

Adam Mickiewicz University

Faculty of Physics

PhD thesis

**Spin-resolved electric and thermoelectric  
transport properties of correlated  
quantum dot systems**

Krzysztof Piotr Wójcik

Supervised by

dr hab. Ireneusz Weymann

Mesoscopic Physics Division, Faculty of Physics,  
Adam Mickiewicz University in Poznań, Poland



Poznań, March 2017



## ACKNOWLEDGEMENTS

The author would like to thank the members of Mesoscopic Physic Division at the Faculty of Physics of Adam Mickiewicz University for many interesting and instructive discussions and a great atmosphere.

The financial support obtained within the following projects is acknowledged:

- Polish State Committee for Scientific Research grant no. N N202 199739,
- Polish Ministry of Science and Higher Education grant *Iuventus Plus* no. IP2011 059471,
- National Science Center in Poland grant *Maestro* no. 2012/04/A/ST3/00372,
- National Science Center in Poland grant *Sonata Bis* no. 2013/10/E/ST3/00213.



Ministry of Science  
and Higher Education

Republic of Poland



NATIONAL SCIENCE CENTRE  
POLAND



*To my beloved wife and daughter.*



# Contents

<b>List of articles constituting the dissertation</b> . . . . .	11
<b>Abstract</b> . . . . .	13
<b>I Introduction</b>	<b>15</b>
<b>1. Motivation and aims</b> . . . . .	17
<b>2. Outline of the methodology</b> . . . . .	21
2.1. General form of the Hamiltonian . . . . .	21
2.1.1. Hamiltonian of quantum dots . . . . .	22
2.1.2. Hamiltonians of leads . . . . .	23
2.1.3. Tunneling Hamiltonian . . . . .	24
2.1.4. Effective Hamiltonian for a quantum dot coupled to a superconductor . . . . .	26
2.2. Linear-response transport coefficients . . . . .	28
2.3. Numerical renormalization group procedure . . . . .	30
2.3.1. Logarithmic discretization . . . . .	30
2.3.2. Mapping onto the Wilson chain . . . . .	31
2.3.3. Iterative diagonalization . . . . .	33
2.3.4. Fixed points of the renormalization group . . . . .	34
2.3.5. The renormalization group and the transmission coefficient . . . . .	35
2.3.6. Implementation of numerical renormalization group procedure in the dissertation . . . . .	35
2.4. Other methods . . . . .	37
2.4.1. Master equation . . . . .	37
2.4.2. Equation of motion for Green's functions . . . . .	38
<b>3. Basic phenomena in transport through quantum dot systems</b> . . . . .	41
3.1. Sequential tunneling and the Coulomb blockade . . . . .	41
3.2. The Kondo effect . . . . .	45
3.3. The two-stage Kondo effect . . . . .	48

3.4. The Fano effect . . . . .	49
3.5. The exchange field . . . . .	51
3.6. Superconducting proximity effect . . . . .	52
3.7. Andreev current through quantum dot . . . . .	53
<b>4. Summary . . . . .</b>	<b>55</b>
<b>5. Streszczenie (Summary in polish) . . . . .</b>	<b>61</b>
<b>The bibliography . . . . .</b>	<b>67</b>
<b>II Articles constituting the dissertation</b>	<b>73</b>
<b>6. Proximity effect on spin-dependent conductance and thermopower of correlated quantum dots [A] . . . . .</b>	<b>75</b>
<b>7. Andreev transport in a correlated ferromagnet-quantum-dot-superconductor device [B] . . . . .</b>	<b>86</b>
<b>8. Perfect spin polarization in T-shaped double quantum dots due to the spin-dependent Fano effect [C] . . . . .</b>	<b>96</b>
<b>9. The magnetic field effects on spin polarization of T-shaped double quantum dots coupled to ferromagnetic leads [D] . . . . .</b>	<b>107</b>
<b>10. Ferromagnets-induced splitting of molecular states of T-shaped double quantum dots [E] . . . . .</b>	<b>110</b>
<b>11. Two-stage Kondo effect in T-shaped double quantum dots with ferromagnetic leads [F] . . . . .</b>	<b>119</b>
<b>12. Thermopower of strongly correlated T-shaped double quantum dots [G] . .</b>	<b>133</b>
<b>13. Strong spin Seebeck effect in Kondo T-shaped double quantum dots [H] . .</b>	<b>147</b>
<b>III Appendix</b>	<b>157</b>
<b>A. Academic achievements . . . . .</b>	<b>159</b>
A.1. Complete list of publications . . . . .	159
A.2. List of schools and conferences . . . . .	160
A.3. List of awards . . . . .	162
A.4. Experience in scientific projects . . . . .	163



**B. Statements concerning authors' contributions** . . . . . 165



# List of articles constituting the dissertation

- [A] K. P. Wójcik, I. Weymann,  
*Proximity effect on spin-dependent conductance and thermopower of correlated quantum dots,*  
Phys. Rev. B **89**, 165303 (2014).
- [B] I. Weymann, K. P. Wójcik,  
*Andreev transport in a correlated ferromagnet-quantum-dot-superconductor device,*  
Phys. Rev. B **92**, 245307 (2015).
- [C] K. P. Wójcik, I. Weymann,  
*Perfect spin polarization in T-shaped double quantum dots due to the spin-dependent Fano effect,*  
Phys. Rev. B **90**, 115308 (2014).
- [D] K. P. Wójcik, I. Weymann,  
*The magnetic field effects on spin polarization of T-shaped double quantum dots coupled to ferromagnetic leads,*  
Acta Phys. Pol. A **127**, 222 (2015).  
(Proceedings of the European Conference *Physics of Magnetism*, Poznań 2014).
- [E] K. P. Wójcik,  
*Ferromagnets-induced splitting of molecular states of T-shaped double quantum dots,*  
Eur. Phys. J. B **88**, 110 (2015).
- [F] K. P. Wójcik, I. Weymann,  
*Two-stage Kondo effect in T-shaped double quantum dots with ferromagnetic leads,*  
Phys. Rev. B **91**, 134422 (2015).

- [G] K. P. Wójcik, I. Weymann,  
*Thermopower of strongly correlated T-shaped double quantum dots*,  
Phys. Rev. B **93**, 085428 (2016).
- [H] K. P. Wójcik, I. Weymann,  
*Strong spin Seebeck effect in Kondo T-shaped double quantum dots*,  
J. Phys.: Condens. Matt. **29**, 055303 (2016).

# Abstract

The subject of the present PhD thesis belongs to a branch of theoretical physics devoted to determination of transport properties of strongly correlated nanoscale systems. It concentrates on mesoscopic structures, in particular these, in which electron correlations lead to the Kondo effect. Single and double quantum-dot structures, coupled to two or three conducting leads, are considered here. A major part of the present dissertation concerns the systems, in which electrodes exhibit ferromagnetic or superconducting correlations, although the case of normal metallic leads is also analyzed. In such structures a diversity of phenomena occur, among which the Coulomb blockade, the Kondo screening, the Fano interference and the Andreev transport are only a few examples of primary interest.

The emphasis is put on the interplay of different correlations. It is shown how the Kondo effect in the structures under consideration is affected by ferromagnetism or superconductivity of the leads. In general, Kondo correlations compete with the exchange field induced by the ferromagnetic leads, as well as with pairing potential induced by superconductor. However, this is not always the case. Under some circumstances, the Kondo temperature may even increase, when the coupling between quantum-dot device and a superconductor is strengthened. The exchange field may compensate for the external magnetic field effects and lead to restoration of the Kondo effect even in strong fields. Thus, the main conclusion of these studies is that *complex many-body phenomena taking place in the correlated quantum-dot systems manifest themselves in a diversity of nontrivial transport properties of these systems.*

The dissertation has the form of a series of eight articles published in international peer-reviewed journals, preceded by an introductory part. Each of the articles addresses a specific problem concerning a particular correlated quantum-dot system. The methodology was optimized for the description of nonperturbative phenomena. For this purpose, the numerical renormalization group procedure is employed as the main calculation technique, and whenever necessary it is complemented by other suitable methods.



# **Part I**

## **Introduction**





# Chapter 1

## Motivation and aims

The giant magnetoresistance effect, discovered in thin layers of ferromagnetic materials by Grünberg and Fert in 1988 [1,2], has found its commercial appliance in reading heads of computer hard disks already in 1997 [3], not even a decade later. Having published his General Theory of Relativity in 1916 [4], Einstein could not have expected that the atomic clocks, build to verify his predictions, will allow the creation of Global Positioning System almost a century later [5]. These two examples illustrate, how strong the impact on the everyday life of society can be exerted by discoveries made by researchers motivated primarily by curiosity, exploring the fields seemingly unrelated to the problems absorbing attention of vast majority of people. Such instances have convinced the author to follow his own interests and to undertake the studies, whose results are described in the following.

The investigations presented in this dissertation are a part of a direction in theoretical basic research, concerning determination of the transport properties of strongly correlated nanoscopic systems. The system is said to be *nanoscopic*, when its characteristic spatial dimensions are within the range of several to a few hundreds nanometers ( $1\text{nm} = 10^{-9}\text{m}$ ). It can be envisioned that development in this field will lead to new discoveries, which could give rise to extraordinary and potentially useful properties of relevant systems. Such findings could be of importance for future applications in nanoelectronics, spintronics, caloritronics or other, possibly yet unknown, fields. However, the main motivation stems from the fact that the low-temperature phenomena at the nanoscale are not yet fully understood, even though appropriate nanoscopic systems can be in practice fabricated, and put under extensive experimental investigations. In particular, systems where different types of correlations compete with each other have recently attracted a great interest. These correlations include the electronic correlations leading to the Kondo ef-

fect, ferromagnetism, superconductivity, and others. Due to the recent rapid development in experimental techniques, the implementation of such systems becomes now possible, so that one can expect experimental verification of theoretical predictions at a relatively short timescale compared to many other basic research areas, such as cosmology or elementary particle physics. At the same time, theoretical description of nanoscale physics is challenging owing to many-body nature of the related phenomena.

The important examples of nanoscopic systems, widely analyzed both theoretically and experimentally, are the systems of quantum dots – the objects of the size smaller than the respective Fermi wavelength, which can be tunnel-coupled to external leads [6]. A quantum dot is usually expected to exhibit single-electron charging effects, which means that the charging energy  $E_C = e^2/(2C)$  fulfills the condition  $E_C \gg k_B T$ . Here,  $e$  denotes the absolute value of the electron charge,  $C$  stands for electric capacity of the considered object, and  $k_B$  is the Boltzmann constant. Hereafter,  $k_B = 1$  by the appropriate choice of units. Moreover, the tunnel junctions need to have a sufficient resistance, large enough for the thermal fluctuations of the number of electrons in the quantum dot to be strongly suppressed.

In the present dissertation quantum dots are often thought of as spatially restricted semiconductor structures, coupled to the electrodes by tunnel junctions [7]. The characteristic feature of such quantum dots is their tunability, *i.e.* the possibility to arbitrarily adjust their basic parameters in experimental setups [8]. Additionally, their rich physical behavior can be often captured by relatively simple model Hamiltonians. Although the solution of them is usually not an easy task, it is still far simpler and computationally less demanding than performing calculations based on first principles. This makes quantum dots an ideal playground for studying the most complicated many-body phenomena. The aim of the present dissertation is to contribute to this field.

The dissertation is focused on determining the transport properties of a few systems, possessing at least two competing energy scales. One could expect that the physics of such systems should be governed by the scale corresponding to the stronger correlation, at least at sufficiently low temperatures. In such cases, the electrical and thermal conductance, the Seebeck coefficient, and other transport coefficients are supposed to resemble the corresponding quantities in the simpler systems. However, there are regimes of parameters, where none of the correlations is dominant. These are the most interesting, since one can hope to find substantially new properties there. Nevertheless, things are not necessarily as simple as one could suppose, and the correlations that may seem to compete can cooperate under some circumstances. For example, as shown in article [A], the coupling to the superconducting lead can actually increase the Kondo temperature. Thus, the conclu-

sion of this study can be formulated as follows: *Complex many-body phenomena taking place in correlated quantum-dot systems manifest themselves in a diversity of nontrivial transport properties of these systems.*

The form of this dissertation is imposed by the fact that it has the form of a series of published articles. The thesis is divided into three parts. Part I is intended to give a possibly simple introduction. It begins with the present chapter outlining the motivation and aims. Subsequently, Chapter 2 is devoted to the methodology. Then, in Chapter 3, the basic physical phenomena occurring in quantum-dot systems are explained and illustrated with calculations performed with the aid of techniques described in Chapter 2. Finally, Chapter 4 contains the summary of the results and conclusions, while Chapter 5 is (somewhat extended) translation of Chapter 4 into polish. Such a form of the introductory part allows for avoiding repetition of the content of introductions of articles constituting Part II, where the history of research in the relevant fields is always discussed. On the contrary, this general introduction aims at showing the basic building blocks of the models analyzed in Part II and at increasing the self-consistency of the thesis.

Being the core of the dissertation, Part II presents the most important results and is constituted by eight articles, written by the author of the present dissertation under the guidance of his supervisor and published in peer-reviewed international journals. Each article corresponds to one chapter of the dissertation (Chapters 6-13).

At last, Part III contains appendices, such as the list of author's academic achievements and statements concerning authors' contributions to the articles constituting Part II.



# Chapter 2

## Outline of the methodology

In the following chapter, the most important aspects of the methodology used in the dissertation are described. The general Hamiltonian of a quantum dot (abbreviated as QD henceforth) system is described in Sec. 2.1. Then, the transport coefficients in the linear response regime are defined and discussed in Sec. 2.2. The numerical renormalization group procedure, being one of the most reliable tools for studying quantum-dot systems at equilibrium, is briefly explained in Sec. 2.3. Finally, in Sec. 2.4 other methods used in Part II are described.

### 2.1. General form of the Hamiltonian

The studied nanostructures can be naturally divided into two parts: quantum dots and leads. The boundary between the two, namely the tunnel junctions, is also an important part of the system, which determines the interaction between QDs and electrodes. Consequently, the total Hamiltonian of a quantum-dot system takes the general form

$$H = H_{\text{QDs}} + \sum_r H_r + \sum_r H_{\text{Tr}}, \quad (2.1)$$

where  $H_{\text{QDs}}$  denotes the Hamiltonian of the quantum dots, including all the interactions between them,  $r$  is an index labeling the contacts,  $H_r$  describes the electrons in the lead  $r$ , while  $H_{\text{Tr}}$  accounts for tunneling between lead  $r$  and QDs. In this Hamiltonian it has been already assumed that there is no direct hopping between the leads.

Before the respective elements of the Hamiltonian are discussed separately in the following subsections, one point seems worth mentioning. Although the quantum dots coupled to the leads and the impurities in the metallic host may seem completely different physical

systems, their spectral properties are in fact nearly identical. For this reason, the models used for the description of QDs are very similar to the well-known quantum impurity models, such as the Anderson model [9] or the Kondo model [10]. These two models are actually closely related [11], although the Anderson model is more general, because it allows for the study of the impurity (or the quantum dot) with a fluctuating occupation number. This is also reflected in richer spectrum of possible low-temperature behavior, especially in the particle-hole asymmetric case [12, 13]. In the present dissertation, description of QDs is based on the Anderson model, to allow for exploration of this wide range of phenomena.

### 2.1.1. Hamiltonian of quantum dots

For the description of quantum dots one usually uses a model Hamiltonian, which captures their basic properties, relevant for the experimentally accessible quantities of the system of interest. In particular, aiming at the calculation of low-temperature transport properties, one can usually restrict the model to only one single-electron orbital per QD. This is justified, because the corresponding level spacing is usually large, due to their limited spatial dimensions. The energy of the orbital relevant for QD labeled by  $i$  is henceforth denoted by  $\varepsilon_i$ . It is usually spin-degenerate, unless an external magnetic field  $B$  is present. In the considered model the interaction between respective QDs takes the form of an electron hopping. Of course, the QD on-site Coulomb (electrostatic) interactions, traditionally denoted by  $U_i$ , should also be taken into account. In the dissertation, the direct exchange coupling between QDs and the inter-dot Coulomb interactions are neglected. These considerations enable one to write the Hamiltonian of QDs in the form suitable for the present analysis,

$$H_{\text{QDs}} = \sum_{i\sigma} (\varepsilon_i + \sigma B) n_{i\sigma} + \sum_i U_i n_{i\uparrow} n_{i\downarrow} + \sum_{\substack{i,j>i \\ \sigma\sigma'}} (t_{i\sigma,j\sigma'} d_{i\sigma}^\dagger d_{j\sigma'} + \text{h.c.}). \quad (2.2)$$

Here,  $i$  indexes the quantum dots.  $n_{i\sigma}$  is the occupation number operator for spin- $\sigma$  electrons in the relevant orbital in  $i$ -th QD, which can be written as a product of respective creation and annihilation operators,  $n_{i\sigma} = d_{i\sigma}^\dagger d_{i\sigma}$ . The first term of Eq. (2.2) describes the energy of an electron residing in  $i$ -th QD, where the magnetic field  $B$  is assumed to be expressed in energy units, such that  $g\mu_B = 1$ . The second term describes on-site Coulomb interactions. The last term contains the sum over all pairs of QDs. For each pair, one can define the hopping matrix elements  $t_{i\sigma,j\sigma'}$ . Phrase h.c. stands for *Hermitean conjugation* of the preceding term. Hopping between quantum dots often conserves spin (*i.e.*, matrix elements  $t_{i\sigma,j\sigma'}$  are nonzero only for  $\sigma = \sigma'$ ).

Although systems with a relatively large number of quantum dots are experimentally realizable [14], structures containing only one or two QDs strongly coupled to correlated leads already host a huge variety of physical phenomena. Moreover, preparation of samples of quality sufficient for measurements of many-body phenomena is even more challenging for more complex nanostructures. For these reasons the present dissertation focuses on single and double quantum-dot systems.

### 2.1.2. Hamiltonians of leads

The leads play a very important role in QD-based structures. Not only are they the reservoirs of electrons and heat, but also strongly affect properties of QDs via interaction with them. In fact, most of the articles constituting the present dissertation analyze the influence of ferromagnetic or superconducting correlations in the leads on the properties of a system of QDs [A, B, C, D, E, F, H]. All leads are normal metals only in article [G].

The typical metallic leads can be modeled as partially filled free-electron sea, with appropriate dispersion relation. Then, the Hamiltonian of each such lead takes the simple form

$$H_r^N = \sum_{\mathbf{k}\sigma} \varepsilon_{r\mathbf{k}} n_{r\mathbf{k}\sigma}, \quad (2.3)$$

where  $\varepsilon_{r\mathbf{k}}$  denotes energy dispersion relation of lead  $r$  for an electron of spin  $\sigma$  and pseudo-momentum  $\mathbf{k}$ , and  $n_{r\mathbf{k}\sigma} = c_{r\mathbf{k}\sigma}^\dagger c_{r\mathbf{k}\sigma}$  with  $c_{r\mathbf{k}\sigma}^{(\dagger)}$  being annihilation (creation) operator of that electron. The summation over  $\mathbf{k}$  runs through the first Brillouin zone. The superscript N was added to  $H_r$  to indicate that the equation applies only to the case of normal metallic lead.

At first sight, the form of the Hamiltonian of a ferromagnetic electrode,

$$H_r^{\text{FM}} = \sum_{\mathbf{k}\sigma} \varepsilon_{r\mathbf{k}\sigma} n_{r\mathbf{k}\sigma}, \quad (2.4)$$

does not really differ from the nonmagnetic case. The only, yet crucial, difference is that the dispersion relation becomes then spin-dependent.

On the contrary, Hamiltonian of a superconducting lead is more complicated. There are various types of superconductors, however, in the dissertation only these described by the BCS theory [15, 16] are considered. The corresponding Hamiltonian is written in the mean-field form,

$$H_r^{\text{SC}} = \sum_{\mathbf{k}\sigma} \varepsilon_{r\mathbf{k}} n_{r\mathbf{k}\sigma} + \sum_{\mathbf{k}} (\Delta_{r\mathbf{k}} c_{r\mathbf{k}\uparrow}^\dagger c_{r-\mathbf{k}\downarrow}^\dagger + \text{h.c.}). \quad (2.5)$$

The dispersion relation  $\varepsilon_{r\mathbf{k}}$  does not depend on spin. The superconducting order parameter is denoted by  $\Delta_{r\mathbf{k}}$  and in general it depends on  $\mathbf{k}$ . Here, it is assumed that this can be neglected, so that the corresponding subscript is omitted,  $\Delta_{r\mathbf{k}} = \Delta_r$ . Note that  $\Delta_r$  is a complex number with an arbitrary phase factor. However, only a difference of such phases between the two superconductors is of physical significance. Thus, in the case of a single superconductor, not only can the subscript be omitted ( $\Delta_r = \Delta$ ), but also  $\Delta$  may be chosen real.

The Hamiltonian given by Eq. (2.5) can be solved by the Bogoliubov transformation [17]. It leads to a new dispersion relation for the quasi-particles, which introduces energy gap of  $2\Delta_r$ , symmetrical around the Fermi level. Additionally, exactly at the Fermi level a condensate of Cooper pairs occurs.

All the lead Hamiltonians presented so far can be combined in a universal form,

$$H_r = \sum_{\mathbf{k}\sigma} \varepsilon_{r\mathbf{k}\sigma} n_{r\mathbf{k}\sigma} + \sum_{\mathbf{k}} (\Delta_r c_{r\mathbf{k}\uparrow}^\dagger c_{r\mathbf{k}\downarrow}^\dagger + \text{h.c.}). \quad (2.6)$$

Of course, none material should be expected to be a ferromagnet and a superconductor at the same time. The purpose of writing Eq. (2.6) is only to give a universal expression for all types of leads considered in this dissertation. Moreover, Hamiltonian given by (2.6) can be also written in the continuous notation,

$$H_r = \int \frac{d^3k}{(2\pi)^3} \left[ \sum_{\sigma} \varepsilon_{r\mathbf{k}\sigma} n_{r\mathbf{k}\sigma} + (\Delta_r c_{r\mathbf{k}\uparrow}^\dagger c_{r\mathbf{k}\downarrow}^\dagger + \text{h.c.}) \right]. \quad (2.7)$$

Here, operators  $c_{r\mathbf{k}\sigma}^{(\dagger)}$  are normalized such that the commutation relation contains the volume of the crystal times the Kronecker delta function, which becomes the Dirac delta function in the limit of an infinite crystal, corresponding to dense Brillouin zone.

### 2.1.3. Tunneling Hamiltonian

Within this dissertation the tunneling Hamiltonian is taken simply as

$$H_{Tr} = \sum_{i\sigma\mathbf{k}\sigma'} (v_{i\sigma,r\mathbf{k}\sigma'} c_{r\mathbf{k}\sigma'}^\dagger d_{i\sigma} + \text{h.c.}), \quad (2.8)$$

where  $v_{i\sigma,r\mathbf{k}\sigma'}$  is the hopping matrix element between the spin- $\sigma$  state in  $i$ -th QD and spin- $\sigma'$  state with momentum  $\mathbf{k}$  in the lead  $r$ . Since  $v_{i\sigma,r\mathbf{k}\sigma'}$  is a coupling between plain-wave-like state in the lead and a localized state in QD, it is inversely proportional to square root of volume of the crystal. With the appropriate changes of normalization of



$v_{i\sigma,r\mathbf{k}\sigma'}$  and operators  $c_{r\mathbf{k}\sigma'}^{(\dagger)}$ , also this part can be expressed in the continuous notation,

$$H_{Tr} = \sum_{i\sigma\sigma'} \int \frac{d^3k}{(2\pi)^3} (v_{i\sigma,r\mathbf{k}\sigma'} c_{r\mathbf{k}\sigma'}^\dagger d_{i\sigma} + \text{h.c.}). \quad (2.9)$$

When written in the spherical basis in the  $\mathbf{k}$ -space, the coefficients  $v_{i\sigma,r\mathbf{k}\sigma'}$  are usually negligible for leads' states of angular momentum different from that of the state localized in QD  $i$ . Then, the 3-dimensional integral may be reduced to the integral over  $k = |\mathbf{k}|$ , while the integrals over angular coordinates give either unity (for states of correct angular momentum) or zero (for the other states). Note, that such decoupled states do not contribute to the transport properties of the system and can be discarded from the Hamiltonian completely (not only from  $H_{Tr}$ ). Moreover, one can use dispersion relation to change the variable from  $k$  to  $\varepsilon$ . Finally, in the present dissertation only co-linear orientations of leads' magnetizations are considered and the assumption concerning spin-conserving tunneling is made. Altogether, these simplifications allow one to write the tunneling Hamiltonian in the form

$$H_{Tr} = \sum_{i\sigma} \int d\varepsilon \sqrt{\rho_{r\sigma}(\varepsilon)} (v_{ir\varepsilon\sigma} c_{r\varepsilon\sigma}^\dagger d_{i\sigma} + \text{h.c.}), \quad (2.10)$$

where  $\rho_{r\sigma}(\varepsilon)$  is the density of states (per unit cell) of lead  $r$ , and the integration is performed over the relevant energy band. In practice, at low temperatures  $\rho_{r\sigma}$  and  $v_{ir\varepsilon\sigma}$  usually do not change significantly for  $\varepsilon$  within the range of a few  $k_B T$  around the Fermi level, so one can consider them as constants without introducing a significant error. In particular, in the present thesis  $\rho_{r\sigma}(\varepsilon)$  is substituted by the constant corresponding to the Fermi level. The tunnel coupling between the lead  $r$  and  $i$ -th QD can then be parametrized by

$$\Gamma_{ir\sigma} = \pi \rho_{r\sigma} |v_{irE_F\sigma}|^2 \quad (2.11)$$

and the phase of  $v_{irE_F\sigma}$ , which is often irrelevant. In all the systems considered in the present dissertation, there is only one QD directly coupled to the leads —say QD labeled with  $i = 1$  or simply QD1. This means that  $\Gamma_{r\sigma} \equiv \Gamma_{1r\sigma}$  is a parameter of the model and  $\Gamma_{ir\sigma} = 0$  for  $i \neq 1$ .

At low temperatures,  $\Gamma_{r\sigma}$  also plays the role of the interaction-induced broadening of QD1 level for spin- $\sigma$  electron. One can further define the (spin-resolved) level broadening as a sum of couplings corresponding to the relevant leads,

$$\Gamma_{(\sigma)} = \sum_r \Gamma_{r(\sigma)}. \quad (2.12)$$

It is convenient to introduce the spin polarization  $p_r$  of lead  $r$ , which obeys

$$\Gamma_{r\sigma} = \Gamma_r (1 \pm p_r \sigma). \quad (2.13)$$

In the above equation, the upper sign corresponds to the situation that spin moment of lead  $r$  is parallel to the quantization axis, while the lower one to its anti-parallel alignment. In this notation, assuming that  $v_{1r\varepsilon\sigma}$  may be taken real and positive, the corresponding tunneling Hamiltonian becomes

$$H_{Tr} = \sum_{\sigma} \sqrt{\frac{\Gamma_{r\sigma}}{\pi}} \int d\varepsilon (c_{r\varepsilon\sigma}^{\dagger} d_{1\sigma} + \text{h.c.}). \quad (2.14)$$

Finally, at equilibrium, in the case of two symmetrically coupled and *not* superconducting leads, *i.e.*  $r \in \{L, R\}$ , a following canonical transformation of the leads states,

$$c_{\varepsilon\sigma} = u_{\sigma} c_{L\varepsilon\sigma} + v_{\sigma} c_{R\varepsilon\sigma}, \quad (2.15)$$

$$\tilde{c}_{\varepsilon\sigma} = -v_{\sigma} c_{L\varepsilon\sigma} + u_{\sigma} c_{R\varepsilon\sigma}, \quad (2.16)$$

with  $u_{\sigma} = \sqrt{\Gamma_{L\sigma}/(\Gamma_{L\sigma} + \Gamma_{R\sigma})}$  and  $v_{\sigma} = \sqrt{1 - u_{\sigma}^2}$ , results in the decoupling of states described by  $\tilde{c}_{\varepsilon\sigma}$  [18]. Note that for  $\Gamma_L = \Gamma_R$  these are simply the states odd with respect to exchange of the leads. This allows for writing the total Hamiltonian in an effective single-channel form,

$$\sum_r H_{Tr} = \sum_{\sigma} \sqrt{\frac{\Gamma_{\sigma}}{\pi}} \int d\varepsilon (c_{\varepsilon\sigma}^{\dagger} d_{1\sigma} + \text{h.c.}), \quad (2.17)$$

$$\sum_r H_r = \sum_{\sigma} \int d\varepsilon \varepsilon n_{\varepsilon\sigma}. \quad (2.18)$$

The integrals in principle run through the whole conduction band, but in practice one can restrict oneself to the section of energies lying within the range  $E_F \pm D$ , with cutoff  $D$  being greater than the largest relevant energy scale.

#### 2.1.4. Effective Hamiltonian for a quantum dot coupled to a superconductor

In general, in the presence of a superconducting lead, the Hamiltonian of the system cannot be transformed to the single-channel form, as described in the previous section, unless the superconducting lead is the only one to which the quantum dot is attached. This stems from the fact, that states not tunnel-coupled directly to the QDs, *i.e.* described by  $\tilde{c}_{\varepsilon\sigma}$  in Eq. (2.16), can still interact with the coupled states (described by  $c_{\varepsilon\sigma}$ ) via a term proportional to  $\Delta$ . Moreover, even in the absence of the voltage bias, the presence of two superconductors characterized by a different phase of their corresponding order parameters is in fact a non-equilibrium situation, as this induces the flow of the Josephson current in the system. On the other hand, if there is only one superconductor, all tunneling processes can be divided into two categories: tunneling of quasi-particles, which is strongly

suppressed at temperatures  $T \ll \Delta$  and low bias, and the Andreev (Cooper pair) tunneling. In the limit of the infinitely large superconducting gap,  $\Delta \rightarrow \infty$ , the former can be neglected, and description of the latter can be significantly simplified.

A new Cooper pair can be created in the superconductor, when two electrons are provided, so that their total energy equals the doubled Fermi energy,  $2E_F$ . Thus, when an electron incident on the superconductor interface has an energy  $\varepsilon > E_F$ , to form a Cooper pair it needs another electron of opposite spin from the Fermi sea. As a result, a hole is left behind in the normal region. Such a process is referred to as the *Andreev reflection*, in memory of a Russian physicist who predicted it [19]. In restricted geometries, due to multiple Andreev reflections, the bound states can form [20, 21], called *Andreev bound states* or *Yu-Shiba-Rusinov states* [22–24]. They can be investigated experimentally by means of scanning tunneling microscopy [25–27]. Moreover, these states determine the transport properties of a QD coupled to the superconductor [28–31].

In order to gain a better insight into the role of the bound states in the transport, consider a single QD coupled to a superconductor (SC) as an example. The subscript  $i$  numbering QDs is now redundant and can be omitted (in particular,  $\varepsilon$  denotes QD level). Additionally, the SC order parameter  $\Delta$  is taken as real and negative, which occurs to be convenient choice. The Hamiltonian of the system under consideration can be written then as

$$H_{\text{QD}} + H_S + H_{\text{TS}} = \sum_{\sigma} (\varepsilon + \sigma B) n_{\sigma} + U n_{\uparrow} n_{\downarrow} + \sum_{\mathbf{k}\sigma} \varepsilon_{S\mathbf{k}} n_{S\mathbf{k}\sigma} \quad (2.19)$$

$$+ \Delta \sum_{\mathbf{k}} (c_{S\mathbf{k}\uparrow}^{\dagger} c_{S\mathbf{k}\downarrow}^{\dagger} + \text{h.c.}) + \sum_{\sigma\mathbf{k}} (v_{S\mathbf{k}} c_{S\mathbf{k}\sigma}^{\dagger} d_{\sigma} + \text{h.c.}).$$

Importantly, the Hamiltonian above can be extremely simplified if one integrates out the quasi-particle excitations. This generates the induced action, which in the limit  $|\Delta| \rightarrow \infty$  is equal to the action corresponding to the effective Hamiltonian [20],

$$H_{\text{eff}} = \sum_{\sigma} (\varepsilon + \sigma B) n_{\sigma} + U n_{\uparrow} n_{\downarrow} + \Gamma_S (d_{\uparrow}^{\dagger} d_{\downarrow}^{\dagger} + \text{h.c.}), \quad (2.20)$$

where  $\Gamma_S = \pi \rho_S |v_S|^2$  and  $\rho_S$  denotes normalized density of states of SC lead at the Fermi level in the normal state, and  $v_S$  equals  $\mathbf{k}$ -independent  $v_{S\mathbf{k}}$  in the wide-band limit. The positive sign of the term proportional to  $\Gamma_S$  is implied by a negative  $\Delta$ . Note that although SC degrees of freedom were excluded from  $H_{\text{eff}}$ , the Hamiltonian does not conserve the number of electrons. In fact, a pair of them may be created or annihilated in QD. This is described by the term proportional to  $\Gamma_S$ , which plays a role of a pairing potential here. The tremendous simplification obtained by introduction of  $H_{\text{eff}}$  rests in the fact, that it can be represented in terms of local states of QD, *i.e.*, as a 4-dimensional matrix, instead of an operator acting on infinitely many degrees of freedom, as in Eq. (2.20).

## 2.2. Linear-response transport coefficients

As explained in Sec. 2.3, numerical renormalization group approach can be used to find the spectrum of the system at equilibrium. However, at equilibrium there is no transport in the system, in particular, there is neither electric nor spin current, and heat does not flow either. Nevertheless, the dynamical properties of the system, such as conductances corresponding to respective currents, can be defined within the linear response theory and calculated from the equilibrium spectrum of the Hamiltonian, as discussed in the following<sup>1</sup>.

Using the Boltzmann equation approach or Kubo linear response theory, and assuming well-defined Fermi level to be the reference point for energy scale, one can derive the linear-response kinetic coefficients connecting currents (the  $x$ -current is denoted by  $I_x$ , where  $x = C$  for charge,  $x = S$  for spin,  $x = Q$  for heat) with forces that induce these currents: voltage  $V$ , spin voltage  $V_S$  and temperature difference  $\Delta T$  [32, 33],

$$\begin{pmatrix} I_C \\ I_S \\ I_Q \end{pmatrix} = \sum_{\sigma} \begin{pmatrix} e^2 L_{0\sigma} & \sigma e^2 L_{0\sigma} & -e L_{1\sigma}/T \\ -\sigma e \frac{\hbar}{2} L_{0\sigma} & -e \frac{\hbar}{2} L_{0\sigma} & \sigma \frac{\hbar}{2} L_{1\sigma}/T \\ -e L_{1\sigma} & -\sigma e L_{1\sigma} & L_{2\sigma}/T \end{pmatrix} \begin{pmatrix} V \\ V_S \\ \Delta T \end{pmatrix}, \quad (2.21)$$

where  $e$  is the absolute value of electron charge,  $\sigma$  corresponds to different spin species,

$$L_{n\sigma} = -\frac{1}{\hbar} \int \omega^n \frac{\partial f(\omega)}{\partial \omega} \mathcal{T}_{\sigma}(\omega) d\omega \quad (2.22)$$

is the appropriate kinetic coefficient,  $f(\omega)$  is the Fermi-Dirac distribution function, and  $\mathcal{T}_{\sigma}(\omega)$  is the spin-resolved transmission coefficient. Henceforth the notation  $L_n = L_{n\uparrow} + L_{n\downarrow}$  and  $M_n = L_{n\uparrow} - L_{n\downarrow}$  will be also used.

The transport properties can be calculated from integrals  $L_{n\sigma}$  using Eq. (2.21). In particular, the electrical and spin conductances are

$$G \equiv \partial_V I_C \Big|_{\substack{V_S=0 \\ \Delta T=0}} = e^2 L_0, \quad (2.23)$$

$$G_S \equiv \partial_{V_S} I_S \Big|_{\substack{V=0 \\ \Delta T=0}} = -e \frac{\hbar}{2} \cdot L_0, \quad (2.24)$$

respectively, where  $\partial_x A|_{y=0}$  denotes partial derivative of  $A(x, y)$  with respect to  $x$ , while the condition  $y = 0$  is fulfilled. Similarly, the heat conductance is given by

$$\kappa \equiv \partial_{\Delta T} I_Q \Big|_{\substack{I_C=0 \\ V_S=0}} = \frac{1}{T} \left( L_2 - \frac{L_1^2}{L_0} \right), \quad (2.25)$$

where the conditions  $I_C = 0$  and  $V_S = 0$  in fact determine  $V$  as a function of  $\Delta T$ .

<sup>1</sup>This section is partially based on article [H] constituting Chapter 13.

The difference between the conductances of respective spin channels can be conveniently described by the linear-response spin polarization of the current,

$$\mathcal{P} = \frac{I_{\uparrow} - I_{\downarrow}}{I} = \frac{G_{\uparrow} - G_{\downarrow}}{G} = \frac{M_0}{L_0}. \quad (2.26)$$

Another important property of the systems with two ferromagnetic leads is their tunneling magnetoresistance [34],

$$\text{TMR} = \frac{G^{\text{P}} - G^{\text{AP}}}{G^{\text{AP}}}, \quad (2.27)$$

where the superscript P refers to the parallel magnetic configuration of the leads, while AP corresponds to the anti-parallel configuration. In the case of direct tunneling between the two ferromagnets,  $G^{\text{P}} > G^{\text{AP}}$  and  $\text{TMR} > 0$ . However, if the two ferromagnets are separated with a strongly interacting quantum-dot system, TMR may reach negative values.

The major thermoelectric property of a nano-device is the Seebeck coefficient, denoted by  $S$  and describing the voltage necessary to prevent the electric current flow in the presence of temperature difference between the two leads. It can be expressed as

$$S = G^{-1} \partial_{\Delta T} I_C \Big|_{\substack{V=0 \\ V_S=0}} = -\frac{1}{eT} \frac{L_1}{L_0}. \quad (2.28)$$

Seebeck coefficient is related to the Peltier coefficient  $\Pi = \partial_{I_C} I_Q \Big|_{\substack{V_S=0 \\ \Delta T=0}}$  by  $\Pi = ST$ . However, at low temperatures it is more useful to study  $S$  instead of  $\Pi$ , because Peltier coefficient is then very small. Indeed, at low temperatures the experimentally realizable temperature differences are also small, so the heat flows are in general reduced.

The spin Seebeck coefficient, known also as the spin thermopower, is conventionally defined in analogy to Eq. (2.28) as

$$S_S = G_S^{-1} \partial_{\Delta T} I_S \Big|_{\substack{V=0 \\ V_S=0}} = -\frac{2}{\hbar T} \frac{M_1}{L_0}. \quad (2.29)$$

Indeed, this definition is used in article [H] (Chapter 13) and corresponds to spin voltage necessary to ensure vanishing spin current in the presence of temperature differences. However, in articles [A] and [G] (*i.e.* Chapters 6 and 12), it was defined somewhat differently. In fact, the situation described in these articles corresponds to complete independence of spin channels. Then, the Seebeck coefficient can be defined for each spin channel individually,

$$S_{\sigma} = G_{\sigma}^{-1} \partial_{\Delta T} I_{\sigma} \Big|_{V_{\sigma}=0} = -\frac{1}{eT} \frac{L_{1\sigma}}{L_{0\sigma}}, \quad (2.30)$$

where  $G_{\sigma}$ ,  $I_{\sigma}$  and  $V_{\sigma}$  denote (correspondingly): the conductance, the electric current, and the voltage, in each case in spin-channel  $\sigma$ . Then,

$$\tilde{S}_S = \frac{1}{2}(S_{\uparrow} - S_{\downarrow}) \quad (2.31)$$

can also be called spin thermopower. Note that the two definitions are *not* equivalent, *i.e.*  $\tilde{S}_S \neq S_S$ . This is caused by the fact that the condition  $V_S = 0$  is in general not fulfilled for independent spin channels. Nevertheless, in Part II  $S_S$  is used to denote both quantities (they do not occur together in any article).

Finally, the (spin) figure of merit can be defined by

$$Z_{(S)}T = S_{(S)}^2 G_{(S)}T / \kappa. \quad (2.32)$$

It is a measure of thermodynamic efficiency of the device treated as a heat engine. The corresponding power factor

$$P = S^2 G \quad (2.33)$$

is related to maximal power of the device and the performance under the fixed flow conditions [35].

## 2.3. Numerical renormalization group procedure

Numerical renormalization group procedure, commonly abbreviated NRG, is an algorithm allowing for very accurate numerical computation of the spectrum of impurity models in equilibrium [38]. The method, proposed by Kenneth G. Wilson, is *not* based on the perturbative expansion in the coupling constant or interaction strength, but rather relies on obtaining a sequence of effective Hamiltonians and was inspired by earlier ideas concerning renormalization. The procedure consists of three major steps: logarithmic discretization of the conduction band, mapping the model onto effective semi-infinite chain, which determines the sequence of effective Hamiltonians and, finally, iterative diagonalization of them. The respective steps are discussed in detail in the following subsections.

### 2.3.1. Logarithmic discretization

The starting point for application of NRG can be a Hamiltonian of a form of Eq. (2.1), with Eq. (2.2) accounting for a single QD (corresponding to single value of  $i$ ), and Eqs. (2.17) and (2.18) representing the tunneling and leads Hamiltonians, respectively. The generalization to the case of a double QD in a T-shaped configuration is rather trivial, as explained further. From now on, we set the Fermi energy to be the reference point for measuring single-particle energies,  $E_F = 0$ , and use the half-bandwidth as a unit of energy,  $D = 1$ .

The first step of NRG is the *logarithmic discretization* of the conduction band. It is achieved in a few stages, which aim at the optimal choice of basis for single-particle states. At the beginning, the energy band is divided into logarithmic intervals,

$$I_n^+ = [\Lambda^{-(n+1)}, \Lambda^{-n}], \quad n \geq 0, \quad (2.34)$$

and  $I^-$  defined analogously for negative energies.  $\Lambda$  is called a discretization parameter and at the moment it is an arbitrary number greater than unity. Large  $\Lambda$  implies large intervals  $I_n^\pm$ , while  $\Lambda \rightarrow 1$  leads to small intervals. Then, in each interval, the Fourier basis is introduced. Note that electron states labeled by energy  $\varepsilon$  and spin  $\sigma$  correspond to a spherically symmetric electronic wave functions extending over the entire volume of the system. Thus, the Fourier basis corresponds to some spatially localized states. In fact, the zero-frequency Fourier state is localized around the center of spherical symmetry, while the remaining states —around some spherical shells surrounding it [38]. The states are said to be *localized around*, not localized *at* some point or shell, because the Fourier basis is introduced in each interval  $I_n^\pm$  separately, so it is not a true Fourier basis in the entire momentum space. Therefore, one can expect a Heisenberg-like uncertainty relation determining the spatial spread of these new basis states. Since QD is a small object and by definition of conduction band basis it is located at the center of spherical symmetry, one can claim that it couples only to the zero-frequency Fourier state. For this reason one can discard the other states and only one state per a single interval  $I_n^\pm$  is left.

It seems worth stressing that logarithmic discretization is possible only if the effective conduction band has a well-defined Fermi level. Clearly, this is not the case for a non-equilibrium systems, which is the strongest restriction upon the applicability of NRG. On the other hand, at equilibrium logarithmic discretization occurs to be very efficient, allowing for separation of energy scales in the Hamiltonian under investigation. This idea has provided the main motivation for the introduction of NRG since its conception proposed by Wilson in his seminal, albeit still rarely mentioned paper [39].

### 2.3.2. Mapping onto the Wilson chain

The next step of the NRG procedure is a tri-diagonalization of the single-particle subspace of the Hamiltonian leading to its mapping onto the semi-infinite chain, the so-called Wilson chain. This chain corresponds to conduction band degrees of freedom and is coupled to the unaffected Hamiltonian of QD. In the case of flat conduction band the tri-diagonalization can be realized analytically [38]. In more complex situations, some integrals have to be calculated numerically, or the whole tri-diagonalization can be per-

formed *e.g.* with the aid of the Lanczos method. In both cases one can define a sequence of Hamiltonians, which for a particle-hole symmetric conduction band has the form

$$H_N = \Lambda^{(N-1)/2} \left[ H_{\text{QD}} + \sum_{\sigma} \sqrt{\frac{\Gamma_{\sigma}}{\pi}} (f_{0\sigma}^{\dagger} d_{\sigma} + d_{\sigma}^{\dagger} f_{0\sigma}) \right. \\ \left. + \frac{1}{2} (1 + \Lambda^{-1}) \sum_{\sigma} \sum_{n=0}^N \Lambda^{-n/2} \xi_n (f_{n\sigma}^{\dagger} f_{(n+1)\sigma} + f_{(n+1)\sigma}^{\dagger} f_{n\sigma}) \right] - E_{\text{GS}}(N), \quad (2.35)$$

where  $f_{n\sigma}$  annihilates an electron of spin  $\sigma$  at site  $n$  of the chain, the term  $-E_{\text{GS}}(N)$  indicates, that  $H_N$  contains additional constant chosen such, that its ground state has energy equal to 0, and

$$\xi_n = \frac{1 - \Lambda^{-(n+1)}}{\sqrt{(1 - \Lambda^{-(2n+1)})(1 - \Lambda^{-(2n+3)})}}. \quad (2.36)$$

The discretization scheme ensures that  $\xi_n \rightarrow 1$  for  $n \rightarrow \infty$  [38]. In the limit  $N \rightarrow \infty$ ,  $H_N$  becomes re-scaled discretized Hamiltonian with ground state shifted to 0 written in a new basis. However, the scale factor becomes then infinite. The reason for introduction of such re-scaling is to make the smallest hopping in the chain the number of the order of unity. At this point it is easy to note that the only difference between the case of a single QD and a T-shaped double QD is an additional QD attached to the first one. The chain itself remains unaffected. Thus, although the second QD can completely change the results, its presence does not alter the NRG procedure.

The sequence  $H_N$  fulfills the following recursion relation, known also as the renormalization group transformation,

$$H_{N+1} = \Lambda^{1/2} H_N + \sum_{\sigma} \xi_N (f_{N\sigma}^{\dagger} f_{(N+1)\sigma} + f_{(N+1)\sigma}^{\dagger} f_{N\sigma}) - E_{\text{GS}}(N+1) \equiv \mathcal{R}(H_N). \quad (2.37)$$

The idea behind the renormalization group is to solve this relation, *i.e.*, understand how  $H_N$  evolves upon iteration of  $N$ . In NRG, one uses Eq. (2.37) as a basis for iterative method of approximate determination of the spectrum of  $H_N$ . Finally, note that although the spectrum of  $H_N$  is discrete, whereas the spectrum of the initial Hamiltonian is continuous, they can lead to practically identical thermodynamic properties, if the distance between energies in a discrete spectrum is much smaller than the temperature. Thus, the smaller  $T$  is, the more densely the spectrum must be probed. On the other hand, at small  $T$  only states close to the ground state are relevant. Therefore,  $H_N$  can be considered as a (re-scaled) effective Hamiltonian at temperatures fulfilling

$$\Lambda^{-(N-1)/2} \ll T \ll 1. \quad (2.38)$$



### 2.3.3. Iterative diagonalization

The last step of NRG is an iterative procedure of diagonalization of NRG effective Hamiltonians (2.35). For some small  $N$ , the whole Hamiltonian  $H_N$  can be diagonalized numerically. Then, another site of the Wilson chain can be added (*i.e.*  $N$  can be increased by unity) and the Hamiltonian re-scaled according to Eq. (2.37). However, for a single-channel calculation the Hilbert space is then increased by a factor of 4. In this way, when consecutive sites of the chain are added, the dimension of the Hilbert space rapidly expands and the problem quickly becomes unmanageable. To avoid such a scenario, before adding a new site, one discards high-energy states and keeps only a fixed number  $N_{\text{kept}}$  of low-energy states. Due to this truncation scheme, the number of states after adding another site equals  $4N_{\text{kept}}$ .  $N_{\text{kept}}$  must be chosen so that the matrix of this size can be diagonalized numerically, and the procedure can be iterated. The discarded states possess energies much larger than the hopping to the newly-added site. Thus, it seems reasonable to assume that they are not affected by the further part of the Wilson chain, corresponding to the lower-energy scales. Such an energy scale separation is the most important feature of the physical system for NRG procedure to be effective.

The postulate to keep  $N_{\text{kept}}$  states of the lowest energies actually cannot be treated literally, because it can lead to huge inaccuracy, if the last kept state and the first state to be discarded are in fact degenerate. When such situation arises, the true eigenstates of  $H_{N+1}$  can be very different from the eigenstates of  $H_N$  extended to the larger Hilbert space, provided that the interaction with the next site of the Wilson chain removes this degeneracy. For this reason, degenerate multiplets should be either entirely kept or entirely discarded. The same applies to *almost degenerate* states, *i.e.*, when the difference in their energy is much smaller than the interaction between them. In the present dissertation, as in Ref. [38], such multiplets are entirely kept.

The number of kept states,  $N_{\text{kept}}$ , can be significantly decreased, if the Hamiltonian exhibits some symmetries, for instance the ones resulting from the conservation of charge or spin  $z$ -component. Also non-Abelian symmetries, such as the total spin  $SU(2)$  symmetry, can be exploited. The Hamiltonian can be then written in the block-diagonal form on the basis of quantum numbers only, and each block can be diagonalized separately. Since CPU time needed for matrix diagonalization grows as cube of its dimension with matrix size, this accelerates the computation tremendously.

The truncated  $H_N$  can still be interpreted as a re-scaled effective Hamiltonian, but now at

temperatures fulfilling much stronger criterion, namely

$$\Lambda^{-(N-1)/2} \ll T \ll E_{\text{dis}}, \quad (2.39)$$

where  $E_{\text{dis}}$  is the energy of the lowest discarded state. The thermodynamics can then be determined from the partition function  $Z_N = \exp(-H_N/T)$ . Nevertheless, as it is explained in Sec. 2.3.6, the effects of finite temperature should be taken into account more precisely.

### 2.3.4. Fixed points of the renormalization group

Except for very small  $N$ , the transformation  $\mathcal{R}: H_N \mapsto H_{N+1}$  conserves a dimension of a Hamiltonian matrix —assuming that one can choose  $N_{\text{kept}}$  so that keeping more states due to their degeneracy is not necessary. Thus, it can happen that  $\mathcal{R}$  has a fixed point, *i.e.*, there exists such an effective Hamiltonian  $H^*$  that  $\mathcal{R}(H^*) = H^*$ . Because of the continuity of  $\mathcal{R}$ , one can expect that if for some  $N$  the Hamiltonian  $H_N$  is close to  $H^*$ , then  $H_{N+1}$  is also close to  $H^*$ , so  $H_N$  and  $H_{N+1}$  are close to each other. Furthermore, if  $H_N$  has any limit for  $N \rightarrow \infty$ , this limit must be a fixed point of  $\mathcal{R}$ . In impurity models, though, such a limit does not exist. On the contrary,  $\mathcal{R}$  causes oscillations for large  $N$  with a period of 2. However, some fixed points exist for the transformation  $\mathcal{R}^2$ , *i.e.*  $\mathcal{R}$  applied twice. In fact, for large  $N$  the Hamiltonian  $H_N$  oscillates between the two fixed points of  $\mathcal{R}^2$ .

The fixed points are important, because they are properties of the renormalization group transformation itself, and not of the initial effective Hamiltonian  $H_0$ ; see Eq. (2.35). If there are many fixed points, and they are not isolated, then small change in the model parameters may change the fixed point to which  $H_N$  converges (for a given parity of  $N$ ). However, in the case of isolated fixed points, the large  $N$  limits may be the same for a wide range of model parameters. Since large  $N$  corresponds to a small temperature, this means a universal low-temperature behavior, a characteristic feature of many Kondo systems.

At the end it seems worth mentioning, that although the term *numerical renormalization group* is nowadays usually identified with the procedure proposed by Wilson in Ref. [38] and described above, there exist other numerical procedures based on the renormalization group ideas. One of many examples is described in Ref. [40].

### 2.3.5. The renormalization group and the transmission coefficient

The transmission coefficient  $\mathcal{T}_\sigma(\omega)$ , which needs to be known for the calculation of the integrals  $L_{n\sigma}$ , see Eq. (2.22), is proportional to the imaginary part of a relevant retarded Green function. In the case of a T-shaped double QD, the Green's function of the QD coupled to the leads needs to be calculated. Using  $d_{1\sigma}$  as the notation for the annihilation operator of the electron with spin  $\sigma$  in this QD irrespective of the number of QDs, the transmission coefficient for the normal or ferromagnetic leads can be written as [36]

$$\mathcal{T}_\sigma(\omega) = -\Gamma_\sigma \text{Im} \langle\langle d_{1\sigma}^\dagger | d_{1\sigma} \rangle\rangle^{\text{ret}}(\omega), \quad (2.40)$$

where the corresponding Green's function is denoted by  $\langle\langle d_{1\sigma}^\dagger | d_{1\sigma} \rangle\rangle^{\text{ret}}(\omega)$  and defined in Sec. 2.4.2. It can be calculated directly in the Lehmann representation, from the spectrum obtained with NRG. Then,  $\mathcal{T}_\sigma(\omega)$  is a sum of the Dirac delta functions, which is easy to integrate directly. This allows for the calculation of coefficients  $L_{n\sigma}$  given by Eq. (2.22).

On the other hand, in the case of transport between the normal lead and the superconductor (via QD), the transmission coefficient for Andreev reflection processes reads [37]

$$\mathcal{T}_\sigma(\omega) = 4\Gamma_\sigma \Gamma_{\bar{\sigma}} \left| \langle\langle d_{1\sigma} | d_{1\bar{\sigma}} \rangle\rangle^{\text{ret}}(\omega) \right|^2, \quad (2.41)$$

where  $\Gamma_\sigma$  is spin-dependent coupling to the normal/ferromagnetic lead and  $\bar{\sigma} \equiv -\sigma$ . Eq. (2.41) is valid only in the continuum limit (with dense Brillouin zone). Otherwise the square of the relevant Green's function is not well-defined (it contains terms proportional to the Dirac delta functions, which cannot be squared). For this reason,  $\langle\langle d_{1\sigma} | d_{1\bar{\sigma}} \rangle\rangle^{\text{ret}}(\omega)$  calculated with NRG (*i.e.* for a discretized system) must be numerically smoothed. This can be obtained *e.g.* by Gaussian broadening of corresponding delta peaks on the logarithmic scale and performing a numerical Hilbert transform to obtain real part of the Green's function. Then, the calculation of squared module of  $\langle\langle d_{1\sigma} | d_{1\bar{\sigma}} \rangle\rangle^{\text{ret}}(\omega)$  is possible. However, one needs to carefully verify the lack of dependence of that result on mesh grid or discretization parameter, because the Hilbert transform is in general difficult to realize numerically.

### 2.3.6. Implementation of numerical renormalization group procedure in the dissertation

In the preceding sections, the NRG procedure was discussed in the form originally presented by Wilson in the famous paper [38]. Since then, NRG has been technically improved in a few points. In particular, in the original formulation, the truncated  $H_N$  is

interpreted as a re-scaled effective Hamiltonian. However, taking into account that all the states discarded during iteration form (after a trivial extension to the full space of states) an approximate complete and ortho-normal set [41, 42], one can obtain the effective density matrix of the system [43]. More precisely, let  $|N, k\rangle$  denote the  $k$ -th discarded eigenstate of  $H_N$ ,  $H_N|N, k\rangle = \tilde{E}_{Nk}|N, k\rangle$ , with  $\tilde{E}_{Nk} = \Lambda^{(N-1)/2}E_{Nk} - E_{\text{GS}}(N)$ ; compare Eq. (2.35). The states  $|N, k\rangle$  can be extended to the full Hilbert space of the chain,  $\mathcal{H}$ , which is  $4^{N_{\text{max}}+2}$ -dimensional for a single QD described with the Anderson model (the Wilson chain has  $N_{\text{max}} + 1$  sites, and there are 4 QD states). However, this extension is not unique. In fact, the subspace of  $\mathcal{H}$  spanned by different extensions of  $|N, k\rangle$  is  $4^{N_{\text{max}}-N}$ -dimensional. The important point is that the full Hamiltonian of the chain restricted to this subspace can be approximated by the eigenvalue of  $H_N$  corresponding to  $|N, k\rangle$  namely  $E_{Nk}$ . Moreover, for  $|\phi\rangle_{Nk}$  and  $|\psi\rangle_{N'k'}$  denoting arbitrary extensions of  $|N, k\rangle$  and  $|N', k'\rangle$ , respectively,  ${}_{Nk}\langle\phi|\psi\rangle_{N'k'} = 0$  for  $N \neq N'$  or  $k \neq k'$ . With this observation one can write the partition function for the full chain as

$$Z_{\text{eff}} = \sum_{Nk} 4^{N_{\text{max}}-N} \exp(-E_{Nk}/T). \quad (2.42)$$

Since the number of different energies  $E_{Nk}$  is (for a single QD) bounded from above by  $(N_{\text{max}} + 2)N_{\text{kept}}$ , the partition function can be in practice calculated, and so can the thermodynamic quantities as well as the relevant Green functions.

In the present dissertation, calculations were performed with slightly modified version of logarithmic discretization [44–46]. The difference is that instead of states whose wave functions are exact plain waves within interval  $I_n^\pm$ , one uses optimized representative states for each interval. The basis states are orthogonal, despite their continuity at the edges of the intervals.

Finally, the so-called  $z$ -averaging trick [47] is in some cases used to enhance the quality of obtained spectral functions. This means that the results are averaged over a few runs of NRG procedure with shifted discretizations. Instead of Eq. (2.34), the discretization intervals are defined by

$$I_0^+ = [\Lambda^{-z}, 1], \quad (2.43)$$

$$I_n^+ = [\Lambda^{-n-z}, \Lambda^{-n+1-z}] \quad \text{for } n > 0, \quad (2.44)$$

and the results obtained for a number  $N_z$  of values of  $z$  are averaged. The used  $z$ -values are  $z = i/N_z$  with  $i$  running from 1 to  $N_z$ . The intervals  $I_n^-$  are defined analogously at the negative energies.

In most of calculations described in the present dissertation  $\Lambda = 2$  was used. All the calculations were performed with the use of the open-access *Flexible DM-NRG* code, de-

veloped at Budapest University of Technology and Economics [48], accordingly adapted to the performed calculations.

## 2.4. Other methods

In the present dissertation also other methods are used whenever suitable. Some of them give some qualitatively correct insight into the problems solved with the numerical renormalization group, and help to understand the characteristic features of numerical results in a simple manner. They also complement the numerical renormalization group, allowing for non-equilibrium calculations in the weak coupling regime. In the following section, the most important ones are briefly described.

### 2.4.1. Master equation

Although the numerical renormalization group is a very strong, non-perturbative tool for studying transport in quantum-dot systems, it does not allow for treating the systems outside the equilibrium, even in the weak coupling regime. For this purpose, the master equation based on the Fermi golden rule is used [6, 49]. In principle, it can be formulated for any  $H_{\text{QDs}}$ . The Hamiltonian of QDs can be written in the diagonal form,

$$H_{\text{QDs}} = \sum_{\alpha} |\alpha\rangle E_{\alpha} \langle\alpha|, \quad (2.45)$$

where  $\alpha$  runs through the eigenstates of  $H_{\text{QDs}}$ . In the case of particle-number-conserving Hamiltonian, states  $|\alpha\rangle$  can possess definite occupation numbers. Only such case is considered in the dissertation.

The time-independent tunneling Hamiltonian  $H_T = \sum_r H_{Tr}$  is treated as a perturbation. The transition rate from the initial state  $|i\rangle$  to the final state  $|f\rangle$  (of the whole system) reads

$$R_{fi} = \frac{2\pi}{\hbar} |\langle f|H_T|i\rangle|^2 \delta(\xi_f - \xi_i), \quad (2.46)$$

where  $\xi_x$  is the unperturbed energy of state  $x$ . This is in fact the Fermi golden rule, which is obtained within time-dependent perturbation theory in the first order in  $\Gamma$ . Thus, the validity of the approach is limited to the weak coupling regime, when  $\Gamma \lesssim T$ . Let  $W_{\alpha\beta}^r$  for  $\alpha \neq \beta$  be the rate, at which the electron tunnels between lead  $r$  and QDs, causing QDs

to change their state from  $\beta$  to  $\alpha$ . Then, for  $\alpha \neq \beta$  and  $\omega_{\alpha\beta} = E_\alpha - E_\beta$ ,

$$W_{\alpha\beta}^r = \frac{1}{\hbar} \sum_{\sigma} \left\{ \Gamma_{r\sigma}(\omega_{\alpha\beta}) \left| \langle \alpha | d_{1\sigma}^\dagger | \beta \rangle \right|^2 f_r(\omega_{\alpha\beta}) + \Gamma_{r\sigma}(-\omega_{\alpha\beta}) \left| \langle \alpha | d_{1\sigma} | \beta \rangle \right|^2 [1 - f_r(-\omega_{\alpha\beta})] \right\}, \quad (2.47)$$

where  $f_r(\omega)$  is the Fermi-Dirac distribution function in the lead  $r$ , and  $\Gamma_{r\sigma}(\omega)$  is to be understood as  $\Gamma_{r\sigma}$  for  $\omega$  in the band of lead  $r$  and as zero for  $\omega$  outside the band. Moreover,  $W_{\alpha\beta}^r$  may be understood as the elements of the matrix  $\mathbf{W}^r$ . It is convenient to define its diagonal by

$$W_{\alpha\alpha}^r = - \sum_{\beta \neq \alpha} W_{\beta\alpha}^r, \quad (2.48)$$

and denote by  $\mathbf{P}$  the vector of probabilities  $P_\alpha$  of respective QDs' states  $|\alpha\rangle$ .  $\mathbf{P}$  is determined by the initial state and the rates encapsulated in  $\mathbf{W} = \sum_r \mathbf{W}^r$ . The master equation can be written in the following matrix form,

$$\frac{\partial}{\partial t} \mathbf{P} = \mathbf{W} \mathbf{P}. \quad (2.49)$$

For determination of a steady state, for which  $\frac{\partial}{\partial t} \mathbf{P} = 0$ , the initial state is irrelevant, and one needs to take into account the constraint of probability normalization,  $\sum_\alpha P_\alpha = 1$ , to guarantee the uniqueness of the solution. Then, the current flowing from the lead  $r$  to QDs can be found from

$$I^r = \sum_{\alpha\beta} e \operatorname{sgn}(n_\beta - n_\alpha) W_{\alpha\beta}^r P_\beta, \quad (2.50)$$

with  $\operatorname{sgn}$  - sign function (equal zero for zero argument) and  $n_\alpha$  - number of electrons on QDs in state  $\alpha$ .

## 2.4.2. Equation of motion for Green's functions

The Hamiltonians which are quadratic forms of the annihilation and creation operators, can be exactly solved with the technique known as the equation of motion (EOM) for Green's functions [50, 51]. This method also allows for calculations of more complicated models, however, in the present dissertation the method is used only in exactly solvable cases or in simple approximations, to present some basic properties of the considered systems. In this section  $\hbar = 1$ .

The retarded Green's function for operators  $A$  and  $B$  is defined in the Heisenberg picture as

$$\langle\langle A|B \rangle\rangle^{\text{ret}}(t, t') = -i\theta(t - t') \langle \{A(t), B(t')\} \rangle, \quad (2.51)$$

where  $\theta$  denotes the Heaviside step function, while  $\langle \dots \rangle$  denotes thermal averaging with a density matrix corresponding to the initial conditions (density matrix does not change in the Heisenberg picture). For time-independent  $H$ , the Green function depends only on the difference of the two times [50, 51],

$$\langle\langle A|B \rangle\rangle^{\text{ret}}(t, t') = \langle\langle A|B \rangle\rangle^{\text{ret}}(t - t'). \quad (2.52)$$

Then, one can define the Fourier-transformed Green's function  $\langle\langle A|B \rangle\rangle^{\text{ret}}(\omega)$  as fulfilling

$$\langle\langle A|B \rangle\rangle^{\text{ret}}(t) = \frac{1}{2\pi} \int e^{-i\omega t} \langle\langle A|B \rangle\rangle^{\text{ret}}(\omega) d\omega. \quad (2.53)$$

Setting in Eq. (2.51)  $t' = 0$  and differentiating over  $t$  one can obtain the "equation of motion" for Green's function, which after the Fourier transform translates to

$$\omega \langle\langle A|B \rangle\rangle^{\text{ret}}(\omega) = \langle\{A, B\}\rangle - \langle\langle [H, A] | B \rangle\rangle^{\text{ret}}(\omega). \quad (2.54)$$

When  $A$  and  $B$  are some annihilation or creation operators, and  $H$  is a quadratic form of such operators, then in the right-hand side a similar Green's function appears. Solution of equation of motion in such a case is reduced to the solution of a set of linear equations. These equations are algebraic in the frequency domain and differential in the time domain. However, if  $H$  is not a quadratic form of annihilation or creation operators, *e.g.*, contains terms representing the Coulomb repulsion, then  $[H, A]$  is not a linear combination of creation or annihilation operators. Thus, the right-hand side of Eq. (2.54) contains the Green's function of a different type (one says : of higher order), and the exact solution is in general not possible.





# Chapter 3

## Basic phenomena in transport through quantum dot systems

Due to spatial restrictions, phenomena in systems of QDs can be different than the corresponding phenomena in the bulk. In particular, their quantum nature may become evident. Moreover, some phenomena are present only in the nanoscale systems. The purpose of the present chapter is to give a brief introduction to the basic phenomena determining transport properties of QD systems, in particular, systems considered in Part II.

### 3.1. Sequential tunneling and the Coulomb blockade

Probably the simplest example of a transport phenomenon in QD systems is tunneling of electrons from one lead to the other via a single QD, weakly coupled to the leads through the tunneling junctions. For a sufficiently weak coupling different tunneling processes can be seen as practically independent from each other. In such a case, an electron can spontaneously tunnel from the leads to QD and vice versa, as long as there exist an unoccupied electron orbital at QD to hop in. At equilibrium the hoppings from/to each of the leads are equally probable and the net current vanishes, even if in QD there is an orbital at the Fermi level. However, the voltage bias introduces asymmetry and the current can flow.

One can consider a more general situation, when the temperature is lower than the charging energy,  $T \ll E_c$ , and resistance of tunnel junctions is much larger than the quantum resistance  $h/(2e^2)$ . This condition does not imply independence of the respective tunneling events. In fact, they can be correlated quite strongly. Nevertheless, electrons are

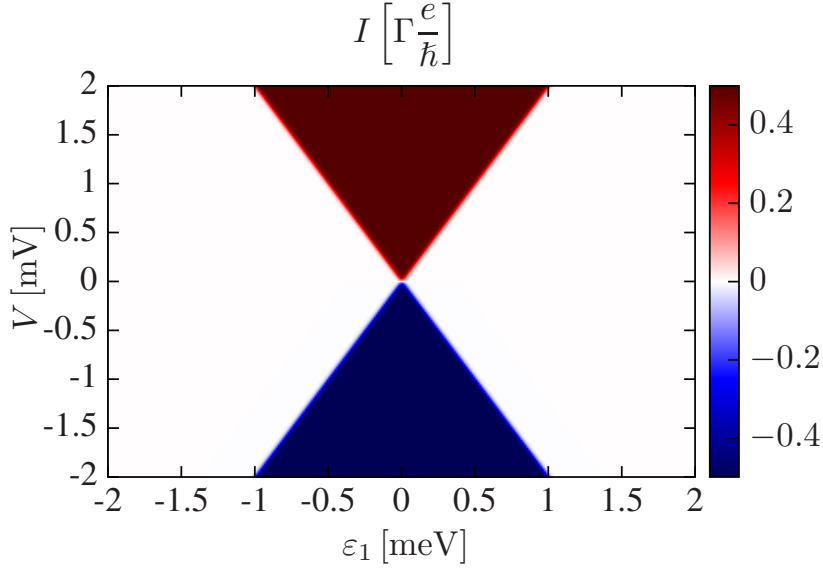


**Figure 3.1:** Current  $I$  flowing through a single-level non-interacting QD for  $T = 0.01\text{meV}$ .

forced to tunnel one after another, *i.e. sequentially*, and not simultaneously. Therefore, the phenomenon is known as sequential tunneling. Here, to give a possibly simple example of a system exhibiting sequential tunneling, the single-level QD is considered.

This system can be treated quantitatively by means of the master equation described in Sec. 2.4.1. The results for a single-level non-interacting QD coupled to two metallic leads with coupling strengths  $\Gamma_L = \Gamma_R = \Gamma/2$  are presented in the following. A symmetric bias voltage  $V$  was assumed, which essentially means that the chemical potentials fulfill  $\mu_L = -\mu_R = eV/2$ . Then, the probability of occupation of QD by an electron of a given spin equals

$$\mathbf{P}_{\text{QD}} = \frac{1}{2} [f_R(\varepsilon_1) + f_L(\varepsilon_1)], \quad (3.1)$$

where  $f_r$  denotes the Fermi-Dirac distribution function for the lead  $r$  and  $\varepsilon_1$  denotes the energy level of QD (the subscript was added for consistency with Sec. 2.1). The obtained electric current equals

$$I = I_\uparrow + I_\downarrow = \frac{-e}{2\hbar} \Gamma [f_L(\varepsilon_1) - f_R(\varepsilon_1)] \quad (3.2)$$

( $I_\sigma$  denotes current in spin-channel  $\sigma$ ). Note, that  $I$  is proportional to  $\Gamma$ , which is the consequence of performing the perturbation theory only to the first order in  $\Gamma$  (second order in hopping matrix element). The differential conductance is at low temperatures given by peaks at  $V = \pm 2\varepsilon_1/e$ , which corresponds to the situation when QD energy level equals the chemical level of one of the leads. The result for the current is presented in the form of a density plot in Fig. 3.1 for the case of  $T = 0.01\text{meV} = 0.116\text{K}$ . For a realistic value of  $\Gamma = 10\mu\text{eV}$  [7], the maximal current equals  $I = 0.5\Gamma e/\hbar = 61.7\text{pA}$ .

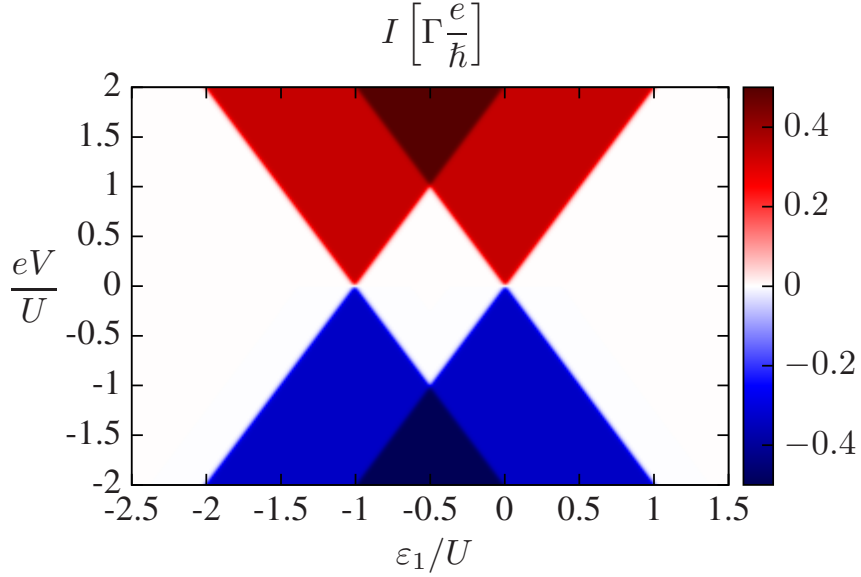


**Figure 3.2:** Current  $I$  flowing through a single-level interacting QD for a realistic  $U = 1\text{meV}$ , and all other parameters the same as in Fig. 3.1.

Up to this point, the non-interacting QD has been considered. However, since QDs are small objects, their charging energies are usually quite large and cannot be neglected. Thus, the model is further extended to the case of finite Coulomb repulsion  $U$  between two electrons occupying QD. The result concerning the current flowing through QD is presented in Fig. 3.2 and discussed below.

In the case of  $\varepsilon_1$  close to the Fermi level and small  $V$ , the plot resembles that in Fig. 3.1, but with the current smaller by a factor of  $2/3$ . This decrease is caused by the fact, that for finite  $U$  the singly and doubly occupied states are no longer degenerate. Consequently, the number of possibilities of tunneling through QD is effectively reduced. On the other hand, the presence of doubly occupied energy level in the transport window allows for low-bias transport for  $\varepsilon_1 \approx -U$ . The two aforementioned regimes of enhanced conductance are separated by the region  $-U \ll \varepsilon_1 \ll 0$  of low conductance and singly occupied QD, sometimes called the Coulomb valley. The fact, that QD does not conduct the current when the applied voltage is smaller than the charging energy (and consequently there is no energy level in the transport window) is called the Coulomb blockade [6, 7]. At this point a note seems justified. Although the current of sequentially tunneling electrons is exponentially suppressed in the Coulomb blockade regime, the next-to-leading-order processes (so-called co-tunneling processes) may give rise to the finite current also in this region [52, 53]. Moreover, the electronic correlations may change the situation even further, leading to the Kondo effect, as explained in Sec. 3.2. Nevertheless, those possibilities are not taken into account in calculations leading to results presented in Fig. 3.2,

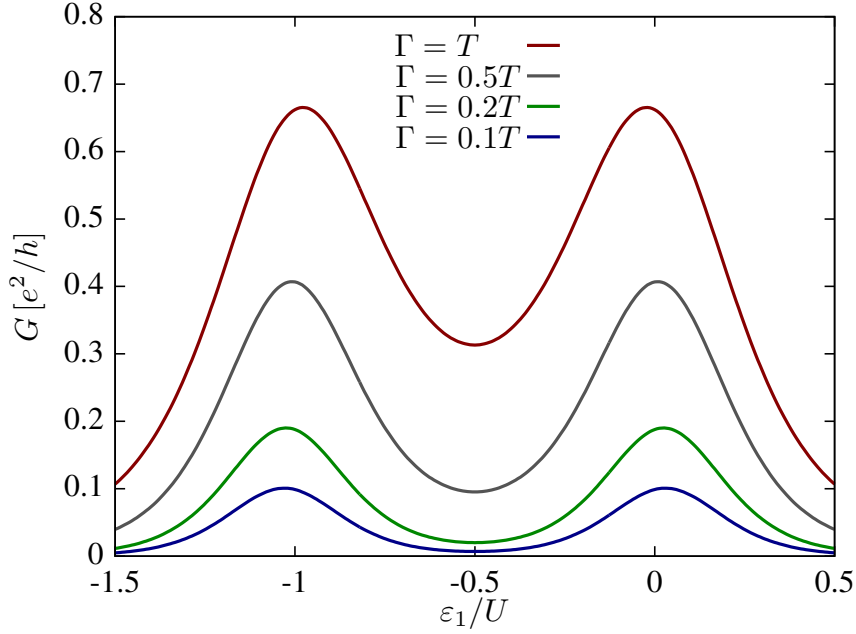


**Figure 3.3:** Linear conductance  $G$  as a function of QD energy level  $\varepsilon_1$  for  $T = U/10$  and different  $\Gamma$ , obtained with the aid of the numerical renormalization group for  $U = 0.1D$ .

which stem from the Fermi golden rule.

The shape of a plot of differential conductance as a function of  $\varepsilon_1$  for  $V = 0$  harmonizes with the name of the region  $-U \ll \varepsilon_1 \ll 0$  (the Coulomb valley). The relevant plot is presented in Fig. 3.3 and shows the peaks of conductance at the resonance positions of  $\varepsilon_1$  and a valley between them. The results in Fig. 3.3 were obtained with the aid of the numerical renormalization group, which allowed for increasing  $\Gamma$  towards the strong coupling regime. As can be easily seen in the figure,  $G$  is not proportional to  $\Gamma$  for  $\Gamma > 0.2T$ , but the results are quantitatively similar also for  $\Gamma = T$ .

Finally, it should be stressed that sequential tunneling as well as the Coulomb blockade phenomena are obviously present also in multilevel QDs. In fact, in experimentally realized QDs the  $\varepsilon_1$  dependence of the linear conductance at low temperatures and for weak coupling exhibits many resonance peaks separated by Coulomb valleys. The corresponding density plots of differential conductance versus bias and gate voltage (the latter is used to tune  $\varepsilon_1$ ), so-called stability diagrams, are known to contain the edges of Coulomb diamonds, similar to that in Fig. 3.2 corresponding to each Coulomb valley.

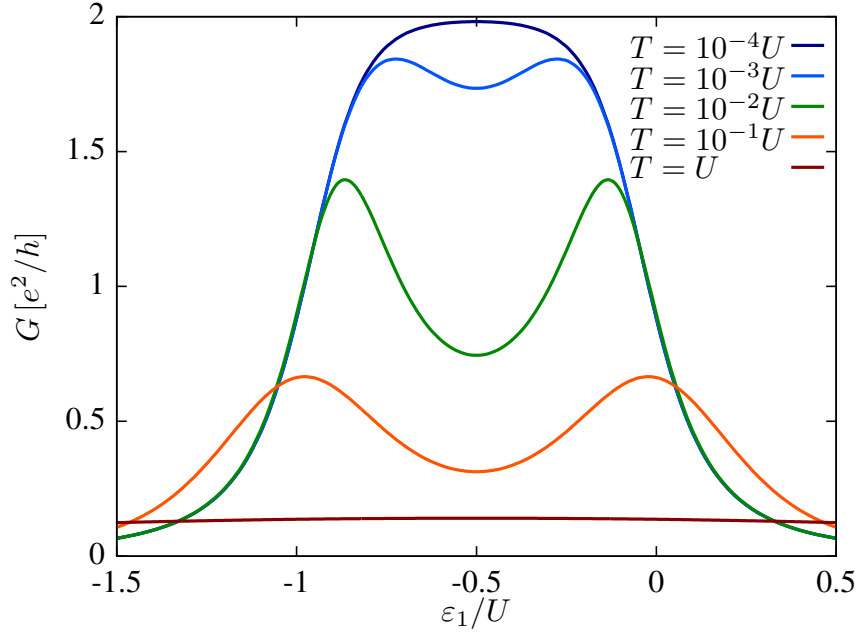


**Figure 3.4:** Linear conductance  $G$  as a function of  $\varepsilon_1$  for different  $T$  and  $\Gamma = U/10$ , obtained from the numerical renormalization group with  $U = 0.1D$ .

### 3.2. The Kondo effect

In Fig. 3.3 presented in the preceding section, one can clearly see an increase of conductance with increasing coupling strength  $\Gamma$ . This agrees with intuition based on understanding of sequential tunneling processes. In turn, the dependence  $G(\varepsilon_1)$  will be analyzed for fixed  $\Gamma$  and a few different temperatures. According to the simple picture described in Sec. 3.1, one can expect two resonant peaks at  $\varepsilon_1 = 0$  and  $\varepsilon_1 = -U$ , separated by a Coulomb blockade regime. Moreover, one can think that the width of the peaks decreases, when  $T$  is lowered. This is indeed the case at high temperatures, as clearly seen in Fig. 3.4. However, the conductance at the particle-hole symmetry point ( $\varepsilon_1 = -U/2$ , *i.e.* in the middle of Coulomb valley) increases with lowering  $T$ . When the system is cooled down sufficiently, it even reaches the limit of  $2e^2/h$ , which means a perfect transmission in both spin channels. This effect is called the mesoscopic Kondo effect and the purpose of the present section is to recall the basic explanation of this effect.

Before explaining the reason for the aforementioned increase of conductance at low temperatures, one more property of this phenomenon will be discussed, on the basis of Fig. 3.5, which presents a plot of the conductance as a function of temperature (the latter on the logarithmic scale) for the case of  $\varepsilon_1 = -U/2$ . As can be seen there, for all  $\Gamma$  the increase of  $G(T)$  has a logarithmic nature. Moreover, the stronger is the coupling strength  $\Gamma$ , the higher is the temperature at which  $G$  starts to increase rapidly. In fact, this

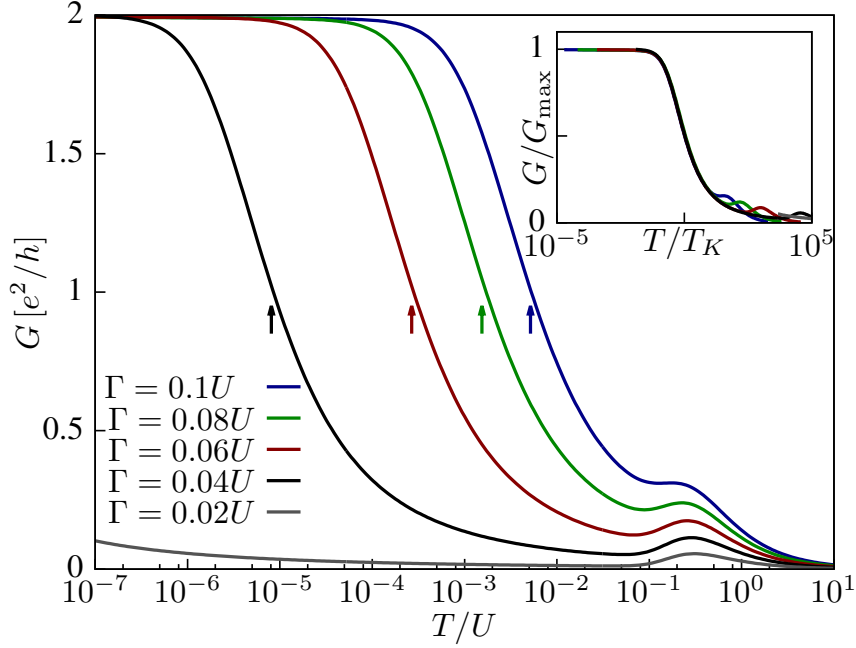


**Figure 3.5:** Linear conductance as a function of temperature for different  $\Gamma$  and  $\varepsilon_1 = -U/2$ , obtained from the numerical renormalization group with  $U = 0.1D$ . Arrows indicate the Kondo temperatures corresponding to each curve (for  $\Gamma = 0.02U$ ,  $T_K \approx 2.1 \cdot 10^{-10}U$  is outside the range of the plot). The inset shows the same curves with  $T$  axis scaled by the corresponding  $T_K$ .

observation can be stated more quantitatively. The temperature at which  $G$  reaches the half of its maximal value,  $G_{\max}/2$ , will be denoted  $T_K$  and called the Kondo temperature. It can be estimated from [54]

$$T_K = \sqrt{\frac{U\Gamma}{2}} \exp\left[\frac{\pi \varepsilon_1(\varepsilon_1 + U)}{2\Gamma U}\right] \quad (3.3)$$

on the basis of scaling theory [55]. The important property of the Kondo effect is that the functions  $G(T)$  are universal in this sense, that for all values of  $\Gamma$  (at temperatures corresponding to the Kondo regime)  $G(T/T_K)/G_{\max}$  is in fact the same function. The increase of the conductance at  $T < T_K$  may be described more precisely with the aid of the asymptotic expansion in powers of  $[\log(T/T_K)]^{-1}$ . The leading term gives [56],

$$G \approx \frac{3\pi^2}{16} G_{\max} \left[ \log\left(\frac{T}{T_K}\right) \right]^{-2}. \quad (3.4)$$

The scaling property of  $G(T)$  resembles the properties of the Kondo effect in the bulk systems, which is described below for comparison. Since the thirties of the last century, the resistance minimum at low temperatures has been observed for different bulk metals [57]. Explanation of this fact was elucidated by Kondo [10]. He pinpointed the fact that the

effect is related to the presence of the magnetic impurities and showed, on the ground of perturbation theory in the coupling of conduction band electrons to the impurity site, that such impurities strongly enhance the scattering of the conduction band electrons. His calculations also predicted a logarithmic increase of the resistance at very low temperatures. However, the result that this increase persists till the smallest temperatures leading to a divergence in resistivity seemed unphysical. Furthermore, more precise perturbative calculation gave even more striking result, namely a divergence of resistivity at finite  $T$ , close to  $T$  corresponding to minimum of resistance [58], which was clearly in contradiction with the experiments. The temperature of divergence is now one of many definitions of  $T_K$  for bulk systems used in the literature. The failure of obtaining the correct temperature dependence of the resistance on the basis of perturbation theory became known as the *Kondo problem*.

The correct theoretical description of the conducting metal with diluted magnetic impurities was given by Wilson on the basis of the numerical renormalization group calculations [38]. While the source of the Kondo problem is the fact that electrons possessing energies of different scales contribute similarly to the perturbative expressions, in NRG the problem is solved scale by scale with the aid of iterative procedure described in Sec. 2.3. Thus, the correct impurity spectral function can be obtained. It occurs to have a peak at the Fermi level with width at half-maximum of the order of  $T_K$ , which is responsible for the increased scattering off the impurity. Not only does NRG correctly predict the universality of resistance versus temperature curve, but also explains it as a consequence of a fixed point structure of the Kondo model [38].

The Kondo effect in the mesoscopic physics has in fact the same physical nature. The main difference is that in the case of QD coupled to the leads, the scattering through QD is in fact the only possibility for an electron to be transmitted from one lead to the other, as opposed to the scattering off the impurity in the bulk metal, which is an obstacle for the transport. As a result, the peak in QD's spectral function at the Fermi level (QD plays a role of an impurity as already discussed in Sec. 2.1) is a source of a maximized conductance through the QD system.

Finally, it is important to stress that the Kondo effect in QD systems is now not only well understood theoretically, but also confirmed experimentally in numerous papers, with the first experiments carried out in 1998 [59, 60]. The new and interesting content of the present dissertation is described in Part II, which treats in particular the systems, where the Kondo effect coexists and interplays with the other electron correlations, such as ferromagnetism or superconductivity.

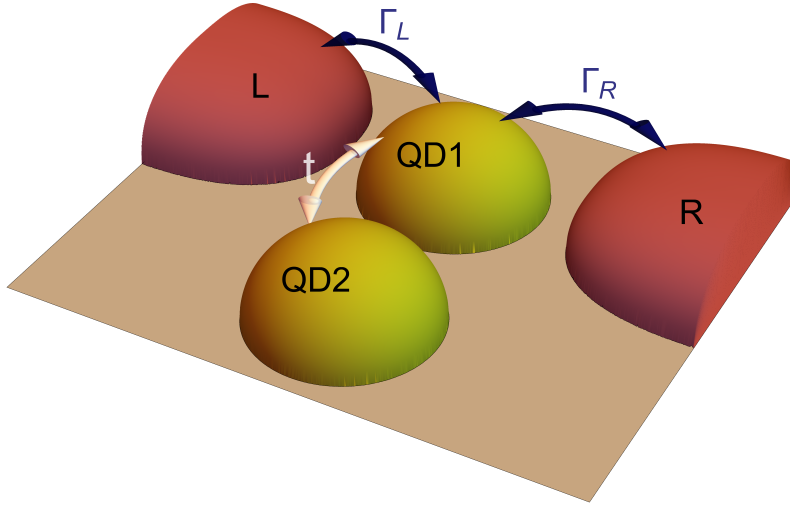


**Figure 3.6:** Illustration of a T-shaped double quantum dot geometry. L and R denote (correspondingly) left and right metallic lead. One of QDs, denoted QD1, is coupled directly to both leads. The second dot, QD2, is not directly coupled to the leads, but only to QD1. The figure comes from article [F].

### 3.3. The two-stage Kondo effect

In the three preceding sections a single QD was used as an example of a QD system. In the present section, the Kondo effect is discussed in the case of a double QD in the T-shaped geometry, shown and explained in Fig. 3.6.

Counter-intuitively, even very small coupling between the two QDs is sufficient for quite a drastic change in the low-temperature behavior of the system. In fact, in the particle-hole symmetric case the zero-temperature conductance of the T-shaped double QD vanishes for any non-zero inter-dot hopping  $t$ . This is illustrated in Fig. 3.7, which presents a plot of conductance as a function of  $T$  for  $\varepsilon_1 = \varepsilon_2 = -U/2$ . The temperature axis is again logarithmic and scaled by  $T_K$  corresponding to  $t = 0$ , *i.e.* completely decoupled QD2. The coupling strength was set to  $\Gamma = U/5$ , with  $U = 0.5D$ . The temperature, at which  $G$  is reduced to the half of its maximal value (while decreasing  $T$ ) will be denoted by  $T^*$ . Similarly to the dependence of  $T_K$  on  $\Gamma$ ,  $T^*$  strongly depends on  $t$ . As explained in the following, this resemblance is not incidental.

The hopping between the two QDs gives rise to the inter-dot exchange coupling. Its strength can be estimated perturbatively to be [61]

$$J_{\text{eff}} = 2t^2 \left( \frac{1}{\varepsilon_1 + U_1 - \varepsilon_2} + \frac{1}{\varepsilon_2 + U_2 - \varepsilon_1} \right). \quad (3.5)$$



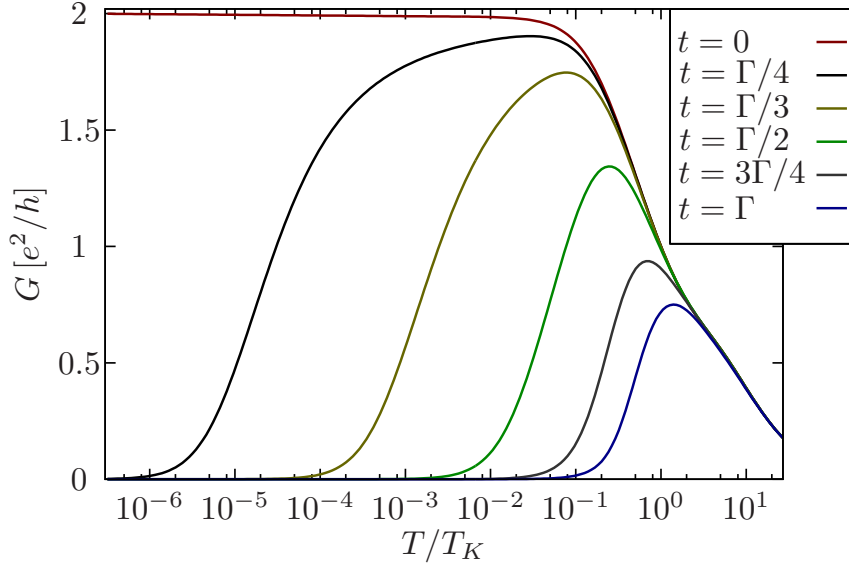


**Figure 3.7:** Conductance  $G$  as a function of  $T$  for different  $t$ ,  $\varepsilon_1 = \varepsilon_2 = -U/2$ , and  $\Gamma = U/5$  obtained from the numerical renormalization group with  $U = 0.5D$ . The figure was adopted from article [F].

In fact, the reason for suppression of the conductance of a T-shaped double QD at low temperatures is again the Kondo effect. For  $T < T_K$ , the role of the impurity is played by QD2, while QD1 and the conduction bands of the leads serve as an effective continuum (note, that the single QD Kondo system has a Fermi-liquid nature, *i.e.*, its energy spectrum can be seen as a quasi-free-particle one). Since QD2 is not directly coupled to the leads, scattering off it is not a source of conductance, but rather an obstacle. Consequently, the resonant scattering caused by the Kondo effect leads to complete suppression of the conductance.  $T^*$  estimated on the basis of this correspondence can be expressed as [62, 63]

$$T^* = aT_K e^{-bT_K/J_{\text{eff}}}, \quad (3.6)$$

where  $a$  and  $b$  are dimensionless numerical constants of the order of unity. Of course, this picture brakes down for large  $t$ , when eigenstates of QD1 and QD2 strongly hybridize, and the transport through a spin singlet formed between the two QDs is blocked.

### 3.4. The Fano effect

In general, the Fano effect is a consequence of an interference between a resonant scattering process and a background process [64]. It can be observed in various nanostructures [65]. In the case of T-shaped double QDs, the considered processes correspond to the transport through double QD single-electron levels. The strongly coupled level is broad-

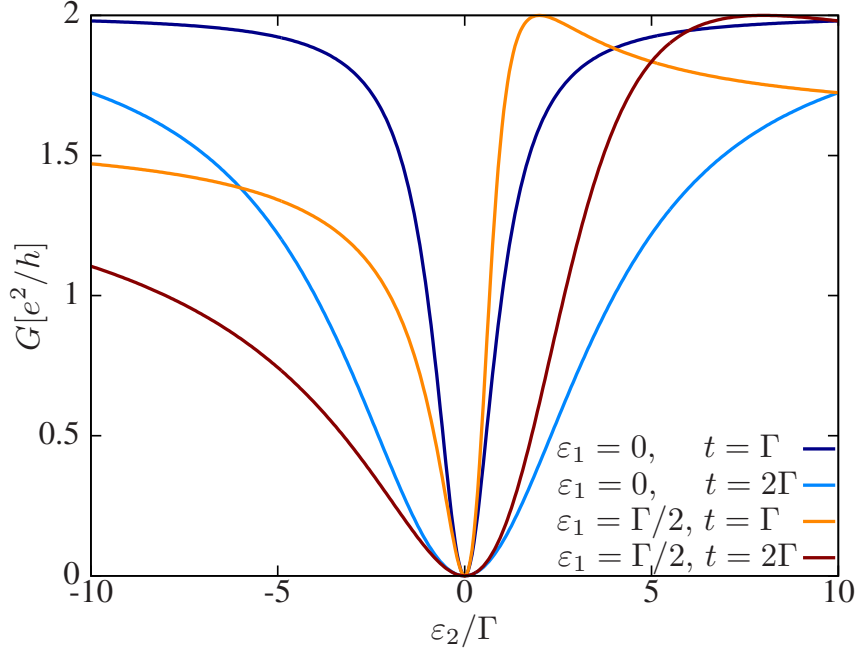


**Figure 3.8:** Conductance versus  $\varepsilon_2$  for  $U_1 = U_2 = 0$  and different  $t$  and  $\varepsilon_1$ . The results were obtained with the aid of equation of motion for Green functions. Figure is based on calculations discussed in article [C].

ened significantly and thus corresponds to the background [66]. The resonance's role is played by the weakly coupled level, whose energy lies within the strongly broadened level. This phenomenon was in fact measured in the T-shaped double QD structure [67] and can be understood within a very simple model.

Actually, with  $U_1 = U_2 = 0$  and for normal metallic leads, the Hamiltonian presented in Sec. 2.1 is quadratic in creation/annihilation operators and as such can be exactly solved with the aid of the equation of motion technique. The spectral function of QD1 is then

$$A_1(\omega) = \frac{2}{\pi} \frac{\Gamma}{[\omega - \varepsilon_1 - t^2/(\omega - \varepsilon_2)]^2 + \Gamma^2}, \quad (3.7)$$

which allows one to write the conductance at  $T = 0$  as

$$G = \frac{2e^2}{h} \frac{\tilde{\varepsilon}_2^2}{\tilde{\varepsilon}_2^2 + (\tilde{\varepsilon}_1 \tilde{\varepsilon}_2 - \tilde{t}^2)^2}, \quad (3.8)$$

where the tilde was used to denote quantities expressed in units of  $\Gamma$ . For  $\tilde{\varepsilon}_1 = 0$ , this becomes the famous Fano formula for the symmetric case, with  $\Gamma \varepsilon_2/t^2$  being the energy variable. This formula is illustrated in Fig. 3.8 for two different  $t$  values. For  $\varepsilon_1 \neq 0$ , the dip in the conductance becomes asymmetric, with maximal conductance at  $\varepsilon_2 = t^2/\varepsilon_1$ ; see Fig. 3.8.

It should be emphasized that this simple model cannot fully explain the results of an experiment such as the ones described in Ref. [67], because in real quantum dots  $U_1$  and

$U_2$  cannot be neglected. For finite  $U_2$  the assumption of  $T = 0$  may also be misleading, because the corresponding  $T^*$  may be really cryogenic [63].

### 3.5. The exchange field

So far, the consequences of (Coulomb) correlations in QDs were discussed. Now, the focus is shifted to the correlations in the leads. In the present section the effects of ferromagnetic leads are considered.

The interaction with lead (or many leads) in general causes the renormalization of the position of energy levels of QDs. As an example, a single QD coupled to a single ferromagnetic lead can be considered. The Hamiltonian is then given by Eq. (2.1) with respective parts described by Eqs. (2.18), (2.17) and (2.2), where only  $i = 1$  is allowed,  $B = 0$  and all the three terms containing sums over  $j$  vanish. The energy shift of QD level can be calculated perturbatively, with  $\Gamma_\sigma$  treated as a small parameter. Let  $|\sigma\rangle^*$  denote the state corresponding to QD occupied by a single electron of spin  $\sigma$  and leads in their ground states, *i.e.* with completely filled Fermi sea and completely empty single-electron states above the Fermi level. The asterisk indicates that this is a state of the whole system, not only of QD. For  $T = 0$ , the leading-order correction to the energy of the state  $|\sigma\rangle^*$  equals

$$\delta E_\sigma = -\frac{\Gamma}{\pi} \left[ (1 - \sigma p) \log \left| \frac{D + (\varepsilon_1 + U)}{\varepsilon_1 + U} \right| + (1 + \sigma p) \log \left| \frac{D - \varepsilon_1}{\varepsilon_1} \right| \right]. \quad (3.9)$$

Clearly, the result diverges for a wide band ( $D \rightarrow \infty$ ) and  $p < 1$ , which is definitely a wrong result. To obtain the correct shift, one would need to use some renormalization techniques. However, the difference between the shifts of the levels corresponding to opposite spins converges in the limit of large  $D$ . In analogy to the magnetic field splitting the spin doublet, the difference  $E_\uparrow - E_\downarrow$  is called the exchange field and reads [68–70]

$$\Delta\varepsilon_{\text{ex}} = \frac{2p\Gamma}{\pi} \log \left| \frac{\varepsilon_1}{\varepsilon_1 + U} \right|. \quad (3.10)$$

In the case of a single QD, the exchange field is in practice equivalent to application of an external magnetic field. Importantly, it can be adjusted by electrical means (by tuning  $\varepsilon_1$ ), which is convenient for application purposes. The splitting of the Kondo peak by the exchange field can be predicted with the numerical renormalization group calculations. This is shown in Fig. 3.9, presenting a density plot of the transmission coefficient as a function of  $\omega$  and  $\varepsilon_1$ . The aforementioned splitting was also observed experimentally and the results obtained with NRG were found to be in a quantitative agreement with experiments [71]. For these reasons, NRG can be considered as a particularly convenient tool for studying transport through QD systems coupled to ferromagnets.

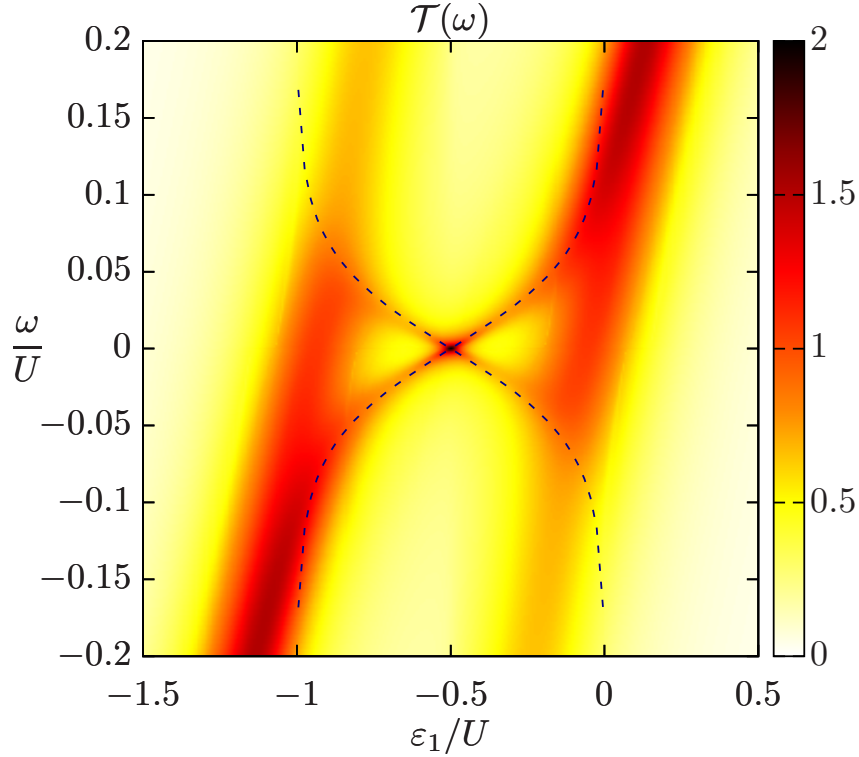


**Figure 3.9:** Transmission coefficient  $\mathcal{T}(\omega)$  of a single QD coupled to ferromagnetic leads of spin polarization  $p = 0.5$  with an effective coupling strength  $\Gamma = U/10$ , as a function of frequency  $\omega$  and QD level  $\varepsilon_1$ , obtained from the numerical renormalization group calculations for  $T = 0$ .

As explained in article [E], the exchange field in the case of multiple QDs is a much more subtle quantity, because the energy levels of individual QDs are well defined only for weak inter-dot couplings. Note also, that in the case of two leads with co-linear magnetizations, the Hamiltonian used in the present section is still valid, with  $\Gamma$  and  $p$  understood as effective quantities. For two leads, the magnetic configuration (parallel or anti-parallel) and the asymmetry of couplings between the two leads and QD become crucial parameters determining the occurring exchange field [72].

### 3.6. Superconducting proximity effect

As explained in the preceding section, the energy levels of QD proximized by the ferromagnet become spin-split, because the spin reversal symmetry, possessed by QD, is broken by the lead. Similarly, QD proximized by a superconductor with large order parameter  $\Delta$  exhibits a tendency for pairing, as explained in Sec. 2.1.4. To illustrate this aspect, the spectrum of such QD coupled to a superconductor is analyzed below.

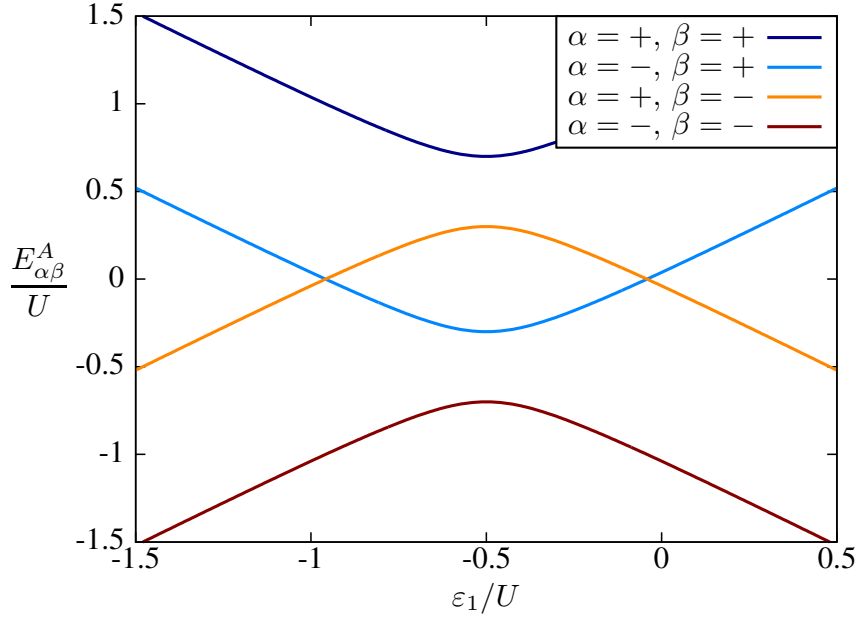


**Figure 3.10:** Energies of Andreev bound states as a function of  $\varepsilon_1$  for  $\Gamma_S = U/5$ .

The effective Hamiltonian  $H_{\text{eff}}$  given by Eq. (2.20) is just a  $4 \times 4$  matrix, which can be divided into two  $2 \times 2$  diagonal blocks. Thus, its eigenvalues can be found analytically and are given by  $\varepsilon_1$  for singly occupied states, whereas

$$E_{\pm} = \varepsilon_1 + \frac{U}{2} \pm \sqrt{\left(\varepsilon_1 + \frac{U}{2}\right)^2 + \Gamma_S^2} \quad (3.11)$$

for combinations of unoccupied and doubly occupied states. This means that the excitation energies between the singlets and the doublet are

$$E_{\alpha\beta}^A = \alpha \frac{U}{2} + \beta \sqrt{\left(\varepsilon_1 + \frac{U}{2}\right)^2 + \Gamma_S^2}, \quad (3.12)$$

where  $\alpha$  and  $\beta$  can be  $+1$  or  $-1$ , depending on the initial and final state. These are called the Andreev bound state energies and are presented in Fig. 3.10 as functions of  $\varepsilon_1$ . They correspond to the sharp peaks in the spectral function of QD coupled to a superconductor, thus, they govern the transport properties of such QD [21].

### 3.7. Andreev current through quantum dot

In a single QD coupled to a superconducting lead, the Kondo correlations in general compete with the pairing potential. When  $\Delta$  is large, the effective Hamiltonian (2.20) is a good approximation and the spectral properties of QD are determined by the Dirac delta functions corresponding to the Andreev bound states energies (3.12). On the other

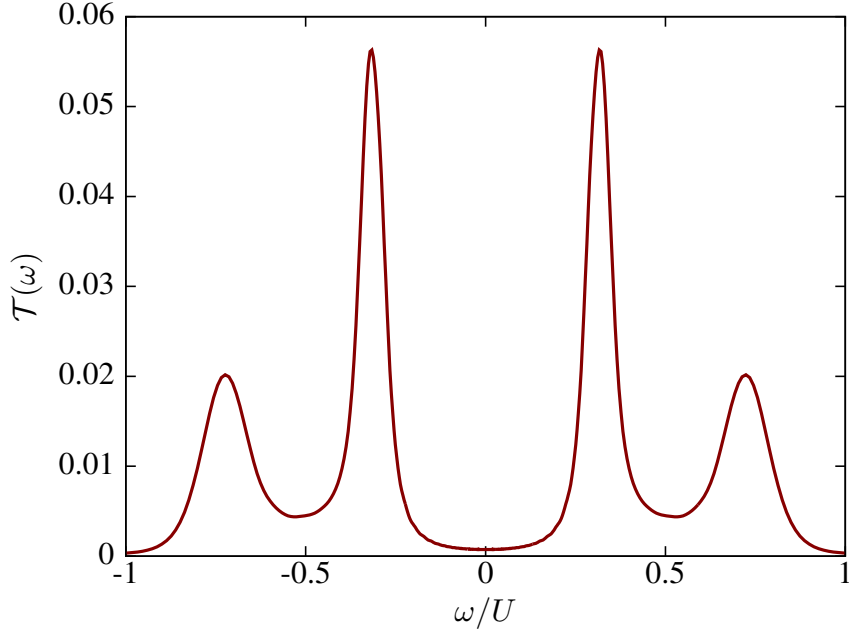


**Figure 3.11:** Andreev transmission coefficient  $\mathcal{T}(\omega)$  for a single QD coupled to one normal (coupling strength  $\Gamma = 0.01U$ ) and one superconducting (coupling strength  $\Gamma_S = 0.2U$ ) lead at the particle-hole symmetry point and  $T = 0$ , calculated with the numerical renormalization group for  $U = 0.1D$ .

hand, the situation changes quite dramatically, when  $\Delta$  is small. Then, the quasi-particle degrees of freedom are relevant and the coupling between them and the QD level may give rise to the Kondo effect, as soon as  $\Delta \lesssim T_K$ . However, if two electrodes are attached to QD, one being superconducting, and the other one metallic, the situation becomes more interesting. Indeed, the sharp in-gap spectral features of QD are broadened by the interaction with normal lead, and the Kondo effect may develop [37]. Moreover, under some circumstances it can even be enhanced by the superconducting pairing [B,73]. Nevertheless, in the weak coupling regime, the Andreev transmission coefficient exhibits peaks at Andreev bound states energies, as shown in Fig. 3.11.

# Chapter 4

## Summary

This PhD thesis has the form of a sequence of published articles [A-H], preceded by the introductory part. It deals with theoretical problems related to the transport properties of a few selected strongly correlated quantum-dot systems. Results obtained for the subsequent systems are described in the following.

The article [A], constituting Chapter 6, presents the results concerning the system containing a single QD coupled to three terminals: two ferromagnetic leads and a superconductor. Its main aim was to determine how the proximity of a superconductor influences the electronic and thermal transport between the ferromagnetic leads.

Transport properties of hybrid QD systems, such as the one considered in article [A], are governed by the interplay of the relevant energy scales. In this case an important role is played by the exchange field generated by the ferromagnets. Another scale is set by the strength of the coupling to the superconducting lead, which enhances pairing of electrons occupying the quantum dot, effectively reducing their Coulomb repulsion. Finally, the last crucial energy scale is given by the Kondo temperature. The superconducting electrode is assumed to possess an energy gap  $\Delta$  much larger than the aforementioned scales. This allows for the use of an effective Hamiltonian (2.20) and reduces the problem to a single-channel one. Within the framework of the numerical renormalization group and the linear response theory the quantities characterizing the transport were calculated. In particular, electrical and heat conductances, as well as the Seebeck and the spin Seebeck coefficients were obtained as functions of temperature, QD energy level, and the strength of the coupling between QD and the superconductor. It was shown that the magnitude of the exchange field in the considered system is significantly changed with respect to a similar system without a superconducting lead and can be expressed in terms of energies

of Andreev bound states. Moreover, in some circumstances, the increase of the coupling to the superconductor leads to an enhancement of the Kondo temperature and can even restore the Kondo effect, otherwise destroyed by a strong exchange field. On the other hand, strongly coupled superconductor destroys the Kondo effect. All these effects are reflected in the electrical and thermal transport properties of the system.

Another vital aspect of hybrid QD systems is the Andreev tunneling through QD embedded in between the ferromagnetic and the superconducting contacts. The results concerning this topic were published in article [B], included in the dissertation as Chapter 7. The main result is that the Andreev transport in the system under consideration is determined by the relations between the relevant energy scales, similarly to the case of the system discussed in article [A]. Indeed, NRG calculations show that the exchange field strongly affects the low-energy properties of the Andreev transmission. In particular, the Kondo resonance is split for strong enough coupling to the ferromagnet. Further consequence of this fact is that the Andreev conductance is a non-monotonic function of the QD energy level. Finally, at very low temperatures the conductance exhibits a peak at the particle-hole symmetry point.

Both aforementioned articles [A, B] undoubtedly prove that in hybrid QD systems the relevant transport characteristics reveal a subtle interplay of the important energy scales and strongly support the thesis formulated in Chapter 1, that correlated quantum-dots exhibit nontrivial transport properties, reflecting many-body nature of such systems. In turn, a second branch of the research described in Part II is discussed, which is focused on the transport properties of a double QD in the T-shaped configuration (further referred to as T-DQD), presented in Fig. 3.6. This seemingly simple system in fact hosts a plethora of interesting physical phenomena, which were described in Chapters 8-13.

The main result of the article [C], included in the dissertation as Chapter 8, is the determination of the circumstances when T-DQD coupled to ferromagnetic leads becomes a source of perfectly spin-polarized current. The phenomenon leading to this interesting property is the Fano effect, which is the origin of an antiresonance in conductance expressed as a function of T-DQD energy levels. The exchange field induced by the magnetism of leads spin-splits these levels, similarly to the magnetic field [74]. Thus, the conductance minima in respective spin channels are also split. Since the exchange field can be adjusted by changing the voltage gating any of the two QDs, the current spin polarization can also be tuned without the need for application of an external magnetic field. The article also explains why the Coulomb interactions in QD *not* coupled directly to the leads (*i.e.* QD2 in Fig. 3.6) are crucial for the effect to occur, while the Coulomb correlations in QD1 are not necessary.



Besides the explanation of the spin-dependent Fano interference, article [C] illustrates the exchange field induced in the side QD with a plot of the corresponding spectral function, which exhibits a Kondo peak split by the exchange field in a way similar to the single QD coupled to magnetic leads (compare Fig. 3.9). Furthermore, the influence of various conditions on the spin-dependent Fano effect was examined. In particular, the effects of finite temperature were analyzed and the role of the Coulomb interaction strength, energy level of a QD coupled to the leads, and the inter-QD hopping was determined.

Chapter 9, constituted by the article [D], is an extension of the work presented in article [C]. It addresses the problem of an external magnetic field acting on the system analogous to considered in Chapter 8. It is based on NRG calculations. Specifically, the role of external magnetic field is determined in particular in the range of its small magnitude, which is the experimentally relevant limit in any system containing ferromagnetic leads. The results presented in article [D] prove that the magnetic field in general does not change the properties of the system qualitatively, although some quantitative differences appear. Indeed, the magnetic field can even sharpen the spin-dependent Fano effect, when it is parallel to the exchange field induced in the side QD. On the other hand, the application of the appropriately tuned opposite magnetic field, *i.e.* antiparallel to the relevant exchange field, may completely suppress the effect.

Further analysis of transport properties of T-DQD coupled to ferromagnetic leads was preceded by a careful study of the exchange field induced in this structure. It was presented in article [E], see Chapter 10. Articles [C] and [D] were focused on the case when the Coulomb interaction in QD coupled to the leads can be neglected. Then, the exchange field induced in QD2 (as depicted in Fig. 3.6) is a well-defined quantity. However, in the presence of Coulomb interactions in QD1, the situation becomes more complex and the exchange field can be defined for all the multiplets of DQD eigenstates. Moreover, although one can naively expect such defined exchange field to be only quantitatively dependent on the inter-QD hopping  $t$ , in fact in some cases, expressed as a function of  $t$ , it exhibits a few sign changes. Furthermore, a precise calculation of the exchange field in all the relevant multiplets allowed for determination the current-voltage characteristics of the system on the basis of the master equation described in Sec. 2.4.1. The manifestation of the existence of the exchange field was predicted. Besides this, results of the paper [E] were helpful for interpreting the results concerning the two-stage Kondo effect, as described in the following.

Article [F], included as Chapter 11, involves the comprehensive analysis of transport properties of T-DQD with ferromagnetic leads in the regime of two-stage Kondo effect, *i.e.* in particular in the case when Coulomb interactions are present in both QDs. The

motivation was to understand the interplay between the exchange field and the Kondo correlations at different temperatures. For this reason, two magnetic configurations were taken into account: the parallel one, when the exchange field is maximal, and the anti-parallel, in which the exchange field vanishes. Not only did this allowed to examine the conductance, but also the tunnel magnetoresistance. The influence of an external magnetic field on the transport properties of the system was also thoroughly analyzed.

The results obtained mainly with the numerical renormalization group technique show that the exchange field can destroy the second stage of the Kondo screening alone, as well as both of them – depending on the leads' spin polarization and a detuning from the particle-hole symmetry point. In the regime of parameters corresponding to the suppression of only the second stage, tunnel magnetoresistance can reach huge values. In other parameter regimes, it can become negative. The article also shows that appropriately strong magnetic field can restore the corresponding screening stage in a way similar to the case of a single QD.

The results presented in Chapter 11 are complementary to those obtained in the preceding chapters. They independently support the hypothesis presented in article [E], concerning the possible role of the exchange field induced in a double QD for the two-stage Kondo screening. Moreover, they also allow for re-interpretation of some of the results of paper [C] as a consequence of the two-stage Kondo effect.

The studies of transport through T-DQD would not have been complete without determination of its caloritronic and spin caloritronic properties. These issues are addressed in Chapter 12 constituted by the article [G], which is devoted to the case of T-DQD coupled to nonmagnetic leads. In particular, the heat conductance and the Seebeck coefficient (called also the thermopower) were calculated within the linear response theory with the aid of NRG. Some of the results were then explained on the basis of simple analytic methods proposed by Mahan and Sofo [75]. Moreover, the thermoelectric figure of merit (related to the thermodynamic efficiency of the device) and the power factor (determining its maximal power and the efficiency under fixed heat flow conditions [35]) were studied. The most important results concern the regime of singly occupied QDs, when the two-stage Kondo effect occurs. The thermopower has a strong maximum at temperatures corresponding to the second stage of the screening. Moreover, the heat conductance in the regime of strong coupling fulfills a modified Wiedemann-Franz law, predicted earlier for the single QD case [76]. The article presents also a systematic analysis of the influence of external magnetic field on the caloritronic properties of the system. In particular, large spin thermopower is reported for appropriately tuned field.

Finally, the research concerning spin caloritronic properties of T-DQDs are closed with the results for the case of magnetic leads, which are presented in article [H] (Chapter 13). The most important conclusion is that for magnetic leads the spin thermopower is enhanced at temperatures corresponding to the second stage of Kondo screening even in the absence of an external magnetic field. Moreover, the effect can be tuned by changing the gate voltage. This is explained in terms of the exchange field generated in QD2 (compare Fig. 3.6) by the continuum formed by QD1 and the leads. Interestingly, the spin-thermoelectric response of the system is found to be highly sensitive to the spin polarization of the leads: in some cases spin polarization of the order of 1% is sufficient for a strong spin Seebeck effect to occur. Additionally, the article proves that the thermal conductance fulfills the modified Wiedemann-Franz law also in the regime of suppression of subsequent stages of Kondo effect by the exchange field, which is also a surprising result. The calculations presented in the paper were performed with the aid of NRG.

To summarize, the research devoted to the analysis of transport properties of T-DQD appeared to give a lot of interesting results, many of which are caused by the two-stage Kondo screening of QDs' local moments. Together with the properties of QD in a hybrid ferromagnet-superconductor heterostructure, they prove that the seemingly simple systems host very rich physics and allow one to state that, as already written in Chapter 1, *complex many-body phenomena taking place in correlated quantum dot systems manifest themselves in a diversity of nontrivial transport properties of these systems.*

Scientific research is a never-ending story and the results and answers obtained within this dissertation gave rise to new questions and uncovered new horizons of knowledge. What properties would a T-shaped double quantum dot have if one proximates it with a superconducting STM tip? What would happen to the multistage Kondo physics in the system with a tripple magnetically frustrated QD in T-shaped configuration with ferromagnetic leads? Those questions seem particularly interesting to the author and are going to shape his future efforts. Their story, however, is only just beginning and will not be described here.



# Chapter 5

## Streszczenie (Summary in polish)

Niniejsza rozprawa doktorska, zatytułowana „*Zależne od spinu własności elektryczne i termoelektryczne układów skorelowanych kropek kwantowych*”, ma formę cyklu ośmiu publikacji [A-H]. Odpowiednie artykuły stanowią kolejne rozdziały (Rozdziały 6-13) w Części II pracy. Są one poprzedzone wprowadzeniem (Część I, Rozdziały 1-5), obejmującym opis motywacji i celów, zarys stosowanej metodologii, opis podstawowych zjawisk zachodzących w rozważanych układach oraz streszczenie otrzymanych wyników, a także niniejsze *Streszczenie* w języku polskim. Dysertacja przedstawia teoretyczną analizę własności transportowych kilku układów silnie skorelowanych kropek kwantowych. Konkluduje ją teza, że *złożone zjawiska wielociałowe zachodzące w rozważanych układach skorelowanych kropek kwantowych objawiają się całą gamą nietrywialnych własności transportowych tych układów*. Wyniki dotyczące poszczególnych analizowanych układów są opisane poniżej.

Praca [A], zatytułowana „*Wpływ bliskości nadprzewodnika na zależną od spinu konduktancję oraz na termositę skorelowanych kropek kwantowych*” i stanowiąca Rozdział 6, przedstawia wyniki dotyczące układu zawierającego pojedynczą kropkę kwantową sprzężoną do trzech zewnętrznych elektrod: dwóch ferromagnetycznych i jednej nadprzewodzącej. Jej głównym celem było określenie wpływu bliskości nadprzewodnika na elektryczny i termiczny transport między elektrodami magnetycznymi.

Własności transportowe hybrydowych układów kropek kwantowych, takich jak ten rozważany w publikacji [A], stanowią wynik oddziaływania między różnymi korelacjami, scharakteryzowanymi przez odpowiadające im skale energii. W omawianym przypadku szczególnie ważną rolę odgrywa pole wymiany indukowane przez ferromagnetyki. Drugą istotną skalę wyznacza sprzężenie kropki kwantowej z elektrodą nadprzewodzącą. Powo-

duje ona parowanie się elektronów w nanostrukturze, efektywnie redukując ich kulombowskie odpychanie. Wreszcie, ostatnią skalą energii odpowiadającą występującym w układzie korelacjom jest temperatura Kondo. O elektrodzie nadprzewodzącej założono, że obecna w jej spektrum przerwa energetyczna  $\Delta$  jest znacznie większa od wszystkich wymienionych wyżej skal energii. Pozwala to na skorzystanie z hamiltonianu efektywnego, w którym stopnie swobody odpowiadające elektronom wewnątrz nadprzewodnika są wyciąkowane, dzięki czemu zagadnienie transportu w rozważanej nanostrukturze sprowadza się do problemu jednokanałowego. Wielkości fizyczne charakteryzujące ten transport zostały obliczone w ramach teorii liniowej odpowiedzi za pomocą procedury numerycznej grupy renormalizacji. W szczególności przewodnictwa: elektryczne i cieplne, a także współczynniki: Seebecka i spinowy Seebecka, zostały określone jako funkcje temperatury, poziomu energetycznego kropki kwantowej oraz sprzężenia między kropką kwantową, a nadprzewodnikiem. Pokazano, że wielkość pola wymiany w rozważanym układzie jest istotnie inna, niż w podobnym układzie bez elektrody nadprzewodzącej; co więcej, może być wyrażona jako funkcja stanów związanych Andriejewa. Ponadto, w pewnych okolicznościach wzrost sprzężenia z nadprzewodnikiem prowadzi do wzrostu temperatury Kondo, a nawet może przywrócić efekt Kondo stłumiony przez pole wymiany. Z drugiej strony, silnie sprzężony z nanostrukturą nadprzewodnik niszczy efekt Kondo. Wszystkie te zjawiska znajdują odbicie w elektrycznych i termoelektrycznych własnościach transportowych układu.

Ważnym aspektem badań hybrydowych układów kropek kwantowych są te dotyczące tunelowania Andriejewa. Analizę tego zjawiska w układzie z kropką kwantową umieszczoną pomiędzy dwiema elektrodami, ferromagnetyczną i nadprzewodzącą, podjęto w pracy [B], zatytułowanej „*Transport Andriejewa w skorelowanych układach typu ferromagnetyk–kropka kwantowa–nadprzewodnik*” i stanowiącej Rozdział 7 niniejszej rozprawy. Najważniejszym z nich jest wykazanie, że transport Andriejewa przez rozważany układ jest określony przez relacje pomiędzy odpowiednimi skalami energii, tak jak to ma miejsce w układzie analizowanym w artykule [A]. Istotnie, rachunki przeprowadzone metodą numerycznej grupy renormalizacji pokazują, że pole wymiany silnie wpływa na niskoenergetyczne własności transportu Andriejewa przez rozważany układ. W szczególności, rezonans Kondo rozszczepia się, gdy sprzężenie z ferromagnetykiem jest wystarczająco silne. Dalszą konsekwencją tego faktu jest niemonotoniczna zależność przewodnictwa Andriejewa od poziomu energetycznego kropki kwantowej. Wreszcie, w bardzo niskich temperaturach przewodnictwo wykazuje pik w punkcie symetrii elektronowodziurowej.

Obydwie opisane wyżej publikacje [A,B] bez wątplenia potwierdzają, że własności trans-

portowe hybrydowych układów kropek kwantowych ujawniają subtelne wzajemne oddziaływanie odpowiednich korelacji. Wyniki te stanowią więc silną przesłankę za tezą rozprawy, przytoczoną wyżej. Pozostałe artykuły stanowiące Część II pracy omawiają drugą poruszaną w niej gałąź badań, skoncentrowaną na własnościach transportowych podwójnych kropek kwantowych w konfiguracji T. Jej cechą szczególną jest to, że tylko jedna z kropek kwantowych, oznaczana dalej QD1 (na podstawie akronimu od angielskiego *quantum dot* – kropka kwantowa), jest bezpośrednio sprzężona z elektrodami, druga natomiast, oznaczana QD2, oddziałuje z nimi wyłącznie za pośrednictwem pierwszej. W tym na pozór prostym układzie występuje w istocie całe mnóstwo interesujących zjawisk fizycznych, omówionych w Rozdziałach 8-13.

Głównym wynikiem artykułu „*Pełna polaryzacja spinowa w podwójnych kropkach kwantowych w konfiguracji T spowodowana zależnym od spinu efektem Fano*” [C], stanowiącego Rozdział 8, jest określenie okoliczności, w których podwójna kropka kwantowa w konfiguracji T sprzężona z ferromagnetycznymi elektrodami staje się źródłem w pełni spinowo-spolaryzowanego prądu. Prowadzącym do tego zjawiskiem jest efekt Fano, powodujący antyrezonans w przewodnictwie wyrażonym jako funkcja poziomów energetycznych podwójnej kropki kwantowej. Pole wymiany wyindukowane przez magnetyzm elektrod rozszczepia spinowo te poziomy. Stąd minima przewodnictwa w poszczególnych kanałach spinowych również ulegają rozszczepieniu. Jako że pole wymiany może być regulowane za pomocą zmian napięcia bramkującego dowolną z kropek kwantowych, polaryzacja spinowa prądu także podlega strojeniu, bez konieczności umieszczenia układu w zewnętrznym polu magnetycznym. Publikacja wyjaśnia również, dlaczego oddziaływanie kulombowskie elektronów w kropce kwantowej QD2, a więc *niesprzężonej* bezpośrednio z elektrodami, decyduje o wystąpieniu zjawiska, podczas gdy odpychanie kulombowskie na kropce kwantowej QD1 nie jest ku temu niezbędne.

Poza wyjaśnieniem spinowo-zależnej interferencji Fano, w publikacji [C] pole wymiany wyindukowane w kropce kwantowej QD2 zilustrowane jest za pomocą wykresu odpowiedniej funkcji spektralnej, w której widać pik Kondo rozszczepiony przez pole wymiany – w sposób podobny do piku Kondo dla pojedynczej kropki kwantowej umieszczonej w polu magnetycznym. Co więcej, zbadany został wpływ różnych warunków na spinowo-zależny efekt Fano. W szczególności, przeanalizowane zostały efekty skończonej temperatury oraz określone role: siły oddziaływań kulombowskich, poziomu energetycznego kropki kwantowej QD1, a także wielkości elementu macierzowego odpowiedzialnego za przeskok między poszczególnymi kropkami kwantowymi.

Rozdział 9, stanowiący przez artykuł [D] zatytułowany „*Wpływ pola magnetycznego na polaryzację spinową podwójnych kropek kwantowych w konfiguracji T sprzężonych z*

*ferromagnetycznymi elektrodami*”, opisuje rozwinięcie badań zaprezentowanych w publikacji [C]. Podjęta w nim analiza kwestii związanych z zewnętrznym polem magnetycznym w analogicznym układzie została oparta na obliczeniach wykonywanych metodą numerycznej grupy renormalizacji. Rola pola magnetycznego jest określona w szczególności dla pola o małych wartościach, które zawsze występuje w fizycznych układach z ferromagnetycznymi elektrodami. Zaprezentowane wyniki dowodzą, że w ogólności pole magnetyczne nie zmienia jakościowo własności układu, aczkolwiek ilościowe różnice są widoczne. Istotnie, pole magnetyczne może prowadzić do zaostrzenia spinowo-zależnego efektu Fano, kiedy jest skierowane zgodnie z polem wymiany wyindukowanym na kropce kwantowej QD2. Z drugiej strony, przyłożenie odpowiednio dostrojonego pola magnetycznego, przeciwnego do odpowiedniego pola wymiany, może skutkować całkowitym wytłumieniem zjawiska.

Dalsza analiza własności transportowych podwójnej kropki kwantowej w konfiguracji T sprzężonej z ferromagnetycznymi elektrodami została poprzedzona uważnym badaniem pola wymiany w tej strukturze. Zostało ono zaprezentowane w artykule [E], zatytułowanym „*Rozszczepienie stanów molekularnych podwójnych kropek kwantowych w konfiguracji T wyindukowane bliskością ferromagnetyków*” i stanowiącym Rozdział 10. Wyniki omawiane w publikacjach [C] i [D] były skupione na przypadku, gdy oddziaływania kulombowskie na kropce kwantowej QD1 mogą być zaniedbane. Wtedy pole wymiany wyindukowane na kropce kwantowej QD2 jest dobrze zdefiniowane. Jednakże w obecności oddziaływań kulombowskich na kropce kwantowej QD1 sytuacja jest bardziej złożona i pole wymiany można zdefiniować dla wszystkich multipletów stanów własnych podwójnej kropki kwantowej. Co więcej, mimo że można by naiwnie przypuszczać, że tak zdefiniowane pole wymiany powinno tylko jakościowo zależeć od elementu macierzowego  $t$  opisującego przeskok elektronu między poszczególnymi kropkami kwantowymi, w niektórych przypadkach okazuje się, że wyrażone jako funkcja  $t$  kilkakrotnie zmienia ono znak. Ponadto precyzyjny rachunek pola wymiany w odpowiednich multipletach pozwolił na określenie charakterystyki prądowo-napięciowej układu na podstawie równania typu master, omówionego w podrozdziale 2.4.1. Istnienie pola wymiany znajduje w niej swoje odbicie. Poza tym, wyniki opisane w artykule [E] były pomocne przy interpretacji rezultatów dotyczących dwustopniowego efektu Kondo, jak opisano niżej.

Publikacja zatytułowana „*Dwustopniowy efekt Kondo w podwójnych kropkach kwantowych w konfiguracji T z ferromagnetycznymi elektrodami*” [F], stanowiąca Rozdział 11, podejmuje wyczerpującą analizę własności transportowych podwójnej kropki kwantowej w konfiguracji T sprzężonej z ferromagnetycznymi elektrodami w reżimie dwustopniowego efektu Kondo, tzn. w szczególności w przypadku gdy oddziaływania kulombowskie



są obecne na obu kropkach kwantowych. Motywacją do jej podjęcia była chęć zrozumienia zależności między polem wymiany i korelacjami prowadzącymi do efektu Kondo w różnych temperaturach. Z tego powodu pod uwagę zostały wzięte dwie konfiguracje magnetyczne. W jednej z nich elektrody były namagnesowane zgodnie – wtedy pole wymiany osiąga maksymalną wartość. W drugiej konfiguracji namagnesowanie elektrod było przeciwne, powodując znikanie pola wymiany. Porównanie wyników w tych dwóch przypadkach pozwoliło zbadać nie tylko przewodnictwo, ale także tunelowy magnetoopór. Wpływ zewnętrznego pola magnetycznego na własności transportowe układu również został dokładnie zbadany.

Wyniki otrzymane przede wszystkim za pomocą procedury numerycznej grupy renormalizacji pokazują, że pole wymiany może stłumić tak wyłącznie drugi stopień ekranowania Kondo, jak i oba – zależnie od stopnia polaryzacji elektrod i odstrojenia od punktu symetrii elektronowo-dziurowej. W zakresie parametrów odpowiadającym stłumieniu tylko drugiego stopnia ekranowania, tunelowy magnetoopór może osiągać olbrzymie wartości. W innych reżimach, może on stać się ujemny. W artykule pokazano także, że odpowiednio silne pole magnetyczne może przywrócić odpowiedni stopień ekranowania, podobnie jak to jest w przypadku pojedynczej kropki kwantowej.

Badania przedstawione w Rozdziale 11 rzucają nowe światło na te opisane w rozdziałach wcześniejszych. Ich wyniki potwierdzają hipotezę postawioną w Rozdziale 10 dotyczącą roli, jaką pole wymiany wyindukowane w podwójnej kropce kwantowej może odgrywać w przypadku dwustopniowego efektu Kondo. Co więcej, pozwalają też na reinterpretację niektórych rezultatów przedstawionych w publikacji [C] jako konsekwencji dwustopniowego efektu Kondo.

Badania dotyczące transportu przez podwójne kropki kwantowe w konfiguracji T nie byłyby pełne bez określenia ich własności termoelektrycznych, w tym spinowych efektów termoelektrycznych. Te problemy zostały podjęte w Rozdziale 12, stanowionym przez artykuł [G] zatytułowany „*Termosiła silnie skorelowanych podwójnych kropek kwantowych w konfiguracji w konfiguracji T*”. Jest on poświęcony strukturze sprzężonej z niemagnetycznymi elektrodami. W szczególności, przewodnictwo cieplne i współczynnik Seebecka (nazywany także termosiałą) zostały obliczone w ramach teorii liniowej odpowiedzi za pomocą metody numerycznej grupy renormalizacji. Niektóre spośród wyników zostały następnie wyjaśnione przy użyciu prostych metod analitycznych. Co więcej, termoelektryczna dobroć układu (związana z jego termodynamiczną wydajnością) oraz związany z nią czynnik mocy (określający jego maksymalną moc oraz wydajność w warunkach ustalonego strumienia cieplnego) zostały zbadane. Najważniejsze wyniki dotyczą reżimu pojedynczo obsadzonych kropek kwantowych, kiedy to zachodzi

dwustopniowy efekt Kondo. Termosiła posiada silne maksimum w temperaturach odpowiadających drugiemu stopniowi ekranowania. Ponadto, przewodnictwo cieplne w reżimie stałego sprężenia spełnia zmodyfikowane prawo Wiedemanna-Franza, przewidziane wcześniej dla pojedynczej kropki kwantowej. Publikacja przedstawia także systematyczną analizę wpływu zewnętrznego pola magnetycznego na termoelektryczne własności układu. W szczególności, zwraca uwagę na znaczną spinową termosiłę dla odpowiednio dostrojonego pola.

Wreszcie, badania spinowych własności termoelektrycznych podwójnych kropek kwantowych w konfiguracji T dopełniają wyniki uzyskane dla przypadku ferromagnetycznych elektrod, zaprezentowane w artykule [H], zatytułowanym „*Silny spinowy efekt Seebecka w podwójnych kropkach kwantowych typu Kondo w konfiguracji T*” i stanowiącym Rozdział 13. Najważniejszym płynącym z nich wnioskiem jest stwierdzenie, że w przypadku magnetycznych elektrod w temperaturach odpowiadających drugiemu stopniowi ekranowania Kondo następuje wzrost spinowej termosiły, nawet pod nieobecność zewnętrznego pola magnetycznego. Co więcej, efekt może być strojony za pomocą zmian napięcia na bramce. Wyniki te są wyjaśnione jako konsekwencja wyindukowania przez kontinuum stworzone przez kropkę kwantową QD1 oraz elektrody pola wymiany na kropce kwantowej QD2. Co ciekawe, spinowa termoelektryczna odpowiedź układu okazuje się bardzo czuła na stopień polaryzacji spinowej elektrod. W niektórych przypadkach nawet polaryzacja rzędu 1% wystarcza, aby pojawił się silny spinowy efekt Seebecka. Ponadto, w publikacji wykazano, że przewodnictwo cieplne rozważanego układu spełnia zmodyfikowane prawo Wiedemanna-Franza także w reżimach, w których poszczególne stopnie efektu Kondo ulegają stłumieniu przez pole wymiany, co można uznać za zaskakujące. Wszystkie rachunki zostały przeprowadzone metodą numerycznej grupy renormalizacji.

Reasumując, badania poświęcone analizie własności transportowych podwójnych kropek kwantowych w konfiguracji T przyniosły wiele interesujących wyników, z których znaczna część dotyczy konsekwencji dwustopniowego ekranowania Kondo momentów magnetycznych poszczególnych kropek kwantowych. Wraz z własnościami kropek kwantowych w hybrydowych heterostrukturach zawierających elektrody zarówno ferromagnetyczne, jak i nadprzewodzące, dowodzą one, że na pozór proste układy może charakteryzować bardzo bogata fizyka i potwierdzają postawioną w dysertacji tezę.

# The bibliography

- [1] G. Binasch, P. Grünberg, F. Saurenbach, W. Zinn, *Enhanced magnetoresistance in layered magnetic structures with antiferromagnetic interlayer exchange*, Phys. Rev. B **39**, 4828 (1989).
- [2] M. N. Baibich, J. M. Broto, A. Fert, F. Nguyen Van Dau, F. Petroff, P. Etienne, G. Creuzet, A. Friederich, J. Chazelas, *Giant magnetoresistance of (001)Fe/(001)Cr magnetic superlattices*, Phys. Rev. Lett. **61**, 2472 (1988).
- [3] [http://www-03.ibm.com/ibm/history/exhibits/storage/storage\\_chrono20b.html](http://www-03.ibm.com/ibm/history/exhibits/storage/storage_chrono20b.html)
- [4] A. Einstein, *Grundlage der allgemeinen Relativitätstheorie*, Annalen der Physik **49**, 769 (1916).
- [5] C. H. Llewellyn Smith, *What's the use of basic science?* (1997). Available at <https://cds.cern.ch/record/388110/files/open-99-011.pdf>.
- [6] H. Grabert, M. H. Devoret (ed.), *Single charge tunneling: Coulomb blockade phenomena in nanostructures*, NATO ASI Series B: Physics **294** (Plenum, New York 1992).
- [7] L.P. Kouwenhoven, G. Schön, and L. Sohn, *Mesoscopic electron transport*, Proceedings of the NATO Advanced Study Institute on Mesoscopic Electron Transport, 1-44, (1997)
- [8] D. Goldhaber-Gordon, J. Göres, M. A. Kastner, H. Shtrikman, D. Mahalu, U. Meirav, *From the Kondo regime to the mixed-valence regime in a single-electron transistor* Phys. Rev. Lett. **81**, 5225 (1998).
- [9] P. W. Anderson, *Localized magnetic states in metals*, Phys. Rev. **124**, 41 (1961).
- [10] J. Kondo, *Resistance minimum in dilute magnetic alloys*, Prog. Theor. Phys. **32**, 37 (1964).

- [11] J.R. Schrieffer, P. A. Wolf, Relation between the Anderson and Kondo Hamiltonians, *Phys. Rev.* **149**, 491 (1966).
- [12] H. R. Krishna-murphy, J. W. Wilkins, K. G. Wilson, *Renormalization-group approach to the Anderson model of dilute magnetic alloys. I. Static properties for the symmetric case*, *Phys. Rev. B* **21**, 1003 (1980).
- [13] H. R. Krishna-murphy, J. W. Wilkins, K. G. Wilson, *Renormalization-group approach to the Anderson model of dilute magnetic alloys. II. Static properties for the asymmetric case*, *Phys. Rev. B* **21**, 1044 (1980).
- [14] M. R. Delbecq, T. Nakajima, T. Otsuka, S. Amaha, J. D. Watson, M. J. Manfra, S. Tarucha, *Full control of quadruple quantum dot circuit charge states in the single electron regime*, *Appl. Phys. Lett.* **104**, 183111 (2014).
- [15] J. Bardeen, L. N. Cooper, J. R. Schrieffer, *Microscopic theory of superconductivity*, *Phys. Rev.* **106**, 162 (1957).
- [16] J. Bardeen, L. N. Cooper, J. R. Schrieffer, *Theory of superconductivity*, *Phys. Rev.* **108**, 1175 (1957).
- [17] N. N. Bogoliubov, *a new method in the theory of superconductivity*, *Sov. Phys. JETP* **34**, 41 (1958).
- [18] L. I. Glazman and M. E. Raikh, *Resonant Kondo transparency of a barrier with quasilocal impurity states*, *J. Exp. Theor. Phys. Lett.* **47**, 452 (1988); *Pis'ma Zh. Exp. Teor. Fiz.* **47**, 378 (1988).
- [19] A. F. Andreev, *The thermal conductivity of the intermediate state in superconductors*, *J. Exptl. Theoret. Phys.* **46**, 1823 (1964) [*Sov. Phys. JETP* **19**, 1228 (1964)].
- [20] A. V. Rozhkov, D. P. Arovas, *Interacting-impurity Josephson junction: Variational wave functions and slave-boson mean-field theory*, *Phys. Rev. B* **62**, 6687 (2000).
- [21] M. R. Buitelaar, W. Belzig, T. Nussbaumer, B. Babić, C. Bruder, C. Schönenberger, *Multiple Andreev reflections in a carbon nanotube quantum dot*, *Phys. Rev. Lett.* **91**, 057005 (2003).
- [22] L. Yu, *Bound state in superconductors with paramagnetic impurity*, *Acta Phys. Sin.* **21**, 75 (1965).
- [23] H. Shiba, *Classical spins in superconductors*, *Prog. Theor. Phys.* **40**, 435 (1968).

- [24] A. I. Rusinov, *Superconductivity near a paramagnetic impurity*, JETP Lett. 9, 85 (1969); [ZhETF Pis. Red. **9**, 146 (1969)].
- [25] A. Yazdani, B. A. Jones, C. P. Lutz, M. F. Crommie, and D. M. Eigler, *Probing the local effects of magnetic impurities on superconductivity*, Science **275**, 1767 (1997).
- [26] K. J. Franke, G. Schulze, and J. I. Pascual, *Competition of superconducting phenomena and Kondo screening at the nanoscale*, Science **332**, 940 (2011).
- [27] A. Jellinggaard, K. Grove-Rasmussen, M. H. Madsen, J. Nygård, *Tuning Yu-Shiba-Rusinov states in a quantum dot*, Phys. Rev. B **94**, 064520 (2016).
- [28] R. S. Deacon, Y. Tanaka, A. Oiwa, R. Sakano, K. Yoshida, K. Shibata, K. Hirakawa, S. Tarucha, *Tunneling spectroscopy of Andreev energy levels in a quantum dot coupled to a superconductor*, Phys. Rev. Lett. **104**, 076805 (2010).
- [29] B.-K. Kim, Y.-H. Ahn, J.-J. Kim, M.-S. Choi, M.-H. Bae, K. Kang, J. S. Lim, R. López, and N. Kim, *Transport measurement of Andreev bound states in a Kondo-correlated quantum dot*, Phys. Rev. Lett. **110**, 076803 (2013).
- [30] J.-D. Pillet, P. Joyez, R. Žitko, and M. F. Goffman, *Tunneling spectroscopy of a single quantum dot coupled to a superconductor: From Kondo ridge to Andreev bound states*, Phys. Rev. B **88**, 045101 (2013).
- [31] J. Schindele, A. Baumgartner, R. Maurand, M. Weiss, and C. Schönenberger, *Non-local spectroscopy of Andreev bound states*, Phys. Rev. B **89**, 045422 (2014).
- [32] R. D. Barnard, *Thermoelectricity in metals and alloys*, (Taylor & Francis, London, 1972).
- [33] R. Kubo, *Statistical Mechanical Theory of Irreversible Processes I*, J. Phys. Soc. Jap. **12**, 570 (1957).
- [34] M. Julliere, *Tunneling between ferromagnetic films*, Phys. Lett. A **54**, 225 (1975).
- [35] D. Narducci, *Do we really need high thermoelectric figures of merit? A critical appraisal to the power conversion efficiency of thermoelectric materials*, App. Phys. Lett. **99**, 102104 (2011).
- [36] Y. Meir, N. S. Wingreen, *Landauer formula for the current through an interacting electron region*, Phys. Rev. Lett. **68**, 2512 (1992).

- [37] T. Domański, A. Donabidowicz, K. I. Wysokiński, *Meservey-Tedrow-Fulde effect in a quantum dot embedded between metallic and superconducting electrodes*, Phys. Rev. B **78**, 144515 (2008).
- [38] K. G. Wilson, *The renormalization group: Critical phenomena and the Kondo problem*, Rev. Mod. Phys. **47**, 773 (1975).
- [39] K. G. Wilson, *Model Hamiltonians for local quantum field theory*, Phys. Rev. **140**, B445 (1965).
- [40] K. P. Wójcik, *Application of a numerical renormalization group procedure to an elementary anharmonic oscillator*, Acta Phys. Pol. B **44**, 69 (2013).
- [41] F. B. Anders, A. Schiller, *Real-time dynamics in quantum-impurity systems: A time-dependent numerical renormalization-group approach*, Phys. Rev. Lett. **95**, 196801 (2005).
- [42] F. B. Anders, A. Schiller, *Spin precession and real-time dynamics in the Kondo model: Time-dependent numerical renormalization-group study*, Phys. Rev. B **74**, 245113 (2006).
- [43] A. Weichselbaum, J. von Delft, *Sum-rule conserving spectral functions from the numerical renormalization group*, Phys. Rev. Lett. **99**, 076402 (2007).
- [44] V. L. Campo Jr., L. N. Oliveira, *Alternative discretization in the numerical renormalization-group method*, Phys. Rev. B **72**, 104432 (2005).
- [45] R. Žitko, T. Pruschke, *Energy resolution and discretization artifacts in the numerical renormalization group*, Phys. Rev. B **79**, 085106 (2009).
- [46] R. Žitko, *Adaptive logarithmic discretization for numerical renormalization group methods*, Comput. Phys. Comm. **180**, 1271 (2009).
- [47] W. C. Oliveira, L. N. Oliveira, *Generalized numerical renormalization-group method to calculate the thermodynamical properties of impurities in metals*, Phys. Rev. B **49**, 11986 (1994).
- [48] See O. Legeza, C. P. Moca, A. I. Tóth, I. Weymann, G. Zaránd, arXiv:0809.3143 for manual (unpublished).  
The code is available at <http://www.phy.bme.hu/~dmnrg/>.
- [49] I. Weymann, J. Barnaś, S. Krompiewski, *Theory of shot noise in single-walled metallic carbon nanotubes weakly coupled to nonmagnetic and ferromagnetic leads*, Phys. Rev. B **76**, 155408 (2007).

- [50] G. D. Mahan, *Many-particle physics*, (Kulwer Academic, New York, 2000).
- [51] A. L. Fetter, L. D. Walecka, *Quantum theory of many-particle systems*, (Dover Publications, New York, 2003).
- [52] D. V. Avarin, A. A. Odintsov, *Macroscopic quantum tunneling of the electric charge in small tunnel junctions*, Phys. Lett. A **140**, 251 (1989).
- [53] D. V. Avarin, Yu. V. Nazarov, *Virtual electron diffusion during quantum tunneling of the electric charge*, Phys. Rev. Lett. **65** 2446, (1990).
- [54] F. D. M. Haldane, *Scaling theory of the asymmetric Anderson model* Phys. Rev. Lett. **40**, 416 (1978).
- [55] P. W. Anderson, *A poor man's derivation of scaling laws for the Kondo problem*, J. Phys. C **3**, 2436 (1970).
- [56] M. Pustilnik, L. Glazman, *Kondo effect in quantum dots*, J. Phys.: Condens. Matt. **16**, R513 (2004).
- [57] W. J. de Haas, J. H. de Boer and G. J. van den Berg, *The electrical resistance of gold, copper and lead at low temperatures*, Physica **1**, 1115 (1934).
- [58] A. A. Abrikosov, *Electron scattering on magnetic impurities in metals and anomalous resistivity effects*, Physics **2**, 5 (1965).
- [59] D. Goldhaber-Gordon, H. Shtrikman, D. Mahalu, D. Abusch-Magder, U. Meirav, M. A. Kastner, *Kondo effect in a single-electron transistor*, Nature (London) **391**, 156 (1998).
- [60] S. Cronenwett, T. H. Oosterkamp, L. P. Kouwenhoven, *A tunable Kondo effect in quantum dots*, Science **281**, 540 (1998).
- [61] Y. Tanaka, N. Kawakami, A. Oguri, *Crossover between two different Kondo couplings in side-coupled double quantum dots*, Phys. Rev. B **85**, 155314 (2012).
- [62] P. S. Cornaglia and D. R. Grempel, *Strongly correlated regimes in a double quantum dot device*, Phys. Rev. B **71**, 075305 (2005).
- [63] R. Žitko, *Fano-Kondo effect in side-coupled double quantum dots at finite temperatures and the importance of two-stage Kondo screening*, Phys. Rev. B **81**, 115316 (2010).

- [64] U. Fano, *Effects of configuration interaction on intensities and phase shifts*, Phys. Rev. **124**, 1866 (1961).
- [65] A. E. Miroschnichenko, S. Flach, Y. S. Kivshar, *Fano resonances in nanoscale structures*, Rev. Mod. Phys. **82**, 2257 (2010).
- [66] P. Trocha, J. Barnaś, *Quantum interference and Coulomb correlation effects in spin-polarized transport through two coupled quantum dots*, Phys. Rev. B **76**, 165432 (2007).
- [67] S. Sasaki, H. Tamura, T. Akazaki, and T. Fujisawa, *Fano-Kondo interplay in a side-coupled double quantum dot*, Phys. Rev. Lett. **103**, 266806 (2009).
- [68] A. N. Pasupathy, R. C. Bialczak, J. Martinek, J. E. Grose, L. A. K. Donev, P. L. McEuen, D. C. Ralph, *The Kondo effect in the presence of ferromagnetism*, Science **306**, 86 (2004).
- [69] J. Martinek, Y. Utsumi, H. Imamura, J. Barnaś, S. Maekawa, J. König, and G. Schön, *Kondo effect in quantum dots coupled to ferromagnetic leads*, Phys. Rev. Lett. **91**, 127203 (2003).
- [70] J. Martinek, M. Sindel, L. Borda, J. Barnaś, J. König, G. Schön, J. von Delft, *Kondo effect in the presence of itinerant-electron ferromagnetism studied with the numerical renormalization group method*, Phys. Rev. Lett. **91**, 247202 (2003).
- [71] M. Gaass, A. K. Hüttel, K. Kang, I. Weymann, J. von Delft, Ch. Strunk, *Universality of the Kondo effect in quantum dots with ferromagnetic leads*, Phys. Rev. Lett. **107**, 176808 (2011).
- [72] K. P. Wójcik, I. Weymann, J. Barnaś, *Asymmetry-induced effects in Kondo quantum dots coupled to ferromagnetic leads*, J. Phys: Condens. Matter **25**, 075301 (2013).
- [73] T. Domański, I. Weymann, M. Barańska, G. Górski, *Constructive influence of the induced electron pairing on the Kondo state*, Sci. Rep. **6**, 23336 (2016).
- [74] L. G. G. V. Dias da Silva, E. Vernek, K. Ingersent, N. Sandler, S. E. Ulloa, *Spin-polarized conductance in double quantum dots: Interplay of Kondo, Zeeman, and interference effects*, Phys. Rev. B **87**, 205313 (2013).
- [75] G. D. Mahan and J. O. Sofo, *The best thermoelectric*, Proc. Natl. Acad. Sci. USA **93**, 7436 (1996).
- [76] T. A. Costi, V. Zlatić, *Thermoelectric transport through strongly correlated quantum dots*, Phys. Rev. B **81**, 235127 (2010).



## **Part II**

### **Articles constituting the dissertation**



**Proximity effect on spin-dependent conductance and thermopower of correlated quantum dots**

Krzysztof P. Wójcik\* and Ireneusz Weymann†

*Faculty of Physics, Adam Mickiewicz University, ulica Umultowska 85, 61-614 Poznań, Poland*

(Received 13 February 2014; published 9 April 2014)

We study the electric and thermoelectric transport properties of correlated quantum dots coupled to two ferromagnetic leads and one superconducting electrode. Transport through such hybrid devices depends on the interplay of ferromagnetic-contact-induced exchange field, superconducting proximity effect, and correlations leading to the Kondo effect. We consider the limit of large superconducting gap. The system can be then modeled by an effective Hamiltonian with a particle-nonconserving term describing the creation and annihilation of Cooper pairs. By means of the full density-matrix numerical renormalization group method, we analyze the behavior of electrical and thermal conductances, as well as the Seebeck coefficient as a function of temperature, dot level position, and strength of the coupling to the superconductor. We show that the exchange field may be considerably affected by the superconducting proximity effect and is generally a function of Andreev bound-state energies. Increasing the coupling to the superconductor may raise the Kondo temperature and partially restore the exchange-field-split Kondo resonance. The competition between ferromagnetic and superconducting proximity effects is reflected in the corresponding temperature and dot level dependence of both the linear conductance and the (spin) thermopower.

DOI: [10.1103/PhysRevB.89.165303](https://doi.org/10.1103/PhysRevB.89.165303)

PACS number(s): 72.25.-b, 72.15.Qm, 73.50.Lw, 74.45.+c

**I. INTRODUCTION**

Systems containing quantum dots (QDs) or molecules coupled to different types of electrodes have been attracting nondecreasing attention for a few decades [1–4]. As one of the most interesting phenomena in such systems the Kondo effect can be considered [5], in which the interaction with conduction electrons gives rise to many-body screening of the localized spin [6]. This results in an additional resonance at the Fermi level in the local density of states and, consequently, to an enhanced conductance through the system for temperatures lower than the Kondo temperature  $T_K$  [7,8].

When the electron reservoirs, to which the dot is coupled, exhibit some correlations, the occurrence of the Kondo effect is conditioned by the ratio of  $T_K$  to the respective characteristic energy scale of correlated leads. In particular, in the case of superconducting electrodes, through multiple Andreev reflections at the QD-superconductor interface, a Cooper pair carrying two electron charges can be transferred through the dot [9–12]. In the Kondo regime this may lead to the conductance enhanced above the unitary limit  $2e^2/h$ , provided  $T_K$  is larger than the superconducting gap  $\Delta$  [13]. If, however,  $\Delta > T_K$ , the Kondo effect becomes suppressed and the conductance displays only small side resonances at energies corresponding to the energy gap [14]. On the other hand, in the case of ferromagnetic leads, transport properties in the Kondo regime strongly depend on the relative orientation of the magnetizations of electrodes; the conductance usually drops when the magnetic configuration switches from antiparallel to parallel [15,16]. This is related with an exchange field  $\Delta\epsilon_{\text{exch}}$  that emerges in the parallel configuration and acts in a similar way as an external magnetic field, splitting the dot level and thus suppressing the linear conductance [15,17–19]. It is thus the magnitude of the ferromagnetic-contact-induced exchange

field that determines the emergence of the Kondo resonance in such systems [20–22].

For QDs coupled to both ferromagnetic and superconducting leads, transport properties are conditioned by a sensitive interplay of the exchange field, correlations leading to the Kondo effect, and the superconductivity. Although transport through such hybrid devices in the Kondo regime has been recently experimentally measured [23], theoretically this problem is still rather unexplored, although some considerations exist [24–33]. These considerations, however, involved mainly the case of rather weak tunnel couplings between the dot and external leads, where the Kondo effect is not fully present and the effects due to the exchange field are not systematically included.

The goal of the present paper is therefore to provide a systematic and reliable analysis of transport properties of QDs with superconducting and ferromagnetic leads in the Kondo regime. To achieve this goal, we employ the full density-matrix numerical renormalization group (fDM-NRG) method [34–37], which allows for calculating various linear-response transport coefficients in an accurate way. In particular, we focus on the role of Andreev reflection in transport through a QD coupled to the left and right ferromagnetic leads in a proximity with the third superconducting lead. We show that the exchange field due to ferromagnetic leads becomes modified by the coupling to the superconductor and is determined by the Andreev bound-state energies. This fact is correspondingly reflected in the dependence of the dot's spectral function and the linear conductance on the dot level position and temperature. Moreover, we demonstrate that the effects due to the proximity with the superconductor can be also resolved in thermoelectric transport properties. Thermoelectricity in confined nanostructures, such as QDs or molecules, has recently attracted a lot of attention due to relatively large values of the figure of merit [38], which makes such nanoscale objects interesting for possible future applications [39]. Besides applicatory aspects, it turns out that measuring temperature dependence of the thermopower

\*kpwojcik@amu.edu.pl

†weymann@amu.edu.pl

may provide additional information about (Kondo) correlations in the system [40]. Recently, the Seebeck and spin Seebeck coefficients in Kondo-correlated QDs were studied for nonmagnetic and ferromagnetic leads [40–43]. Here we extend these studies to hybrid QDs with superconducting and ferromagnetic electrodes. To determine the thermopower in these hybrid devices, we assume that there is a temperature gradient between the ferromagnetic leads and analyze how the proximity effect influences the heat conductance and (spin) thermopower of the considered system in the Kondo regime.

The paper is organized as follows. In Sec. II we present the theoretical framework for our calculations. The model, relevant transport coefficients and method used in calculations are described therein. In Sec. III the numerical results on the dot's spectral function are presented and the analytical formula for the exchange field is derived. Section IV is devoted to the discussion of the linear conductance and tunnel magnetoresistance of the system, while in Sec. V we analyze the thermoelectric transport properties for different coupling strengths to the superconductor. Finally, the concluding remarks are given in Sec. VI.

## II. THEORETICAL FRAMEWORK

### A. Model

We consider a single-level QD coupled to two ferromagnetic leads whose magnetizations can form either parallel (P) or antiparallel (AP) magnetic configuration; see Fig. 1. There is a temperature gradient  $\delta T$  applied between the ferromagnetic leads and the dot is additionally coupled to a superconducting lead. The Hamiltonian of the system is given by

$$H = H_{\text{QD}} + H_{\text{F}} + H_{\text{S}} + H_{\text{TF}} + H_{\text{TS}}, \quad (1)$$

where  $H_{\text{QD}} = \sum_{\sigma} \varepsilon d_{\sigma}^{\dagger} d_{\sigma} + U d_{\uparrow}^{\dagger} d_{\uparrow} d_{\downarrow}^{\dagger} d_{\downarrow}$  describes the QD, with  $d_{\sigma}^{\dagger}$  being the creation operator of an electron with spin  $\sigma$  and energy  $\varepsilon$  in the dot and  $U$  denoting the Coulomb correlations. The ferromagnetic leads are modeled within the noninteracting quasiparticle approximation,

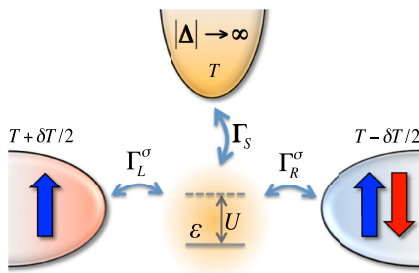


FIG. 1. (Color online) Schematic of the considered system. Quantum dot, with dot level energy  $\varepsilon$  and Coulomb correlation  $U$ , is connected to two ferromagnetic leads and one superconducting lead.  $\Gamma_L^{\sigma}$  ( $\Gamma_R^{\sigma}$ ) describes the spin-dependent coupling between the dot and the left (right) ferromagnetic lead and  $\Gamma_S$  is the coupling to the superconductor. The magnetizations of ferromagnets can form either parallel or antiparallel magnetic configuration, as indicated. There is a temperature gradient  $\delta T$  applied between the two ferromagnetic leads.

$H_{\text{F}} = \sum_{\alpha k \sigma} \varepsilon_{\alpha k \sigma} c_{\alpha k \sigma}^{\dagger} c_{\alpha k \sigma}$ , where  $\alpha = L$  ( $\alpha = R$ ) for the left (right) lead and  $c_{\alpha k \sigma}^{\dagger}$  creates an electron of spin  $\sigma$  and momentum  $\mathbf{k}$  in lead  $\alpha$  with the corresponding energy  $\varepsilon_{\alpha k \sigma}$ . The  $s$ -wave superconductor is described by  $H_{\text{S}} = \sum_{\mathbf{k} \sigma} \xi_{\mathbf{k} \sigma} a_{\mathbf{k} \sigma}^{\dagger} a_{\mathbf{k} \sigma} - \Delta \sum_{\mathbf{k}} (a_{\mathbf{k} \uparrow}^{\dagger} a_{-\mathbf{k} \downarrow}^{\dagger} + a_{-\mathbf{k} \downarrow} a_{\mathbf{k} \uparrow})$ , where  $\xi_{\mathbf{k} \sigma}$  denotes the relevant single-particle energy,  $a_{\mathbf{k} \sigma}^{\dagger}$  is the corresponding creation operator, and  $\Delta$  is the superconducting order parameter, which is assumed to be real and positive.

Finally, the last two terms of the Hamiltonian (1) describe tunneling processes between the dot and ferromagnetic and superconducting leads. They are respectively given by

$$H_{\text{TF}} = \sum_{\alpha=L,R} \sum_{\mathbf{k} \sigma} V_{\alpha k \sigma} (d_{\sigma}^{\dagger} c_{\alpha k \sigma} + c_{\alpha k \sigma}^{\dagger} d_{\sigma}), \quad (2)$$

$$H_{\text{TS}} = \sum_{\mathbf{k} \sigma} V_{S k \sigma} (d_{\sigma}^{\dagger} a_{\mathbf{k} \sigma} + a_{\mathbf{k} \sigma}^{\dagger} d_{\sigma}), \quad (3)$$

where  $V_{\alpha k \sigma}$  denotes the tunnel matrix elements between the dot and ferromagnetic leads, while  $V_{S k \sigma}$  is the tunnel matrix element between superconducting electrode and the dot. The strength of the coupling to ferromagnetic lead  $\alpha$  for spin  $\sigma$  is given by  $\Gamma_{\alpha}^{\sigma} = (1 + \sigma p_{\alpha}) \Gamma$ , where  $p_{\alpha}$  is the spin polarization of ferromagnetic lead  $\alpha$ ,  $p_{\alpha} = (\Gamma_{\alpha}^{\uparrow} - \Gamma_{\alpha}^{\downarrow}) / (\Gamma_{\alpha}^{\uparrow} + \Gamma_{\alpha}^{\downarrow})$ , and  $\Gamma = \Gamma_L + \Gamma_R$ , with  $\Gamma_{\alpha} = (\Gamma_{\alpha}^{\uparrow} + \Gamma_{\alpha}^{\downarrow}) / 2$  and  $\Gamma_{\alpha}^{\sigma} = \pi \rho_{\alpha}^{\sigma} V_{\alpha \sigma}^2$ . Here  $\rho_{\alpha}^{\sigma}$  is the spin-dependent density of states of lead  $\alpha$  and we assumed momentum independent matrix elements  $V_{\alpha k \sigma} \equiv V_{\alpha \sigma}$ . In the following we also assume that the system is symmetric,  $p_L = p_R \equiv p$  and  $\Gamma_L = \Gamma_R \equiv \Gamma/2$ . On the other hand, the coupling between the dot and the superconductor is given by  $\Gamma_S = \pi \rho_S V_S^2$ , where  $\rho_S$  is the density of states of the superconductor in the normal state and we assumed momentum and spin-independent tunnel matrix elements  $V_{S k \sigma} \equiv V_S$ .

In this paper we focus on the linear-response spin-dependent transport properties of QDs in the proximity with the superconductor. We assume that the superconducting gap is larger than the corresponding charging energy of the dot. It implies that at low temperatures the only processes between the dot and superconducting lead are due to the Andreev reflection. We note that the charging energy in typical QDs can range from fractions of meV up to a few meV, while the superconducting energy gap can be as large as a couple of meV [44,45]. Consequently, there are systems where the condition  $U < \Delta$  is fulfilled. Aiming to focus on transport between the two ferromagnets, we set the electrochemical potential of the superconducting lead to zero and assume a small symmetric bias between ferromagnetic electrodes. Then, for symmetric couplings, the net current between the dot and the superconductor vanishes. In the limit of large  $\Delta$ , the QD with superconducting lead can be modeled by the following effective Hamiltonian [46–48]:

$$H_{\text{QD}}^{\text{eff}} = H_{\text{QD}} + \Gamma_S (d_{\uparrow}^{\dagger} d_{\downarrow}^{\dagger} + d_{\downarrow} d_{\uparrow}). \quad (4)$$

In this Hamiltonian the superconducting degrees of freedom have been integrated out and the possibility of creating or annihilating Cooper pairs in the superconductor is now included in the last, particle-nonconserving term proportional to  $\Gamma_S$ . This effective Hamiltonian can be easily diagonalized and has the following eigenstates: singly occupied dot states,  $|\uparrow\rangle$  and  $|\downarrow\rangle$ ,

with energy  $\varepsilon$ , and the two states being combinations of empty ( $|0\rangle$ ) and doubly occupied ( $|\uparrow\downarrow\rangle$ ) dot states

$$|\pm\rangle = \alpha_{\mp}|0\rangle \pm \alpha_{\pm}|\uparrow\downarrow\rangle, \quad (5)$$

with the coefficients  $\alpha_{\pm} = \sqrt{1 \pm \delta/(\delta^2 + \Gamma_S^2)}/\sqrt{2}$  and  $\delta = \varepsilon + U/2$  denoting the detuning of the dot level from the particle-hole symmetry point  $\varepsilon = -U/2$ . The eigenenergies of the above eigenstates are given by  $E_{\pm} = \delta \pm \sqrt{\delta^2 + \Gamma_S^2}$ , correspondingly. The excitation energies of the effective Hamiltonian (4) result in Andreev bound-state energies

$$E_{\gamma\eta}^A = \gamma \frac{U}{2} + \eta \sqrt{\delta^2 + \Gamma_S^2}, \quad (6)$$

with  $\gamma, \eta = \pm$ . They correspond to respective excitations between the doublet and singlet states of the dot.

### B. Transport coefficients

All the relevant linear-response transport coefficients can be expressed in terms of the integral

$$L_{n\sigma} = -\frac{1}{h} \int d\omega \omega^n \frac{\partial f(\omega)}{\partial \omega} T_{\sigma}(\omega), \quad (7)$$

where  $f(\omega)$  is the Fermi-Dirac distribution function and  $T_{\sigma}(\omega)$  denotes the transmission coefficient. The spin-resolved linear conductance is then given by

$$G_{\sigma} = e^2 L_{0\sigma}. \quad (8)$$

In the case of ferromagnetic leads, depending on the spin relaxation time in ferromagnets, the voltage drop induced by temperature gradient can become spin dependent, giving rise to spin accumulation,  $\delta V_{\sigma} = \delta V + \sigma V_S$ , where  $V_S$  is the spin voltage. One can thus generally distinguish two different situations: (i) the first one when the spin relaxation is fast enough to assure  $V_S = 0$  and (ii) the second one when spin relaxation is slow and  $V_S \neq 0$ . Moreover, in the three-terminal setup considered here, one needs to be careful about the current which can flow to the superconducting lead [31]. To prevent the average current from flowing into the superconductor, we apply the temperature gradient  $\delta T$  symmetrically (see Fig. 1) and assume that the voltage guaranteeing the absence of the current  $J$  induced by temperature gradient is also applied symmetrically; that is,  $\mu_l = -\mu_r = \delta V/2$  and  $\mu_S = 0$ . Consequently, in the absence of spin accumulation,  $V_S = 0$ , the thermal conductance is given by

$$\kappa \equiv \left( \frac{\delta J_Q}{\delta T} \right)_{J=0} = \frac{1}{T} \left[ L_2 - \frac{L_1^2}{L_0} \right], \quad (9)$$

where  $L_n = \sum_{\sigma} L_{n\sigma}$ . On the other hand, the Seebeck coefficient is defined as

$$S \equiv -\left( \frac{\delta V}{\delta T} \right)_{J=0} = -\frac{1}{|e|T} \frac{L_1}{L_0}. \quad (10)$$

The spin-dependent thermopower in the case of finite spin accumulation,  $V_S \neq 0$ , is defined by

$$S_{\sigma} \equiv -\left( \frac{\delta V_{\sigma}}{\delta T} \right)_{J_{\sigma}=0} = -\frac{1}{|e|T} \frac{L_{1\sigma}}{L_{0\sigma}}, \quad (11)$$

where  $J_{\sigma}$  denotes the current flowing in the spin channel  $\sigma$ . One can then define the thermopower and the spin thermopower, respectively, as

$$S_{ac} = \frac{1}{2}(S_{\uparrow} + S_{\downarrow}), \quad (12)$$

$$S_S = \frac{1}{2}(S_{\uparrow} - S_{\downarrow}). \quad (13)$$

### C. Method

To obtain reliable, experimentally testable predictions for transport properties of correlated QDs with ferromagnetic leads in the proximity with the superconductor, we employ the fDM-NRG method [34–37]. This method allows us to study the dot's local density of states (dot-level spectral function) as well as the electric and thermoelectric transport properties in the full range of parameters in a very accurate way. In NRG, the conduction band is discretized logarithmically and the Hamiltonian is mapped onto a tight binding chain with exponentially decaying hoppings, which can be then diagonalized iteratively. In our calculations we kept 1024 states per iteration and used the Abelian symmetry for the total spin  $z$ th component.

To perform the analysis, we first applied an orthogonal left-right transformation to map the effective two-lead Hamiltonian to a new Hamiltonian, in which the dot couples only to an even linear combination of electron operators of the left and right leads, with a new coupling strength  $\Gamma = \Gamma_L + \Gamma_R$ . We note that for left-right symmetric systems, such as considered in this paper, in the AP configuration the effective coupling is the same for spin-up and spin-down electrons. As a result, transport characteristics are then qualitatively similar to those observed for nonmagnetic systems, except for a polarization-dependent factor. In the P configuration, on the other hand, the effective couplings do depend on spin polarization of ferromagnets, giving rise to various interesting effects.

The main quantity we are interested in is the spin-dependent transmission coefficient

$$T_{\sigma}(\omega) = \frac{4\Gamma_L^{\sigma}\Gamma_R^{\sigma}}{\Gamma_L^{\sigma} + \Gamma_R^{\sigma}} \pi A_{\sigma}(\omega), \quad (14)$$

with  $A_{\sigma}(\omega)$  being the spin-dependent spectral function of the dot,  $A_{\sigma}(\omega) = -\frac{1}{\pi} \text{Im} G_{\sigma}^R(\omega)$ , where  $G_{\sigma}^R(\omega)$  is the Fourier transform of the retarded Green's function of the QD for spin  $\sigma$ . In the P and AP magnetic configurations the spin-resolved transmission coefficient acquires relatively simple form,

$$T_{\sigma}^P(\omega) = (1 + \sigma p) \pi \Gamma A_{\sigma}^P(\omega), \quad (15)$$

$$T_{\sigma}^{AP}(\omega) = (1 - p^2) \pi \Gamma A_{\sigma}^{AP}(\omega), \quad (16)$$

respectively. Having determined the transmission,  $T_{\sigma}(\omega)$ , one can then calculate the integrals  $L_{n\sigma}$  [Eq. (7)] and find the respective electric and thermoelectric transport coefficients. However, since in NRG one usually collects the spectral data in logarithmic bins that are then broadened to obtain a smooth curve, which may introduce some errors, we determine the transport coefficients directly from the discrete, high-quality NRG data [41,42]. Nevertheless, when discussing the behavior of the dot spectral function, to improve its quality and suppress

possible broadening artifacts [50], in calculations we employ the  $z$ -averaging trick with the number of twist parameters  $N_z = 5$  [51].

### III. LOCAL DENSITY OF STATES AND EXCHANGE FIELD

#### A. Antiparallel configuration

The normalized spectral function in the AP configuration,  $\mathcal{A}^{\text{AP}}(\omega) = \sum_{\sigma} \pi \Gamma_{\sigma}^{\text{AP}} A_{\sigma}^{\text{AP}}(\omega)$ , is shown in Fig. 2 for different couplings to the superconductor  $\Gamma_S$ . As mentioned above, in the AP configuration the effective couplings  $\Gamma_{\sigma}^{\text{AP}}$  become spin-independent and the system behaves as if coupled to nonmagnetic leads. Consequently, for  $\Gamma_S = 0$ , the spectral function exhibits the full Kondo resonance at  $\omega = 0$ . The Kondo temperature for the assumed parameters and for  $\Gamma_S = 0$  is  $T_K/U \simeq 1.8 \times 10^{-3}$ . There are also two Hubbard resonances, which for  $\delta = 0$  occur at energies  $\omega = \pm U/2$  (note the logarithmic scale in Fig. 2). The proximity of superconducting lead results in gradual suppression of the Kondo effect with increasing  $\Gamma_S$ . For finite  $\Gamma_S$ , the virtual states for the spin-flip cotunneling processes driving the Kondo effect are the states  $|+\rangle$  and  $|-\rangle$ , the energy of which greatly depends on  $\Gamma_S$ . This leads to a strong dependence of the Kondo temperature on the coupling to the superconductor. As can be seen in Fig. 2, increasing  $\Gamma_S$  generally raises the Kondo temperature. Moreover, for finite  $\Gamma_S$ , one can also observe two resonances for larger  $\omega$ , which correspond to Andreev bound states of energies  $E_{++}^A$  and  $E_{+-}^A$ ; see Fig. 2 for, e.g.,  $\Gamma_S/U = 0.2$ . When the coupling to the superconductor increases, the energies of the bound states change and, for larger  $\Gamma_S$ , the resonance at  $\omega = E_{+-}^A$  merges with the Kondo peak; see the curve for  $\Gamma_S/U = 0.4$  in Fig. 2.

The increase of the Kondo temperature for finite  $\Gamma_S$  is due to the fact that the excitation energies from the doublet state to singlet states  $|+\rangle$  and  $|-\rangle$  become decreased. As a consequence, an effective exchange interaction between the spin in the dot and the conduction electrons becomes enhanced with increasing  $\Gamma_S$ .

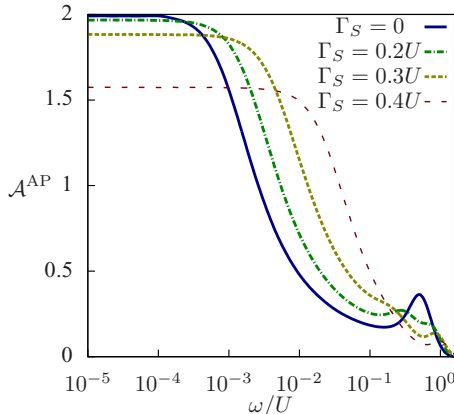


FIG. 2. (Color online) The energy dependence of the normalized spectral function in the AP magnetic configuration  $\mathcal{A}^{\text{AP}}$  calculated for  $\delta = 0$  and different couplings to superconducting lead  $\Gamma_S$ . The parameters are  $U = 1$ ,  $\Gamma = U/12$ ,  $T = 0$ , and  $p = 0.4$ .

Another interesting feature visible in Fig. 2 is the decrease of the spectral function at the Fermi level with increasing  $\Gamma_S$ . In the case of  $\Gamma_S = 0$ , by the Friedel sum rule [6,52], the spectral function  $A_{\sigma}(0)$  at  $\omega = 0$  is given by  $A_{\sigma}(0) = (\pi\Gamma)^{-1}$ , with  $\Gamma_{\uparrow} = \Gamma_{\downarrow} \equiv \Gamma$ . To understand the behavior of the spectral function in the presence of superconducting lead, let us have a look at the Green's function  $\langle\langle d_{\sigma} | d_{\sigma}^{\dagger} \rangle\rangle_{\omega}$  of the dot level, which in the wide band approximation is given by

$$\langle\langle d_{\sigma} | d_{\sigma}^{\dagger} \rangle\rangle_{\omega} = \left[ \omega - \varepsilon - \Sigma_{\sigma} + i\Gamma - \frac{\Gamma_S^2}{\omega + \varepsilon + \Sigma_{\sigma}^S + i\Gamma} \right]^{-1}, \quad (17)$$

where the self-energies are defined as

$$\Sigma_{\sigma} = U \frac{\langle\langle d_{\sigma} n_{\bar{\sigma}} | d_{\sigma}^{\dagger} \rangle\rangle}{\langle\langle d_{\sigma} | d_{\sigma}^{\dagger} \rangle\rangle} \quad \text{and} \quad \Sigma_{\sigma}^S = U \frac{\langle\langle d_{\sigma}^{\dagger} n_{\bar{\sigma}} | d_{\sigma}^{\dagger} \rangle\rangle}{\langle\langle d_{\sigma}^{\dagger} | d_{\sigma}^{\dagger} \rangle\rangle}.$$

For the noninteracting case  $U = 0$ , and for  $\varepsilon = 0$ , the spectral function at  $\omega = 0$  is  $A_{\sigma}(0) = (\pi\tilde{\Gamma})^{-1}$ , with a renormalized coupling,

$$\tilde{\Gamma} = \Gamma \left( 1 + \frac{\Gamma_S^2}{\Gamma^2} \right). \quad (18)$$

Clearly, the presence of the superconducting lead results in an enhancement of the effective level half width  $\tilde{\Gamma}$ . The height of the spectral function at the Fermi level then decreases with increasing  $\Gamma_S$ . The same tendency also holds for the fully interacting case (see Fig. 2); the increase in the effective coupling is, however, smaller than in the noninteracting case, since the denominator in Eq. (18) is larger due to finite self-energy  $\Sigma_{\sigma}^S$ ; see Eq. (17). Note that for  $\varepsilon = -U/2$  (the particle-hole symmetry point of the Anderson model),  $\text{Re}\{\Sigma_{\sigma}^S(\omega = 0)\} \neq U/2$ , contrary to the self-energy  $\Sigma_{\sigma}$ , which then fulfills  $\text{Re}\{\Sigma_{\sigma}(\omega = 0)\} = U/2$ .

#### B. Parallel configuration

Figure 3 presents the energy and level detuning dependence of the normalized spectral function in the P magnetic configuration,  $\mathcal{A}^{\text{P}}(\omega) = \sum_{\sigma} \pi \Gamma_{\sigma}^{\text{P}} A_{\sigma}^{\text{P}}(\omega)$ .  $\mathcal{A}^{\text{P}}(\omega)$  is calculated for a few different values of the coupling to the superconductor  $\Gamma_S$ , as indicated in the figure. By changing the level detuning  $\delta$ , the occupancy of the dot changes. For  $|\delta| < \sqrt{U^2/4 - \Gamma_S^2}$ , the dot is singly occupied, while for  $|\delta| > \sqrt{U^2/4 - \Gamma_S^2}$ , the occupancy is even; i.e., the dot is in state  $|+\rangle$  for  $\delta < -\sqrt{U^2/4 - \Gamma_S^2}$ , and in state  $|-\rangle$  for  $\delta > \sqrt{U^2/4 - \Gamma_S^2}$ .

In the singly occupied regime, for  $T < T_K$ , the electronic correlations may give rise to a resonance at the Fermi level due to the Kondo effect. This is indeed what one observes for the AP magnetic configuration; see Fig. 2. However, due to the dependence of tunneling processes on spin, in the P configuration the dot levels for spin-up and spin-down become renormalized and shift in opposite directions, leading to a spin splitting of the dot level,  $\Delta\varepsilon_{\text{exch}}$ . This exchange field created by the presence of ferromagnetic leads suppresses the Kondo effect once  $|\Delta\varepsilon_{\text{exch}}| > T_K$ . Moreover,  $\Delta\varepsilon_{\text{exch}}$  displays a particular dependence on the level detuning  $\delta$ , it vanishes for  $\delta = 0$  and changes sign at the particle-hole symmetry point. Although by splitting the dot level the exchange field acts in

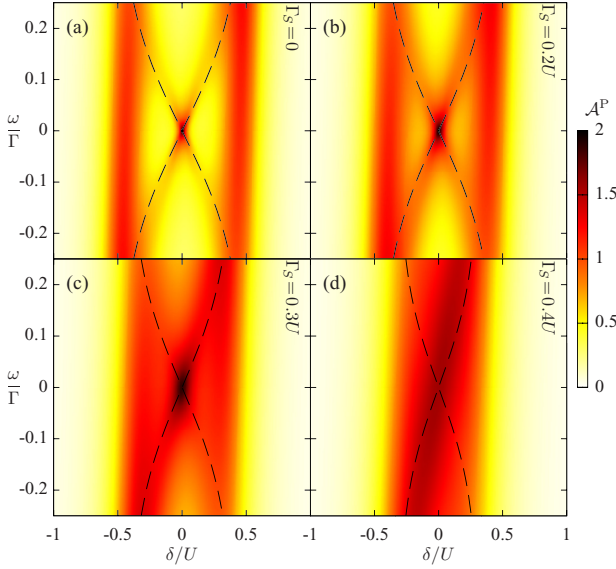


FIG. 3. (Color online) The normalized spectral function  $\mathcal{A}^P$  in the P magnetic configuration as a function of energy  $\omega$  and level detuning  $\delta = \varepsilon + U/2$  for different couplings to superconducting lead: (a)  $\Gamma_S = 0$ , (b)  $\Gamma_S/U = 0.2$ , (c)  $\Gamma_S/U = 0.3$ , (d)  $\Gamma_S/U = 0.4$ . The dashed lines show the exchange field  $\Delta\varepsilon_{\text{exch}}$  obtained from the analytical formula (20). The parameters are the same as in Fig. 2.

a similar way as an external magnetic field, it possesses an extra asset, namely that its magnitude and sign can be tuned by purely electrical means, i.e., by changing  $\delta$  with a gate voltage.

All the above-mentioned features can be clearly visible in Fig. 3(a), which presents the spectral function for  $\Gamma_S = 0$ . First, the zero-energy spectral function  $\mathcal{A}^P(0)$  has two maxima broadened by  $2\Gamma$  at resonant energies  $\delta = \pm U/2$ . Second, in the singly occupied dot regime, one observes the Kondo resonance for  $\delta = 0$ , which then becomes split as the level detuning increases,  $|\delta| > 0$ . The split Kondo resonance due to the presence of ferromagnetic leads has already been observed in a number of experiments and is rather well understood [15–22]. Here we in particular want to analyze how the superconducting proximity effect affects the exchange field and, thus, the split Kondo resonance. For finite  $\Gamma_S$ , the resonant energies are  $\delta = \pm\sqrt{U^2/4 - \Gamma_S^2}$ . This implies that the singly occupied regime shrinks with increasing the coupling to the superconductor. Consequently, the Kondo temperature increases, since the excitation energies from singly occupied to evenly occupied virtual states,  $|+\rangle$  and  $|-\rangle$ , become lowered. Moreover, the magnitude of the exchange field also becomes enhanced with increasing  $\Gamma_S$ . However, while the increase of  $\Delta\varepsilon_{\text{exch}}$  with  $\Gamma_S$  is algebraic, the  $T_K$  dependence on  $\Gamma_S$  is rather exponential. Therefore, for large  $\Gamma_S$ , the effects due to the proximity with ferromagnets become eventually overwhelmed by the Kondo correlations. This is visible in Fig. 3, where the width of the split Kondo resonances become increased, until they eventually merge for large  $\Gamma_S$ ; see Fig. 3(d). In fact, for  $\Gamma_S = 0.4U$ , the local moment regime of the dot is rather narrow and due to the broadening of the resonant peaks, one

observes only a single low-energy resonance for  $\delta = 0$ . The height of this resonance is, however, lower as compared to the case of smaller  $\Gamma_S$ , which indicates that although the strong coupling to the superconductor can suppress the effects due to the exchange field, it may also destroy the Kondo effect.

### C. Perturbative analysis

To estimate the magnitude of the exchange field in the P configuration in the presence of the superconductor, one can use the second-order perturbation theory to determine the spin-dependent dot level renormalization  $\delta\varepsilon_\sigma$  due to the coupling to ferromagnets. We thus treat  $H_{\text{TF}}$  as a perturbation to  $H_0 = H_{\text{QD}}^{\text{eff}} + H_{\text{F}}$  and find that the shift of the level is given by

$$\delta\varepsilon_\sigma = -\frac{\Gamma_\sigma}{\pi} \int d\omega \left[ \frac{\alpha_+^2 f^-(\omega)}{\omega - E_{+-}^A} + \frac{\alpha_-^2 f^-(\omega)}{\omega - E_{--}^A} \right] - \frac{\Gamma_{\bar{\sigma}}}{\pi} \int d\omega \left[ \frac{\alpha_+^2 f(\omega)}{\omega - E_{++}^A} + \frac{\alpha_-^2 f(\omega)}{\omega - E_{+-}^A} \right], \quad (19)$$

where  $f^-(\omega) = 1 - f(\omega)$ . The exchange field can be then obtained from  $\Delta\varepsilon_{\text{exch}} = \delta\varepsilon_\uparrow - \delta\varepsilon_\downarrow$  and is given by

$$\Delta\varepsilon_{\text{exch}} = \frac{2p\Gamma}{\pi} \frac{\delta}{\sqrt{\delta^2 + \Gamma_S^2}} [\phi(E_{+-}^A) - \phi(E_{++}^A)], \quad (20)$$

where  $\phi(\omega) = \text{Re}\{\Psi(\frac{1}{2} + i\frac{\omega}{2\pi T})\}$  and  $\Psi(z)$  is the digamma function. Clearly, the exchange field is a function of the Andreev bound-state energies and can be tuned not only by  $\delta$ , but also by  $\Gamma_S$ . Although  $\Delta\varepsilon_{\text{exch}}$  results directly from the proximity effect with the ferromagnetic leads, the superconducting proximity effect may considerably affect it. The formula for the exchange field, Eq. (20), can be somewhat simplified at zero temperature when  $\phi(E_{+-}^A) - \phi(E_{++}^A) = \log|E_{+-}^A/E_{++}^A|$ , while for  $\Gamma_S = 0$  one gets [17,20–22]  $\Delta\varepsilon_{\text{exch}} = \frac{2p\Gamma}{\pi} \log|\frac{\delta-U/2}{\delta+U/2}|$ .

The exchange field obtained from Eq. (20) as a function of level detuning  $\delta$  is plotted in Fig. 4. The perturbation theory breaks down at resonances for  $|\delta| = \sqrt{U^2/4 - \Gamma_S^2}$ , where the exchange field diverges at  $T = 0$ . We plotted  $\Delta\varepsilon_{\text{exch}}$  in the full range of  $\delta$  to present how the resonances move towards the middle of the Coulomb blockade regime with increasing  $\Gamma_S$ . Another feature visible in Fig. 4 is the enhancement of the magnitude of the exchange field in the singly occupied dot regime with raising the coupling to the superconductor.  $\Delta\varepsilon_{\text{exch}}$  obtained from formula (20) is also shown in Fig. 3 by dashed lines. One can see that the agreement between the split Kondo resonances visible in the spectral function obtained by NRG and the estimation for  $\Delta\varepsilon_{\text{exch}}$  based on Eq. (20) is indeed very good. For large coupling to the superconductor, however, the spectral function displays only one broad Kondo resonance and the splitting is no longer visible due to the broadening of Andreev levels by the coupling to ferromagnetic leads  $\Gamma$ .

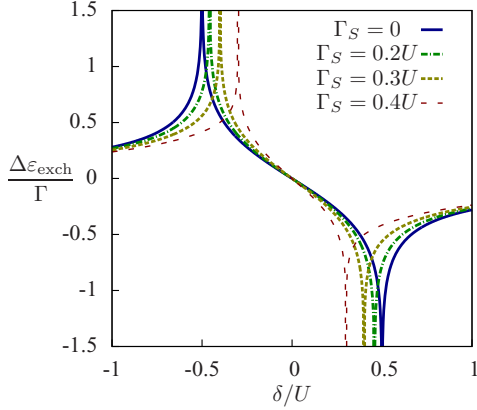


FIG. 4. (Color online) The exchange field in the P magnetic configuration for a few values of  $\Gamma_S$  obtained from Eq. (20) at  $T = 0$ . The other parameters are as in Fig. 2.

#### IV. LINEAR CONDUCTANCE AND TUNNEL MAGNETORESISTANCE

In this section we focus on the role of superconducting proximity effect on the spin-resolved electric transport coefficients. In particular, we study the level detuning and temperature dependence of the linear conductance in the P ( $G^P$ ) and AP ( $G^{AP}$ ) magnetic configurations, as well as the resulting tunnel magnetoresistance, which is defined as [49]  $\text{TMR} = G^P/G^{AP} - 1$ .

##### A. Level detuning dependence

In Fig. 5 we show the level detuning dependence of the linear conductance and the TMR for different temperatures and couplings to the superconductor. At low temperatures,  $T < T_K$ , in the AP configuration there is a Kondo plateau in the singly occupied regime where  $G^{AP} = 2(1 - p^2)e^2/h$  [see Fig. 5(a)], which becomes suppressed with increasing  $\Gamma_S$ . At intermediate temperatures,  $T/U = 10^{-2}$  [Fig. 5(b)], for  $\Gamma_S = 0$ , the Kondo effect is suppressed since  $T > T_K$ ; however, by increasing the coupling to the superconductor, one also increases the Kondo temperature and for  $\Gamma_S/U = 0.4$  there is a single resonance around  $\delta = 0$ . Note, however, that this maximum in  $G^{AP}$  is mainly due to the fact that the resonant energies become very close and the two resonant peaks merge due to the broadening of Andreev levels by the coupling to ferromagnetic leads. In the case of relatively high temperatures,  $T/U = 10^{-1}$ , the general dependence is similar to the previous case, but the conductance is suppressed.

In the P configuration, the linear conductance at low temperatures shows a clear signature of the exchange field that suppresses the Kondo effect for  $\delta \neq 0$ , while for  $\delta = 0$  the conductance is maximum,  $G^P = 2e^2/h$ ; see Fig. 5(d). With increasing  $\Gamma_S$ , the effects due to the exchange field are effectively decreased and almost completely disappear for  $\Gamma_S/U = 0.4$ , as explained in Sec. III. On the other hand, for higher temperatures,  $|\Delta\varepsilon_{\text{exch}}| < T$ , such that thermal fluctuations smear out the effects due to the exchange field, the dependence of  $G^P$  on  $\delta$  is qualitatively similar to that for  $G^{AP}$ ,

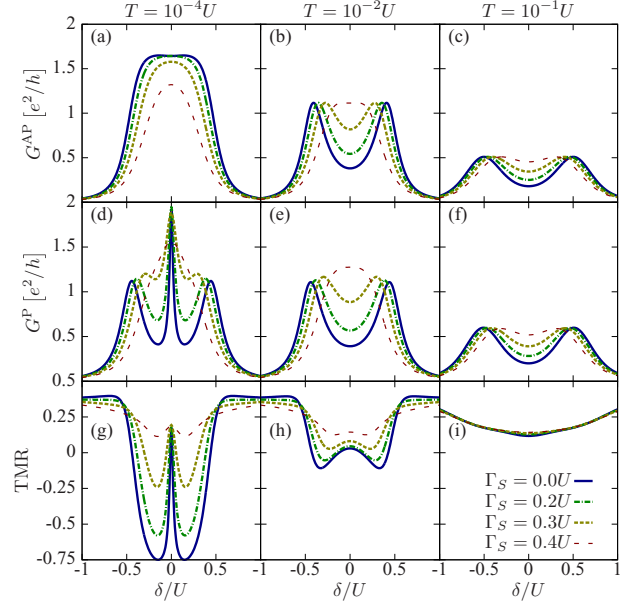


FIG. 5. (Color online) The level detuning dependence of the linear conductance in the AP ( $G^{AP}$ ) (a)–(c) and P ( $G^P$ ) (d)–(f) magnetic configurations, as well as the resulting TMR (g)–(i) for different couplings to the superconductor and temperatures. The left, middle, and right columns correspond to  $T/U = 10^{-4}$ ,  $T/U = 10^{-2}$ , and  $T/U = 10^{-1}$ , respectively. The other parameters are as in Fig. 2.

with a general tendency that for  $T \gtrsim \Gamma$ ,  $G^P > G^{AP}$ ; compare Figs. 5(c) and 5(f).

The difference in  $G^P$  and  $G^{AP}$  gives rise to nonzero TMR presented in Figs. 5(g)–5(i). While for  $T < T_K$  and  $\Gamma_S = 0$ , the TMR exhibits a highly nontrivial dependence on level detuning  $\delta$  [21], with increasing either  $\Gamma_S$  or  $T$ , the TMR dependence on  $T$  becomes less dramatic. First of all, when raising  $\Gamma_S$ , the effects due to the exchange field become suppressed and the TMR becomes positive in the whole range of  $\delta$ . Moreover, for larger temperatures, the proximity of the superconductor plays a smaller role and for  $T/U = 10^{-1}$  [see Fig. 5(i)], the TMR is roughly independent of  $\Gamma_S$ .

##### B. Temperature dependence

The behavior described above is also visible in the temperature dependence of the linear conductance and TMR shown in Fig. 6, which is calculated for several values of  $\delta$  and  $\Gamma_S$ . For the particle-hole symmetric case  $\delta = 0$  presented in the left column of Fig. 6, both  $G^P$  and  $G^{AP}$  exhibit dependence on  $T$ , which is typical for QDs in the Kondo regime [21]. They just differ by a polarization-dependent factor, which in the Kondo regime is equal to  $1 - p^2$ , and with increasing temperature becomes decreased for  $T \approx T_K$  to raise again once thermally activated sequential processes become possible. As a result, the TMR is given by  $\text{TMR} = p^2/(1 - p^2)$ ; in the Kondo regime,  $T < T_K$ , and in the sequential tunneling regime,  $T \gtrsim \Gamma$  and becomes suppressed for  $T \approx T_K$  [see Fig. 6(g)]. With increasing the coupling to the superconductor, these features basically persist, but the Kondo temperature becomes



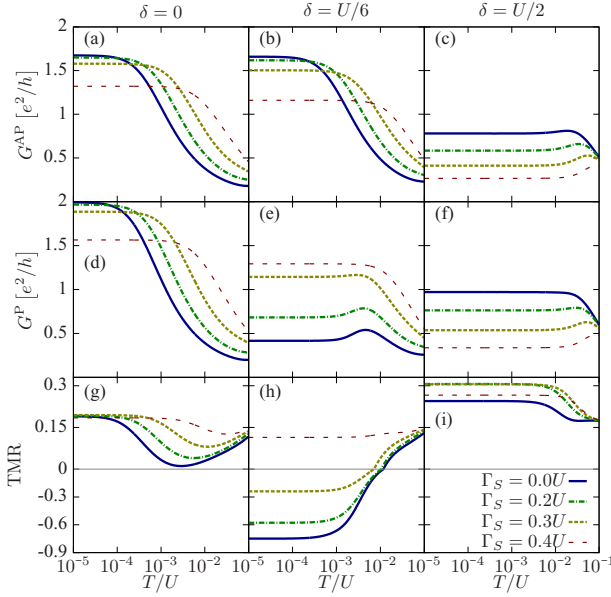


FIG. 6. (Color online) The temperature dependence of  $G^{\text{AP}}$  (a)–(c),  $G^{\text{P}}$  (d)–(f), and the TMR (g)–(i) for different couplings  $\Gamma_S$ . The left, middle, and right columns correspond to  $\delta = 0$ ,  $\delta = U/6$ , and  $\delta = U/2$ , respectively. The other parameters are the same as in Fig. 2.

increased; see Figs. 6(a) and 6(d). In addition, one can observe that the height of the Kondo resonance is gradually suppressed with increasing  $\Gamma_S$ . This can be understood by realizing that the proximity of the superconductor effectively diminishes the repulsion of electrons in the dot. Since the Coulomb repulsion is necessary for the Kondo effect to occur, an increase of  $\Gamma_S$  will inevitably lead to the suppression of the Kondo resonance.

In the Coulomb blockade regime when the particle-hole symmetry is broken, the exchange field starts playing an important role. This situation is presented in the middle column of Fig. 6, which is calculated for  $\delta = U/6$ . While the temperature dependence of  $G^{\text{AP}}$  is very similar to the case of  $\delta = 0$  [see Figs. 6(a) and 6(b)], the linear conductance in the P configuration is completely different.  $G^{\text{P}}$  is generally suppressed as compared to the particle-hole symmetric case, which is due to the presence of exchange field. The Kondo resonance is suppressed and the linear conductance in P configuration displays only a small maximum for temperatures of the order of the Kondo temperature; see Fig. 6(e). This results in highly nontrivial dependence of the TMR on  $T$  [Fig. 6(h)], which now takes large negative values for  $T < T_K$  and then becomes positive with increasing temperature. However, when the coupling to superconducting lead increases, there appears a competition between the exchange field and the superconducting proximity effect, so that the role of the exchange field becomes diminished and the difference in conductances for both magnetic configurations is lowered; see Figs. 6(b) and 6(e). Consequently, for relatively strong coupling  $\Gamma_S$ , the TMR becomes positive in the whole range of temperatures; see the case of  $\Gamma_S/U = 0.4$  in Fig. 6(h).

The right column of Fig. 6 presents the case when  $\delta = U/2$ ; i.e., for  $\Gamma_S = 0$  the system is on resonance. With increasing

$\Gamma_S$ , the resonance moves towards the middle of the Coulomb blockade and the dot becomes occupied by the state  $|+\rangle$ . This results in lowering of the linear conductance with increasing  $\Gamma_S$ , irrespective of the magnetic configuration of the system; see Figs. 6(c) and 6(f). In fact, when raising the coupling to the superconductor, the transport regime changes from resonant to cotunneling regime. As a consequence, the TMR increases with  $\Gamma_S$  to reach the value  $\text{TMR} = 2p^2/(1-p^2)$ , characteristic of non-spin-flip cotunneling regime [53]. However, for higher temperatures,  $T \gtrsim \Gamma$ , the thermally activated sequential transport dominates and TMR becomes lowered, reaching  $\text{TMR} = p^2/(1-p^2)$ ; see Fig. 6(i).

## V. SEEBECK AND SPIN SEEBECK COEFFICIENTS

We now move to the discussion of thermoelectric transport properties of the system. For this, we assume that there is a temperature gradient  $\delta T$  applied to the left and right ferromagnetic leads; see Fig. 1. The formulas for the relevant thermoelectric coefficients are presented in Sec. II B. First, we study the influence of the proximity effect on the thermoelectric coefficients in the case of no spin accumulation in the leads

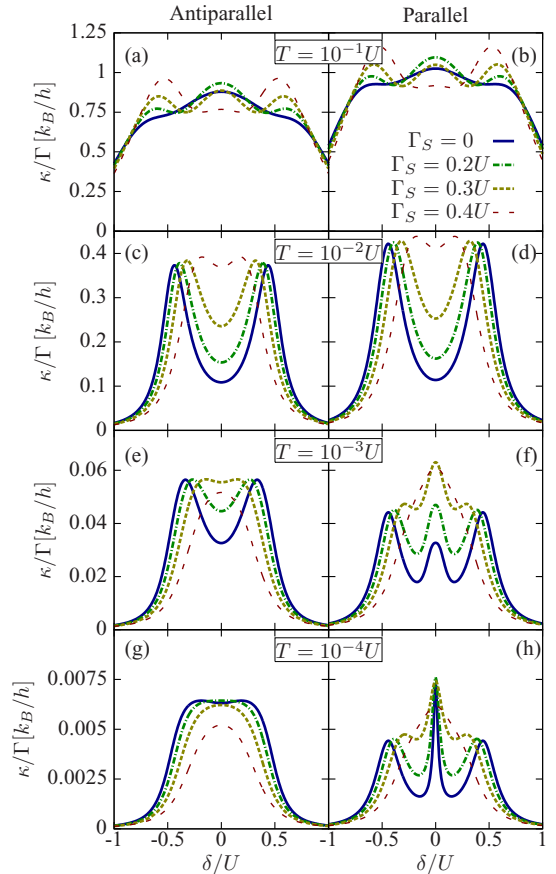


FIG. 7. (Color online) The thermal conductance  $\kappa$  as a function of detuning  $\delta$  for the AP (left column) and P (right column) configurations and for different couplings to the superconductor  $\Gamma_S$ . Each row corresponds to different temperature, as indicated. The parameters are the same as in Fig. 2.

and then proceed to the case of finite spin accumulation and the analysis of the spin Seebeck effect.

#### A. Absence of spin accumulation in the leads

Before analyzing the behavior of the thermopower, in Fig. 7 we show the thermal conductance  $\kappa$  as a function of the level detuning  $\delta$  for different temperatures and couplings to superconducting lead. The left column corresponds to the AP configuration, while the right column shows the results in the P configuration. When decreasing temperature, the thermal conductance becomes generally suppressed; however, specific shape of its dependence on  $\delta$  also changes. At high temperatures,  $T/U = 0.1$ ,  $\kappa$  displays a maximum for  $\delta = 0$ , where the particle and hole processes equally contribute to transport. This is visible in both magnetic configurations [see Figs. 7(a) and 7(b)], although  $\kappa$  is larger in the P configuration as compared to the AP one. With increasing the coupling to the superconductor, the maximum changes into local minimum, while two maxima for  $\delta \approx \pm U/2$  develop. For intermediate temperatures,  $T/U = 0.01$ , the shape of the  $\delta$  dependence of  $\kappa$  becomes similar to the detuning dependence of the linear conductance; cf. Fig. 5. A similar tendency can be also observed for lower temperatures; however, while the conductance increases with decreasing  $T$ , the thermal conductance becomes suppressed to disappear completely at zero temperature. Furthermore, at low temperatures, when  $|\Delta\varepsilon_{\text{exch}}| \gtrsim T$ , the exchange field starts playing an important role and the difference between both magnetic configurations becomes clearly visible. When raising  $\Gamma_S$ , the influence of the exchange field on transport becomes relatively weakened. The suppressed thermal conductance in the P configuration in the Coulomb blockade regime then becomes enhanced. On the other hand, in the AP configuration, the Kondo effect becomes gradually destroyed and  $\kappa$  drops in the local moment regime with increasing  $\Gamma_S$ ; see Figs. 7(g) and 7(h).

Figure 8 shows the  $\delta$  dependence of the Seebeck coefficient in both magnetic configurations for different temperatures and couplings  $\Gamma_S$ . The behavior of the thermopower is mostly determined by the shape of the Kondo peak in the local density of states. For  $\delta = 0$ , the Kondo resonance is fully symmetric around the Fermi level and, consequently, the particle and hole currents compensate each other and the thermopower vanishes. When moving away from the particle-hole symmetry point, the Seebeck coefficient becomes nonzero and its sign depends on the relative magnitude of the particle and hole currents.  $S$  is thus an odd function of  $\delta$ . At higher temperatures, the behavior of  $S$  is qualitatively similar in both magnetic configurations; see Figs. 8(a) and 8(b). The thermopower has a local maximum (minimum) for  $0 < \delta < U/2$  ( $-U/2 > \delta > 0$ ). The differences between  $S$  in the P and AP configuration start showing up with lowering temperature, when the exchange field starts playing a role. In the AP configuration, for  $0 < \delta < U/2$ , the local maximum in  $S$  for  $T/U = 0.1$  gradually merges with a local minimum, the position of which moves from  $\delta \approx U$  towards  $\delta = 0$  with lowering temperature. When increasing the coupling to superconducting lead, the thermopower in the AP configuration (and in the P configuration for  $T > |\Delta\varepsilon_{\text{exch}}|$ ) becomes generally suppressed; however, its qualitative dependence on  $\delta$  remains the same. This is opposite to what we have

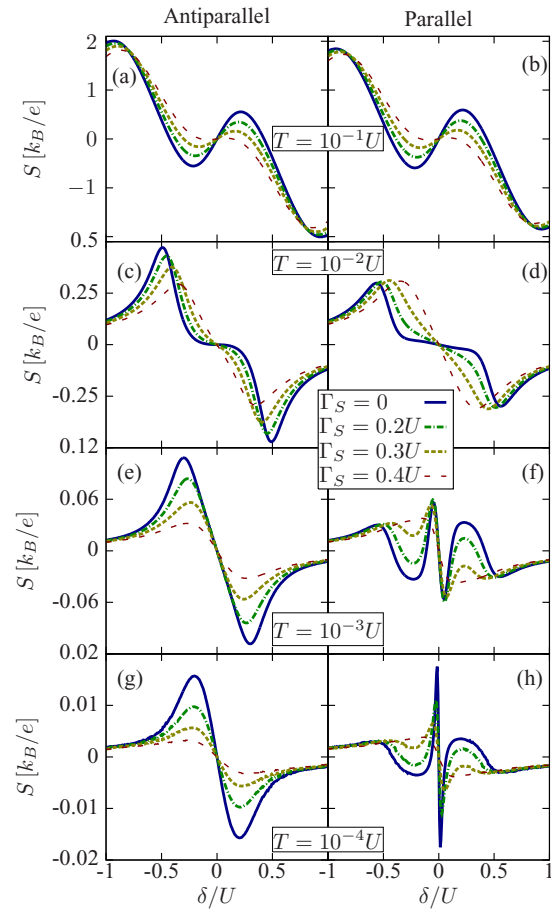


FIG. 8. (Color online) The thermopower as a function of  $\delta$  for the AP (left column) and P (right column) configurations and for different  $\Gamma_S$  and  $T$ , as indicated. The other parameters are as in Fig. 2.

in the P configuration, especially at low temperatures, when  $T < |\Delta\varepsilon_{\text{exch}}|$ ; see Figs. 8(f) and 8(h). Then, for  $0 < \delta < U/2$ ,  $S$  exhibits a local minimum, which becomes sharper and moves towards  $\delta = 0$  with lowering  $T$ . With increasing  $\delta$ , this minimum changes into a local maximum to drop again for  $\delta \approx U/2$ . As a consequence, for  $\delta > 0$ ,  $S$  changes sign twice in the Coulomb blockade regime. This is related to the exchange field, which suppresses the Kondo resonance, once  $|\Delta\varepsilon_{\text{exch}}| > T_K T$ . Since  $\Delta\varepsilon_{\text{exch}}$  depends strongly on  $\delta$ , it leads to the aforementioned behavior of the thermopower around the particle-hole symmetry point  $\delta = 0$ . Interestingly, when the coupling to the superconductor is increased, the  $\delta$  dependence of  $S$  changes drastically. In particular, for large  $\Gamma_S$ , when the exchange field effects are suppressed by superconducting proximity effect, the difference between the two magnetic configurations is decreased, and  $S$  in the P configuration behaves similarly to  $S$  in the AP configuration. Altogether, this gives rise to a nontrivial dependence of the low-temperature thermopower on  $\Gamma_S$  in the P configuration. The interplay of the three relevant energy scales—superconducting gap, exchange field, and Kondo temperature—is then clearly revealed; see Fig. 8.

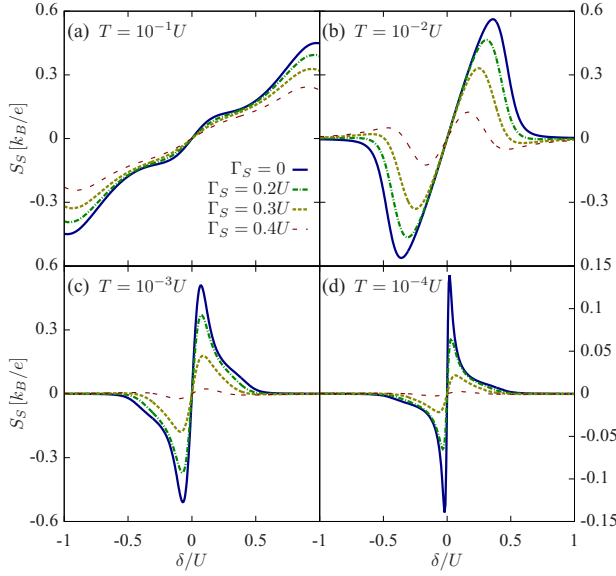


FIG. 9. (Color online) The spin thermopower in the P configuration as a function of  $\delta$  for different  $\Gamma_S$  and for (a)  $T/U = 10^{-1}$ , (b)  $T/U = 10^{-2}$ , (c)  $T/U = 10^{-3}$ , and (d)  $T/U = 10^{-4}$ . The other parameters are the same as in Fig. 2.

### B. Finite spin accumulation in the leads

We now discuss the behavior of the spin thermopower in the P magnetic configuration in the case of finite spin accumulation in the leads. Such a situation arises when the spin relaxation in the leads is slow and the shifts of the chemical potential for spin-up and spin-down electrons induced by the temperature gradient are not equal. The  $\delta$  dependence of the spin Seebeck coefficient is presented in Fig. 9 for different temperatures and couplings to the superconductor. For  $T/U = 0.1$ , the spin thermopower changes monotonically with sweeping  $\delta$  from  $-U$  to  $U$ ; see Fig. 9(a). Finite coupling to the superconductor leads only to the suppression of  $S_S$ . For smaller temperatures, however,  $S_S$  exhibits a maximum (minimum) for  $\delta > 0$  ( $\delta < 0$ ); see the case of  $T/U = 0.01$  in Fig. 9. This maximum is still present when the coupling to the superconductor becomes stronger, while its position moves towards the middle of the Coulomb blockade with increasing  $\Gamma_S$ . Moreover, for relatively strong coupling to the superconductor,  $\Gamma_S/U = 0.4$ , one can see that the  $\delta$  dependence of the spin thermopower has changed qualitatively. Now,  $S_S$  for  $\delta > 0$  exhibits a sign change in the Coulomb blockade regime, which was not present in the case of  $\Gamma_S = 0$ . When further decreasing the temperature, the maximum in  $S_S$  for positive detuning moves towards the particle-hole symmetry point  $\delta = 0$  and its magnitude becomes suppressed; see Figs. 9(c) and 9(d). For given temperature, increasing the strength of the coupling to superconducting lead results in a large suppression of the spin thermopower. The spin Seebeck coefficient for  $T \lesssim T_K$  becomes almost fully suppressed in the case of strong coupling to the superconductor.

For completeness, in Fig. 10 we show the detuning dependence of the Seebeck coefficient for different temperatures and couplings  $\Gamma_S$  in the case of finite spin accumulation

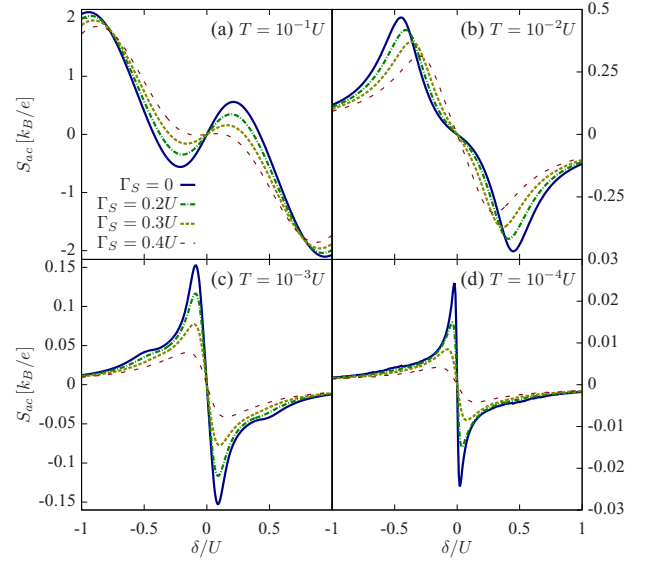


FIG. 10. (Color online) The thermopower in the P configuration as a function of  $\delta$  for different  $\Gamma_S$  and for different temperatures in the case of finite spin accumulation. The parameters are the same as in Fig. 2.

in the leads. Except for opposite sign, the dependence of  $S_{ac}$  on  $\delta$ ,  $T$ , and  $\Gamma_S$  is quite similar to the dependence of the spin Seebeck coefficient (cf. Figs. 9 and 10), although some differences still appear. First of all, for temperatures considered in Fig. 10,  $S_{ac}$  exhibits a nonmonotonic dependence on  $\delta$ , contrary to  $S_S$ , which for  $T/U = 0.1$  changed rather monotonically. Moreover, the dependence on  $\Gamma_S$  for  $S_{ac}$  is now weaker as compared to  $S_S$ . Increasing the coupling to the superconductor results only in quantitative changes, leading generally to the suppression of the thermopower  $S_{ac}$ ; see Fig. 10.

Finally, it is also interesting to study the temperature dependence of  $S_S$  and  $S_{ac}$  in the P configuration for different coupling  $\Gamma_S$ ; see Fig. 11. The left (right) column corresponds to  $\delta = U/6$  ( $\delta = U/2$ ). Let us first consider the case of  $\delta = U/6$ , when the system is in the Coulomb blockade regime. For very high ( $T > U$ ) or very low ( $T < T_K$ ) temperatures, both  $S_S$  and  $S_{ac}$  tend to zero for all values of  $\Gamma_S$ ; see Figs. 11(a) and 11(c). However, for intermediate temperatures,  $T \sim T_K$ , the spin Seebeck coefficient exhibits a maximum, the height of which diminishes with increasing  $\Gamma_S$ . The temperature at which the maximum occurs increases when the coupling to the superconductor is stronger. In addition, for  $\Gamma_S = 0$  there is also a small local maximum for  $T \approx \Gamma$ , however, which merges with the large peak when  $\Gamma_S$  is increased; see Fig. 11(a). Contrary to  $S_S$ , the temperature dependence of  $S_{ac}$  reveals two sign changes. With increasing  $T$ ,  $S_{ac}$  first drops to a local minimum for  $T \sim T_K$ , then changes sign and reaches a local maximum for  $T \sim \Gamma$  to drop again for  $T \sim U$  with another sign change; see Fig. 11(c). When increasing the coupling to the superconductor, the temperature at which the first minimum occurs increases, while the positions of other extrema are rather unchanged. Moreover, the overall magnitude of  $S_{ac}$  becomes generally suppressed

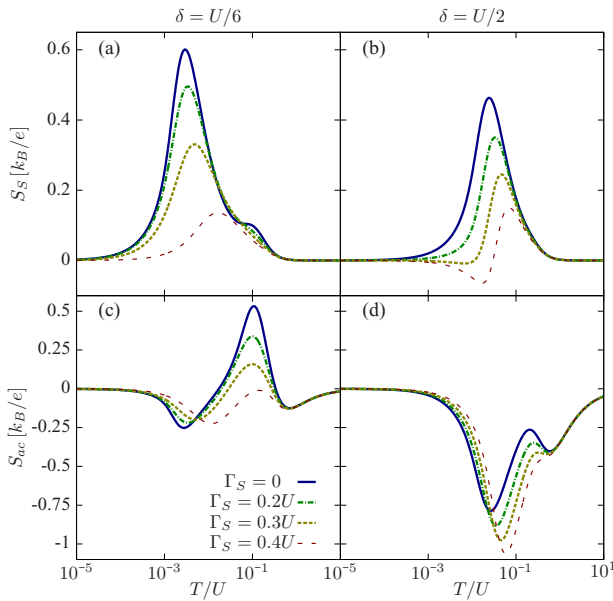


FIG. 11. (Color online) The spin thermopower (a),(b) and thermopower (c),(d) in the P configuration as a function of temperature for different  $\Gamma_S$  in the case of finite spin accumulation. The left column corresponds to  $\delta = U/6$ , while the right column to  $\delta = U/2$ . The parameters are as in Fig. 2.

with increasing  $\Gamma_S$ , which is especially visible for  $T \sim \Gamma$ ; see Fig. 11(c).

For larger detuning,  $\delta = U/2$ , the system is on resonance for  $\Gamma_S = 0$ . The temperature dependence of the spin thermopower displays then a single maximum for temperatures of the order of the coupling  $\Gamma$ . With increasing the coupling to the superconductor, this maximum transforms into a local minimum and  $S_S$  exhibits a sign change when increasing temperature; see Fig. 11(b). This is opposite to  $S_{ac}$ , which is now negative in the whole range of temperatures, irrespective of  $\Gamma_S$ ; see Fig. 11(d). The Seebeck coefficient has two local minima for  $T \sim \Gamma$  and  $T \sim U$ , separated by a local maximum, which merge together with increasing  $\Gamma_S$  into a large single minimum for  $T \sim \Gamma$ . Consequently, the proximity of the superconductor generally enhances the Seebeck coefficient  $S_{ac}$ . This behavior is opposite to that of  $S_S$  and  $S_{ac}$  in the case of  $\delta = U/6$  discussed above, for which the proximity effect led to a general suppression of the (spin) thermopower.

Finally, we would like to note that although the range of temperatures studied in Fig. 11 may be slightly too large to

assure that the description based on effective Hamiltonian in the limit of large superconducting gap is reasonable, we showed the data at high temperatures  $T \gtrsim U$  for completeness and consistency. Nevertheless, the most interesting behavior of the Seebeck and spin Seebeck coefficients discussed above occurs in the temperature range where the assumptions used are correct.

## VI. CONCLUDING REMARKS

In the present paper we analyzed the electric and thermoelectric transport properties of Kondo-correlated QDs coupled to the left and right ferromagnetic leads and additionally coupled to one superconducting lead. In such hybrid devices, transport characteristics are determined by the interplay of ferromagnetic-contact-induced exchange field, the superconducting proximity effect and correlations leading to the Kondo effect. By using the fDM-NRG method, we determined the dot's spectral function, linear electric and thermal conductances, the TMR, and the (spin) Seebeck coefficient for different temperatures, level positions, and couplings to the superconductor in the limit of large superconducting gap. We showed that the superconducting proximity effect may considerably affect the exchange field, which is a function of Andreev bound-state energies. For the exchange field, we provided an approximative analytical formula that agrees well with the NRG calculations. The exchange field leads to a spin-splitting of the dot level, which can suppress the Kondo resonance. We demonstrated that increasing the coupling to the superconductor may raise the Kondo temperature and partially restore the exchange-field-split Kondo resonance. This subtle competition between ferromagnetic and superconducting proximity effects is clearly visible in the corresponding temperature and level detuning dependence of both the electric and the thermoelectric transport coefficients of the system.

## ACKNOWLEDGMENTS

The discussions with J. Barnaś, K. Bocian, W. Rudziński, and P. Trocha are gratefully acknowledged. We also thank J. Barnaś and P. Trocha for critical reading of the manuscript. This work is supported by “Iuventus Plus” Project No. IP2011 059471 for years 2012–2014 and the National Science Center in Poland as Project No. DEC-2012/04/A/ST3/00372. This research was also supported by a Marie Curie FP-7-Reintegration-Grants (Grant No. CIG-303 689) within the 7th European Community Framework Programme.

- [1] H. Grabert and M. H. Devoret (eds.), *Single Charge Tunneling: Coulomb Blockade Phenomena in Nanostructures*, NATO ASI Series B: Physics 294 (Plenum, New York 1992).
- [2] L. L. Sohn, L. P. Kouwenhoven, and G. Schön (eds.), *Mesoscopic Electron Transport* (Kluwer, Dordrecht 1997).
- [3] D. D. Awschalom, D. Loss, and N. Samarth (eds.), *Semiconductor Spintronics and Quantum Computation* (Springer, Berlin, 2002).

- [4] S. Andergassen, V. Meden, H. Schoeller, J. Splettstoesser, and M. R. Wegewijs, *Nanotechnology* **21**, 272001 (2010).
- [5] J. Kondo, *Prog. Theor. Phys.* **32**, 37 (1964).
- [6] A. C. Hewson, *The Kondo Problem to Heavy Fermions* (Cambridge University Press, Cambridge, UK, 1993).
- [7] D. Goldhaber-Gordon, H. Shtrikman, D. Mahalu, D. Abusch-Magder, U. Meirav, and M. A. Kastner, *Nature (London)* **391**, 156 (1998).

- [8] S. Cronenwett, T. H. Oosterkamp, and L. P. Kouwenhoven, *Science* **281**, 540 (1998).
- [9] M. R. Buitelaar, W. Belzig, T. Nussbaumer, B. Babic, C. Bruder, and C. Schönberger, *Phys. Rev. Lett.* **91**, 057005 (2003).
- [10] H. I. Jorgensen, K. Grove-Rasmussen, T. Novotny, K. Flensberg, and P. E. Lindelof, *Phys. Rev. Lett.* **96**, 207003 (2006).
- [11] J. A. van Dam, Y. V. Nazarov, E. P. A. M. Bakkers, S. De Franceschi, and L. P. Kouwenhoven, *Nature (London)* **442**, 667 (2006).
- [12] T. Tsuneta, L. Lechner, and P. J. Hakonen, *Phys. Rev. Lett.* **98**, 087002 (2007).
- [13] M. R. Buitelaar, T. Nussbaumer, and C. Schönberger, *Phys. Rev. Lett.* **89**, 256801 (2002).
- [14] T. Hecht, A. Weichselbaum, J. von Delft, and R. Bulla, *J. Phys.: Condens. Matter* **20**, 275213 (2008).
- [15] A. N. Pasupathy, R. C. Bialczak, J. Martinek, J. E. Grose, L. A. K. Donev, P. L. McEuen, and D. C. Ralph, *Science* **306**, 86 (2004).
- [16] J. Barnaś and I. Weymann, *J. Phys.: Condens. Matter* **20**, 423202 (2008).
- [17] J. Martinek, M. Sindel, L. Borda, J. Barnaś, J. König, G. Schön, and J. von Delft, *Phys. Rev. Lett.* **91**, 247202 (2003).
- [18] J. Hauptmann, J. Paaske, and P. Lindelof, *Nat. Phys.* **4**, 373 (2008).
- [19] M. Gaass, A. K. Hüttel, K. Kang, I. Weymann, J. von Delft, and Ch. Strunk, *Phys. Rev. Lett.* **107**, 176808 (2011).
- [20] M. Sindel, L. Borda, J. Martinek, R. Bulla, J. König, G. Schön, S. Maekawa, and J. von Delft, *Phys. Rev. B* **76**, 045321 (2007).
- [21] I. Weymann, *Phys. Rev. B* **83**, 113306 (2011).
- [22] K. P. Wójcik, I. Weymann, and J. Barnaś, *J. Phys.: Cond. Matter* **25**, 075301 (2013).
- [23] L. Hofstetter, A. Geresdi, M. Aagesen, J. Nygard, C. Schönberger, and S. Csonka, *Phys. Rev. Lett.* **104**, 246804 (2010).
- [24] Y. Zhu, Q.-F. Sun, and T.-H. Lin, *Phys. Rev. B* **65**, 024516 (2001).
- [25] J.-F. Feng and S.-J. Xiong, *Phys. Rev. B* **67**, 045316 (2003).
- [26] X. F. Cao, Y. Shi, X. Song, S. Zhou, and H. Chen, *Phys. Rev. B* **70**, 235341 (2004).
- [27] P. Zhang and Y.-X. Li, *J. Phys.: Condens. Matter* **21**, 095602 (2009).
- [28] D. Futterer, M. Governale, M. G. Pala, and J. König, *Phys. Rev. B* **79**, 054505 (2009).
- [29] B. Sothmann, D. Futterer, M. Governale, and J. König, *Phys. Rev. B* **82**, 094514 (2010).
- [30] E. C. Siqueira and G. G. Cabrera, *Phys. Rev. B* **81**, 094526 (2010).
- [31] K. I. Wysokiński, *J. Phys.: Condens. Matter* **24**, 335303 (2012).
- [32] K. Bocian and W. Rudziński, *Eur. Phys. J. B* **86**, 439 (2013).
- [33] I. Weymann and P. Trocha, *Phys. Rev. B* **89**, 115305 (2014).
- [34] K. G. Wilson, *Rev. Mod. Phys.* **47**, 773 (1975).
- [35] R. Bulla, T. A. Costi, and T. Pruschke, *Rev. Mod. Phys.* **80**, 395 (2008).
- [36] A. Weichselbaum and J. von Delft, *Phys. Rev. Lett.* **99**, 076402 (2007).
- [37] We used an open-access Budapest NRG code, <http://www.phy.bme.hu/~dmnrg/>; O. Legeza, C. P. Moca, A. I. Tóth, I. Weymann, and G. Zaránd, [arXiv:0809.3143](https://arxiv.org/abs/0809.3143).
- [38] P. Trocha and J. Barnaś, *Phys. Rev. B* **85**, 085408 (2012).
- [39] L. D. Hicks and M. S. Dresselhaus, *Phys. Rev. B* **47**, 16631 (1993).
- [40] T. A. Costi and V. Zlatic, *Phys. Rev. B* **81**, 235127 (2010).
- [41] T. Rejec, R. Zitko, J. Mravlje, and A. Ramsak, *Phys. Rev. B* **85**, 085117 (2012).
- [42] I. Weymann and J. Barnaś, *Phys. Rev. B* **88**, 085313 (2013).
- [43] R. Chirla and C. P. Moca, *Phys. Rev. B* **89**, 045132 (2014).
- [44] J. Nagamatsu, N. Nakagawa, T. Muranaka, Y. Zenitani, and J. Akimitsu, *Nature (London)* **410**, 63 (2001).
- [45] B. W. Heinrich, L. Braun, J. I. Pascual, and K. J. Franke, *Nat. Phys.* **9**, 765 (2013).
- [46] A. V. Rozhkov and D. P. Arovas, *Phys. Rev. B* **62**, 6687 (2000).
- [47] C. Karrasch and V. Meden, *Phys. Rev. B* **79**, 045110 (2009).
- [48] T. Meng, S. Florens, and P. Simon, *Phys. Rev. B* **79**, 224521 (2009).
- [49] M. Julliere, *Phys. Lett. A* **54**, 225 (1975).
- [50] R. Zitko and T. Pruschke, *Phys. Rev. B* **79**, 085106 (2009).
- [51] V. L. Campo and L. N. Oliveira, *Phys. Rev. B* **72**, 104432 (2005).
- [52] J. Friedel, *Can. J. Phys.* **34**, 1190 (1956).
- [53] I. Weymann, J. König, J. Martinek, J. Barnaś, and G. Schön, *Phys. Rev. B* **72**, 115334 (2005).



**Andreev transport in a correlated ferromagnet-quantum-dot-superconductor device**

I. Weymann\* and K. P. Wójcik

*Faculty of Physics, Adam Mickiewicz University, ulica Umultowska 85, 61-614 Poznań, Poland*

(Received 13 October 2015; published 14 December 2015)

The spin-resolved Andreev reflection processes in a hybrid ferromagnet-quantum-dot-superconductor device are theoretically studied. In particular, the transport coefficients, such as the Andreev transmission as well as the linear-response Andreev conductance, are calculated by means of the numerical renormalization group method. It is shown that, generally, transport properties are conditioned by the interplay of correlations leading to the Kondo effect, superconducting proximity effect, and ferromagnetic-contact-induced exchange field. The exchange field is shown to greatly affect the low-energy behavior of the Andreev transmission by splitting the Kondo resonance. Moreover, it leads to a nonmonotonic dependence of the Andreev conductance on the dot level position. At low temperatures, the conductance has a peak at the particle-hole symmetry point, which however becomes quickly suppressed with increasing the temperature. The mechanisms responsible for those effects are thoroughly discussed.

DOI: [10.1103/PhysRevB.92.245307](https://doi.org/10.1103/PhysRevB.92.245307)

PACS number(s): 73.23.-b, 72.15.Qm, 74.45.+c, 72.25.-b

**I. INTRODUCTION**

Transport properties of hybrid quantum dot systems, involving both superconducting and normal electrodes, have recently been extensively studied both theoretically [1–28] and experimentally [29–34]. In such systems, at sufficiently low temperatures, the physics is determined by an interplay between the superconducting proximity effect and the correlations leading to the Kondo effect [35–38]. For a magnetic impurity coupled to a superconductor, the existence of the Kondo phenomenon is conditioned by the relative ratio of the Kondo temperature  $T_K$  to the superconducting energy gap  $\Delta$  [39–41]. The Kondo phenomenon is present when  $T_K > \Delta$ . On the other hand, in the opposite situation when  $\Delta$  exceeds  $T_K$ , the Kondo effect is suppressed and the so-called Yu-Shiba-Rusinov bound states form inside the energy gap [42–44]. Such proximity-induced bound states can be probed in a mesoscopic device consisting of a quantum dot, in which Andreev reflection [45] leads to the formation of similar long-lived states. In fact, Andreev bound states have been recently measured in bias spectroscopy experiments by attaching a second normal electrode to the dot acting as a weakly coupled probe [30–34]. However, when the coupling to the second electrode increases, such that the Kondo temperature associated with this normal reservoir becomes relevant, the system can again exhibit conductance enhancement due to the Kondo correlations. It was shown recently in the limit of large superconducting energy gap that, quite counterintuitively, in a hybrid normal-metal-quantum-dot-superconductor system increasing the strength of the coupling to superconducting electrode can lead to an enhancement of the Kondo temperature [26–28]. This is associated with the fact that the pairing correlations induced in the dot decrease the excitation energies to virtual states of the dot, leading to an increase in the effective exchange interaction, which consequently results in an increase of  $T_K$ .

An even more interesting situation occurs when the normal lead is ferromagnetic. Then, another energy scale becomes

relevant, namely, the one associated with a spin-splitting of the dot level caused by the so-called effective exchange field [46–51]. When the exchange field is large enough, it can affect the Kondo state in a very considerable way by splitting or even fully suppressing the Kondo peak. The interplay of exchange field, Kondo, and proximity effects has been recently studied experimentally in a hybrid ferromagnet-quantum-dot-superconductor device [52]. It was shown that the coexistence of itinerant ferromagnetism with superconducting and Kondo correlations leads to a very complex differential conductance spectra, containing both signatures of subgap states and split Kondo resonance.

The main goal of this paper is to provide further insight into Andreev transport properties of such systems. By employing the nonperturbative and very accurate numerical renormalization group (NRG) method [53–55], we determine transport due to Andreev reflection in the full parameter space, where both the Kondo correlations, superconducting proximity effect, and ferromagnet-induced exchange field coexist. We analyze the dot level and temperature dependence of the Andreev transmission coefficient and the associated linear-response conductance for various coupling strengths to both superconducting and normal leads. We show that generally the transport properties are conditioned by a subtle interplay of the aforementioned energy scales. In particular, for relatively weak couplings to superconducting electrode, the Kondo resonance becomes split due to the exchange field. However, with increasing the coupling strength, the proximity effect leads to an enhancement of  $T_K$  and the Kondo resonance becomes reinstated.

The paper is organized in the following way. Theoretical framework is presented in Sec. II, where we first describe the model Hamiltonian (Sec. II A), define the quantities of interest (Sec. II B), and briefly describe the method used in calculations (Sec. II C). The main part of the paper is presented in Sec. III, in which we first describe the behavior of the local density of states of the dot (Sec. III A) and then analyze the Andreev transmission and the linear-response conductance (Sec. III B). Finally, the conclusions are given in Sec. IV.

\*weymann@amu.edu.pl

## II. THEORETICAL DESCRIPTION

### A. Effective Hamiltonian

The schematic of the system is shown in Fig. 1. It consists of a quantum dot coupled to one ferromagnetic (FM) and one  $s$ -wave superconducting (SC) lead. Since in this paper we are mainly interested in the Andreev reflection processes, we consider the superconducting energy gap  $\Delta$  to be the largest energy scale in the problem. In such a case, the system can be described by the following effective Hamiltonian [56]:

$$H = H_{\text{QD}}^{\text{eff}} + H_{\text{F}} + H_{\text{TF}}, \quad (1)$$

where

$$H_{\text{QD}}^{\text{eff}} = \sum_{\sigma} \varepsilon d_{\sigma}^{\dagger} d_{\sigma} + U d_{\uparrow}^{\dagger} d_{\downarrow}^{\dagger} d_{\downarrow} + \Gamma_{\text{S}} (d_{\uparrow}^{\dagger} d_{\downarrow}^{\dagger} + d_{\downarrow} d_{\uparrow}). \quad (2)$$

Here,  $d_{\sigma}^{\dagger}$  creates a spin- $\sigma$  electron of energy  $\varepsilon$  in the quantum dot and  $U$  is the correlation energy between two electrons occupying the dot. The last term takes into account the creation and annihilation of Cooper pairs in the superconductor, the degrees of freedom of which were integrated out in the limit of  $\Delta \rightarrow \infty$ , where  $\Gamma_{\text{S}}$  denotes the strength of the coupling between the SC lead and the quantum dot [56]. The electrons in the ferromagnetic lead are modeled as noninteracting particles,  $H_{\text{F}} = \sum_{\mathbf{k}\sigma} \varepsilon_{\mathbf{k}\sigma} c_{\mathbf{k}\sigma}^{\dagger} c_{\mathbf{k}\sigma}$ , with  $c_{\mathbf{k}\sigma}^{\dagger}$  being the creation operator of a spin- $\sigma$  electron with momentum  $\mathbf{k}$  and energy  $\varepsilon_{\mathbf{k}\sigma}$ . The last term of the Hamiltonian,  $H_{\text{TF}}$ , describes tunneling processes between the FM lead and the quantum dot. It is given by  $H_{\text{TF}} = \sum_{\mathbf{k}\sigma} V_{\mathbf{k}\sigma} (d_{\sigma}^{\dagger} c_{\mathbf{k}\sigma} + c_{\mathbf{k}\sigma}^{\dagger} d_{\sigma})$ , where  $V_{\mathbf{k}\sigma}$  denotes the tunnel matrix elements between the dot and the ferromagnet, which are assumed to be energy independent. The coupling to the FM lead gives rise to the broadening of the dot level, the half width of which is given by  $\Gamma = (\Gamma^{\uparrow} + \Gamma^{\downarrow})/2$ . Assuming the flat density of states of width  $2D$ , with  $D \equiv 1$  used as energy unit, the spin-dependent coupling strength is given by  $\Gamma^{\sigma} = \pi |V_{\sigma}|^2/2$ . It can be further expressed in terms of the spin polarization  $p = (\Gamma^{\uparrow} - \Gamma^{\downarrow})/(\Gamma^{\uparrow} + \Gamma^{\downarrow})$  of the FM lead as  $\Gamma^{\sigma} = (1 \pm p)\Gamma$  [46,48,50].

The effective quantum dot Hamiltonian (2) is not diagonal in the local basis spanned by the following four states:  $|0\rangle$ ,  $|\sigma\rangle$ ,  $|d\rangle$ , for empty, singly occupied with spin  $\sigma$  and doubly occupied dot. However, it can be easily diagonalized and its

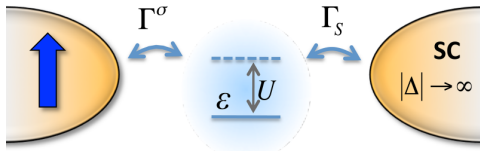


FIG. 1. (Color online) Schematic of the considered system. A single-level quantum dot is coupled to a ferromagnetic and superconducting (SC) lead with coupling strengths  $\Gamma^{\sigma}$  and  $\Gamma_{\text{S}}$ , respectively. The dot level energy is denoted by  $\varepsilon$ , while  $U$  is the Coulomb correlation energy. The superconducting energy gap  $\Delta$  is assumed to be the largest energy scale in the problem, so that the only tunneling processes are exclusively due to the Andreev reflection.

eigenstates are  $|\sigma\rangle$ ,  $|+\rangle$ ,  $|-\rangle$ , where

$$|\pm\rangle = \frac{1}{\sqrt{2}} \left( \sqrt{1 \mp \frac{\delta}{\sqrt{\delta^2 + \Gamma_{\text{S}}^2}}} |0\rangle \pm \sqrt{1 \pm \frac{\delta}{\sqrt{\delta^2 + \Gamma_{\text{S}}^2}}} |d\rangle \right), \quad (3)$$

and  $\delta = \varepsilon + U/2$  denotes the detuning from the particle-hole symmetry point of the dot. On the other hand, the energies of the above states are correspondingly given by  $E_{\pm} = \delta \pm \sqrt{\delta^2 + \Gamma_{\text{S}}^2}$ . The excitation energies of the effective dot Hamiltonian  $H_{\text{QD}}^{\text{eff}}$  result in the following Andreev bound-state energies [16,18,25,26]:

$$E_{\alpha\beta}^A = \alpha \frac{U}{2} + \beta \sqrt{\delta^2 + \Gamma_{\text{S}}^2}, \quad (4)$$

with  $\alpha, \beta = \pm$ .

### B. Andreev transmission and conductance

The transmission coefficient for Andreev processes between the ferromagnetic and superconducting lead is given by [2,4,5,11]

$$T_A(\omega) = \sum_{\sigma} 4\Gamma^{\sigma} \Gamma^{\bar{\sigma}} |\langle\langle d_{\sigma} | d_{\bar{\sigma}} \rangle\rangle_{\omega}^r|^2, \quad (5)$$

where  $\langle\langle d_{\sigma} | d_{\bar{\sigma}} \rangle\rangle_{\omega}^r$  is the Fourier transform of the corresponding off-diagonal retarded Green's function,  $\langle\langle d_{\sigma} | d_{\bar{\sigma}} \rangle\rangle_t^r = -i\Theta(t)\langle\{d_{\sigma}(t), d_{\bar{\sigma}}(0)\}\rangle$ . The linear-response Andreev conductance can be then found from [2,4,5,11]

$$G_A = \frac{2e^2}{h} \int d\omega T_A(\omega) \left( -\frac{\partial f(\omega)}{\partial \omega} \right), \quad (6)$$

with  $f(\omega)$  denoting the Fermi-Dirac distribution function.

### C. Calculation method

Because all the relevant linear-response transport coefficients are expressed in terms of the transmission coefficient,  $T_A(\omega)$ , the main task is to calculate its full energy and dot level detuning dependence. To perform this task in the most accurate manner, we employ the numerical renormalization group method [53–55]. Within this method the conduction band of FM lead is described by a tight-binding chain with exponentially decaying hoppings, which allows one to diagonalize the Hamiltonian iteratively and to find its full many-body eigenstates and eigenenergies. These can then be used to calculate any expectation value of both static and dynamic observables. Since in calculations it is crucial to keep a large number of states at each iteration, it is of vital importance to exploit as many symmetries the Hamiltonian possesses as possible. However, in the present problem, due to the superconducting pairing term in the effective Hamiltonian [cf. Eq. (2)] and the spin dependence of tunneling processes, only the  $z$ th component of the total spin is conserved, which makes the calculations challenging. In particular, here we kept  $N_K = 4^6$  states at each iteration, exploiting one Abelian symmetry for the total spin  $z$ th component, and used the band discretization parameter  $\Lambda = 2$ . To find the Andreev transmission coefficient, we first determined the imaginary part of relevant Green's functions and then, from the



Kramers-Kronig relation, calculated the respective real parts. To obtain most reliable spectral functions from discrete NRG data, we employed the optimal broadening method [57] and used a  $z$ -averaging trick [58], averaging over two different discretizations.

### III. RESULTS AND DISCUSSION

In this section we present and discuss the transport properties of the quantum dot connected to superconducting and ferromagnetic leads. We first study the behavior of the dot's local density of states in the Kondo regime on the strength of the coupling to superconducting lead. In particular, we analyze how the Kondo temperature  $T_K$  changes when  $\Gamma_S$  increases. Then, we study the detuning dependence of the Andreev transmission coefficient and the linear conductance for different temperatures, different coupling strengths, and spin polarization of the ferromagnetic lead.

#### A. Local density of states and the Kondo temperature

The local density of states of the dot is represented by the normalized spectral function  $\pi \Gamma A(\omega) \equiv \sum_{\sigma} \pi \Gamma^{\sigma} A_{\sigma}(\omega)$ , with  $A_{\sigma}(\omega) = -(1/\pi) \text{Im} \langle \langle d_{\sigma} | d_{\sigma}^{\dagger} \rangle \rangle_{\omega}^r$  and  $\langle \langle d_{\sigma} | d_{\sigma}^{\dagger} \rangle \rangle_{\omega}^r$  being the Fourier transform of  $\langle \langle d_{\sigma} | d_{\sigma}^{\dagger} \rangle \rangle_t = -i \Theta(t) \langle \{ d_{\sigma}(t), d_{\sigma}^{\dagger}(0) \} \rangle$ . Figure 2 presents the energy dependence of the normalized dot's level spectral function for different couplings to the superconducting lead  $\Gamma_S$ , as indicated. The spectral function is calculated both in the absence and presence of detuning, i.e., for  $\varepsilon/U = -0.5$  ( $\delta/U = 0$ ) and for  $\varepsilon/U = -0.495$  ( $\delta/U = 0.005$ ). Note that, in principle, in the case of the ferromagnetic lead the Kondo effect is generally suppressed due to the presence of ferromagnetic-contact-induced exchange field  $\Delta \varepsilon_{\text{exch}}$ . Such an exchange field splits the dot levels, removing thus the degeneracy of the ground state, and the Kondo effect becomes destroyed when  $|\Delta \varepsilon_{\text{exch}}| \gtrsim T_K$  [46,47,49,51]. However, the exchange field has this special property that it vanishes at the particle-hole symmetry point  $\delta = 0$ . This is why in Fig. 2(a) the signatures of the Kondo effect are clearly visible, while in Fig. 2(b) the Kondo effect for small  $\Gamma_S$  is suppressed.

Let us first discuss the former case. When  $\Gamma_S = 0$ , the spectral function exhibits the Kondo-Abrikosov-Suhl resonance at the Fermi energy due to the Kondo effect, where  $\pi \Gamma A(0) = 1$  [36]. When the coupling to the superconducting lead increases, the excitation energies between the singly occupied states and the states  $|+\rangle$  and  $|-\rangle$  decrease. As a result, the effective exchange interaction between the dot and the normal lead is increased, and so is the Kondo temperature [28]. This behavior can be clearly seen in Fig. 2(a). Moreover, when  $\Gamma_S$  is relatively large, the height of the resonance becomes diminished. This is associated with the fact that for  $\Gamma_S = U/2$ , all the dot's states become degenerate and the system is truly in the mixed-valence regime, so that the Kondo effect is absent.

For the considered hybrid device, by performing the Schrieffer-Wolff transformation, one can find the effective exchange interaction between the dot and the ferromagnetic lead, which then allows one to estimate the Kondo temperature

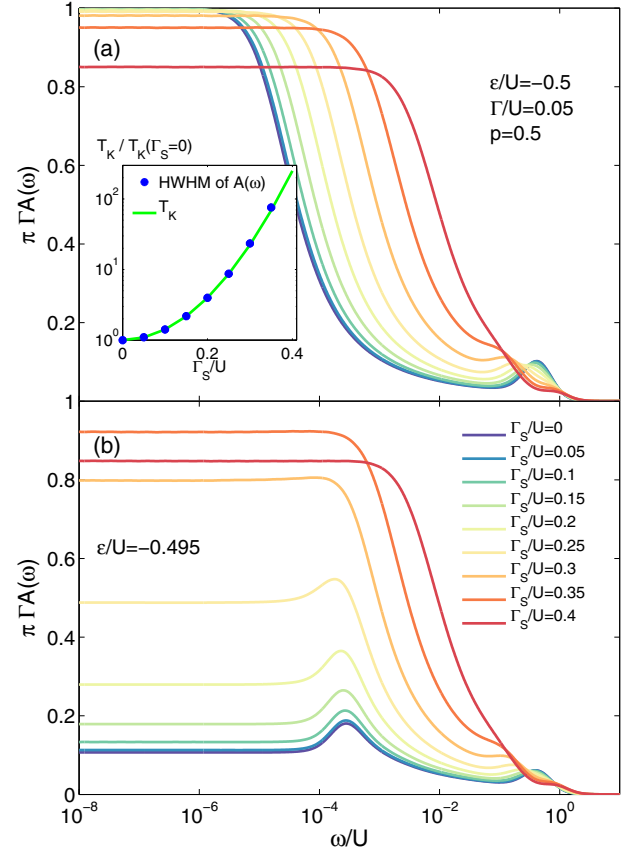


FIG. 2. (Color online) The normalized spectral function of the dot level,  $\pi \Gamma A(\omega)$ , as a function of energy  $\omega$  for different coupling strengths to the superconductor  $\Gamma_S$  calculated for (a)  $\delta/U = 0$  and (b)  $\delta/U = 0.005$ . The inset in (a) shows the  $\Gamma_S$  dependence of the Kondo temperature extracted from the half width at half maximum (HWHM) of the spectral function (points) and the fit as obtained from Eq. (7) with  $\eta \approx 1.5$ . The parameters are  $U/D = 0.1$ ,  $\Gamma/U = 0.05$ ,  $T = 0$ , and  $p = 0.5$ . Note the logarithmic energy scale.

[27,28,59],

$$T_K = \eta \sqrt{\frac{\Gamma U}{2}} \exp \left\{ \frac{\pi [\varepsilon(\varepsilon + U) + \Gamma_S^2]}{2\Gamma U} \frac{\text{arctanh}(p)}{p} \right\}, \quad (7)$$

with  $\eta$  being a constant of the order of unity. From the above formula it clearly follows that increasing  $\Gamma_S$  raises  $T_K$ . Moreover, in the case of ferromagnetic lead and in the absence of exchange field, the Kondo temperature is decreased by a spin polarization dependent factor [46]. The Kondo temperature estimated from the half width at half maximum (HWHM) of the spectral function plotted as a function of  $\Gamma_S$  is shown as bullets in the inset to Fig. 2(a). Clearly, the Kondo temperature rises with increasing the strength of the coupling to the superconducting lead. For comparison, the solid line in the inset shows the Kondo temperature obtained by using Eq. (7). The agreement with numerical data is indeed very good and the numerical constant was found to be  $\eta \approx 1.5$ .

In the case of finite detuning from the particle-hole symmetry point, the Kondo effect is generally suppressed.

Figure 2(b) shows the spectral function calculated for such  $\delta$  that for assumed parameters the exchange field is slightly larger than  $T_K$ . In this situation the interplay of relevant energy scales is clearly visible. When  $\Gamma_S = 0$ , the Kondo resonance is suppressed since  $|\Delta\varepsilon_{\text{exch}}| > T_K$ . However, when increasing the pairing correlations with  $\Gamma_S$ , the Kondo temperature rises and, once  $T_K \gtrsim |\Delta\varepsilon_{\text{exch}}|$ , the Kondo peak becomes restored; see, e.g., the curves for larger  $\Gamma_S$  in Fig. 2(b). Further increase of the coupling to the superconductor eventually kills the Kondo effect, since the system enters the mixed-valence regime.

## B. Andreev transmission and conductance

### 1. Dependence on the coupling strength $\Gamma$

The Andreev transmission coefficient plotted as a function of energy  $\omega$  and dot level detuning  $\delta$  is shown in Fig. 3 for different values of the coupling to the normal lead  $\Gamma$ . The left column corresponds to the case of a nonmagnetic lead, while the right column presents the case when the lead is ferromagnetic. The dashed lines show the energy of respective Andreev bound states; cf. Eq. (4). In the case of a nonmagnetic lead and when the coupling is small,  $T_A(\omega)$  exhibits narrow peaks around the energies corresponding to resonances between the bound states, which occur for  $\delta = \pm\sqrt{U^2/4 - \Gamma_S^2}$ .

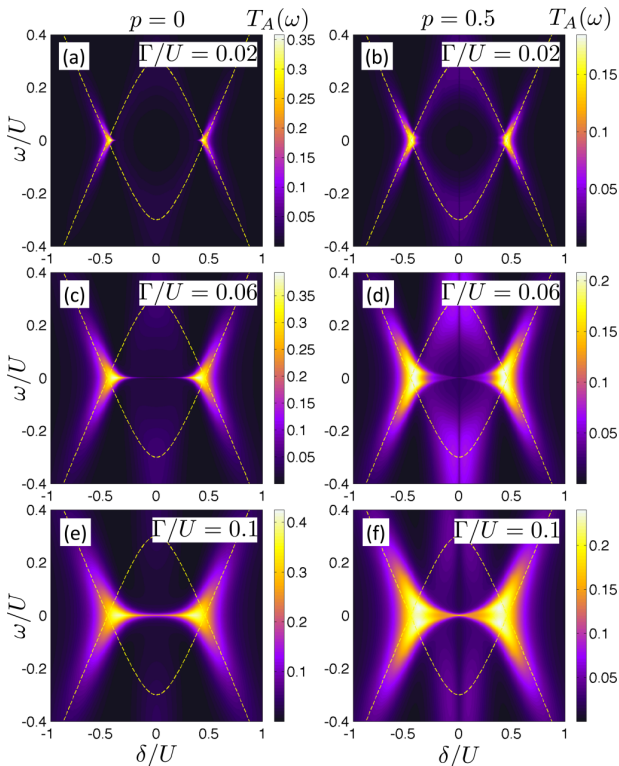


FIG. 3. (Color online) The Andreev transmission coefficient  $T_A(\omega)$  as a function of energy  $\omega$  and dot level detuning  $\delta = \varepsilon + U/2$  in the case of nonmagnetic (left column,  $p = 0$ ) and ferromagnetic (right column,  $p = 0.5$ ) lead calculated for different couplings to normal lead  $\Gamma$ , as indicated in the figure. The dashed line shows the Andreev bound-state energies obtained from Eq. (4). The parameters are  $U/D = 0.1$ ,  $\Gamma_S/U = 0.2$ , and  $T = 0$ .

However, with increasing  $\Gamma$ , the width of those peaks increases and, in addition, an extra resonance at  $\omega = 0$  develops for  $|\delta| \lesssim \sqrt{U^2/4 - \Gamma_S^2}$ ; see Fig. 3(e). In this transport regime the dot is singly occupied and the resonance in  $T_A(\omega)$ , which occurs at the Fermi energy, is due to the Kondo effect.

When the lead is ferromagnetic, the transmission coefficient is suppressed by approximately a factor of 2 as compared to the nonmagnetic case; see Fig. 3. This is due to the fact that transferring Cooper pairs between the superconductor and ferromagnet involves two electrons of opposite spins. While one of those electrons belongs to the spin-majority subband of ferromagnetic lead, the other one is a spin-minority electron. The density of states of minority carriers becomes then a bottleneck for Cooper pair transport [25,26].

While for detunings  $|\delta| > \sqrt{U^2/4 - \Gamma_S^2}$ , that is in the case when the dot occupancy is even, the behavior of  $T_A(\omega)$  is similar to that in the case of  $p = 0$ ; this is completely not the case when the dot is singly occupied, especially for larger  $\Gamma$ . First, one can see that transmission coefficient is enhanced in the singly occupied dot regime not only at low energies, but this enlargement extends to high energies,  $|\omega| \approx U/2$ . Second, the Kondo resonance is now split, which is most visible in the case of  $\Gamma/U = 0.06$ ; see Fig. 3(d). This splitting is due to the proximity effect with a ferromagnetic lead, which results in the exchange field. If  $|\Delta\varepsilon_{\text{exch}}| \gtrsim T_K$ , the Kondo resonance becomes suppressed and there are only side resonances occurring at  $\omega = \pm\Delta\varepsilon_{\text{exch}}$ . Moreover, one can also see that the splitting of the zero-energy peak in  $T_A(\omega)$  changes with  $\delta$ . This is due to a particular dependence of  $\Delta\varepsilon_{\text{exch}}$  on the dot detuning:  $\Delta\varepsilon_{\text{exch}} = 0$  for  $\delta = 0$  and it changes sign when  $\delta$  crosses zero [26]. In fact, a similar split Kondo resonance has recently been observed experimentally in a ferromagnet-quantum-dot-superconductor device [52]. When the coupling to the normal lead increases, both  $T_K$  and  $\Delta\varepsilon_{\text{exch}}$  are enhanced. However, while  $\Delta\varepsilon_{\text{exch}}$  grows algebraically with  $\Gamma$  [26],  $T_K$  increases in an exponential way [36]; cf. Eq. (7). Consequently, for  $\Gamma/U = 0.1$ , the splitting of the Kondo resonance becomes obscured, see Fig. 3(f), since the condition  $|\Delta\varepsilon_{\text{exch}}| \gtrsim T_K$  is only very weakly satisfied.

From the transmission coefficient, by using Eq. (6), one can calculate the dot-level detuning dependence of the linear-response conductance. This is presented in Fig. 4, where the left (right) column corresponds to the nonmagnetic (ferromagnetic) case. Note the different scale for  $G_A$  in the left and right columns of the figure: the conductance for  $p = 0.5$  is approximately two times smaller compared to that in the case of  $p = 0$ . When the coupling is relatively small, see the case for  $\Gamma/U = 0.02$ , the qualitative difference between the  $p = 0$  and  $p > 0$  cases is hardly visible. The linear conductance shows then only two resonant peaks for  $\delta = \pm\sqrt{U^2/4 - \Gamma_S^2}$ , the height of which becomes suppressed with increasing the temperature; see Figs. 4(a) and 4(b). However, for larger couplings between the dot and the normal lead, the differences become more pronounced. This is especially visible in the transport regime where the dot is singly occupied and the interplay of the exchange field and the correlations leading to the Kondo effect become essential.

First of all, one can see that the resonance peaks occurring for  $\delta = \pm\sqrt{U^2/4 - \Gamma_S^2}$  become broadened when increasing the coupling strength  $\Gamma$ . Moreover, the low-temperature

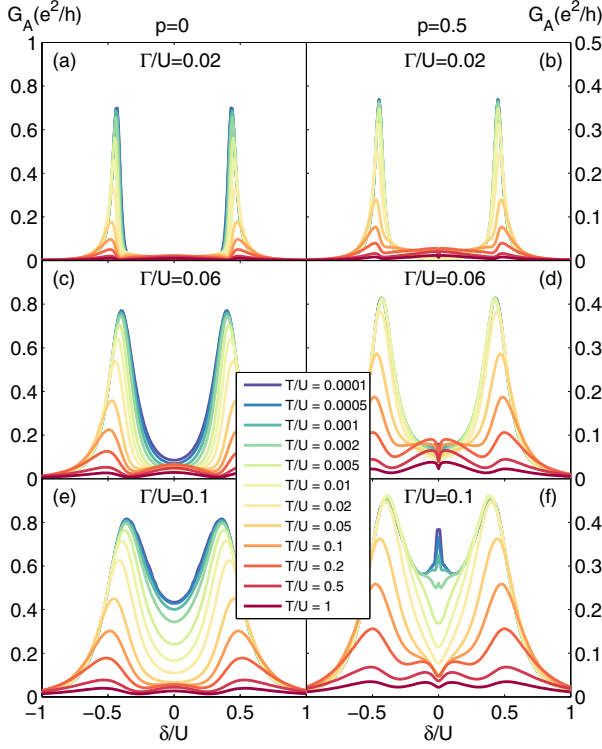


FIG. 4. (Color online) The detuning dependence of the linear-response conductance due to Andreev processes calculated for different temperatures  $T$  and couplings to normal lead  $\Gamma$ , as indicated. The left column corresponds to the case of  $p = 0$ , while the right column shows the case of  $p = 0.5$ . The parameters are the same as in Fig. 3. Note that the scale in the case of  $p = 0.5$  is smaller by a factor of 2 compared to the case of  $p = 0$ .

conductance in the singly occupied regime,  $-\sqrt{U^2/4 - \Gamma_S^2} < \delta < \sqrt{U^2/4 - \Gamma_S^2}$ , rises with enhancing  $\Gamma$ . These two effects result simply from the fact that increasing  $\Gamma$  leads to broadening of the dot levels and to an increase of the Kondo temperature. It reveals as a gradual enhancement of the low- $T$  conductance in the transport regime where the dot is singly occupied. This general tendency can be seen in the case of both nonmagnetic and ferromagnetic leads. However, there are important differences visible especially for  $\Gamma/U = 0.1$ ; see Figs. 4(e) and 4(f). While in the case of a nonmagnetic lead,  $G_A$  in the Kondo valley rises rather uniformly with decreasing  $T$ ; for a ferromagnetic lead, this enhancement is most pronounced for  $\delta = 0$ . In fact, when the dot level is detuned from the particle-hole symmetry point the conductance suddenly drops. This results in a peak in  $G_A$  as a function of  $\delta$ , occurring for  $\delta = 0$ . When the temperature increases, however, this peak becomes smeared and disappears. The occurrence of this peak can be understood by invoking the relevant energy scales in this problem:  $T_K$  and  $\Delta\varepsilon_{\text{exch}}$  (for fixed  $\Gamma_S$ ). By detuning the dot level from  $\delta = 0$ , the exchange field becomes finite and increases with increasing  $|\delta|$ . Consequently, once  $\delta$  is such that  $|\Delta\varepsilon_{\text{exch}}| \gtrsim T_K$ , the Kondo resonance becomes obscured and the conductance drops. In fact, the maximum value of  $G_A$  for  $\delta = 0$  is comparable in both cases of  $p = 0$  and  $p = 0.5$ ;

see Figs. 4(e) and 4(f). In the nonmagnetic case, however,  $G_A$  changes monotonically when moving away from  $\delta = 0$  towards resonances, contrary to the ferromagnetic case, when  $G_A$  behaves in a nonmonotonic way.

## 2. Dependence on the coupling strength $\Gamma_S$

The Andreev transmission coefficient as a function of energy  $\omega$  and dot level detuning  $\delta$  for different couplings to superconducting lead  $\Gamma_S$  is shown in Fig. 5. Again, the right column presents the ferromagnetic lead case, while the left one, for comparison, corresponds to the nonmagnetic case. This figure illustrates how the transmission coefficient changes when  $\Gamma_S$  increases from low to high values, where for

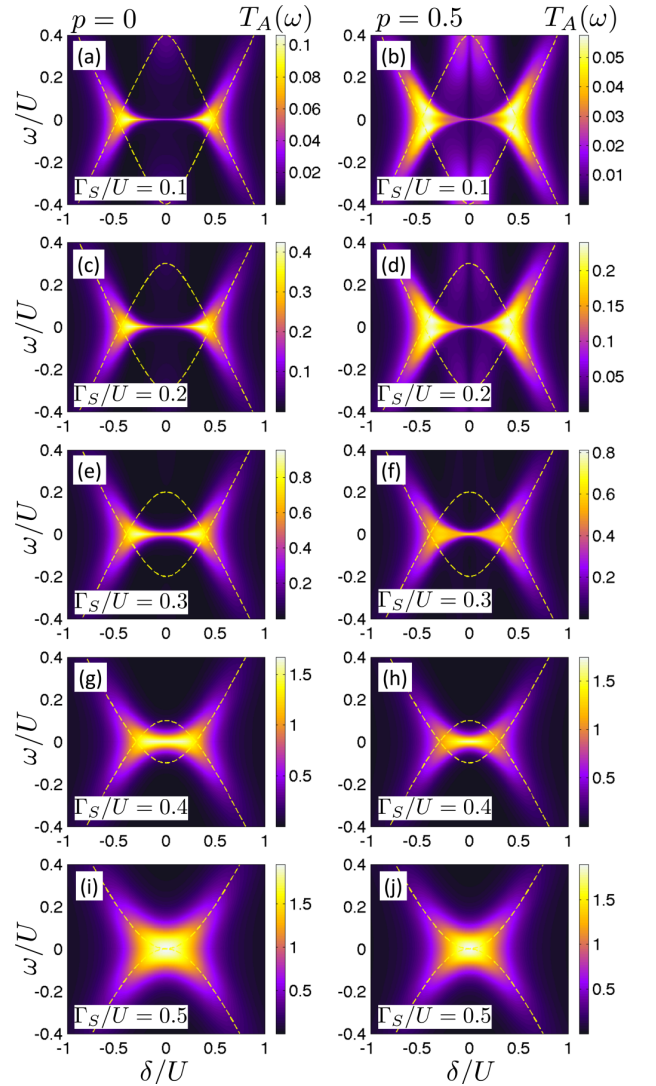


FIG. 5. (Color online) The Andreev transmission coefficient  $T_A(\omega)$  as a function of energy  $\omega$  and dot level detuning  $\delta$  in the case of nonmagnetic (left column,  $p = 0$ ) and ferromagnetic (right column,  $p = 0.5$ ) lead for different couplings to superconducting lead  $\Gamma_S$ , as indicated in the figure. Parameters are the same as in Fig. 3 with  $\Gamma/U = 0.1$ .

$\Gamma_S = U/2$  the Kondo valley is absent and all Andreev bound states are at resonance for  $\delta = 0$ .

First, let us discuss a general tendency, which is visible irrespective of the spin polarization of the normal lead. When  $\Gamma_S$  increases, the resonances for  $\delta = \pm\sqrt{U^2/4 - \Gamma_S^2}$  move towards the particle-hole symmetry point and merge when  $\Gamma_S = U/2$ . Increasing  $\Gamma_S$  is also associated with an enhancement of the Kondo temperature; cf. Eq. (7). As a consequence, one can see that the width of the Kondo peak slightly increases with  $\Gamma_S$ . However, for larger values of  $\Gamma_S$ , see, e.g.,  $\Gamma_S/U \gtrsim 0.4$ , the Kondo peak gets merged with the two resonant peaks and only a single resonant peak occurs with  $T_A(\omega) = 2$ ; see Figs. 5(i) and 5(j).

The difference between the ferromagnetic and nonmagnetic cases is most visible when the coupling to superconductor is relatively low; see the case of  $\Gamma_S/U \lesssim 0.2$  in Fig. 5. For  $\Gamma_S/U \lesssim 0.2$ , one can clearly see the split Kondo resonance in the transmission coefficient. However, further increase of  $\Gamma_S$  decreases the ratio of  $|\Delta\varepsilon_{\text{exch}}|/T_K$ , such that the exchange field effects become suppressed and  $T_A(\omega)$  shows the restored Kondo peak. (Note that  $T_K$  depends exponentially on  $\Gamma_S$  and increases with rising the coupling to the superconductor.) In other words, superconducting correlations win over the ferromagnetic contact proximity effects and the transmission coefficient for  $\Gamma_S/U \gtrsim 0.3$  starts behaving very similarly in both the  $p = 0$  and the finite- $p$  case; see Fig. 5.

This tendency is also clearly visible in the detuning dependence of the linear conductance calculated for different temperatures and values of  $\Gamma_S$  corresponding to Fig. 5, which is shown in Fig. 6. In the nonmagnetic case, increasing  $\Gamma_S$  leads to an enhancement of the linear conductance, until it eventually reaches its maximum value,  $G_A = 4e^2/h$ , for  $\delta = 0$  and  $\Gamma_S = U/2$ . Note that this value persists to relatively high temperatures and starts decreasing when  $T/U \gtrsim 0.01$ ; see Fig. 6(i).

Comparing the left and right column of Fig. 6 reveals the nontrivial differences between the case of ferromagnetic and nonmagnetic leads. Moreover, the differences are now much better resolved compared to Fig. 5, especially at low temperatures. In the case of finite  $p$ , one can clearly see a resonant peak at  $\delta = 0$  for  $\Gamma_S/U \lesssim 0.3$ . As mentioned above, this peak is associated with the fact that the exchange field vanishes at the particle-hole symmetry point and the Kondo peak develops, while it becomes suddenly suppressed at small but finite detuning. For larger couplings to superconducting lead, the superconducting proximity effects dominate, and the differences between the ferromagnetic and nonmagnetic cases are suppressed. Consequently, the detuning dependence of the conductance is then qualitatively the same in both cases, though small quantitative differences can still be observed; see Fig. 6.

### 3. Dependence on the spin polarization $p$

In the previous sections we have discussed the detuning dependence of both  $T_A(\omega)$  and  $G_A$  when either  $\Gamma$  or  $\Gamma_S$  was varied. Now, we assume constant couplings and study how the Andreev transport properties depend on the degree of spin polarization of ferromagnetic lead. In other words, while approximately keeping the same superconducting parity

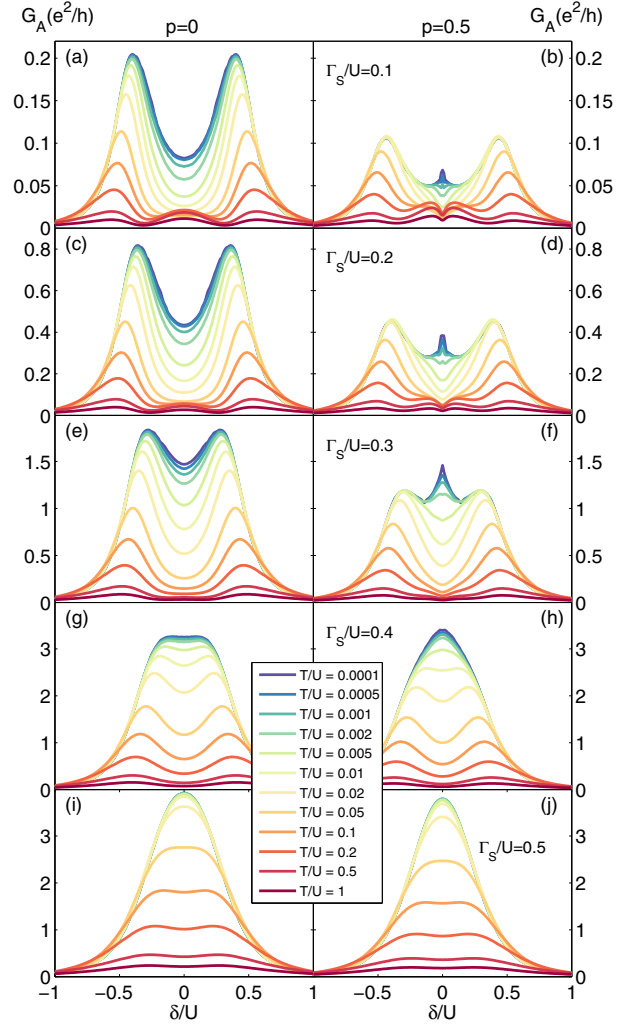


FIG. 6. (Color online) The detuning dependence of the linear conductance due to Andreev reflection for different temperatures. The left column corresponds to the case of  $p = 0$ , and the right column to the case of  $p = 0.5$ . Each row presents the results obtained for different coupling  $\Gamma_S$ , as indicated in the panels on the right-hand side. Parameters are the same as in Fig. 3 with  $\Gamma/U = 0.1$ .

correlations and correlations leading to the Kondo effect, we gradually increase the ferromagnetic proximity effects.

The corresponding detuning and energy dependence of the Andreev transmission coefficient is shown in Fig. 7, where each panel corresponds to different  $p$ , starting from  $p = 0$  to  $p = 0.9$ . Two main features can be immediately noticed. First, increasing spin polarization leads to an overall suppression of  $T_A(\omega)$ . The reason for it has already been explained earlier and is related with the mismatch between the majority and minority subbands of the ferromagnet. Injecting or subtracting Cooper pairs involves two electrons of opposite spin, thus in an ideal case of a half metal, the Andreev reflection will be fully blocked. Second, the splitting of the Kondo peak with increasing  $p$  can be clearly visible. It can be seen that this splitting increases with increasing  $p$ , which is directly

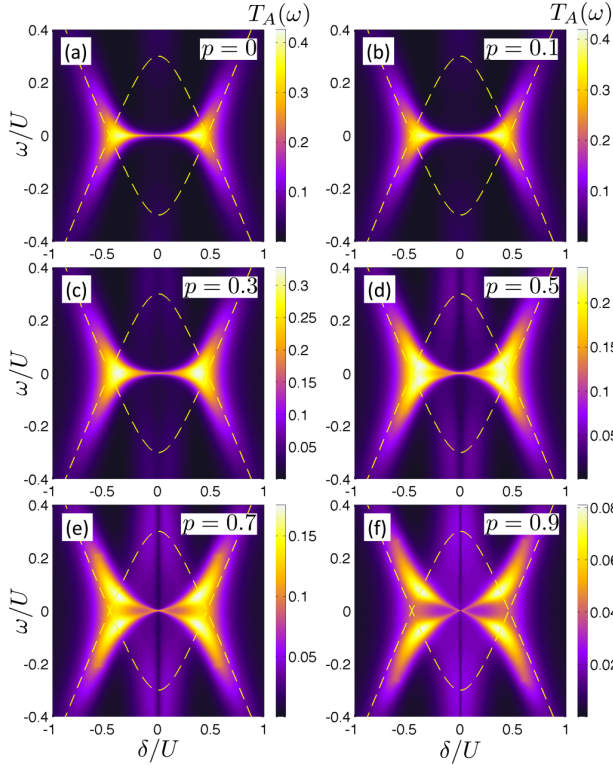


FIG. 7. (Color online) The energy and dot level detuning dependence of the Andreev transmission coefficient for different spin polarization  $p$  of ferromagnetic lead, as indicated. Parameters are the same as in Fig. 3 with  $\Gamma/U = 0.1$  and  $\Gamma_S/U = 0.2$ .

associated with the fact that the magnitude of  $\Delta\varepsilon_{\text{exch}}$  grows with rising  $p$  [26].

Interestingly, one can also note that rising spin polarization  $p$  leads to an enhancement of  $T_A(\omega)$  in the singly occupied regime for energies much larger than those corresponding to the split Kondo resonance. In fact, this enhancement can be seen in the whole range of energy  $\omega$  considered in the figure, except for  $\omega \approx 0$ ; see, e.g., Fig. 7(f). Moreover, a similar enhancement could be also observed in other figures presenting the energy and detuning dependence of  $T_A(\omega)$ ; cf. Figs. 3(d) and 5(b). The maximum of  $T_A(\omega)$  in this energy range occurs around the position of the Andreev bound states. Furthermore, although such enhancement of Andreev transmission occurs in both cases of ferromagnetic and nonmagnetic leads, it is more pronounced in the former case. This finding implies that ferromagnetic proximity effects are relevant not only at low-energy scales, of the order of  $\Delta\varepsilon_{\text{exch}}$  where they condition the occurrence of the Kondo effect, but they also play an important role at larger energy scales. This is in accordance with an observation that the exchange field can lead to a full spin polarization of the Hubbard resonances in the spectral function of the dot level, even when  $|\Delta\varepsilon_{\text{exch}}| \ll U$  [60].

Intuitively, the enhancement of the Andreev transmission for  $p > 0$  can be explained as follows. For ferromagnetic lead the local density of states of the quantum dot  $A_\sigma(\omega)$  becomes spin polarized at all energy scales. This polarization is such that if  $A_\uparrow(\omega)$  is enhanced with respect to the  $p = 0$  case,

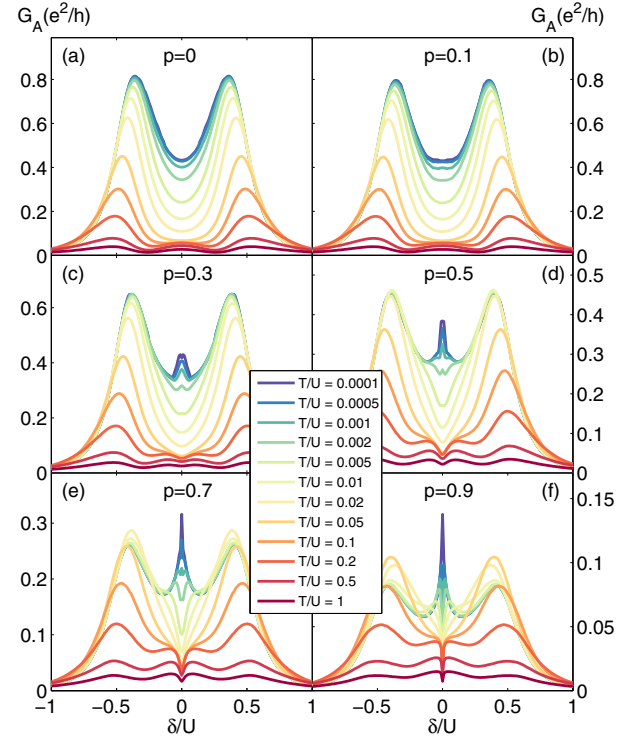


FIG. 8. (Color online) The dot level detuning dependence of the Andreev conductance for different temperatures and for different spin polarization  $p$ , as indicated. Parameters are the same as in Fig. 3 with  $\Gamma/U = 0.1$  and  $\Gamma_S/U = 0.2$ .

then  $A_\downarrow(-\omega)$  is also enhanced, while  $A_\downarrow(\omega)$  and  $A_\uparrow(-\omega)$  are suppressed. Thus, the probability of finding a pair of electrons with opposite spins and energies increases. Consequently, in the case of ferromagnetic lead the Andreev transport becomes enhanced. However, one needs to keep in mind that since Andreev transmission is proportional to  $(1 - p^2)\Gamma^2$ , cf. Eq. (5), increasing the spin polarization of the ferromagnetic lead will eventually result in the suppression of  $T_A(\omega)$ .

The dependence of the linear conductance on the detuning parameter  $\delta$  calculated for different spin polarization  $p$  and temperature  $T$  is shown in Fig. 8. When the spin polarization increases, the magnitude of the low-temperature Andreev conductance gets suppressed and a peak for  $\delta = 0$  develops. The relative height of this peak increases with rising  $p$ . This is due to the fact that  $\Delta\varepsilon_{\text{exch}}$  grows with  $p$  [26]. When the temperature increases, the peak in  $G_A$  as a function of  $\delta$  in the center of the Coulomb blockade becomes smeared out, since thermal fluctuations suppress the Kondo effect. Interestingly, at high temperatures the dependence of conductance on the parameter  $\delta$  in the singly occupied dot regime again becomes nonmonotonic.  $G_A$  shows then a small minimum, which develops for  $\delta = 0$ ; see Fig. 8. This minimum is associated with the fact that  $T_A(\omega)$  in the case of a ferromagnetic lead is suppressed in a narrow region around  $\delta = 0$  for energies larger than the Kondo temperature; see also Figs. 3(d), 5(b), and 7.

## IV. CONCLUSIONS

In this paper we have studied the transport properties of a hybrid superconductor-quantum-dot-ferromagnet device, focusing on the Andreev reflection processes. The system was modeled by an effective Hamiltonian with an on-dot pairing term in the limit of large superconducting energy gap. The calculations were performed by using the numerical renormalization group method, employing the optimal broadening, and  $z$ -averaging tricks to obtain high quality spectral data for the determination of the Andreev transmission coefficient. Generally, all transport characteristics revealed a subtle interplay of the three important energy scales in the problem: the Kondo temperature, the superconducting pairing correlations, and the effective exchange field.

In particular, it was shown that the Andreev transmission exhibits the Kondo resonance in the singly occupied dot regime, which can be split by the exchange field. Moreover, a suppression of the Andreev transmission was found at the particle-hole symmetry point for energies larger than the Kondo temperature. These effects were also revealed in the dot level detuning dependence of the Andreev conductance for different temperatures. At low  $T$ ,  $G_A$  showed a peak for

$\delta = 0$  due to the Kondo effect, however, for larger temperatures this peak developed into a local minimum. Furthermore, the exchange-field effects were shown to dominate transport behavior by splitting the Kondo resonance for moderate couplings to the superconducting lead. With increasing the strength of this coupling, the ferromagnetic proximity effects were however becoming less and less important. This was associated with an increase of the Kondo temperature when increasing the superconducting pairing correlations, which led to a lowering of the relevant excitation energies and, thus, to an enhancement of the exchange interaction between the spin in the dot and spins of itinerant electrons.

## ACKNOWLEDGMENTS

We acknowledge discussions with J. Barnaś and P. Trocha. This work was supported by the National Science Centre in Poland through the Project No. DEC-2013/10/E/ST3/00213 and Marie Curie FP-7-Reintegration-Grants (Grant No. CIG-303 689) within the 7th European Community Framework Programme.

- 
- [1] R. Fazio and R. Raimondi, *Phys. Rev. Lett.* **80**, 2913 (1998).
  - [2] Q.-F. Sun, J. Wang, and T.-H. Lin, *Phys. Rev. B* **59**, 3831 (1999).
  - [3] J. C. Cuevas, A. Levy Yeyati, and A. Martín-Rodero, *Phys. Rev. B* **63**, 094515 (2001).
  - [4] Y. Zhu, Q.-F. Sun, and T.-H. Lin, *Phys. Rev. B* **65**, 024516 (2001).
  - [5] J.-F. Feng and S.-J. Xiong, *Phys. Rev. B* **67**, 045316 (2003).
  - [6] Y. Avishai, A. Golub, and A. D. Zaikin, *Phys. Rev. B* **67**, 041301(R) (2003).
  - [7] M. Krawiec and K. I. Wysokiński, *Supercond. Sci. Technol.* **17**, 103 (2004).
  - [8] Y. Tanaka, N. Kawakami, and A. Oguri, *J. Phys. Soc. Jpn.* **76**, 074701 (2007).
  - [9] T. Domański, A. Donabidowicz, and K. I. Wysokiński, *Phys. Rev. B* **76**, 104514 (2007).
  - [10] J. Bauer, A. Oguri, and A. C. Hewson, *J. Phys.: Condens. Matter* **19**, 486211 (2007).
  - [11] T. Domański, A. Donabidowicz, and K. I. Wysokiński, *Phys. Rev. B* **78**, 144515 (2008).
  - [12] C. Karrasch, A. Oguri, and V. Meden, *Phys. Rev. B* **77**, 024517 (2008).
  - [13] T. Hecht, A. Weichselbaum, J. von Delft, and R. Bulla, *J. Phys.: Condens. Matter* **20**, 275213 (2008).
  - [14] C. Karrasch and V. Meden, *Phys. Rev. B* **79**, 045110 (2009).
  - [15] T. Meng, S. Florens, and P. Simon, *Phys. Rev. B* **79**, 224521 (2009).
  - [16] D. Fütterer, M. Governale, M. G. Pala, and J. König, *Phys. Rev. B* **79**, 054505 (2009).
  - [17] V. Koerting, B. M. Andersen, K. Flensberg, and J. Paaske, *Phys. Rev. B* **82**, 245108 (2010).
  - [18] B. Sothmann, D. Fütterer, M. Governale, and J. König, *Phys. Rev. B* **82**, 094514 (2010).
  - [19] B. M. Andersen, K. Flensberg, V. Koerting, and J. Paaske, *Phys. Rev. Lett.* **107**, 256802 (2011).
  - [20] K. I. Wysokiński, *J. Phys.: Condens. Matter* **24**, 335303 (2012).
  - [21] D. Fütterer, J. Swiebodzinski, M. Governale, and J. König, *Phys. Rev. B* **87**, 014509 (2013).
  - [22] A. Oguri, Y. Tanaka, and J. Bauer, *Phys. Rev. B* **87**, 075432 (2013).
  - [23] J. Barański and T. Domański, *J. Phys.: Condens. Matter* **25**, 435305 (2013).
  - [24] K. Bocian and W. Rudziński, *Eur. Phys. J. B* **86**, 439 (2013).
  - [25] I. Weymann and P. Trocha, *Phys. Rev. B* **89**, 115305 (2014).
  - [26] K. P. Wójcik and I. Weymann, *Phys. Rev. B* **89**, 165303 (2014).
  - [27] R. Zitko, J. S. Lim, R. López, and R. Aguado, *Phys. Rev. B* **91**, 045441 (2015).
  - [28] T. Domański, I. Weymann, M. Barańska, and G. Górski (unpublished).
  - [29] R. S. Deacon, Y. Tanaka, A. Oiwa, R. Sakano, K. Yoshida, K. Shibata, K. Hirakawa, and S. Tarucha, *Phys. Rev. Lett.* **104**, 076805 (2010); *Phys. Rev. B* **81**, 121308(R) (2010).
  - [30] E. J. H. Lee, X. Jiang, R. Aguado, G. Katsaros, C. M. Lieber, and S. De Franceschi, *Phys. Rev. Lett.* **109**, 186802 (2012).
  - [31] J. D. Pillet, P. Joyez, R. Žitko, and M. F. Goffman, *Phys. Rev. B* **88**, 045101 (2013).
  - [32] E. J. H. Lee, X. Jiang, M. Houzet, R. Aguado, Ch. M. Lieber, S. De Franceschi, *Nat. Nanotechnol.* **9**, 79 (2014).
  - [33] J. Schindele, A. Baumgartner, R. Maurand, M. Weiss, and C. Schönenberger, *Phys. Rev. B* **89**, 045422 (2014).
  - [34] A. Kumar, M. Gaim, D. Steininger, A. Levy Yeyati, A. Martín-Rodero, A. K. Hüttel, and C. Strunk, *Phys. Rev. B* **89**, 075428 (2014).
  - [35] J. Kondo, *Prog. Theor. Phys.* **32**, 37 (1964).
  - [36] A. C. Hewson, *The Kondo Problem to Heavy Fermions* (Cambridge University Press, Cambridge, UK, 1993).
  - [37] D. Goldhaber-Gordon, H. Shtrikman, D. Mahalu, D. Abusch-Magder, U. Meirav, and M. A. Kastner, *Nature (London)* **391**, 156 (1998).
  - [38] S. Cronenwett, T. H. Oosterkamp, and L. P. Kouwenhoven, *Science* **281**, 540 (1998).

- [39] S. De Franceschi, L. Kouwenhoven, C. Schönberger, and W. Wernsdorfer, *Nat. Nanotechnol.* **5**, 703 (2010).
- [40] A. Martín-Rodero and A. Levy-Yeyati, *Adv. Phys.* **60**, 899 (2011).
- [41] Ch. Schoenenberger and R. Maurand, *Physics* **6**, 75 (2013).
- [42] L. Yu, *Acta Phys. Sin.* **21**, 75 (1965).
- [43] H. Shiba, *Prog. Theor. Phys.* **40**, 435 (1968).
- [44] A. I. Rusinov, *Zh. Eksp. Teor. Fiz.* **56**, 2047 (1969) [*Sov. Phys. JETP* **29**, 1101 (1969)].
- [45] A. F. Andreev, *J. Exptl. Theoret. Phys.* **46**, 1823 (1964) [*Sov. Phys. JETP* **19**, 1228 (1964)].
- [46] J. Martinek, Y. Utsumi, H. Imamura, J. Barnaś, S. Maekawa, J. König, and G. Schön, *Phys. Rev. Lett.* **91**, 127203 (2003).
- [47] A. N. Pasupathy, R. C. Bialczak, J. Martinek, J. E. Grose, L. A. K. Donev, P. L. McEuen, and D. C. Ralph, *Science* **306**, 86 (2004).
- [48] M. Sindel, L. Borda, J. Martinek, R. Bulla, J. König, G. Schön, S. Maekawa, and J. von Delft, *Phys. Rev. B* **76**, 045321 (2007).
- [49] J. Hauptmann, J. Paaske, and P. Lindelof, *Nat. Phys.* **4**, 373 (2008).
- [50] I. Weymann, *Phys. Rev. B* **83**, 113306 (2011).
- [51] M. Gaass, A. K. Hüttel, K. Kang, I. Weymann, J. von Delft, and Ch. Strunk, *Phys. Rev. Lett.* **107**, 176808 (2011).
- [52] L. Hofstetter, A. Geresdi, M. Aagesen, J. Nygard, C. Schönberger, and S. Csonka, *Phys. Rev. Lett.* **104**, 246804 (2010).
- [53] K. G. Wilson, *Rev. Mod. Phys.* **47**, 773 (1975).
- [54] R. Bulla, T. A. Costi, and T. Pruschke, *Rev. Mod. Phys.* **80**, 395 (2008).
- [55] We used an open-access Budapest NRG code, <http://www.phy.bme.hu/~dmnrg/>; O. Legeza, C. P. Moca, A. I. Tóth, I. Weymann, and G. Zaránd, [arXiv:0809.3143](https://arxiv.org/abs/0809.3143).
- [56] A. V. Rozhkov and D. P. Arovas, *Phys. Rev. B* **62**, 6687 (2000).
- [57] A. Freyn and S. Florens, *Phys. Rev. B* **79**, 121102(R) (2009).
- [58] V. L. Campo and L. N. Oliveira, *Phys. Rev. B* **72**, 104432 (2005).
- [59] M. M. Salomaa, *Phys. Rev. B* **37**, 9312 (1988).
- [60] Sz. Csonka, I. Weymann, and G. Zarand, *Nanoscale* **4**, 3635 (2012).





## Perfect spin polarization in T-shaped double quantum dots due to the spin-dependent Fano effect

Krzysztof P. Wójcik\* and Ireneusz Weymann†

Faculty of Physics, Adam Mickiewicz University, Umultowska 85, 61-614 Poznań, Poland

(Received 16 June 2014; revised manuscript received 26 August 2014; published 16 September 2014)

We study the spin-resolved transport properties of T-shaped double quantum dots coupled to ferromagnetic leads. Using the numerical renormalization group method, we calculate the linear conductance and the spin polarization of the current for various model parameters and at different temperatures. We show that an effective exchange field due to the presence of ferromagnets results in different conditions for Fano destructive interference in each spin channel. This spin dependence of the Fano effect leads to perfect spin polarization, the sign of which can be changed by tuning the dots' levels. Large spin polarization occurs due to Coulomb correlations in the dot, which is not directly coupled to the leads, while finite correlations in the directly coupled dot can further enhance this effect. Moreover, we complement accurate numerical results with a simple qualitative explanation based on analytical expressions for the zero-temperature conductance. The proposed device provides a prospective example of an electrically controlled, fully spin-polarized current source, which operates without an external magnetic field.

DOI: 10.1103/PhysRevB.90.115308

PACS number(s): 72.25.Mk, 73.63.Kv, 85.75.-d, 73.23.Hk

## I. INTRODUCTION

Efficient generation and control of spin currents at the nanoscale is one of the main goals of spin nanoelectronics [1–5]. This is because highly spin-polarized currents can be used to address and detect the spin state of a magnetic nanostructure, such as, e.g., a magnetic quantum dot or a single molecular magnet [6–8], which is of vital importance for applications in information storage technologies. One of the easiest ways to generate high spin polarization  $\mathcal{P}$  of the current is to apply an external magnetic field to the system. If one considers then a singly occupied quantum dot, the current becomes fully spin-polarized provided the transport voltage is smaller than the corresponding Zeeman splitting of the dot's level. However, this method has two drawbacks: First, the magnetic field needs to be strong enough to ensure that  $\mathcal{P} \approx 1$  in a sufficiently large range of bias voltage, which, however, can lead to undesired effects in the nanosystem, on which the spin-polarized current is to act. Second, changing the sign of  $\mathcal{P}$  requires a change in the direction of the magnetic field, which in typical experiments cannot be realized at a rate comparable to operations one would like to perform in a competitive spintronic device.

It has recently been shown that these disadvantages can be overcome by using a quantum dot or a molecule strongly coupled to ferromagnetic leads [9]. The presence of ferromagnets results then in the occurrence of an exchange field, which leads to the splitting of the dot level similarly to an external magnetic field [10–14]. Now one obtains a splitting, whose sign and magnitude can be controlled by a gate voltage, without any need to apply an external magnetic field. This splitting can lead to an enhancement of the spin polarization. However, to reach full spin polarization, the system needs to be highly left-right asymmetric [9,15].

In this paper, we propose a device with which one can induce perfect spin polarization without an external magnetic

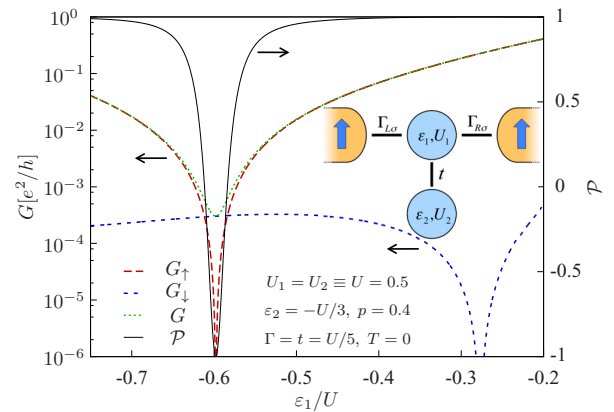


FIG. 1. (Color online) The spin-resolved linear conductance,  $G_\sigma$ , the total conductance,  $G$ , and the spin polarization,  $\mathcal{P}$ , obtained by the numerical renormalization group method, as a function of the first dot level  $\varepsilon_1$  for typical DQD parameters indicated in the figure. The spin-dependent Fano effect leads to perfect spin polarization, the sign of which can be controlled by tuning the dot level position. See Sec. II for details of the model and method.

field that can be controlled by purely electrical means. The device does not need to be asymmetric either. It consists of a double quantum dot (DQD) in a T-shaped geometry coupled to external ferromagnetic leads. In this geometry, only one of the dots is coupled directly to the leads, while the second dot is coupled indirectly, through the first dot; see the inset of Fig. 1. In T-shaped DQDs, the interference of different conduction paths can lead to Fano antiresonance in the linear conductance [16–18]. In addition, the exchange field induced by the coupling to ferromagnets gives rise to the spin splitting of the dots' levels. We will show that this leads to different conditions for destructive Fano interference in each spin channel. As a result, there is a range of DQD level positions where the difference between the conductance in each spin channel is as large as a few orders of magnitude, and the spin polarization becomes essentially perfect. This is illustrated in Fig. 1, which shows the linear conductance

\*kpwojck@amu.edu.pl

†weymann@amu.edu.pl

and the spin polarization as a function of the first dot level position for typical DQD parameters indicated in the figure, calculated by using the numerical renormalization group (NRG) method [19]. The mechanism leading to  $|\mathcal{P}| \rightarrow 1$  is clearly visible: the spin-resolved conductance  $G_\sigma$  displays Fano antiresonance at different  $\varepsilon_1$ . This gives rise to full spin polarization, which changes sign just at the level position where  $G$  is minimum. Importantly, the whole operation is performed without any external magnetic field and can be controlled by only electrical means.

Recently, the transport properties of T-shaped DQDs coupled to nonmagnetic leads have been analyzed by Dias da Silva *et al.* [20]. They focused on the role of an external magnetic field and demonstrated that such a system may work as a spin valve, producing spin polarization of the current  $\mathcal{P} \approx \pm 1$  in an appropriately adjusted field. This effect also stems from the spin-dependent Fano effect, in which the positions of Fano dips in respective spin channels are shifted with respect to each other. Similar spin filtering effects have also been studied in transport through a quantum dot side-coupled to a quantum wire [21–23]. In our device with ferromagnetic contacts, we show that the same is possible without applying any magnetic field. The spin polarization is then controlled by tuning the DQD's levels, which is, no doubt, preferable from an application point of view. We note that the transport properties of T-shaped DQDs with ferromagnetic contacts have already been addressed in a few papers [24–27]. These considerations were, however, restricted to a rather weak-coupling regime, and the effects of the exchange field were not properly taken into account. Our analysis is performed with the aid of NRG, which allows us to study the effects related to a ferromagnetic-contact-induced exchange field in a very accurate way.

This paper has the following structure: Having introduced the model and method in Sec. II, in Sec. III we discuss the behavior of the spectral function determining the linear conductance, and we explain the physical reasons for the occurrence of enhanced spin polarization in the system. We also provide approximate analytical formulas for the exchange field, which agree well with the NRG results. Finally, we present the results of NRG calculations for the linear conductance and the spin polarization in Sec. IV, and we conclude the paper in Sec. V.

## II. MODEL AND METHOD

We consider a double quantum dot forming a T-shaped configuration coupled to ferromagnetic leads whose magnetizations are oriented in parallel; see the inset of Fig. 1. The first dot is coupled directly to the left (right) lead with coupling strength  $\Gamma_{L\sigma}$  ( $\Gamma_{R\sigma}$ ), while the second dot is coupled to the first one through the hopping parameter  $t$ . The Hamiltonian of the system has the form

$$H = H_F + H_T + H_{\text{DQD}}, \quad (1)$$

where

$$H_F = \sum_{r=L,R} \sum_{k\sigma} \varepsilon_{rk\sigma} c_{rk\sigma}^\dagger c_{rk\sigma} \quad (2)$$

is the Hamiltonian of ferromagnetic leads treated in a noninteracting particle approximation, the tunneling Hamiltonian is

given by

$$H_T = \sum_{r=L,R} \sum_{k\sigma} V_{rk\sigma} (d_{1\sigma}^\dagger c_{rk\sigma} + c_{rk\sigma}^\dagger d_{1\sigma}), \quad (3)$$

and the DQD Hamiltonian reads

$$H_{\text{DQD}} = \sum_{j\sigma} \varepsilon_{j\sigma} d_{j\sigma}^\dagger d_{j\sigma} + \sum_j U_j d_{j\uparrow}^\dagger d_{j\uparrow} d_{j\downarrow}^\dagger d_{j\downarrow} + t \sum_\sigma (d_{1\sigma}^\dagger d_{2\sigma} + d_{2\sigma}^\dagger d_{1\sigma}). \quad (4)$$

Here,  $d_{j\sigma}$  annihilates an electron with spin  $\sigma$  on dot  $j$ ,  $c_{rk\sigma}$  annihilates an electron with spin  $\sigma$  and momentum  $k$  in lead  $r$ ,  $\varepsilon_{j\sigma}$  and  $\varepsilon_{rk\sigma}$  denote the energies of respective electrons,  $U_j$  is the Coulomb interaction on dot  $j$ , and  $V_{rk\sigma}$  denotes the corresponding tunnel matrix element. The spin-dependent coupling to the contact  $r$  is given by  $\Gamma_{r\sigma} = \sum_k \pi \rho_{r\sigma} |V_{rk\sigma}|^2$ , where  $\rho_{r\sigma}$  is the spin-dependent, normalized density of states of lead  $r$ . Here, we model the coupling by  $\Gamma_{r\sigma} = (1 + \sigma p)\Gamma_r$ , where  $p$  is the spin polarization of the ferromagnets and  $\Gamma_r = (\Gamma_{r\uparrow} + \Gamma_{r\downarrow})/2$ . In the following, we assume  $\Gamma_L = \Gamma_R \equiv \Gamma/2$ . We also assume that the Coulomb correlations between the two dots are very weak and can be neglected. We use the band half-width as the energy unit,  $D \equiv 1$ .

The linear-response conductance in spin channel  $\sigma$  can be found from [28]

$$G_\sigma = \frac{e^2}{h} \Gamma_\sigma \int d\omega \frac{\partial f(\omega)}{\partial \omega} \text{Im} \langle\langle d_{1\sigma} | d_{1\sigma}^\dagger \rangle\rangle_\omega^{\text{ret}}, \quad (5)$$

where  $\Gamma_\sigma = \Gamma_{L\sigma} + \Gamma_{R\sigma}$ ,  $f(\omega)$  is the Fermi-Dirac distribution function, and  $\langle\langle d_{1\sigma} | d_{1\sigma}^\dagger \rangle\rangle_\omega^{\text{ret}}$  denotes the Fourier transform of the retarded Green's function of the first quantum dot.

To obtain reliable results of high accuracy for our strongly interacting system, we employ the numerical renormalization group method [19]. By using the complete eigenbasis of the NRG Hamiltonian, we construct the thermal density matrix of the system [29,30], which allows us to calculate various correlation functions at arbitrary temperatures. Here, to perform calculations, we use the Budapest Flexible DM-NRG code [31,32].

The main quantity in which we are interested, apart from linear conductance, is the spin polarization, which is defined as

$$\mathcal{P} \equiv \frac{G_\uparrow - G_\downarrow}{G_\uparrow + G_\downarrow}. \quad (6)$$

At zero temperature, formula (5) simplifies considerably to  $G_\sigma = (e^2/h)\pi \Gamma_\sigma \mathcal{A}_{1\sigma}(0)$ , where  $\mathcal{A}_{1\sigma}(\omega) = -\text{Im} \langle\langle d_{1\sigma} | d_{1\sigma}^\dagger \rangle\rangle_\omega^{\text{ret}} / \pi$  denotes the spin-resolved spectral function of the first dot. Then, the spin polarization can be expressed in terms of the normalized spectral function,  $\mathcal{A}_{1\sigma}(\omega) = \pi \Gamma_\sigma \mathcal{A}_{1\sigma}(\omega)$ , taken at  $\omega = 0$ , as  $\mathcal{P} = [\mathcal{A}_{1\uparrow}(0) - \mathcal{A}_{1\downarrow}(0)] / \mathcal{A}_1(0)$ , with  $\mathcal{A}_1(\omega) = \sum_\sigma \mathcal{A}_{1\sigma}(\omega)$ .

## III. ORIGIN OF ENHANCED SPIN POLARIZATION

Since the linear conductance and the spin polarization are expressed in terms of the first dot's spectral function, we will focus on its behavior. To understand the origin of large spin polarization in the considered system, we first consider the case

of noninteracting T-shaped DQD and then study the effect of Coulomb correlations.

### A. Noninteracting case

For  $U_1 = U_2 = 0$ , with the aid of the equation of motion, the spectral function of the first dot can be expressed as

$$A_{1\sigma}(\omega) = \frac{1}{\pi} \frac{\Gamma_\sigma}{[\omega - \varepsilon_{1\sigma} - t^2/(\omega - \varepsilon_{2\sigma})]^2 + \Gamma_\sigma^2}. \quad (7)$$

Then, the spin-resolved linear conductance at zero temperature is given by

$$G_\sigma = \frac{e^2}{h} \frac{\Gamma_\sigma^2}{(\varepsilon_{1\sigma} - t^2/\varepsilon_{2\sigma})^2 + \Gamma_\sigma^2}. \quad (8)$$

Let us now consider some limiting cases. For nonmagnetic leads,  $p = 0$ , and in the absence of magnetic field,  $\varepsilon_{j\sigma} = \varepsilon_j$ , the linear conductance at  $T = 0$  is given by

$$G = \frac{2e^2}{h} \frac{\Gamma^2}{(\varepsilon_1 - t^2/\varepsilon_2)^2 + \Gamma^2}, \quad (9)$$

which for  $\varepsilon_1 = 0$  yields

$$G = \frac{2e^2}{h} \frac{E^2}{1 + E^2}, \quad (10)$$

with  $E = \varepsilon_2/\Gamma_2$  and  $\Gamma_2 = t^2/\Gamma$ . This is the well-known Fano formula describing symmetric antiresonance as a function of energy  $E$  [16,33]. For  $\varepsilon_1 = 0$ , the half-width of the minimum in  $G$  is given by  $t^2/\Gamma$ . When  $\varepsilon_1 \neq 0$ , the antiresonance is still located at  $\varepsilon_2 = 0$ , however it becomes asymmetric [18].

In the presence of an external magnetic field  $B$ , the position of the Fano antiresonance depends on spin, see Eq. (8), since it occurs at  $\varepsilon_{2\sigma} = \varepsilon_2 + \sigma B/2 = 0$ , where  $g\mu_B \equiv 1$ . Consequently, while for one spin direction the conductance is finite, for the other one it can be fully suppressed, leading to  $|\mathcal{P}| = 1$ . Assuming  $p = 0$  and  $\varepsilon_{1\sigma} = \varepsilon_{2\sigma} = \varepsilon + \sigma B/2$ , the spin polarization is then given by

$$\mathcal{P} = \frac{\varepsilon B[t^4 - (\varepsilon^2 - B^2/4)^2]}{(\varepsilon^2 + B^2/4)t^4 + (\varepsilon^2 - B^2/4)^2(\varepsilon^2 + B^2/4 + \Gamma^2 - 2t^2)}. \quad (11)$$

For  $\varepsilon = B/2$ , one has  $\mathcal{P} = 1$ , while for  $\varepsilon = -B/2$ ,  $\mathcal{P} = -1$ . Thus, for finite  $B$ , the spin polarization can be enhanced to its maximum value, and its sign can be changed, depending on the DQD's levels. This effect is completely destroyed in  $B = 0$ , unless  $p \neq 0$ . In the case of ferromagnetic leads and in the absence of magnetic field (henceforth we assume  $\varepsilon_{j\sigma} \equiv \varepsilon_j$ ), for the spin polarization of the linear conductance, one finds

$$\mathcal{P} = \frac{2p}{1 + p^2} \frac{(\varepsilon_1 - t^2/\varepsilon_2)^2}{(\varepsilon_1 - t^2/\varepsilon_2)^2 + (1 - p^2)\Gamma^2/(1 + p^2)}. \quad (12)$$

From this formula, it follows that  $\mathcal{P} = 0$  for  $\varepsilon_1\varepsilon_2 = t^2$  and  $\mathcal{P} = 2p^2/(1 + p^2)$  for  $\varepsilon_2 = 0$ , irrespective of  $\varepsilon_1$ . Thus, the spin polarization is finite,  $0 \leq \mathcal{P} \leq 2p/(1 + p^2)$ , but it does not change sign and is always smaller than unity for  $p < 1$ .

The spin-resolved conductance and the spin polarization for noninteracting dots are plotted in Fig. 2. In the absence of magnetic field, for  $\varepsilon_1 = 0$ , the linear conductance in each spin

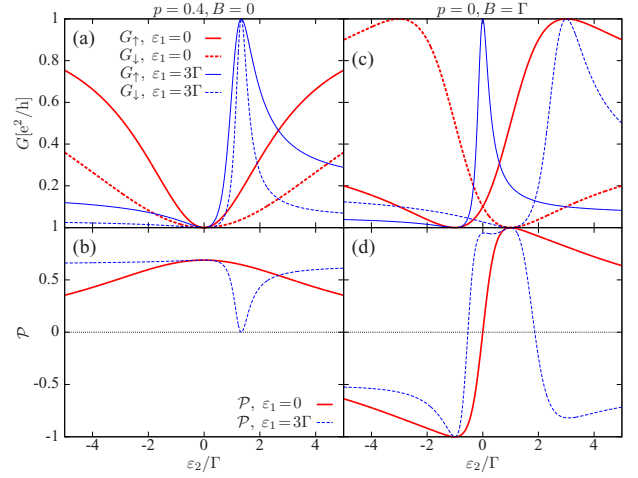


FIG. 2. (Color online) The spin-resolved linear conductance (first row) and the spin polarization (second row) as a function of  $\varepsilon_2$  for two values of  $\varepsilon_1$ , as indicated, and for  $t = 2\Gamma$  in the case of noninteracting DQDs. The left column corresponds to  $p = 0.4$  and  $B = 0$ , while the right column to  $p = 0$  and  $B = \Gamma$ .

channel displays a symmetric antiresonance as a function of  $\varepsilon_2$  located at  $\varepsilon_2 = 0$ , which becomes asymmetric once  $\varepsilon_1 \neq 0$ ; see Fig. 2(a). The spin polarization is also asymmetric for  $\varepsilon_1 \neq 0$ . Moreover,  $\mathcal{P}$  is positive in the whole range of  $\varepsilon_2$  and becomes fully suppressed for  $\varepsilon_2/\Gamma = t^2/(\varepsilon_1\Gamma) = 4/3$ ; see Fig. 2(b). At this point, the linear conductance reaches its maximum value, irrespective of spin channel  $\sigma$ . In the case of a finite magnetic field and nonmagnetic leads, the Fano antiresonance is asymmetric in each spin channel even for  $\varepsilon_1 = 0$  [Fig. 2(c)], and the minimum in  $G_\sigma$  occurs at different  $\varepsilon_2$ . This leads to full spin polarization  $\mathcal{P}$ , which can change sign in a certain range of  $\varepsilon_2$ ; see Fig. 2(d). Figure 2 clearly demonstrates the difference between the two cases discussed above. In the case of noninteracting dots, spin-dependent tunneling due to  $\Gamma_\uparrow \neq \Gamma_\downarrow$  (in the absence of  $B$ ) does not lead to a spectacular dependence of  $\mathcal{P}$  on the DQD's levels.

### B. Interacting case

The spin polarization of the T-shaped DQD with ferromagnetic contacts for  $B = 0$  can be enhanced considerably when one includes the interactions in the dots. For finite  $U_1$  and  $U_2$ , the Green's function of the first dot is given by

$$\langle\langle d_{1\sigma} | d_{1\sigma}^\dagger \rangle\rangle_\omega^{-1} = \omega - \varepsilon_1 - \Sigma_{1\sigma}(\omega) - \frac{t^2}{\omega - \varepsilon_2 - \Sigma_{2\sigma}(\omega)} + i\Gamma_\sigma, \quad (13)$$

where the self-energy  $\Sigma_{j\sigma}$  is defined as

$$\Sigma_{j\sigma}(\omega) = U_j \frac{\langle\langle d_{j\sigma} n_{j\bar{\sigma}} | d_{1\sigma}^\dagger \rangle\rangle_\omega}{\langle\langle d_{j\sigma} | d_{1\sigma}^\dagger \rangle\rangle_\omega} \quad (\bar{\sigma} \equiv -\sigma). \quad (14)$$

One can now use the equation-of-motion technique to find the higher-order Green's functions and solve the problem by using an appropriate decoupling scheme. This is, however, not the goal of our paper, since we calculate the Green's

functions by NRG, which enables us to obtain very accurate results. Nevertheless, to get some intuitive understanding of what happens in correlated T-shaped DQDs, let us consider the zero-temperature conductance (note that for  $w = 0$ , the self-energy is real),

$$G_\sigma = \frac{e^2}{h} \frac{\Gamma_\sigma^2}{\{\varepsilon_1 + \Sigma_{1\sigma}(0) - t^2/[\varepsilon_2 + \Sigma_{2\sigma}(0)]\}^2 + \Gamma_\sigma^2}. \quad (15)$$

Then, we employ the simplest mean-field approximation to the self-energies,  $\Sigma_{j\sigma} \approx U_j \langle n_{j\bar{\sigma}} \rangle$ , which allows us to extract a few interesting conclusions from Eq. (15). The most important one is that when  $\varepsilon_2 + U_2 \langle n_{2\bar{\sigma}} \rangle = 0$ , the conductance in spin channel  $\sigma$  becomes suppressed due to the Fano destructive interference. If  $\langle n_{2\uparrow} \rangle \neq \langle n_{2\downarrow} \rangle$ , the conditions for conductance suppression are different in each spin channel. The spin imbalance in dot-level occupation can be induced by the presence of an exchange field, as described in the following subsection.

The difference in the positions of Fano antiresonances for different spin channels is illustrated in Fig. 1. Indeed,  $G_\uparrow$  has a minimum for different  $\varepsilon_1$  compared to  $G_\downarrow$ , and the resulting  $\mathcal{P}$  reaches  $\pm 1$ . Moreover, it can be observed that  $\mathcal{P}$  changes sign at the level position for which the total conductance is minimum.

The second significant conclusion, which can be drawn from Eq. (15), is that it is sufficient to have different occupations for given spin only in the second dot. This implies that the first dot does not need to be interacting. Finally, the enhanced spin polarization occurs when the second dot is in the local moment regime,  $-U_2 < \varepsilon_2 < 0$ , while no such restriction is imposed on the first dot.

### C. Exchange field

The coupling to external leads gives rise to renormalization of the DQD's levels. Since in the case of ferromagnetic leads the coupling  $\Gamma_\sigma$  depends on spin direction, the level renormalization is also spin-dependent. This results in spin-splitting of the levels,  $\Delta\varepsilon_{\text{exch}}^{(j)} = \delta\varepsilon_{j\uparrow} - \delta\varepsilon_{j\downarrow}$ , where  $\Delta\varepsilon_{\text{exch}}^{(j)}$  is the exchange field on dot  $j$  and  $\delta\varepsilon_{j\sigma}$  denotes the respective spin-dependent level renormalization.

Contrary to the Zeeman splitting caused by an external magnetic field, the sign and magnitude of the splitting induced by ferromagnetic leads can be tuned by changing the position of the quantum dot levels [10,34]. To understand the effect of an exchange field on transport through T-shaped DQDs, we will consider some limiting situations. In the case of  $t = 0$ , the exchange field on the first dot can be found within the perturbation theory, which in the second order gives [10,34]

$$\Delta\varepsilon_{\text{exch}}^{(1)} = \frac{2p\Gamma}{\pi} \log \left| \frac{\varepsilon_1}{\varepsilon_1 + U_1} \right|. \quad (16)$$

Note that  $\Delta\varepsilon_{\text{exch}}^{(1)}$  clearly results from correlations and vanishes for  $U_1 = 0$ . Moreover, it also vanishes at the particle-hole symmetry point,  $\delta_1 = 0$ , with  $\delta_j = \varepsilon_j + U_j/2$ , denoting the detuning of dot  $j$  from the symmetry point.

Now, let us see what happens in the second dot. Since, as follows from previous discussion, to obtain large spin polarization it is sufficient to have interactions only in the second dot, we now assume  $U_1 = 0$ . The hybridization of the

second dot depends on the local density of states of the first dot,  $\Gamma_{2\sigma}(\omega) = \pi A_{1\sigma}^0(\omega)t^2$ , where  $A_{1\sigma}^0(\omega)$  denotes the spectral function of the first dot in the case of  $t = 0$ ,

$$A_{1\sigma}^0(\omega) = \frac{1}{\pi} \frac{\Gamma_\sigma}{(\omega - \varepsilon_1)^2 + \Gamma_\sigma^2}. \quad (17)$$

In this way, the model becomes equivalent to the Anderson model with a Lorentzian density of states. Since the leads are ferromagnetic,  $A_{1\sigma}^0(\omega)$  depends on spin through  $\Gamma_\sigma$ , and so does  $\Gamma_{2\sigma}(\omega)$ , which for low energies ( $\omega = 0$ ) and  $\varepsilon_1 = 0$  becomes equal to  $t^2/\Gamma_\sigma$ . Note that the dependence of couplings on spin is opposite in each dot: while  $\Gamma_\uparrow > \Gamma_\downarrow$ , for the second dot the spin-down level is more strongly coupled than the spin-up one,  $\Gamma_{2\uparrow}(0) < \Gamma_{2\downarrow}(0)$ . In the second order of perturbation theory, renormalization of the second dot's level is given by

$$\delta\varepsilon_{2\sigma} = \frac{1}{\pi} \int d\omega \left[ \frac{\Gamma_{2\sigma}(\omega)f^-(\omega)}{\varepsilon_2 - \omega} + \frac{\Gamma_{2\bar{\sigma}}(\omega)f(\omega)}{\omega - \varepsilon_2 - U_2} \right], \quad (18)$$

where  $f^-(\omega) = 1 - f(\omega)$ . When assuming the limit of zero temperature, taking  $\varepsilon_1 = 0$ , and approximating the hybridization by  $\Gamma_{2\sigma}(\omega) = t^2/\Gamma_\sigma$ , for the exchange field  $\Delta\varepsilon_{\text{exch}}^{(2)}$  one finds

$$\Delta\varepsilon_{\text{exch}}^{(2)} = -\frac{t^2}{\pi\Gamma} \frac{2p}{1-p^2} \log \left| \frac{\varepsilon_2}{\varepsilon_2 + U_2} \right|. \quad (19)$$

Although this formula is very simplified, it still allows us to correctly extract the intuitive behavior of the system. First of all, one can see that the presence of ferromagnets is also revealed in the second dot. It leads to the exchange field, which has a similar dependence on the level position, in the way that it vanishes for  $\delta_2 = 0$ , but it has a different magnitude and sign (for given detuning) compared to  $\Delta\varepsilon_{\text{exch}}^{(1)}$ ; cf. Eq. (16). Thus, if one would like to mimic the effect of an external magnetic field by the exchange field, the detuning in each dot should have an opposite sign. However, it is worth stressing that the exchange field offers much more flexibility, since it allows the spin-splitting to be tuned in each dot separately by gate voltages. For completeness, we also present the zero-temperature formula for the exchange field  $\Delta\varepsilon_{\text{exch}}^{(2)}$  in the case of  $\varepsilon_1 \neq 0$  and for energy-dependent hybridization  $\Gamma_{2\sigma}(\omega)$ . It is given by

$$\begin{aligned} \Delta\varepsilon_{\text{exch}}^{(2)} = & \sum_\sigma \sigma \frac{t^2}{2} [L_{\Gamma_\sigma}(U_2 - \Delta) - L_{\Gamma_\sigma}(\Delta)] \\ & - \sum_\sigma \sigma \frac{t^2}{\pi} \arctan \left( \frac{\varepsilon_1}{\Gamma_\sigma} \right) [L_{\Gamma_\sigma}(U_2 - \Delta) + L_{\Gamma_\sigma}(\Delta)] \\ & - \sum_\sigma \sigma \frac{t^2}{2\pi} L_{U_2 - \Delta}(\Gamma_\sigma) \log \frac{(\varepsilon_2 + U_2)^2}{\varepsilon_1^2 + \Gamma_\sigma^2} \\ & + \sum_\sigma \sigma \frac{t^2}{2\pi} L_\Delta(\Gamma_\sigma) \log \frac{\varepsilon_2^2}{\varepsilon_1^2 + \Gamma_\sigma^2}, \end{aligned} \quad (20)$$

where  $L_y(x) = x/(x^2 + y^2)$  and  $\Delta = \varepsilon_1 - \varepsilon_2$ .

We note that in the case of a noninteracting first dot, the model corresponds to the single-impurity Anderson model with nonconstant density of states. At low temperatures, one should then expect a single-stage Kondo effect to occur [20,35–40]. However, due to the presence of the exchange

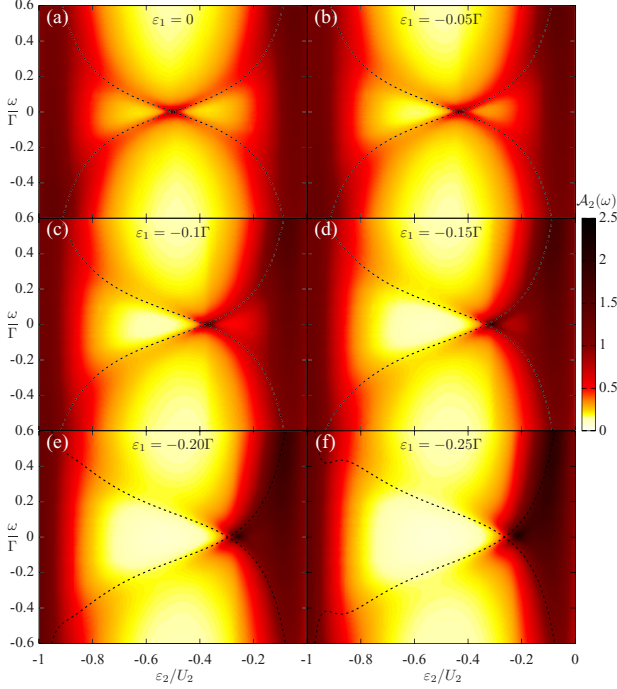


FIG. 3. (Color online) The normalized spectral function of the second dot  $\mathcal{A}_2(\omega)$  plotted as a function of energy  $\omega$  and position of the second dot level  $\epsilon_2$  for (a)  $\epsilon_1 = 0$ , (b)  $\epsilon_1 = -0.05\Gamma$ , (c)  $\epsilon_1 = -0.1\Gamma$ , (d)  $\epsilon_1 = -0.15\Gamma$ , (e)  $\epsilon_1 = -0.2\Gamma$ , and (f)  $\epsilon_1 = -0.25\Gamma$ . The dashed lines present the results obtained from analytical formula (20). The parameters are  $U_1 = 0$ ,  $U_2 = U = 0.5$ ,  $\Gamma = U/5$ ,  $t = \Gamma/2$ , and  $p = 0.4$ .

field, the Kondo resonance becomes suppressed, which happens once  $|\Delta\epsilon_{\text{exch}}^{(2)}| \gtrsim T_K$ , where  $T_K$  is the Kondo temperature. Thus, for T-shaped DQDs with ferromagnetic contacts, the Kondo effect is generally suppressed. In Fig. 3, we show the NRG results on the normalized spectral function of the second quantum dot,  $\mathcal{A}_2(\omega) = \sum_{\sigma} \pi t^2 A_{2\sigma}(\omega) / \Gamma_{\sigma}$ , where  $A_{2\sigma}(\omega)$  denotes the spectral function of the second dot. For  $\epsilon_1 = 0$ , at the particle-hole symmetry point,  $\delta_2 = 0$ , the effect of the exchange field is negligible and the spectral function exhibits Kondo resonance [35–37]. The Kondo temperature, defined as the half-width at half-maximum of the Kondo peak in the spectral function, for parameters assumed in Fig. 3 and for  $\epsilon_1 = 0$  and  $\delta_2 = 0$ , is equal to  $T_K \approx 0.005\Gamma$ . When  $\delta_2 \neq 0$  and  $|\Delta\epsilon_{\text{exch}}^{(2)}| \gtrsim T_K$ , the exchange field leads to the spin splitting of the Kondo resonance; see Fig. 3(a). We note that such a splitting of the Kondo effect due to the presence of ferromagnets has already been observed experimentally in single quantum dots [11–13]. When  $\epsilon_1 \neq 0$ , the splitting of the Kondo resonance becomes asymmetric around  $\delta_2 = 0$ , and the point where the exchange field is suppressed moves toward the resonance at  $\epsilon_2 = 0$  until it actually merges with the resonant peak. One observes then a spin splitting whose magnitude can be tuned, but the sign does not change; see Fig. 3. In the case of  $|\Delta\epsilon_{\text{exch}}^{(2)}| \gtrsim T_K$ , the Kondo peak is split and the spectral function shows only side resonances, which occur at  $\omega = \pm|\Delta\epsilon_{\text{exch}}^{(2)}|$  [13]. The dashed lines in Fig. 3 show

the positions of these resonances based on Eq. (20). As can be seen, they match nicely with the numerical data for all values of  $\epsilon_1$  presented in the figure.

As follows from the above discussion, the effective exchange field induced by the presence of ferromagnets can be conveniently tuned by sweeping the gate voltages and adjusting the positions of the DQD’s levels. This is of importance from an experimental point of view. We also note that in general the splitting of the Kondo peak can also occur in the case of relatively large hopping between the dots [38–40]. However, for parameters assumed in Fig. 3, such splitting is absent [39]. The observed splitting is exclusively due to the presence of the exchange field.

#### IV. NUMERICAL RESULTS

In the following, we present and discuss the numerical results on the spin-resolved linear conductance  $G_{\sigma}$  and the spin polarization  $\mathcal{P}$ . Previous discussion showed that for the full spin polarization to occur, it is necessary to have interactions in the second dot, while the first dot can be noninteracting. Therefore, we first study the case of  $U_1 = 0$  and finite  $U_2$ , and then we also include the interactions in the first dot and analyze how they influence the linear conductance and the spin polarization of the system. Finally, we discuss the effect of finite temperature on transport properties.

We also note that to observe an enhanced spin polarization and tune its sign, one can fix the level of one of the dots and tune the other one. Since it is crucial to have an exchange field in the second dot, we thus fix the level of the second dot, such that  $\delta_2 \neq 0$ , and tune the position of the first dot. (This is what is presented in Fig. 1 for a general interacting case.) Nevertheless, we also present the density plot of the spin polarization as a function of both  $\epsilon_1$  and  $\epsilon_2$ .

##### A. The case of noninteracting first dot

The total linear conductance and spin polarization in the case of  $U_1 = 0$  and  $U_2 = U = 0.5$  are shown in Fig. 4 for two values of the coupling  $\Gamma$  and for different hoppings  $t$  between the dots. The position of the second dot level is  $\epsilon_2 = -U/3$ , to assure that the exchange field effects are present in the system. Since the strength of the exchange field is proportional to  $\Gamma_2 = t^2/\Gamma$ , cf. Eq. (19), by increasing  $t$  one also increases the magnitude of the exchange-field-induced spin splitting of the second dot’s level. As a consequence, the conditions for destructive interference change in each spin channel with tuning  $t$ , and the dependence on  $t$  is different for each coupling  $\Gamma$ ; see Fig. 4.

First of all, one can see that by increasing  $t$ , the total conductance decreases. For large  $t$  [see, e.g., the case of  $t = 1.5\Gamma$  in Fig. 4(a) or  $t = \Gamma$  in Fig. 4(b)], the conductance is three or four orders of magnitude smaller than the conductance quantum. Although these values are rather small, they are still measurable experimentally. In fact, similar values of  $G$  occur in quantum dots in the cotunneling regime [41]. For  $\epsilon_1$ , where  $G$  takes its minimum value, the spin polarization changes sign and becomes negative. This sign change becomes enhanced upon increasing the exchange field (increasing  $t$ ), and for large

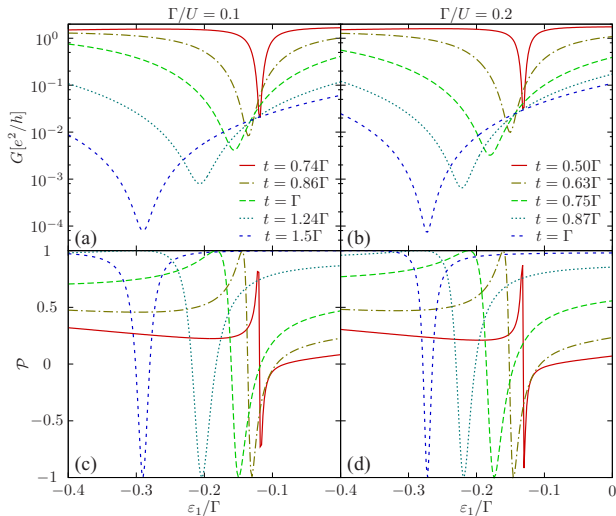


FIG. 4. (Color online) The linear conductance (first row) and the spin polarization (second row) as a function of  $\varepsilon_1$  for  $\Gamma/U = 0.1$  (left column) and  $\Gamma/U = 0.2$  (right column) calculated for different values of the hopping  $t$  between the dots, as indicated. The parameters are  $U_1 = 0$ ,  $U_2 = U = 0.5$ ,  $\varepsilon_2 = -U/3$ ,  $p = 0.4$ , and  $T = 0$ .

$t$ , the spin polarization becomes perfect and changes sign from  $+1$  to  $-1$ . Thus, for given  $t$  and nonzero detuning  $\delta_2 \neq 0$ , the spin polarization can be tuned by only electrical means, namely by shifting the position of the first dot level with a gate voltage. The role of the exchange field is crucial here, which can be deduced from the fact that the effect disappears for  $\delta_2 = 0$  when  $\Delta\varepsilon_{\text{exch}}^{(2)} = 0$ ; cf. Eq. (19).

The minimum in  $G_\sigma$  occurs for such  $\varepsilon_1$  that  $\Sigma_{2\sigma}(\omega = 0) = -\varepsilon_2$ ; cf. Eq. (15). This is explicitly illustrated in Fig. 5, which shows the spin-dependent conductance,  $G_\sigma$ , and self-energy for  $\omega = 0$ ,  $\Sigma_{2\sigma}(\omega = 0)$ , and a function of  $\varepsilon_1$  for two different hoppings:  $t = 0.7\Gamma$  (left column) and  $t = \Gamma$  (right column). Since in calculations we assumed  $\varepsilon_2/U_2 = -1/3$ , the minimum in  $G_\sigma$  occurs precisely at the point where  $\Sigma_{2\sigma}(\omega = 0) = 1/3$ ; see Fig. 5.

As mentioned in the preceding section, for  $U_1 = 0$  the model is equivalent to the single-impurity Anderson model with a Lorentzian density of states. Then, the Friedel sum rule [42] allows one to relate the conductance through the system to the spin-resolved occupation of the second dot. For  $t \ll \Gamma$ , it can be written as  $G_\sigma = (e^2/h) \cos^2(\pi \langle n_{2\sigma} \rangle)$  [23]. Thus, the conductance in spin channel  $\sigma$  should be suppressed when  $\langle n_{2\sigma} \rangle = 1/2$ . However, for stronger hoppings,  $t \sim \Gamma$ , the condition  $\langle n_{2\sigma} \rangle = 1/2$  is not necessarily fulfilled and the application of the Friedel sum rule becomes more complicated. The spin-resolved occupations of the second dot as a function of  $\varepsilon_1$  are shown in Figs. 5(c) and 5(d). The critical occupation for which the conductance becomes minimum is still of the order of  $1/2$ , but its precise value is different. On the other hand, for larger values of  $t$ , the phase shift, which determines the position of the conductance minimum, is given by a rather complex expression even in the particle-hole symmetry point [20]. In the case of significant particle-hole symmetry breaking, as considered in this paper (note that

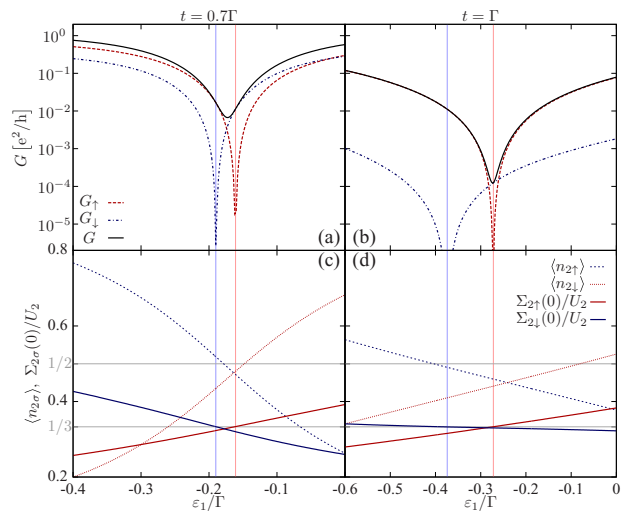


FIG. 5. (Color online) (a) and (b) The spin-resolved and total conductances, and (c) and (d) the spin-dependent occupations together with the self-energies for  $\omega = 0$  of the side-coupled quantum dot as a function of  $\varepsilon_1$  calculated by NRG for  $\Gamma/U = 0.2$ ,  $t = 0.7\Gamma$  (left column), and  $t = \Gamma$  (right column). The vertical dotted lines mark the positions where the minima in spin-dependent conductance occur. The horizontal lines correspond to  $-\varepsilon_2/U_2 = 1/3$  and  $1/2$ . The minimum of  $G_\sigma$  occurs at the crossing of  $\Sigma_{2\sigma}(0)/U_2$  with  $1/3$ ; cf. Eq. (15). The Friedel sum rule predicts the minimum to occur when  $\langle n_{2\sigma} \rangle = 1/2$ . The other parameters are the same as in Fig. 4.

this is a necessary condition to have the exchange field present in the system), it is very difficult to utilize the Friedel sum rule; nevertheless, the condition  $\Sigma_{2\sigma}(\omega = 0) = -\varepsilon_2$  is always correct as long as  $T = 0$ . Finally, one can notice that the simplest mean-field approximation used in Sec. III,  $\Sigma_{2\sigma} = U_2 \langle n_{2\sigma} \rangle$ , leading to the condition  $\langle n_{2\sigma} \rangle = -\varepsilon_2/U_2$  for the minimum in  $G_\sigma$ , is also violated; see Figs. 5(c) and 5(d). However, the qualitative analysis of the system behavior based on this approximation is still sound.

The explicit dependence of the linear conductance and spin polarization on both  $\varepsilon_1$  and  $t$  is shown in Fig. 6 for  $\Gamma/U = 0.2$ . The conductance is plotted on a logarithmic scale to indicate the position of the conductance minimum due to the Fano effect. Clearly, the minimum occurs at different level positions in each spin channel; see Figs. 6(c) and 6(d). Moreover, the spin-up conductance is generally much larger than the spin-down conductance, except for the level position where  $G_\uparrow$  is suppressed by the Fano effect. Consequently, for this level position, the total conductance has a minimum [Fig. 6(b)], while the spin polarization changes sign and becomes  $\mathcal{P} \approx -1$ , otherwise  $\mathcal{P} \approx 1$ ; see Fig. 6(a). Note also that the position of the minimum in  $G_\sigma$  occurs at different  $\varepsilon_1$  for different  $t$ , which results directly from the dependence of the exchange field on  $t$ .

## B. Fully interacting case

Let us now include the interactions in the first dot,  $U_1 \neq 0$ . The linear conductance and spin polarization as a function of the first dot detuning  $\delta_1$  for different correlations  $U_1$  are shown

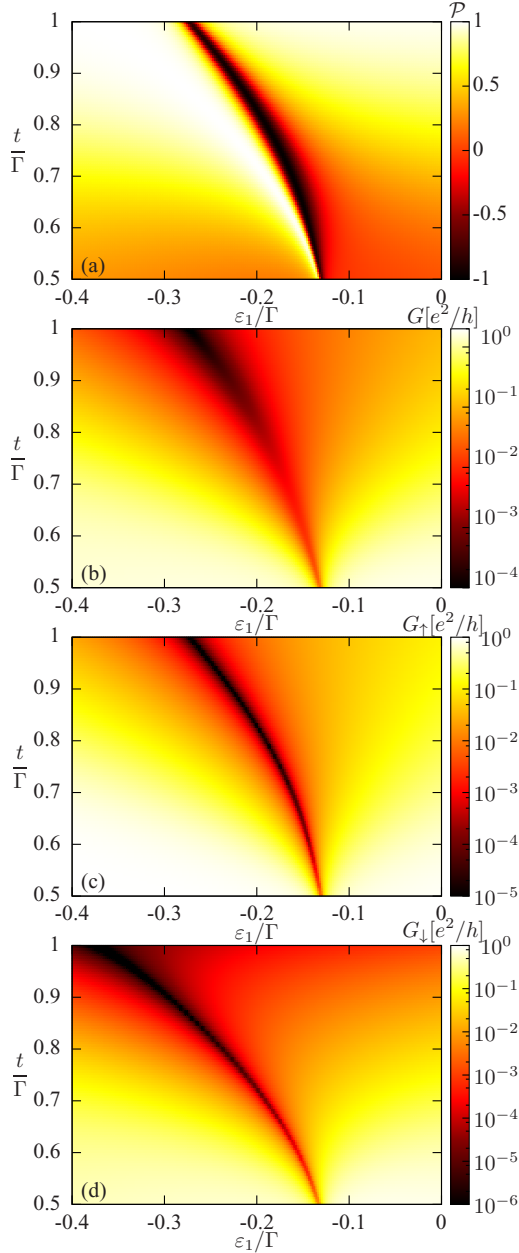


FIG. 6. (Color online) The spin polarization  $\mathcal{P}$  (a) and the logarithm of the linear conductance  $G$  (b),  $G_{\uparrow}$  (c), and  $G_{\downarrow}$  (d) as a function of  $\varepsilon_1$  and  $t$  calculated for parameters the same as in Fig. 4 with  $\Gamma/U = 0.2$ .

in Fig. 7. This figure is calculated for  $U_2 = 0.5$ ,  $\Gamma = t = U_2/5$ , and  $\varepsilon_2 = -U_2/3$ . For finite  $U_1$  and  $\delta_1 \neq 0$ , the exchange field also develops in the first dot, cf. Eq. (16). We note that treating the exchange field in each dot separately is mainly to increase the intuitive understanding of the physics. However, we need to stress that for larger hoppings,  $t \gtrsim \Gamma$ , transport occurs through molecular many-body states of the DQD, and formulas (19) and (20) based on perturbation theory in  $t$  present only very crude estimations.

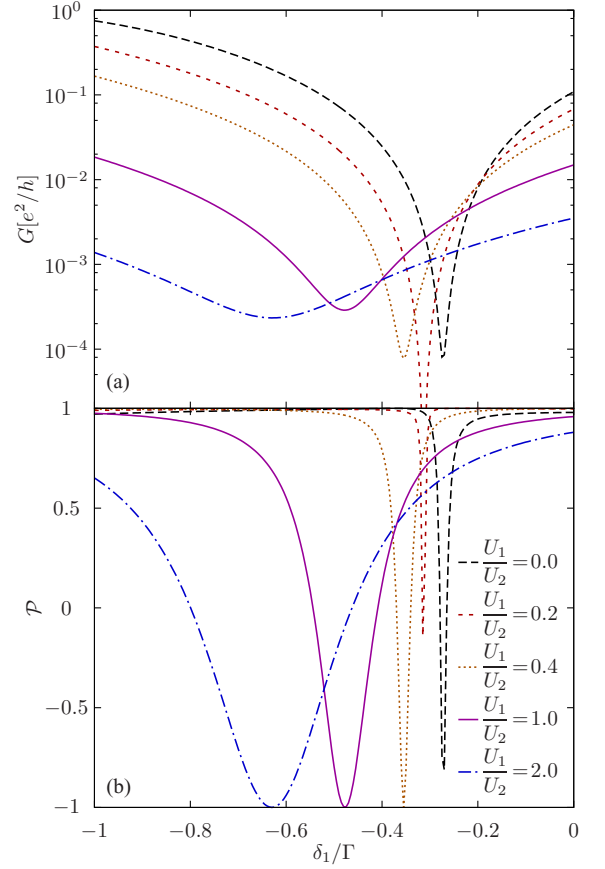


FIG. 7. (Color online) The linear conductance (a) and the spin polarization (b) as a function of the first dot detuning  $\delta_1$  calculated for different Coulomb correlations in the first dot, as indicated. The other parameters are  $U_2 = 0.5$ ,  $\Gamma = t = U_2/5$ ,  $\varepsilon_2 = -U_2/3$ ,  $p = 0.4$ , and  $T = 0$ .

By increasing  $U_1$ , the exchange field effects become generally enhanced. It can be seen that the minimum in  $G$  and  $\mathcal{P}$  as a function of  $\delta_1$  changes position with  $U_1$ ; see Fig. 7. Moreover, the width of both the conductance minimum and the spin-polarization sign change also increase with increasing  $U_1$ . For example, when  $U_1 = U_2$ , both  $G$  and  $\mathcal{P}$  exhibit an approximately symmetric minimum as a function of  $\delta_1$ . Interestingly, for  $U_1 = U_2/5$ , the effect of the spin-polarization sign change is weakened, while the conductance suppression is then very large. For these parameters, the conditions for the Fano effect in each spin channel become roughly equal, and the minimum in  $G_{\sigma}$  occurs at comparable  $\delta_1$  in each spin channel. We also note that for positive detuning,  $\delta_1 > 0$  (notice also that  $\delta_2 > 0$  in Fig. 7), the spin polarization is approximately equal to 1 and no sign change occurs. This can be understood by realizing that the exchange field mimics the effect of an external magnetic field only when  $\delta_1/|\delta_1| = -\delta_2/|\delta_2|$ , i.e., when the detuning in each dot has different sign; cf. Eqs. (16) and (19). Consequently, one should expect that the sign change of spin polarization will occur when  $\delta_1 \leq 0$  and  $\delta_2 \geq 0$ . This is indeed what we observe in the fully interacting case, as can be seen in Fig. 8 calculated for  $U_1 = U_2$ , which shows the spin

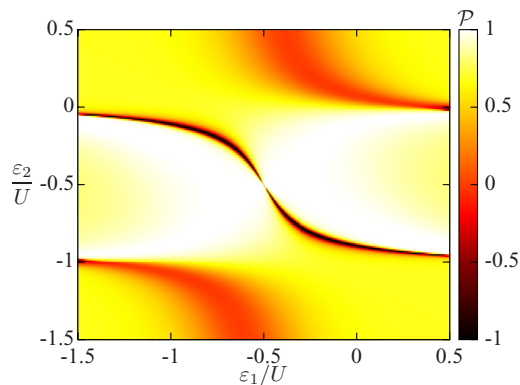


FIG. 8. (Color online) The spin polarization as a function of the DQD levels  $\varepsilon_1$  and  $\varepsilon_2$  calculated for  $U_1 = U_2 = U = 0.5$ . The other parameters are the same as in Fig. 7.

polarization as a function of the double quantum dot levels  $\varepsilon_1$  and  $\varepsilon_2$ .

Figure 8 clearly demonstrates all the features expected on the basis of analytical formulas presented in Sec. III. The spin polarization is very large (approximately equal to 1) and may change sign (reaching  $\mathcal{P} = -1$ ) as a function of either  $\varepsilon_1$  or  $\varepsilon_2$ . However, this sign change occurs when the detunings  $\delta_1$  and  $\delta_2$  have opposite signs. Moreover, this interesting behavior of the spin polarization occurs when the second dot is in the local moment regime,  $-U < \varepsilon_2 < 0$ , irrespective of the first dot's occupancy. In other words, for any  $\varepsilon_2$  such that  $-U < \varepsilon_2 < 0$  and  $\varepsilon_2 \neq -U/2$ , there exists such  $\varepsilon_1$ , that the spin polarization changes sign and becomes  $-1$ . This sign change occurs at the level position where the linear conductance exhibits a minimum. The magnitude of the conductance is then of the order of that in the cotunneling regime.

### C. Finite temperature

Finally, we consider the effect of finite temperature on the operation of our spin-polarized current source. The  $\delta_1$  dependence of the linear conductance and the spin polarization calculated for different temperatures  $T$  is shown in Fig. 9 for the fully interacting case with  $U_1 = U_2 = U$ . This figure was calculated for  $\varepsilon_2 = -U_2/3$ , which implies that the exchange field is much larger than the Kondo temperature, and the Kondo effect is suppressed. Thus, there is no universal energy scale. Because the coupling  $\Gamma$  is directly measurable and determines another important energy scale, namely the exchange field, in Fig. 9 we express the temperature in units of  $\Gamma = U/5$ . One can see that by increasing  $T$ , the conductance suppression becomes weakened, since thermal fluctuations generally suppress the Fano effect. Consequently, the absolute value of the spin polarization is also decreased. Moreover, the effect of the sign change of  $\mathcal{P}$ , directly associated with the spin-dependent Fano effect, also becomes smeared out by finite temperature. As can be seen in Fig. 9, the desired device operation persists only at low temperatures, while already at  $T = \Gamma/10$  the conductance does not show any minimum due to interference effects and the spin polarization is almost independent of  $\delta_1$ , with  $\mathcal{P} \approx p$ .

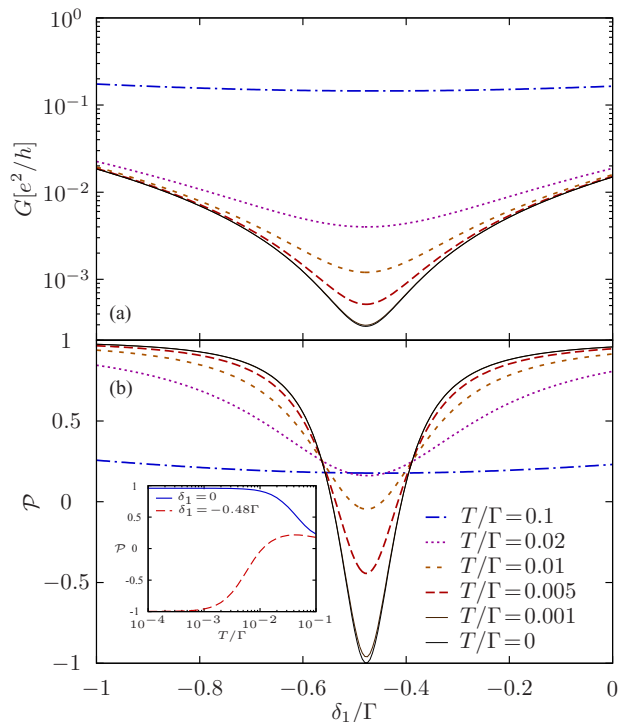


FIG. 9. (Color online) The linear conductance (a) and the spin polarization (b) as a function of  $\delta_1$  calculated for different temperatures  $T$  and for  $U_1 = U_2 = U = 0.5$ . The inset in (b) presents the temperature dependence of  $\mathcal{P}$  for  $\delta_1 = 0$  and  $\delta_1/\Gamma = -0.48$ . The other parameters are the same as in Fig. 7.

The explicit dependence of the spin polarization for two representative level detunings is shown in the inset of Fig. 9(b). For  $\delta = -0.48\Gamma$ ,  $\mathcal{P} = -1$  for  $T \rightarrow 0$ , however once  $T > \Gamma/1000$ , the absolute value of spin polarization starts slowly decreasing. On the other hand, for  $\delta = 0$ , the spin polarization is equal to unity at low temperatures and decreases once  $T > \Gamma/100$ . In fact, the relevant energy scale is given by the magnitude of the exchange field. For realistic parameters, with  $\Gamma \sim \text{meV}$ , the device should operate at clearly cryogenic temperatures. However, for molecules, where both  $U$  and  $\Gamma$  can be larger, the relevant temperature range could be increased.

### V. CONCLUSIONS

In this paper, we have considered transport properties of T-shaped double quantum dots coupled to ferromagnetic leads. The calculations have been performed with the aid of the numerical renormalization group method, which allowed us to accurately determine the spectral functions, the linear conductance, and the spin polarization of the current. Transport properties of the considered system are determined by the Fano effect, which reveals itself as an antiresonance in linear conductance when changing the DQD levels. On the other hand, the presence of ferromagnets results in an exchange field that splits the levels in the dots. This results in the spin dependence of the Fano effect—the conditions for Fano destructive interference are different in each spin channel.



Because the magnitude and sign of the exchange field can be controlled by changing the DQD's levels, one can tune the conductance suppression in each spin channel. As a consequence, there is a range of parameters where one of the conductances is much larger than the other one and the device exhibits perfect spin polarization. Moreover, because the sign of the spin polarization can be changed by tuning the levels, the operation of the device can be controlled by purely electrical means, namely by appropriately sweeping the gate voltages. Our device thus provides a prospective example of an electrically controlled, fully spin-polarized current source, which operates without the need to apply an external magnetic field.

From analytical analysis, we have found that to get perfect spin polarization, it is necessary to have finite Coulomb correlations in the dot, which is not directly coupled to the leads (the second dot). Moreover, this dot should be in the local moment regime, while no such restriction is imposed on the first dot, which can be noninteracting. These findings have been confirmed by detailed NRG calculations, which also revealed that finite Coulomb correlations in the first dot can further increase the range of parameters where the sign change of spin polarization occurs. Studying the conductance at finite temperatures, we have shown that thermal fluctuations

smear out the effects of interest, which persist only at low temperatures.

Finally, we note that T-shaped DQDs can exhibit other interesting effects, such as, e.g., the two-stage Kondo effect [43–46]. In this effect, with lowering temperature, at the first stage the spin in the first dot becomes screened by conduction electrons giving rise to maximum conductance, and then at lower temperatures, the second stage of screening occurs, leading to conductance suppression. In fact, the conductance suppression due to interference effects, which occurs in T-shaped DQDs, can also be explained by invoking the two-stage Kondo effect [17,18]. However, a detailed analysis of the two-stage Kondo effect in the presence of itinerant-electron ferromagnetism goes beyond the scope of the present paper and will be considered elsewhere [47].

#### ACKNOWLEDGMENTS

This work was supported by an “Iuventus Plus” project No. IP2011 059471 in the years 2012–2014 and the National Science Center in Poland under Project No. DEC-2013/10/E/ST3/00213. I.W. also acknowledges support from the EU Grant No. CIG-303 689. Computing time at Poznań Superconducting and Networking Center is acknowledged.

- 
- [1] *Semiconductor Spintronics and Quantum Computation*, edited by D. D. Awschalom, D. Loss, and N. Samarth (Springer, Berlin, 2002).
- [2] S. Maekawa and T. Shinjo, *Spin Dependent Transport in Magnetic Nanostructures* (Taylor and Francis, New York, 2002).
- [3] I. Zutic, J. Fabian, and S. Das Sarma, *Rev. Mod. Phys.* **76**, 323 (2004).
- [4] P. Seneor, A. Bernard-Mantel, and F. Petroff, *J. Phys.: Condens. Matter* **19**, 165222 (2007).
- [5] J. Barnaś and I. Weymann, *J. Phys.: Condens. Matter* **20**, 423202 (2008).
- [6] C. Timm and F. Elste, *Phys. Rev. B* **73**, 235304 (2006).
- [7] M. Misiorny and J. Barnaś, *Phys. Rev. B* **75**, 134425 (2007).
- [8] S. Loth, K. von Bergmann, M. Ternes, A. Otte, C. Lutz, and A. Heinrich, *Nat. Phys.* **6**, 340 (2010).
- [9] Sz. Csonka, I. Weymann, and G. Zarand, *Nanoscale* **4**, 3635 (2012).
- [10] J. Martinek, Y. Utsumi, H. Imamura, J. Barnaś, S. Maekawa, J. König, and G. Schön, *Phys. Rev. Lett.* **91**, 127203 (2003).
- [11] A. N. Pasupathy, R. C. Bialczak, J. Martinek, J. E. Grose, L. A. Donev, P. L. McEuen, and D. C. Ralph, *Science* **306**, 86 (2004).
- [12] J. R. Hauptmann, J. Paaske, and P. E. Lindelof, *Nat. Phys.* **4**, 373 (2008).
- [13] M. Gaass, A. K. Hüttel, K. Kang, I. Weymann, J. von Delft, and C. Strunk, *Phys. Rev. Lett.* **107**, 176808 (2011).
- [14] I. Weymann, *Phys. Rev. B* **83**, 113306 (2011).
- [15] K. P. Wójcik, I. Weymann, and J. Barnaś, *J. Phys. Condens. Matter* **25**, 075301 (2013).
- [16] U. Fano, *Phys. Rev.* **124**, 1866 (1961).
- [17] S. Sasaki, H. Tamura, T. Akazaki, and T. Fujisawa, *Phys. Rev. Lett.* **103**, 266806 (2009).
- [18] R. Žitko, *Phys. Rev. B* **81**, 115316 (2010).
- [19] K. G. Wilson, *Rev. Mod. Phys.* **47**, 773 (1975).
- [20] L. G. G. V. Dias da Silva, E. Vernek, K. Ingersent, N. Sandler, and S. E. Ulloa, *Phys. Rev. B* **87**, 205313 (2013).
- [21] M. E. Torio, K. Hallberg, A. H. Ceccatto, and C. R. Proetto, *Phys. Rev. B* **65**, 085302 (2002).
- [22] M. E. Torio, K. Hallberg, S. Flach, A. E. Miroschnichenko, and M. Titov, *Eur. Phys. J. B* **37**, 399 (2004).
- [23] A. A. Aligia and L. A. Salguero, *Phys. Rev. B* **70**, 075307 (2004).
- [24] F.-B. Yang, S.-Q. Wu, and W.-L. Sun, *Chin. Phys. Lett.* **24**, 2056 (2007).
- [25] F.-B. Yang, S.-Q. Wu, C.-H. Yan, R. Huang, T. Hou, and A.-H. Bi, *Chin. Phys. B* **17**, 1383 (2008).
- [26] T. Hou, S.-Q. Wu, A.-H. Bi, F.-B. Yang, J.-F. Chen, and M. Fan, *Chin. Phys. B* **18**, 783 (2009).
- [27] H. Rui, W. Shao-Quan, and H. Tao, *Commun. Theor. Phys.* **57**, 161 (2012).
- [28] Y. Meir and N. S. Wingreen, *Phys. Rev. Lett.* **68**, 2512 (1992).
- [29] F. B. Anders and A. Schiller, *Phys. Rev. Lett.* **95**, 196801 (2005); *Phys. Rev. B* **74**, 245113 (2006).
- [30] A. Weichselbaum and J. von Delft, *Phys. Rev. Lett.* **99**, 076402 (2007).
- [31] We use the open-access Budapest NRG code, O. Legeza, C. P. Moca, A. I. Tóth, I. Weymann, and G. Zarand, arXiv:0809.3143. The code is available at <http://www.phy.bme.hu/~dmnrg/>
- [32] A. I. Tóth, C. P. Moca, Ö. Legeza, and G. Zarand, *Phys. Rev. B* **78**, 245109 (2008).
- [33] A. E. Miroschnichenko, S. Flach, and Y. S. Kivshar, *Rev. Mod. Phys.* **82**, 2257 (2010).

- [34] J. Martinek, M. Sindel, L. Borda, J. Barnaś, R. Bulla, J. König, G. Schön, S. Maekawa, and J. von Delft, *Phys. Rev. B* **72**, 121302 (2005).
- [35] J. Kondo, *Prog. Theor. Phys.* **32**, 37 (1964).
- [36] D. Goldhaber-Gordon, H. Shtrikman, D. Mahalu, D. Abusch-Magder, U. Meirav, and M. A. Kastner, *Nature (London)* **391**, 156 (1998).
- [37] S. M. Cronenwett, T. H. Oosterkamp, and L. P. Kouwenhoven, *Science* **281**, 540 (1998).
- [38] L. G. G. V. Dias da Silva, N. P. Sandler, K. Ingersent, and S. E. Ulloa, *Phys. Rev. Lett.* **97**, 096603 (2006).
- [39] L. Vaugier, A. A. Aligia, and A. M. Lobos, *Phys. Rev. B* **76**, 165112 (2007).
- [40] L. G. G. V. Dias da Silva, K. Ingersent, N. Sandler, and S. E. Ulloa, *Phys. Rev. B* **78**, 153304 (2008).
- [41] A. Kogan, S. Amasha, D. Goldhaber-Gordon, G. Granger, M. A. Kastner, and H. Shtrikman, *Phys. Rev. Lett.* **93**, 166602 (2004).
- [42] D. C. Langreth, *Phys. Rev.* **150**, 516 (1966).
- [43] M. Vojta, R. Bulla, and W. Hofstetter, *Phys. Rev. B* **65**, 140405(R) (2002).
- [44] P. S. Cornaglia and D. R. Grempel, *Phys. Rev. B* **71**, 075305 (2005).
- [45] R. Žitko and J. Bonča, *Phys. Rev. B* **73**, 035332 (2006).
- [46] C.-H. Chung, G. Zarand, and P. Wölfle, *Phys. Rev. B* **77**, 035120 (2008).
- [47] K. P. Wójcik and I. Weymann (unpublished).

# The Magnetic Field Effects on Spin Polarization of T-Shaped Double Quantum Dots Coupled to Ferromagnetic Leads

K.P. WÓJCIK\* AND I. WEYMANN

Faculty of Physics, Adam Mickiewicz University, Umultowska 85, 61-614 Poznań, Poland

We analyze the spin-dependent conductance and spin polarization of a double quantum dot in a T-shape configuration coupled to ferromagnetic leads in the presence of external magnetic field. The calculations are performed with the aid of the numerical renormalization group method. We show that in the antiparallel configuration, finite magnetic field can give rise to the full spin polarization of the current, which can be controlled by tuning the dots' levels. On the other hand, for parallel configuration enhanced spin polarization can be generated by an exchange field due to the presence of ferromagnetic leads and can be also tuned by changing level position or external magnetic field. The magnetic field can be thus used to improve the spin-resolved properties of the system.

DOI: [10.12693/APhysPolA.127.222](https://doi.org/10.12693/APhysPolA.127.222)

PACS: 73.23.Hk, 73.63.Kv, 85.75.-d

## 1. Introduction

Transport properties of double quantum dots (DQDs) have recently attracted a lot of attention [1]. Since the behavior of such systems mimics the behavior of real molecules, DQDs provide ideal playground to examine various correlations at the nanoscale. When only one of the dots is directly coupled to the leads, while the second dot is coupled indirectly through the first dot, the interference between different conduction paths can give rise to the Fano effect [2]. On the other hand, in the case of strong coupling between the DQD and the leads, the electronic correlations can give rise to the Kondo effect [3]. In fact, transport properties of T-shaped DQDs are determined by the interplay of the Fano and Kondo effects [4, 5]. Another interesting effect occurs in the presence of external magnetic field. It was shown that the conductance through the system can be then fully spin polarized, and the sign and degree of spin polarization can be controlled by the position of the DQD's levels [6].

In this paper we study the spin-polarized conductance of T-shaped DQDs coupled to ferromagnetic leads in the presence of external magnetic field. It is known that the presence of ferromagnetic leads gives rise to an exchange field that acts in a similar way to an external magnetic field, splitting the dots' levels [7, 8]. By using the numerical renormalization group (NRG) method [9, 10], we show that one can obtain full spin polarization  $\mathcal{P}$  of the linear conductance in DQDs with ferromagnetic contacts without the need to apply magnetic field. We also analyze how the presence of external magnetic field modifies the spin-resolved transport properties of the system.

\*corresponding author; e-mail: [kpojczik@amu.edu.pl](mailto:kpojczik@amu.edu.pl)

## 2. Model and method

We consider DQD in a T-shape configuration coupled to ferromagnetic leads, whose magnetizations can form either parallel or antiparallel configuration, see Fig. 1. The Hamiltonian of the system has the form,  $H = H_F + H_T + H_{\text{DQD}}$ .  $H_F = \sum_{r=L,R} \sum_{\mathbf{k}\sigma} \varepsilon_{r\mathbf{k}\sigma} c_{r\mathbf{k}\sigma}^\dagger c_{r\mathbf{k}\sigma}$  is the Hamiltonian of ferromagnetic leads,  $H_T = \sum_{r=L,R} \sum_{\mathbf{k}\sigma} V_{r\mathbf{k}\sigma} (d_{1\sigma}^\dagger c_{r\mathbf{k}\sigma} + c_{r\mathbf{k}\sigma}^\dagger d_{1\sigma})$  is the tunneling Hamiltonian and the DQD Hamiltonian reads

$$H_{\text{DQD}} = \sum_{j\sigma} \varepsilon_{j\sigma} n_{j\sigma} + \sum_{\sigma} t (d_{1\sigma}^\dagger d_{2\sigma} + \text{H.c.}) + U_2 n_{2\uparrow} n_{2\downarrow}, \quad (1)$$

with  $n_{j\sigma} = d_{j\sigma}^\dagger d_{j\sigma}$ . Here,  $c_{r\mathbf{k}\sigma}$  ( $d_{j\sigma}$ ) annihilates an electron with spin  $\sigma$ , carrying momentum  $\hbar\mathbf{k}$  in lead  $r$  (located on dot  $j$ ), correspondingly, and  $\varepsilon_{r\mathbf{k}\sigma}$  ( $\varepsilon_{j\sigma}$ ) is the respective single-particle energy. We assume that only the second dot is interacting, with  $U_2$  denoting the Coulomb correlation parameter. In the presence of magnetic field, the dots' levels become split,  $\varepsilon_{j\sigma} = \varepsilon_j + \sigma B/2$ , where  $B$  is the external magnetic field applied along the  $z$ -th direction and  $g\mu_B \equiv 1$ . The coupling between the first dot and the lead  $r$  is given by  $\Gamma_{r\sigma} = \sum_{\mathbf{k}} \pi \rho_{r\sigma} |V_{r\mathbf{k}\sigma}|^2$ , where  $\rho_{r\sigma}$  denotes the respective spin-resolved density of states. The coupling can be rewritten as  $\Gamma_{r\sigma} = (1 + \sigma p) \Gamma_r/2$ , where  $p$  is the spin-polarization of ferromagnets ( $p_L \equiv p$ ), and  $\Gamma_L = \Gamma_R \equiv \Gamma/2$ .

The linear conductance through the system can be found from the Meir-Wingreen formula,

$$G_\sigma = \frac{e^2}{h} \frac{4\Gamma_{L\sigma}\Gamma_{R\sigma}}{\Gamma_{L\sigma} + \Gamma_{R\sigma}} \int d\omega \frac{\partial f(\omega)}{\partial \omega} \Im \langle \langle d_{1\sigma} | d_{1\sigma}^\dagger \rangle \rangle^{\text{ret}}, \quad (2)$$

where  $f(\omega)$  is the Fermi-Dirac distribution function and  $\langle \langle d_{1\sigma} | d_{1\sigma}^\dagger \rangle \rangle^{\text{ret}}$  denotes the Fourier transform of the retarded Green function of the first dot, which we calculate with the aid of NRG [9, 10]. In calculations we assume the following parameters (the first dot is noninteracting):  $U_2 = 0.5D$ ,  $\Gamma = 0.02D$ ,  $t = 0.04D$  and  $p = 0.4$ , where  $D \equiv 1$  is the band halfwidth used as energy unit.

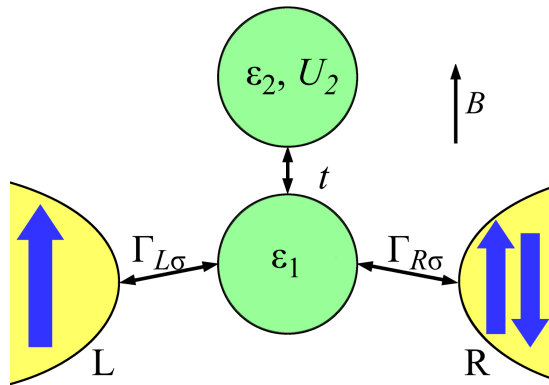


Fig. 1. Schematic of DQD in a T-shape geometry coupled to ferromagnetic leads with either parallel or antiparallel alignment of magnetizations. The first dot is coupled to the leads with strength  $\Gamma_{L(R)\sigma}$  and to the second dot via hopping  $t$ .

### 3. Results and discussion

In the following, we analyze the behavior of the spin-resolved conductance  $G_\sigma$  and the spin polarization  $\mathcal{P}$ , defined as  $\mathcal{P} = (G_\uparrow - G_\downarrow)/(G_\uparrow + G_\downarrow)$ , in both the antiparallel (AP) and parallel (P) magnetic configurations of the system.

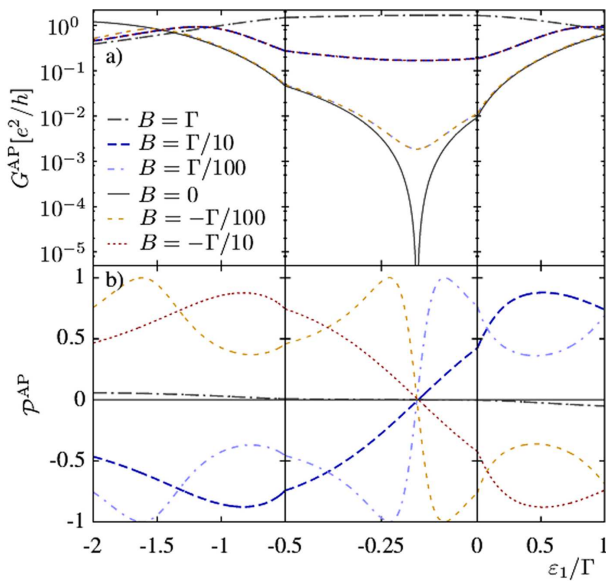


Fig. 2. Dependence of the linear conductance  $G^{\text{AP}}$  (a) and spin polarization  $\mathcal{P}^{\text{AP}}$  (b) on  $\varepsilon_1$ , for different strengths of magnetic field  $B$  in the antiparallel configuration and for  $\varepsilon_2 = -U_2/3$ . The  $x$ -axis for  $\varepsilon_1 \in [-0.5, 0]$  was multiplied by 3 to zoom in the range where the most interesting features occur (curves are smooth in homogeneous scale). In (a) curves for different signs of  $B$  overlap.

In the antiparallel configuration, for left-right symmetric systems as considered here, the couplings for spin-up

and spin-down DQD levels become equal and the system behaves as if coupled to nonmagnetic leads, except for additional factor of  $(1 - p^2)$  in  $G_\sigma$ . Figure 2 shows the linear conductance and spin polarization in the antiparallel configuration as a function of  $\varepsilon_1$  for  $\varepsilon_2 = -U_2/3$ . As can be clearly seen in Fig. 2a, for  $B = 0$ , there is a strong antiresonance in  $G^{\text{AP}}$  due to the Fano destructive interference. It occurs for  $\varepsilon_1 = \varepsilon_0 \approx -\Gamma/6$ . The fact that  $\varepsilon_0 \neq 0$  comes from the lack of electron-hole symmetry in the system, since  $\varepsilon_2 = -U_2/3$ . We note that for  $\varepsilon_2 = -U_2/2$  the conductance in the presence of  $B$  was analyzed in Ref. [6] for nonmagnetic leads.

While for  $B = 0$  the suppression of  $G^{\text{AP}}$  is complete, the presence of magnetic field weakens this effect and leads to finite conductance. This is due to the fact that finite  $B$  removes spin degeneracy and the conditions for Fano destructive interference become different in each spin channel. Then, if  $G_\sigma^{\text{AP}} \rightarrow 0$  for given  $\varepsilon_1$ ,  $G_\sigma^{\text{AP}} \neq 0$ , so that the total conductance,  $G^{\text{AP}} = G_\uparrow^{\text{AP}} + G_\downarrow^{\text{AP}}$ , is finite in the whole range of  $\varepsilon_1$ , provided  $B \neq 0$ , see Fig. 2a. This holds even for very weak  $B$ , while for strong magnetic field  $G^{\text{AP}} = 2(1 - p^2)e^2/h$ . Another feature visible in Fig. 2a is the approximate symmetry of the linear conductance around the point  $\varepsilon_1 = \varepsilon_0$ .

$G^{\text{AP}}$  does not depend on the sign of  $B$ , only on its magnitude, this is contrary to the spin polarization, which is shown in Fig. 2b. Since for  $B = 0$  nothing perturbs the spin  $SU(2)$  symmetry,  $\mathcal{P}^{\text{AP}} = 0$  in this case. However, even as tiny magnetic field as  $B = \Gamma/100$  is sufficient to cause  $\mathcal{P}^{\text{AP}}$  to reach  $\pm 1$ . In agreement with intuition, the change of sign of  $B$  leads to the change of sign of  $\mathcal{P}^{\text{AP}}$  and all the curves are approximately antisymmetric around  $\varepsilon_1 = \varepsilon_0$ . Nevertheless, the dependence of  $\mathcal{P}^{\text{AP}}$  on  $\varepsilon_1$  for  $B = \pm\Gamma/100$  is highly non-trivial. It displays two local maxima with  $\mathcal{P}^{\text{AP}} \approx 1$  and two minima with  $\mathcal{P}^{\text{AP}} \approx -1$ . On the other hand, the dependence of  $\mathcal{P}^{\text{AP}}$  on  $\varepsilon_1$  for stronger  $B$  is less spectacular, i.e. the achieved values of  $\mathcal{P}^{\text{AP}}$  are now much smaller,  $|\mathcal{P}^{\text{AP}}| < 0.1$ , see the curves for  $B = \pm\Gamma$  in Fig. 2b. This holds also outside the range of Fig. 2, for  $-15\Gamma < \varepsilon_1 < 15\Gamma$ .

Consider now the case of parallel magnetic configuration. Now the couplings for spin-up and spin-down are different leading to different level renormalization for each spin direction. This gives rise to a spin splitting of the levels even in the case of  $B = 0$  [7]. The magnitude and sign of this ferromagnetic-contact induced exchange field can be tuned by changing the level position. Moreover, it is clearly an interaction effect since it vanishes for vanishing Coulomb correlations and at the particle-hole symmetry point of the model. In the case studied here with noninteracting first dot, the exchange field develops in the second dot. The hybridization of the second dot is  $\Gamma_{2\sigma} = t^2/\Gamma_\sigma$ , and, clearly, the dependence of  $\Gamma_{2\sigma}$  on  $p$  is opposite to the that of  $\Gamma_\sigma$  [7, 8]. Consequently, for given levels' position, the sign of exchange field is opposite as compared to single dot case. This is reflected in the  $B$ -dependence of  $G$  and  $\mathcal{P}$ , as discussed in the sequel.

The dependence of linear conductance  $G^P$  and spin polarization  $\mathcal{P}^P$  on  $\varepsilon_1$  is shown in Fig. 3. One can see that even for  $B = 0$  the suppression of the conductance due to Fano destructive interference is only partial. Due to the presence of exchange field, Fano antiresonances in different spin channels are shifted against each other, leading to finite conductance  $G^P$  for all  $\varepsilon_1$ . Moreover, the spin polarization is very high,  $\mathcal{P}^P \approx 1$ , except for the point where  $G^P$  is minimum, at which the spin polarization changes sign and becomes  $\mathcal{P}^P \approx -1$ . Thus, without any external magnetic field, due to the presence of exchange field, one can obtain perfect spin polarization of the linear conductance, which can be tuned by changing the level position. This undoubtedly interesting result is analyzed in more detail in Ref. [11].

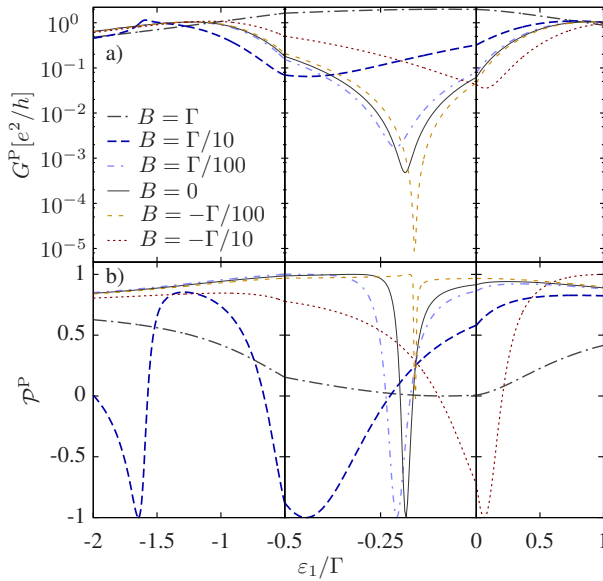


Fig. 3. The same as Fig. 2 calculated for the parallel magnetic configuration of the system.

In the presence of magnetic field, the operation of the device can be changed. If one turns on small negative  $B$ , see the curves for  $B = -\Gamma/100$  in Fig. 3, the Fano antiresonance becomes restored and  $\mathcal{P}$  is almost constant showing only small dip without any sign change. This is due to the fact that this magnetic field compensates the splitting induced by the exchange field. Note that this is contrary to single dot case, where to compensate for exchange field one needs to apply  $B$  along the magnetization of the leads ( $B > 0$ ) [8]. This is related with different dependence of the couplings on  $p$  discussed above.

For small positive field, see the case of  $B = \Gamma/100$  in Fig. 3, the minimum of  $G^P$  is slightly shifted and a bit shallower, while the dip of  $\mathcal{P}^P$  reaches  $-1$  and is wider as compared to the case of  $B = 0$ . This can be understood by realizing that positive  $B$  enhances the splitting induced by the exchange field. The splitting can be enhanced further with larger  $B$  leading to even broader minimum in both  $G^P$  and  $\mathcal{P}^P$ , see the case of  $B = \Gamma/10$

in Fig. 3. Interestingly, a second minimum of  $\mathcal{P}^P$  occurs at  $\varepsilon_1 \approx -1.65\Gamma$ . At this point  $G^P$  is enhanced and exhibits a small local maximum.

The change of sign of  $B$  is in this case qualitatively equivalent to change of the curve to its mirror image with respect to the point where  $G^P$  has minimum. This is due to the fact that for  $|B| \gtrsim \Gamma/10$ , the magnetic field surpasses the exchange field, thus decreasing its influence on transport. In fact, for magnetic fields of the order of the coupling strength,  $|B| = \Gamma$ , the spin polarization becomes much suppressed, it is clearly smaller than unity and does not change sign.

Finally, we note that large spin polarization is also present in the case when the first dot is interacting. Then, the exchange field plays an important role on both dots and it can lead to further enhancement of the range of parameters where perfect spin polarization occurs [11].

### Acknowledgments

This work was supported by the Polish Ministry of Science and Higher Education through a research project No. N N202 199739 in years 2010–2013. I.W. also acknowledges support from the EU grant No. CIG-303 689.

### References

- [1] W.G. van der Wiel, S. De Franceschi, J.M. Elzerman, T. Fujisawa, S. Tarucha, L.P. Kouwenhoven, *Rev. Mod. Phys.* **75**, 1 (2003).
- [2] U. Fano, *Phys. Rev.* **124**, 1866 (1961).
- [3] A.C. Hewson, *The Kondo Problem to Heavy Fermions*, Cambridge University Press, Cambridge 1993.
- [4] S. Sasaki, H. Tamura, T. Akazaki, T. Fujisawa, *Phys. Rev. Lett.* **103**, 266806 (2009).
- [5] R. Žitko, *Phys. Rev. B* **81**, 115316 (2010).
- [6] L.G.G.V. Dias da Silva, E. Vernek, K. Ingersent, N. Sandler, S.E. Ulloa, *Phys. Rev. B* **87**, 205313 (2013).
- [7] J. Martinek, Y. Utsumi, H. Imamura, J. Barnaś, S. Maekawa, J. König, G. Schön, *Phys. Rev. Lett.* **91**, 127203 (2003).
- [8] M. Gaass, A.K. Hüttel, K. Kang, I. Weymann, J. von Delft, Ch. Strunk, *Phys. Rev. Lett.* **107**, 176808 (2011).
- [9] K.G. Wilson, *Rev. Mod. Phys.* **47**, 773 (1975).
- [10] We use the open-access Budapest NRG code, O. Legéza, C.P. Moca, A.I. Tóth, I. Weymann, G. Zaránd, [arXiv:0809.3143](https://arxiv.org/abs/0809.3143) (2008), unpublished. The code is available at: <http://www.phy.bme.hu/dmrg/>.
- [11] K.P. Wójcik, I. Weymann, *Phys. Rev. B* **90**, 115308 (2014).



# Ferromagnets-induced splitting of molecular states of T-shaped double quantum dots

Krzysztof P. Wójcik<sup>a</sup>

Faculty of Physics, Adam Mickiewicz University, Umultowska 85, 61-614 Poznań, Poland

Received 27 November 2014 / Received in final form 11 February 2015

Published online 4 May 2015

© The Author(s) 2015. This article is published with open access at [Springerlink.com](http://Springerlink.com)

**Abstract.** The exchange field for molecular states of double quantum dot, induced by two ferromagnets coupled to the device in T-shaped configuration, is defined and calculated. It is found, that in the regime of strong coupling between quantum dots, the dependence of the exchange field on this coupling becomes nontrivial. In particular, it changes the sign a few times to eventually vanish in the limit of infinite inter-dot coupling. The excitation energies of double quantum dot are calculated and the results used to predict the conditions for suppression of the two-stage Kondo effect in the considered nanostructure.

## 1 Introduction

When a discrete level is coupled to a large system of continuous energy spectrum, it is not only broadened, but also shifted [1]. This applies, in particular, to a quantum dot (QD) coupled to a metallic lead: the charge fluctuations give rise to the renormalization of the dot level [2]. If the coupling to the lead is spin dependent, this renormalization also depends on spin, leading to the splitting of the dot's level, often called *the exchange field*. It can be estimated through the Anderson's scaling approach [3,4] or numerical renormalization group calculations [5,6], as well as within the perturbation theory, second order in the interaction with the lead, where usual logarithmic divergences cancel out when one takes the difference of the shifts for levels of opposite spins [7]. The exchange field was also observed experimentally [8,9]. Its values are of the order of fraction of meV; the magnetic field corresponding to such a splitting for an electron with spin  $s = 1/2$  and gyromagnetic ratio  $g = 2$  is a few Tesla [9]. The estimations of the exchange field based on numerical renormalization group calculations were found to be in good agreement with experiment [9]. Moreover, as dependent significantly on the dot's energy level, the exchange field is very important for spintronic applications, as a tool enabling manipulation of the single electron's spin (localized on the quantum dot) by only electrical means [10].

In the past few years, transport properties of double quantum dots (DQDs), from which only one is coupled directly to the leads, and the second is side-coupled to the first one, were addressed in a number of papers [11–14]<sup>1</sup>. This configuration is often referred to as

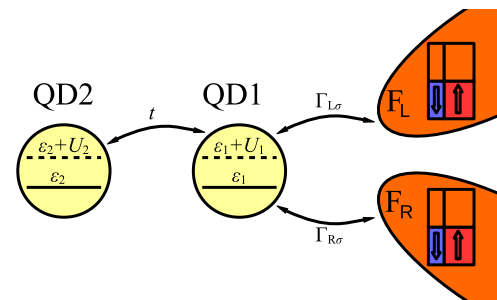


Fig. 1. Scheme of the considered system.

T-shaped DQD. In such systems, the two-stage Kondo effect occurs: the usual Kondo effect is suppressed at sufficiently low temperatures, due to singlet formation in DQD subsystem [12,15,16]. This singlet, however, can be broken by the magnetic field, which restores the Kondo effect [17]. In the present paper a similar system with ferromagnetic electrodes (Fs) is considered (see Fig. 1). It is shown, by means of perturbative calculation, that the exchange field can be considered as an alternative mechanism of breaking the singlet and restoring the Kondo effect. This is confirmed by numerical renormalization group calculations [18].

It is worth stressing, that all the correlations in DQD subsystem are treated analytically. The exchange field is properly defined for all the eigenstates, whose energies are obtained exactly for a rather general case<sup>2</sup>. In particular, adjusting of Coulomb energies and energy levels of both dots independently is allowed. The latter is especially important for applications, where one should be able to tune the exchange field by changing the energy levels of QDs.

<sup>a</sup> e-mail: [kpwojcik@amu.edu.pl](mailto:kpwojcik@amu.edu.pl)

<sup>1</sup> See also references cited in references [11–14].

<sup>2</sup> Less general case was studied in reference [19].

The article is organized as follows. In Section 2 the Hamiltonian of DQD is presented and its eigenvalues and eigenstates are calculated. Then, in Section 3 the exchange field for eigenstates of DQD is defined and the formula for it is derived. Finally, the results are presented in Section 4.

## 2 The double-dot system

The Anderson model is used to describe quantum dots. It is also assumed, that their mutual interaction is reduced to the hopping between the dots. Thus, the Hamiltonian of DQD subsystem has the form

$$H_{\text{DQD}} = \sum_{\alpha\sigma} \varepsilon_{\alpha} d_{\alpha\sigma}^{\dagger} d_{\alpha\sigma} + \sum_{\sigma} t \left( d_{1\sigma}^{\dagger} d_{2\sigma} + h.c. \right) + \sum_{\alpha} \frac{U_{\alpha}}{2} \left( \sum_{\sigma} d_{\alpha\sigma}^{\dagger} d_{\alpha\sigma} - 1 \right)^2 - \frac{U_1 + U_2}{2}. \quad (1)$$

The constant term is set such that unoccupied DQD has energy equal to 0. The index  $\alpha \in \{1, 2\}$  corresponds to number of QD (see Fig. 1), while  $\sigma = \pm 1$  denotes direction of the spin.  $t$  denotes the hopping between the dots.  $d_{\alpha\sigma}^{\dagger}$  annihilates (creates) an electron of spin  $\sigma$  in dot  $\alpha$ . The Coulomb energy of dot  $\alpha$  is  $U_{\alpha}$ , while the energy level for an electron of spin  $\sigma$  in the dot  $\alpha$  is  $\varepsilon_{\alpha}$ . The mean detuning of dot's level from particle-hole symmetric point is  $\varepsilon = (\varepsilon_2 + \varepsilon_1)/2 + U$ , where  $U = (U_2 + U_1)/4$ . For convenience the following notation is used:  $\Delta = (U_2 - U_1)/4$ ,  $\delta = (\varepsilon_2 - \varepsilon_1)/2 + \Delta$ .

In addition,  $q$  denotes the normal-ordered charge of DQD. Similarly,  $S$  denotes the total spin of DQD, and  $S_z$  is used for its  $z$  component. Eigenstates are denoted  $|e_i\rangle$ , with  $i \in \{1, \dots, 16\}$ , while states from the basis of definite occupation numbers have form  $|\chi_1\chi_2\rangle$ , where  $\chi_{\alpha} \in \{0, \uparrow, \downarrow, 2\}$  is the state of QD $\alpha$ .

The eigenvalues of  $H_{\text{DQD}}$  are listed in Table 1. One can clearly see charge U(1) and spin SU(2) symmetries. The energies of the states in the  $q = 0$ ,  $S = 0$  subspace are the roots of the following cubic polynomial,

$$\omega^3 + (2U - 6\varepsilon)\omega^2 - 4(t^2 + 2U\varepsilon + \delta^2 - 3\varepsilon^2)\omega + 8[t^2\varepsilon + U(\varepsilon^2 - \delta^2) + \delta^2\varepsilon - \varepsilon^3] = 0. \quad (2)$$

They can be expressed through radicals, but the resulting expressions are somewhat cumbersome and for this reason were not explicitly listed in Table 1. However, for special cases they significantly simplify. Eigenvalues for some of these cases are presented in Table 2. For  $\varepsilon = \delta = 0$  ( $\varepsilon_1 = -U_1/2$ ,  $\varepsilon_2 = -U_2/2$ ) the charge symmetry also becomes SU(2). Then, states:  $|e_1\rangle$ ,  $|e_{11}\rangle$ , and  $|e_{16}\rangle$ , form the triplet of  $E = 0$  (see column  $\delta = 0$  in Tab. 2 for  $E_{11}$ ). Simultaneously,  $S = 1/2$  doublets with  $q = \pm 1$  become degenerated.

In turn, the eigenstates are listed in Table 3. These corresponding to highest quantum numbers ( $q = \pm 2$ ,  $S = 1$ ) are trivial. Expressions for states forming doublets are

**Table 1.** Exact eigenvalues of  $H_{\text{DQD}}$ . Solutions of cubic secular equation in  $q = 0$ ,  $S = 0$  subspace were not written explicitly.

State	$q$	$S_z$	$E_i$
$ e_1\rangle$	-2	0	0
$ e_2\rangle,  e_3\rangle$	-1	$-\frac{1}{2}, \frac{1}{2}$	$\varepsilon - U - \sqrt{(\Delta - \delta)^2 + t^2}$
$ e_4\rangle,  e_5\rangle$	-1	$-\frac{1}{2}, \frac{1}{2}$	$\varepsilon - U + \sqrt{(\Delta - \delta)^2 + t^2}$
$ e_6\rangle,  e_7\rangle,  e_8\rangle$	0	-1, 0, 1	$2(\varepsilon - U)$
$ e_9\rangle$	0	0	$E_9$
$ e_{10}\rangle$	0	0	$E_{10}$
$ e_{11}\rangle$	0	0	$E_{11}$
$ e_{12}\rangle,  e_{13}\rangle$	+1	$-\frac{1}{2}, \frac{1}{2}$	$3\varepsilon - U - \sqrt{(\Delta + \delta)^2 + t^2}$
$ e_{14}\rangle,  e_{15}\rangle$	+1	$-\frac{1}{2}, \frac{1}{2}$	$3\varepsilon - U + \sqrt{(\Delta + \delta)^2 + t^2}$
$ e_{16}\rangle$	+2	0	$4\varepsilon$

**Table 2.** Values of eigenenergies  $E_9$ ,  $E_{10}$  and  $E_{11}$  for different limiting cases [19]. Each row corresponds to one of the three solutions of equation (2) expressed through radicals.

State	$t = 0$	$\delta = 0$	$U = 0$
$ e_9\rangle$	$2(\varepsilon + \delta)$	$2\varepsilon - U + \sqrt{U^2 + 4t^2}$	$2(\varepsilon + \sqrt{t^2 + \delta^2})$
$ e_{10}\rangle$	$2(\varepsilon - U)$	$2\varepsilon - U - \sqrt{U^2 + 4t^2}$	$2(\varepsilon - \sqrt{t^2 + \delta^2})$
$ e_{11}\rangle$	$2(\varepsilon - \delta)$	$2\varepsilon$	$2\varepsilon$

only a bit more complicated. They all can be written using coefficients

$$\nu_{\pm} = \frac{1}{\sqrt{2}} \sqrt{1 \pm \frac{\delta - \Delta}{\sqrt{t^2 + (\delta - \Delta)^2}}}, \quad (3)$$

$$\tilde{\nu}_{\pm} = \frac{1}{\sqrt{2}} \sqrt{1 \pm \frac{\delta + \Delta}{\sqrt{t^2 + (\delta + \Delta)^2}}}. \quad (4)$$

Note, that for  $t = 0$ ,  $\nu_{\pm}$  ( $\tilde{\nu}_{\pm}$ ) are either 0 or 1, depending on the sign of  $\delta - \Delta$  ( $\delta + \Delta$ ), correspondingly. The three remaining states,  $|e_9\rangle$ ,  $|e_{10}\rangle$ ,  $|e_{11}\rangle$ , can be reasonably simply expressed through the coefficients dependent on the respective eigenvalues,

$$\xi_i^1 = \frac{P_i Q_i / t - 2t}{\sqrt{8t^2 + 2P_i^2 - 4P_i Q_i + P_i^2 Q_i^2 / t^2}}, \quad (5)$$

$$\xi_i^2 = -\frac{\sqrt{2} P_i}{\sqrt{8t^2 + 2P_i^2 - 4P_i Q_i + P_i^2 Q_i^2 / t^2}}, \quad (6)$$

$$\xi_i^3 = \frac{2t}{\sqrt{8t^2 + 2P_i^2 - 4P_i Q_i + P_i^2 Q_i^2 / t^2}}, \quad (7)$$

where  $P_i = 2(\varepsilon + \delta) - E_i$  and  $Q_i = 2(\varepsilon - U) - E_i$ . Note, that dependence of  $\xi_i^a$  on  $E_i$  (through  $P_i$  and  $Q_i$ ), means in fact a complicated dependence on all the parameters of the model. Moreover, if two of the energies  $E_9$ ,  $E_{10}$ ,  $E_{11}$



**Table 3.** Eigenvectors of  $H_{\text{DQD}}$ .

$ e_1\rangle =  00\rangle,$
$ e_2\rangle = \nu_+ \downarrow 0\rangle - \nu_- 0\downarrow\rangle,$
$ e_3\rangle = \nu_+ \uparrow 0\rangle - \nu_- 0\uparrow\rangle,$
$ e_4\rangle = \nu_- \downarrow 0\rangle + \nu_+ 0\downarrow\rangle,$
$ e_5\rangle = \nu_- \uparrow 0\rangle + \nu_+ 0\uparrow\rangle,$
$ e_6\rangle =  \downarrow\downarrow\rangle,$
$ e_7\rangle = ( \downarrow\uparrow\rangle +  \uparrow\downarrow\rangle)/\sqrt{2},$
$ e_8\rangle =  \uparrow\uparrow\rangle,$
$ e_9\rangle = \xi_9^1 20\rangle + \xi_9^2\frac{ \downarrow\uparrow\rangle -  \uparrow\downarrow\rangle}{\sqrt{2}} + \xi_9^3 02\rangle,$
$ e_{10}\rangle = \xi_{10}^1 20\rangle + \xi_{10}^2\frac{ \downarrow\uparrow\rangle -  \uparrow\downarrow\rangle}{\sqrt{2}} + \xi_{10}^3 02\rangle,$
$ e_{11}\rangle = \xi_{11}^1 20\rangle + \xi_{11}^2\frac{ \downarrow\uparrow\rangle -  \uparrow\downarrow\rangle}{\sqrt{2}} + \xi_{11}^3 02\rangle,$
$ e_{12}\rangle = \tilde{\nu}_- \downarrow 2\rangle - \tilde{\nu}_+ 2\downarrow\rangle,$
$ e_{13}\rangle = \tilde{\nu}_- \uparrow 2\rangle - \tilde{\nu}_+ 2\uparrow\rangle,$
$ e_{14}\rangle = \tilde{\nu}_+ \downarrow 2\rangle - \tilde{\nu}_- 2\downarrow\rangle,$
$ e_{15}\rangle = \tilde{\nu}_+ \uparrow 2\rangle - \tilde{\nu}_- 2\uparrow\rangle,$
$ e_{16}\rangle =  22\rangle.$

should happen to coincide, these expressions must become ill-defined, because they constitute the components of the eigenvectors, which must be different even if the eigenvalues are the same. Thus, one must be careful when analyzing cases possessing special symmetries, where such degeneracy may occur.

Similarly to the eigenvalues  $E_i$ , the coefficients  $\xi_i^a$  simplify tremendously in some special cases, in particular

$$\begin{aligned} \lim_{t \rightarrow 0} (\xi_9^1, \xi_9^2, \xi_9^3) &= (0, 0, \pm 1), \\ \lim_{t \rightarrow 0} (\xi_{10}^1, \xi_{10}^2, \xi_{10}^3) &= (0, \pm 1, 0), \\ \lim_{t \rightarrow 0} (\xi_{11}^1, \xi_{11}^2, \xi_{11}^3) &= (\pm 1, 0, 0), \\ \lim_{\delta \rightarrow 0} (\xi_9^1, \xi_9^2, \xi_9^3) &= (-1, 0, 1)/\sqrt{2}, \\ \lim_{\delta \rightarrow 0} (\xi_{10}^1, \xi_{10}^2, \xi_{10}^3) &= (1, -\sqrt{2}, 1)/2, \\ \lim_{\delta \rightarrow 0} (\xi_{11}^1, \xi_{11}^2, \xi_{11}^3) &= (1, +\sqrt{2}, 1)/2. \end{aligned}$$

Note, that for  $t = 0$  the eigenstates correspond to states of definite occupation. The signs may vary depending on model parameters.

### 3 The exchange field

Ferromagnets (Fs) are modeled very simply, neglecting the Stoner splitting and the dependence of density of states and hoppings on energy (for energies smaller than the cutoff  $\pm W$ , with 0 at the Fermi energy). The ferromagnetism is then taken into account via spin-dependent coupling between Fs and DQD. In the linear response

regime, these assumptions allow for showing that two parallelly magnetized leads are equivalent by the unitary transformation [20] to the one effective lead F. Denoting by  $a_{r\omega\sigma}$  annihilation operator of an electron of energy  $\omega$  and spin  $\sigma$  in left ( $r = L$ ) or right ( $r = R$ ) ferromagnet, normalized such that the anti-commutator  $\{a_{r\omega\sigma}, a_{r'\omega'\sigma'}^\dagger\} = \delta_{rr'}\delta_{\sigma\sigma'}\delta(\omega - \omega')$ , the transformation reads the introduction of new operators,

$$c_{\omega\sigma} = u_\sigma a_{L\omega\sigma} + v_\sigma a_{R\omega\sigma}, \quad (8)$$

$$f_{\omega\sigma} = -v_\sigma a_{L\omega\sigma} + u_\sigma a_{R\omega\sigma}, \quad (9)$$

where  $u_\sigma = \sqrt{\Gamma_{L\sigma}/(\Gamma_{L\sigma} + \Gamma_{R\sigma})}$  and  $v_\sigma = \sqrt{1 - u_\sigma^2}$ . Then, both new operators fulfill the fermionic anticommutation relations. Moreover,  $f$ -operators do not appear in the tunnelling term of the Hamiltonian and can be omitted. On the other hand,  $c$ -operators' coupling is  $\Gamma_\sigma = \Gamma_{L\sigma} + \Gamma_{R\sigma}$ .

In order to treat the coupling between DQD and F with a perturbation theory, we write the Hamiltonian as  $H = H_0 + H_I$ , with

$$H_0 = H_{\text{DQD}} + \sum_\sigma \int_{-W}^W \omega c_{\omega\sigma}^\dagger c_{\omega\sigma} d\omega, \quad (10)$$

$$H_I = \sum_\sigma \int_{-W}^W \sqrt{\frac{\Gamma_\sigma}{\pi}} \left( d_{1\sigma}^\dagger c_{\omega\sigma} + h.c. \right) d\omega. \quad (11)$$

The coupling can be expressed as  $\Gamma_\sigma = (1 + p\sigma)\Gamma$ , where  $p$  denotes the spin polarization of F. Denoting by  $|e_i^*\rangle$  the state of the system, in which DQD is in the state  $|e_i\rangle$  and the effective F is in its ground state (all single-electron levels below the Fermi surface are occupied, all above are empty), one can write the zero-temperature expression for the shift of the energy level  $E_i$  in the second order in  $H_I$ ,

$$\delta E_i = \sum_{\psi \neq e_i^*} \langle e_i^* | H_I | \psi \rangle \frac{1}{E_i - E_\psi} \langle \psi | H_I | e_i^* \rangle, \quad (12)$$

where  $|\psi\rangle$  runs through all of the intermediate states in the basis  $|e_i^*\rangle$ . Note that if the intermediate states had been taken from the basis  $|\chi_1\chi_2\rangle$ , their unperturbed energy  $E_\psi$  would not have been defined and the operator  $(E_i - H_0)^{-1}(1 - |e_i^*\rangle\langle e_i^*|)$  would have to be considered instead of the sum over intermediate states in equation (12).

Since  $H_I$  allows only single hops, all the possible intermediate states are of the form  $c_{\omega\sigma}^{(\dagger)}|e_j^*\rangle$ , with the energy  $E_\psi = E_i + [\pm\omega + (E_j - E_i)]$ . This results in the shift,

$$\begin{aligned} \delta E_i &= \sum_{j\sigma} \frac{\Gamma_\sigma}{\pi} \left\{ |\langle e_j | d_{1\sigma}^\dagger | e_i \rangle|^2 \int_{-W}^W \frac{1 - \theta(\omega)}{\omega - (E_j - E_i)} d\omega \right. \\ &\quad \left. - |\langle e_j | d_{1\sigma} | e_i \rangle|^2 \int_{-W}^W \frac{\theta(\omega)}{\omega + (E_j - E_i)} d\omega \right\}. \quad (13) \end{aligned}$$

Notice that  $\delta E_i$  is linear in  $\Gamma$  and contains two parts: one independent of  $p$ , and one linear in  $p$ . Let the exchange field in the state  $|e_i\rangle$  be denoted  $\Delta\varepsilon_i^{\text{ex}}$  and defined as the

latter of those, normalized by the  $z$ -component of the spin of  $|e_i\rangle$ , i.e.  $\delta E_i = \delta E_i|_{p=0} + S_z \Delta \varepsilon_i^{\text{ex}}$ , if only  $S_z \neq 0$ . For  $S_z = 0$ , the modules of respective matrix elements of  $d_{1\sigma}^{(\dagger)}$  do not depend on spin direction, nor do the energies of all states, thus, the terms corresponding to different  $\sigma$  cancel out and the exchange field is 0. Extracting the part proportional to  $p$  and performing elementary integrals, one obtains the general, exact expression for the exchange field,

$$\Delta \varepsilon_i^{\text{ex}} = \sum_{j\sigma} \frac{\sigma p \Gamma}{\pi S_z} \log \left| \frac{E_j - E_i}{W + (E_j - E_i)} \right| \times \left( | \langle e_j | d_{1\sigma}^\dagger | e_i \rangle |^2 + | \langle e_j | d_{1\sigma} | e_i \rangle |^2 \right). \quad (14)$$

$S_z$  was introduced to the definition of the exchange field to make the clear correspondence between  $\Delta \varepsilon^{\text{ex}}$  and the effective magnetic field  $B = \Delta \varepsilon^{\text{ex}} / (g \mu_B)$ , which would cause the same splitting of the multiplets.

## 4 Results

In Section 4.1 it is shown, how the exchange field obtained for a single QD is affected by the presence of QD2. Then, in Section 4.2 the exchange fields in different states are compared and their influence on the ground state of the DQD subsystem is analyzed. The signature of the exchange field in the conductance of the system is discussed in Section 4.3. Finally, in Section 4.4, the limitations of the considered method are examined.

### 4.1 The role of inter-dot interaction

Setting  $t = 0$  and  $U_2 = \varepsilon_2 = 0$ , one practically obtains a single QD coupled to the ferromagnet, plus a free orbital of zero energy. For  $t = 0$  the basis states  $|e_i\rangle$  coincide with states  $|\chi_1 \chi_2\rangle$ , except for  $|e_7\rangle$  and  $|e_8\rangle$ , where, respectively, the sum and the difference of two such states occurs. For any of basis state  $|e_i\rangle$  having the form  $|\sigma \chi_2\rangle$ , the result (14) simplifies to

$$S_z \Delta \varepsilon_{|\sigma \chi_2\rangle}^{\text{ex}} = \frac{\sigma p \Gamma}{\pi} \log \left| \frac{\varepsilon_1}{\varepsilon_1 + U_1} \cdot \frac{W + (\varepsilon_1 + U_1)}{W - \varepsilon_1} \right|, \quad (15)$$

which has a nice limit for  $W \rightarrow \infty$ , namely

$$S_z \Delta \varepsilon_{|\sigma \chi_2\rangle}^{\text{ex}} \xrightarrow{W \rightarrow \infty} \frac{\sigma p \Gamma}{\pi} \log \left| \frac{\varepsilon_1}{\varepsilon_1 + U_1} \right|. \quad (16)$$

This is the result obtained by Martinek et al. in reference [4] for a single quantum dot coupled to a ferromagnetic lead.

Note, that  $U_1 = 0$  implies  $\Delta \varepsilon^{\text{ex}} = 0$ , also for finite  $W$ . This is caused by the fact, that particle-like and hole-like processes cancel each other. The exchange field diverges for resonant positions of the dot's level and vanishes in the particle-hole symmetric point (cf. Fig. 2), solid line.

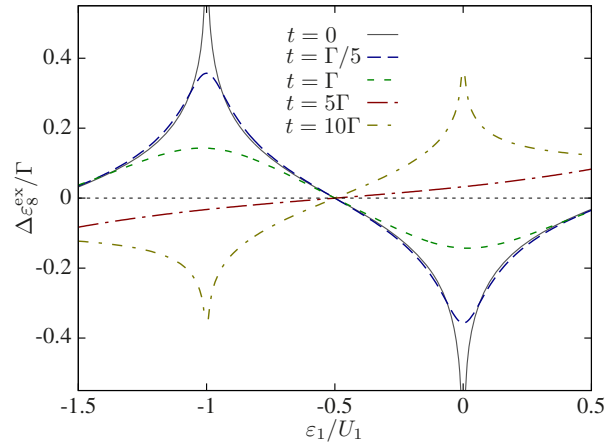


**Fig. 2.** The dependence of the exchange field in the spin-up triplet component  $|e_8\rangle$  on QD1 level position, for finite  $U_1 = W/2 = 5\Gamma$ ,  $p = 0.4$ ,  $U_2 = \varepsilon_2 = 0$  and different  $t$ .

Notice, that in general also  $\Delta \varepsilon^{\text{ex}}$  may become divergent in the limit  $W \rightarrow \infty$ . For this reason that limit was avoided and  $W$  of the order of the highest relevant energy scale was used, as suggested by the scaling theory [2].

In Figure 2, it is shown how the result from equation (16) changes, when  $t$  becomes nonzero (for both dots occupied with a single spin-up electron each). It is clearly seen, that the divergences at the resonances are then removed and the peaks diminish, eventually the exchange field changes sign for really strong  $t$ . In the particle-hole symmetric point,  $\varepsilon_1 = -U_1/2$ ,  $\Delta \varepsilon_8^{\text{ex}} = 0$  for all  $t$ .

Finally, in Figure 3, the density plots of a dependence of the exchange field in the triplet state on both dots' energy levels are presented, for different values of  $t$ , in the case of equal Coulomb interactions on both dots. In Figure 3a, one can clearly see, that for  $t = 0$  the results are qualitatively equivalent to those obtained in Figure 2, where only QD1 was interacting. In agreement with intuition,  $\varepsilon_2$  plays no role in such a situation. However, with increasing  $t$ , the importance of the QD2 level position becomes clear (cf. Fig. 3b). Further increase of  $t$  causes the peaks of  $\Delta \varepsilon^{\text{ex}}$  to change their positions (see Figs. 3c–3e), such that for  $t = 10\Gamma$  the sign of the exchange field is at most of the dots' level positions opposite to the one for  $t = 0$  (see Fig. 3f). After another significant changes of peaks positions while increasing  $t$  even further (cf. Figs. 3g and 3h), the exchange field starts to diminish for  $t = 20\Gamma$  (see Fig. 3i), to vanish completely in the limit  $t \rightarrow \infty$ . Actually, the fact that  $\Delta \varepsilon_i^{\text{ex}} \rightarrow 0$  for  $t \rightarrow \infty$  is rigorously true for all the molecular states and can be proven as follows.

At first, note, that all the matrix elements of  $d_{\alpha\sigma}^{(\dagger)}$  in the eigenbasis have finite limits. On the contrary, all the energies of states with  $S = 1/2$  asymptotically equal  $\pm t$ .  $E_8$  and  $E_9$  asymptotically equal  $\pm 2t$ , the other energies have finite, nonzero limits for  $t \rightarrow \infty$ . In equation (14) energies are present under the logarithm, always as differences. The logarithm containing energy difference  $(E_j - E_i)$  has nonzero coefficient only for such pairs  $(i, j)$ , that some of

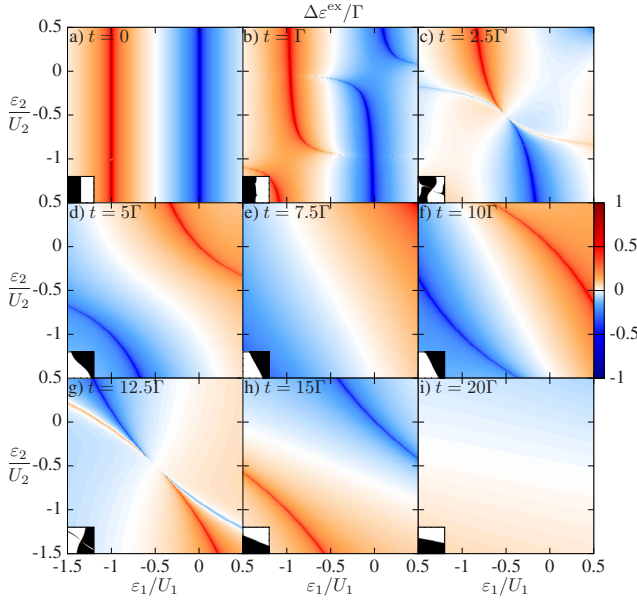


**Fig. 3.** The dependence of the exchange field in the spin-up triplet component  $\Delta\varepsilon_s^x$  on the level positions of both dots for  $U_1 = U_2 = W/2 = 5\Gamma$ ,  $p = 0.4$  and different  $t$ , as indicated in the figure. Insets in the bottom left corners indicate the range of positive (negative) data in black (white), for readability of the plots in the gray-scale.

$\langle e_i | d_{\alpha\sigma}^\dagger | e_j \rangle$  is nonzero. As can be easily checked case by case, all the important energy differences diverge in the limit  $t \rightarrow \infty$ , so the corresponding logarithms vanish (cf., Eq. (14)). This means, that for very large  $t$ , the eigenstates of DQD are too far from each other (in the sense of energy difference) to allow significant charge fluctuations.

#### 4.2 The exchange field for different states

In the case of a single quantum dot coupled to F, the exchange field is either zero (for states of  $S_z = 0$ ), or given by equation (16). This means that it influences the energy spectrum of the dot identically to the magnetic field  $B = \Delta\varepsilon^x / (g\mu_B)$ . It is not exactly the case for DQD. Here, the corresponding magnetic field must be different for different states. However, the multiplet structure of the eigenbasis is preserved. This is illustrated in Figure 4. If the corresponding magnetic field were the same in all the states, all the curves in Figure 4 would coincide. Instead, the peaks appear at different positions for different curves. In the range of small negative values of  $\varepsilon_1$ ,  $\Delta\varepsilon_i^x$  even changes the sign, depending on  $i$ .

Even more interesting result is obtained, when one analyzes the ground state of the DQD subsystem with correction coming from the exchange field. Having defined the ground state energy as  $E_{GS} \equiv \min_i E_i$  (for a fixed set of model parameters), the unperturbed excitation energies  $E_i - E_{GS}$  are plotted as functions of QD1 level position in Figure 5a, and the excitation energies corrected by the exchange field,  $E_i + S_z \Delta\varepsilon_i^x - E_{GS}$ , are shown in

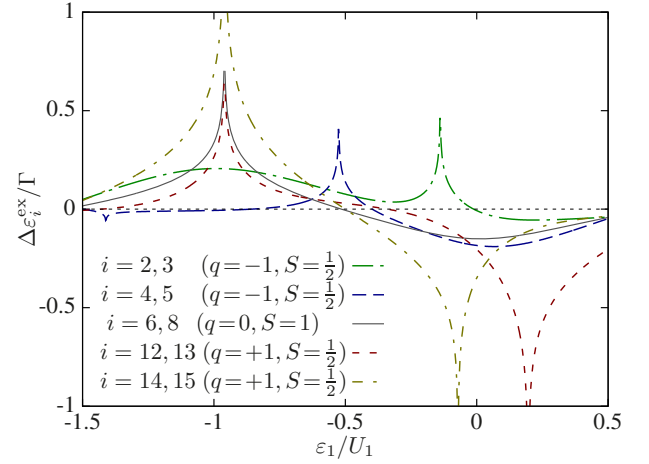


**Fig. 4.** The dependence of the exchange field on the QD1 level position, for  $U_1 = U_2 = W/2 = 5\Gamma$ ,  $p = 0.4$ ,  $\varepsilon_2 = 0$  and  $t = \Gamma$ . In the states not listed in the legend,  $\Delta\varepsilon_i^x = 0$ .

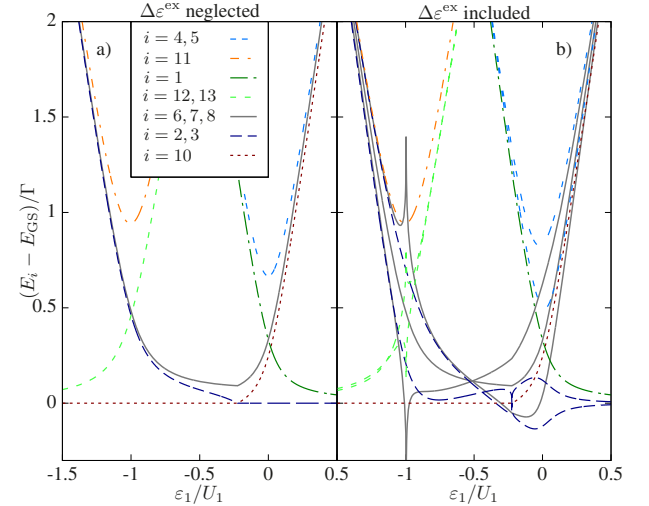


**Fig. 5.** (a) The difference between  $E_i$  and the ground state energy  $E_{GS}$  vs.  $\varepsilon_1$ , for  $U_1 = U_2 = W/2 = 5\Gamma$ ,  $p = 0.4$ ,  $\varepsilon_2 = 0$  and  $t = \Gamma/3$ . (b) The same for  $E_i + S_z \Delta\varepsilon_i^x$  instead of  $E_i$ , with  $E_{GS}$  still obtained without  $\Delta\varepsilon_i^x$ .

Figure 5b. It is visible, that in the Coulomb blockade regime, the ground state of isolated DQD is either the singlet state  $|e_{10}\rangle$ , or degenerate doublet,  $|e_2\rangle, |e_3\rangle$ . The triplet  $|e_6\rangle, |e_7\rangle, |e_8\rangle$  is a low-lying excited state. However, when DQD is coupled to F, due to strong renormalization by the exchange field, the state  $|e_6\rangle$  becomes the ground state for  $\varepsilon_1 \approx -U_1$ , while in very narrow region around  $\varepsilon_1 \approx -0.25U_1$ ,  $|e_8\rangle$  is the ground state. Moreover,  $|e_6\rangle$  becomes degenerate with a singlet state  $|e_{10}\rangle$  in the vicinity of  $\varepsilon_1 = -U_1$ . Because these two states differ in  $S_z$  by unity and have the same charge, they are degenerate states connected by a single spin-flip process, and as so, they can contribute to the formation of the single-stage Kondo effect. The second stage, when the singlet is non-degenerate ground state of DQD, is suppressed. Thus, the

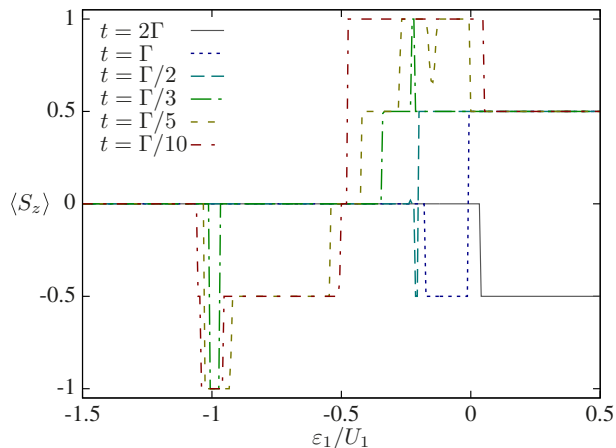


**Fig. 6.** The average value of  $z$ -component of DQD spin for  $T = 10^{-4}\Gamma$ , different  $t$  and other parameters the same as in Figure 5.

large exchange field in triplet state is the condition for the two-stage Kondo effect to be suppressed. This is indeed confirmed by the numerical renormalization group calculations [18].

Knowing energies of DQD states, corrected by  $\Delta\varepsilon^{\text{ex}}$ , one can calculate expectation values of different operators, assuming equilibrium probabilities for eigenstates. Here, the  $z$  component of DQD spin is considered (see Fig. 6). Small finite temperature,  $T = 10^{-4}\Gamma$ , was used to make the curves smoother in the regions of degenerated ground state. For weak  $t$ , see curve for  $t = \Gamma/10$ ,  $\langle S_z \rangle \neq 0$  in the region of Coulomb blockade. It is negative ( $-1/2$ ) for negative detuning, and reaches  $+1$  for positive detuning. However, it vanishes in the small region around particle-hole symmetric point. For  $\varepsilon_1 \approx -U_1$  the triplet component becomes the ground state, resulting in  $\langle S_z \rangle = -1$ . For large, positive detunings,  $\langle S_z \rangle = +1/2$ . On the contrary to the case of small  $t$ , for  $t = 2\Gamma$ ,  $\langle S_z \rangle = 0$  for most of QD1 level positions. Only when  $\varepsilon_1 > 0$ , the average spin becomes  $-1/2$ , which is opposite to what happens for  $t = \Gamma/10$ . This is caused by the fact, that  $\Delta\varepsilon^{\text{ex}}$  can change the sign with increasing  $t$ ; compare Figure 2. For intermediate values of the inter-dot coupling,  $\Gamma/5 < t < \Gamma$ , the region of  $\langle S_z \rangle = 0$  in the center of Coulomb valley becomes larger upon increasing  $t$ , and the region of  $\langle S_z \rangle = +1/2$  appears for  $\varepsilon_1$  slightly larger than  $-U_1/2$ . Moreover, for  $\varepsilon_1 \approx -0.25U_1$  the  $t$ -dependence of  $\langle S_z \rangle$  becomes highly nontrivial. For  $t = \Gamma/5$ , there occurs a dip, suggesting degeneracy between states of  $S_z = 1$  and  $S_z = 1/2$ . For  $t = \Gamma/3$ , the  $S_z = 1$  state is the ground state only in very narrow region of  $\varepsilon_1$  (see also Fig. 5). For  $t = \Gamma/2$ , one sees a sharp dip, reaching  $\langle S_z \rangle = -1/2$ , instead of peak reaching  $\langle S_z \rangle = 1$ , present for  $t = \Gamma/3$ . This dip is significantly wider for  $t = \Gamma$ . Nevertheless, even in this case, for  $\varepsilon_1 > 0$ ,  $\langle S_z \rangle = +1/2$ , contrary to the case of  $t = 2\Gamma$ . The fact that large range of  $\langle S_z \rangle$  values is possible in the region  $-0.25U_1 < \varepsilon_1 < 0$  corresponds to large variety of values of  $\Delta\varepsilon^{\text{ex}}$  for different states, visible in Figure 4 for the case of  $t = \Gamma$ . In particular, note that

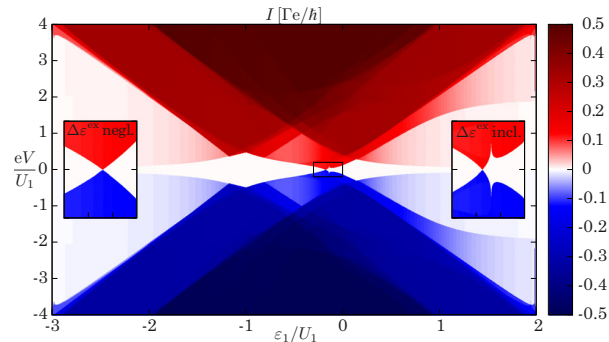


**Fig. 7.** The current through DQD for  $T = 10^{-4}\Gamma$ ,  $t = \Gamma$  and other parameters the same as in Figure 5, obtained with DQD eigenstates energies corrected by the exchange field. Right inset shows enlarged region  $\varepsilon_1 \in [-0.3, 0]U_1$ ,  $eV \in [-0.2, 0.2]U_1$ , marked also with a rectangle in the main plot. The left inset shows the same region as the right one, but with the exchange field neglected.

$\Delta\varepsilon^{\text{ex}}$  can have different sign for different multiplets, thus, states possessing different sign of  $\langle S_z \rangle$  may become the ground state.

### 4.3 The I-V characteristics

The exchange field influences not only the static properties, such as the magnetization of DQD presented in Figure 6. As claimed earlier, also the conductance exhibits its signatures. To present this, the current through the system was calculated using master equation method [21,22], with tunneling rates given by the Fermi golden rule. Moreover, in this subsection we use two leads, with  $\Gamma_{r\sigma} = (1 + \sigma p)\Gamma/2$ , because the transformation given by equations (8) and (9) does not decouple  $f$  operators outside the equilibrium. The results, presented in Figure 7, are valid only in the sequential tunneling regime, since any higher terms are neglected. However, the influence of the exchange field on the  $I$ - $V$  characteristics near the resonance is clearly visible.

In general, one can see large regions of approximately constant current. Each such region corresponds to a fixed set of many-body DQD states, whose energy differences fit in the energy window of a voltage bias. The whole plot resembles a bit a structure characteristic of single interacting QD. However, the inter-dot interaction  $t$  causes the edges of fixed-current regions to band, and the increased number of states reflects itself in the splitting of just a few regions present in the single-QD case. The fact that the plot is not symmetric with respect to  $\varepsilon_1 = -U_1/2$  comes from the lack of particle-hole symmetry in QD2, since  $\varepsilon_2 = 0 \neq -U_2/2$  was assumed. All these features, visible in Figure 7, are valid also when one neglects the existence of  $\Delta\varepsilon^{\text{ex}}$ .

The effects of  $\Delta\varepsilon^{\text{ex}} \neq 0$  are explicitly shown in the insets. The right one shows the enlargement of the region  $-0.3U_1 < \varepsilon_1 < 0$ ,  $|V| < 0.2U_1/e$ . The left one – the results obtained in the same region by neglecting  $\Delta\varepsilon^{\text{ex}}$ .

Note, that according to Figure 5, in this region the ground state becomes magnetic due to the exchange field. The result is clearly visible: the lack of degeneracy leads to the splitting of the X-like structure, which resembles the effect of external magnetic field (here magnetic field is absent).

#### 4.4 Limitations of the method

The considerations in this paper rely on the perturbative expansion in  $\Gamma$ . For transport properties, this is very strong assumption, which limits the range of validity of the results obtained in Section 4.3. One can expect the best accuracy in the sequential tunneling regime, worse in the co-tunneling regime, and completely false in the Kondo regime. However, the inter-dot interaction  $t$  was treated exactly, so the interference effects between different conduction paths, containing arbitrary number of hops of an electron between the dots are properly taken into account.

On the other hand, the renormalization of levels caused by the interaction with magnetically polarized bath obtained with second order perturbation theory proved to be in a good agreement with more sophisticated methods, in particular with numerical renormalization group calculations, for different systems and also in the strong coupling regime [7,14]. For this reason, one can hope that they can be quite generally valid in the linear response regime. Nevertheless, higher order terms may play an important role for particle-hole symmetric point, where  $\Delta\varepsilon^{\text{ex}} = 0$ . For QDs possessing large-spin ground state, they give rise to formation of the effective magnetic quadrupolar field, not vanishing at the symmetric point [23].

Moreover, an important note can be done, if one considers the case  $U_2 = 0$ . Then, one can propose a definition of the exchange field induced on QD2 by both F and QD1 (as opposed to the exchange field for molecular states defined earlier). This is done as follows. Since the only nonquadratic terms in the Hamiltonian are related to the Coulomb interactions, the subsystem containing F and QD1 can now be diagonalized exactly. The whole model is then equivalent to the Anderson impurity (corresponding to QD2) coupled to the lead possessing Lorentzian density of states (corresponding to the diagonalized subsystem containing F and QD1) [24]. Then, treating  $t$  perturbatively to the second order and defining  $\Delta\varepsilon_{\text{QD2}}^{\text{ex}}$  to be the difference between the shifts of different spins for the singly occupied QD2, we obtain [14]

$$\begin{aligned} \Delta\varepsilon_{\text{QD2}}^{\text{ex}} = & \sum_{\sigma} \sigma \frac{t^2}{2} [L_{U_2+\tilde{\delta}}(\Gamma_{\sigma}) - L_{-\tilde{\delta}}(\Gamma_{\sigma})] \\ & - \sum_{\sigma} \sigma \frac{t^2}{\pi} \arctan\left(\frac{\varepsilon_{-1}}{\Gamma_{\sigma}}\right) \\ & \times [L_{U_2+\tilde{\delta}}(\Gamma_{\sigma}) + L_{-\tilde{\delta}}(\Gamma_{\sigma})] \\ & - \sum_{\sigma} \sigma \frac{t^2}{2\pi} L_{\Gamma_{\sigma}}(U_2 + \tilde{\delta}) \log \frac{(\varepsilon_2 + U_2)^2}{\varepsilon_1^2 + \Gamma_{\sigma}^2} \\ & + \sum_{\sigma} \sigma \frac{t^2}{2\pi} L_{\Gamma_{\sigma}}(-\tilde{\delta}) \log \frac{\varepsilon_2^2}{\varepsilon_1^2 + \Gamma_{\sigma}^2}, \end{aligned} \quad (17)$$

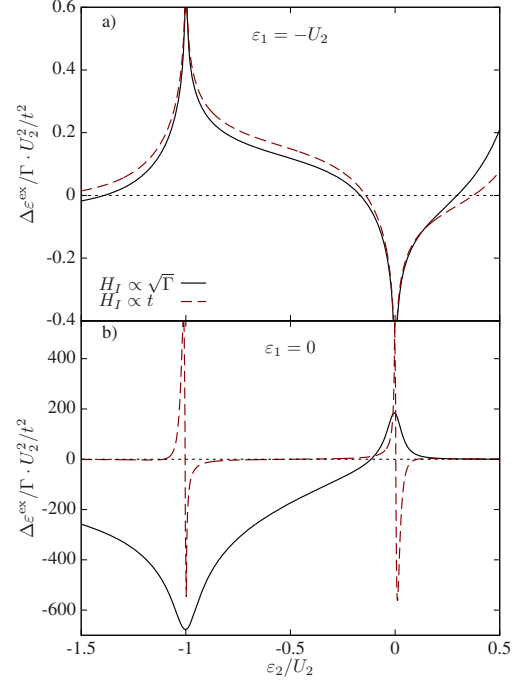


**Fig. 8.** The dependence of the exchange field on QD2 level position calculated from equation (14) for the state  $|e_{13}\rangle$  ( $q = +1$ ,  $S_z = +1/2$ , solid line), and from equation (17) (dashed line), for  $U_1 = 0$ ,  $U_2 = W/2$ ,  $t = \Gamma = W/100$ ,  $p = 0.4$ , and (a)  $\varepsilon_1 = -U_2$ , (b)  $\varepsilon_1 = 0$ .

where  $L_y(x) = y/(x^2 + y^2)$  and  $\tilde{\delta} \equiv \varepsilon_2 - \varepsilon_1 = 2\delta - U_2/2$ . Interestingly,  $\Delta\varepsilon_{\text{QD2}}^{\text{ex}}$  does not vanish for  $U_2 = 0$ . This peculiarity changes if equation (17) is expanded in the power series in  $\Gamma$ . Then, zeroth order vanishes, and in the first order one obtains the result, in which  $U_2 = 0$  implies  $\Delta\varepsilon_{\text{QD2}}^{\text{ex}} = 0$ .

The question if the result (17) can be reasonably compared with equation (14) is not trivial. First of all, while in equation (14) we treated  $t$  exactly and  $\Gamma$  perturbatively, it was the other way around in equation (17). Thus, if these two are to be correct simultaneously, both  $t$  and  $\Gamma$  must be small, when compared to  $U_2$ . This is, however, not the whole story yet. The even bigger problem is that equation (17) corresponds to the situation, in which QD2 is singly occupied, while the subsystem containing F and QD1 is in its ground state. The occupancy of QD1 in this ground state is not well defined for the general case. Thus, the reasonable comparison can be made only in the special cases. One of them is the case of large  $|\varepsilon_1|$ . Indeed, QD1 is practically doubly occupied for  $\varepsilon_1 \ll -\Gamma$  and practically unoccupied for  $\varepsilon_1 \gg \Gamma$ . The comparison of  $\Delta\varepsilon^{\text{ex}}$  obtained in this case from equations (14) and (17) is presented in Figure 8a. The same comparison for  $\varepsilon_1 = 0$  does not make sense, which is illustrated in Figure 8b. This demonstrates, that the validity of the results obtained in this paper is limited to the case of  $\Gamma$  weak enough for DQD occupation to be determined from  $H_{\text{DQD}}$  eigenenergies only. In particular, the spin-dependent Fano-like interference occurring

at extremely low temperatures is better described with the aid of formula (17) then by equation (14) [14].

## 5 Conclusions

In the present article we have defined and calculated the exchange field induced in the molecular states of a double quantum dot by the coupling to the ferromagnetic leads in the T-shaped configuration. It was shown that the exchange field is different in different molecular states, so it is not acting exactly like a real magnetic field. However, it acts very similarly, reversing the sign of the shift upon spin-reversal in the considered state.

The results for small  $t$  agree with well-known formula (16). However, the dependence on  $t$  for stronger inter-dot hopping is complex, and perturbative treatment of  $t$  would have to be performed to very high order to give results consistent with equation (14), in particular for the parameters used in Figure 3. Because changing  $t$  can change sign and magnitude of  $\Delta\varepsilon^{\text{ex}}$ , it can be used to tune the exchange field as well as  $\varepsilon_1$  or  $\varepsilon_2$ .

The validity of equation (14) is limited by the validity of perturbative treatment of  $\Gamma$  and by the assumption, that the molecular states are relevant for the physical situation of the interest. For the case of strong  $\Gamma$  and weak  $t$ , this is not the case.

The author thanks I. Weymann for fruitful discussions and P. Baláz for critical reading of the manuscript. Research was supported by the National Science Center in Poland through Project No. DEC-2013/10/E/ST3/00213.

## References

1. U. Fano, Phys. Rev. **124**, 1866 (1961)
2. F.D.M. Haldane, Phys. Rev. Lett. **40**, 416 (1978)
3. P.W. Anderson, J. Phys. C **3**, 2436 (1970)
4. J. Martinek, Y. Utsumi, H. Imamura, J. Barnaś, S. Maekawa, J. König, G. Schön, Phys. Rev. Lett. **91**, 127203 (2003)
5. K.G. Wilson, Rev. Mod. Phys. **47**, 773 (1975)
6. M.S. Choi, D. Sanchez, R. Lopez, Phys. Rev. Lett. **92**, 056601 (2004)
7. J. Martinek, M. Sindel, L. Borda, J. Barnaś, R. Bulla, J. König, G. Schön, S. Maekawa, J. von Delft, Phys. Rev. B **72**, 121302 (2005)
8. A.N. Pasupathy, R.C. Bialczak, J. Martinek, J.E. Grose, L.A. Donev, P.L. McEuen, D.C. Ralph, Science **306**, 86 (2004)
9. M. Gaass, A.K. Hüttel, K. Kang, I. Weymann, J. von Delft, C. Strunk, Phys. Rev. Lett. **107**, 176808 (2011)
10. J.R. Hauptmann, J. Paaske, P.E. Lindelof, Nat. Phys. **4**, 373 (2008)
11. S. Sasaki, H. Tamura, T. Akazaki, T. Fujisawa, Phys. Rev. Lett. **103**, 266806 (2009)
12. R. Žitko, Phys. Rev. B **81**, 115316 (2010)
13. I.L. Ferreira, P.A. Orellana, G.B. Martins, F.M. Souza, E. Vernek, Phys. Rev. B **84**, 205320 (2011)
14. K.P. Wójcik, I. Weymann, Phys. Rev. B **90**, 115308 (2014)
15. M. Pustilnik, L.I. Glazman, Phys. Rev. Lett. **87**, 216601 (2001)
16. C.-H. Chung, G. Zarand, P. Wölfle, Phys. Rev. B **77**, 035120 (2008)
17. L.G.G.V. Dias da Silva, E. Vernek, K. Ingersent, N. Sandler, S.E. Ulloa, Phys. Rev. B **87**, 205313 (2013)
18. K.P. Wójcik, I. Weymann, Phys. Rev. B, accepted
19. B.R. Bułka, T. Kostyrko, Phys. Rev. B **70**, 205333 (2004)
20. L.I. Glazman, M.E. Raikh, J. Exp. Theor. Phys. Lett. **47**, 452 (1988)
21. H. Grabert, M.H. Devoret, *Single Charge Tunneling* (Springer US, New York, 1992)
22. I. Weymann, J. Barnaś, S. Krompiewski, Phys. Rev. B **76**, 155408 (2007)
23. M. Misiorny, M. Hell, M.R. Wegewijs, Nat. Phys. **9**, 801 (2013)
24. L. Vaugier, A.A. Aligia, A.M. Lobos, Phys. Rev. B **76**, 165112 (2007)

**Open Access** This is an open access article distributed under the terms of the Creative Commons Attribution License (<http://creativecommons.org/licenses/by/4.0>), which permits unrestricted use, distribution, and reproduction in any medium, provided the original work is properly cited.

**Two-stage Kondo effect in T-shaped double quantum dots with ferromagnetic leads**

Krzysztof P. Wójcik\* and Ireneusz Weymann

*Faculty of Physics, Adam Mickiewicz University, Umultowska 85, 61-614 Poznań, Poland*

(Received 29 January 2015; revised manuscript received 27 March 2015; published 21 April 2015)

The linear-response transport properties of a T-shaped double quantum dot strongly coupled to external ferromagnetic leads are studied theoretically by using the numerical renormalization group method. It is shown that when each dot is occupied by a single electron, for antiparallel alignment of leads' magnetizations, the system exhibits the two-stage Kondo effect. For parallel alignment, however, the second stage of the Kondo effect becomes suppressed due to the presence of ferromagnetic-contact-induced exchange field. The difference between the two magnetic configurations results in highly nontrivial behavior of the tunnel magnetoresistance, which for some parameters can take giant values. In addition, the dependence of the linear conductance and tunnel magnetoresistance on external magnetic field, the double-dot levels' position, and the spin polarization of the leads is thoroughly analyzed. It is shown that the second stage of the Kondo effect can be restored by fine-tuning of the magnetic field or the dots' levels. The effect of spin-dependent tunneling on the low-temperature transition from the high to low conducting state of the system, which occurs when changing the hopping between the dots, is also discussed.

DOI: [10.1103/PhysRevB.91.134422](https://doi.org/10.1103/PhysRevB.91.134422)

PACS number(s): 73.23.-b, 73.21.La, 72.15.Qm, 72.25.-b

**I. INTRODUCTION**

Screening of a magnetic impurity's spin by conduction electrons of the host metal occurs at sufficiently low temperatures and results in an increase of the resistance [1]. The mechanism leading to this effect is associated with spin-flip scattering processes between the impurity's spin and conduction electrons, as first elucidated by Kondo [2]. Similar screening can also occur in a quantum dot hosting an unpaired spin, but now instead of resistance enhancement one observes an increased conductance through the system [3]. Multiple spin-flip processes give rise to an additional resonance in the dot's local density of states at the Fermi level. This results in enhanced transmission through the system, yielding, for temperatures  $T$  smaller than the Kondo temperature  $T_K$ , maximum conductance,  $G = 2e^2/h$ . The Kondo effect in quantum dots and molecules has already been a subject of extensive studies for more than two decades [4–8], and its more complex and exotic versions that occur in multi-dot systems still draw a nondecreasing attention [9–12].

While in simple one-impurity systems the screening usually has a single-stage character, in multi-impurity systems screening can be realized in a multistage way [3]. In this regard, one of the simplest examples is the two-impurity Kondo problem, in which the interplay of the RKKY interaction between the impurity spins with the correlations leading to the Kondo effect results in two-stage screening [13]. The two-stage Kondo effect also occurs in side-coupled double quantum dot (DQD) systems, where the antiferromagnetic coupling between the dots' spins competes with the Kondo effect [14–23]. The two-stage nature of screening is revealed especially in the temperature dependence of the conductance, which is not monotonic: With lowering the temperature, for  $T \approx T_K$ , the conductance first increases due to the Kondo effect; however, with further decrease of  $T$ , for  $T < T^*$ , where  $T^*$  is the temperature characteristic of the second-stage screening, the conductance drops to zero [21].

Recently, various aspects of the two-stage Kondo effect in T-shaped DQDs have been extensively studied, both experimentally [14–17] and theoretically [18–30]. However, these considerations dealt mainly with the case of nonmagnetic leads. The goal of the present paper is therefore to extend those studies and analyze the two-stage Kondo effect in the presence of itinerant ferromagnetism. Transport properties of quantum dots with ferromagnetic leads in the Kondo regime have been attracting considerable attention for the last decade [31–40]. For example, it was shown that the conductance depends greatly on the relative orientation of ferromagnets. For single quantum dots, when the leads' magnetizations are oriented in parallel, the Kondo effect can be suppressed due to the presence of an effective exchange field, while no such suppression occurs in the antiparallel configuration where the exchange field is absent for symmetric systems [31–34]. The suppression of the Kondo resonance is due to a spin splitting of the dot level, which is caused by the exchange field and can be controlled by a gate voltage [41]. One can expect that the impact of exchange field effects on transport characteristics of T-shaped double quantum dots is even more complex [42]. Despite vast existing literature on spin-resolved transport through quantum dots, the two-stage Kondo effect remains in this context to a large extent unexplored. Therefore, this problem is addressed in the present paper.

Using the numerical renormalization group method [43] we calculate the linear response conductance in the parallel and antiparallel magnetic configurations, as well as the resulting tunnel magnetoresistance (TMR). We show that the temperature dependence of the linear conductance in the parallel configuration greatly depends on the splitting caused by the exchange field, which can be tuned by gate voltages. While in the antiparallel configuration the conductance becomes suppressed at sufficiently low temperatures, in the parallel configuration the second stage of screening is destroyed and the conductance is finite. Moreover, for some gate voltages, the second stage of screening can be totally suppressed. This results in highly nontrivial behavior of the TMR, which at low temperatures is greatly enhanced and takes giant values. We also study the dependence of the low-temperature value

\*kpwojcik@amu.edu.pl

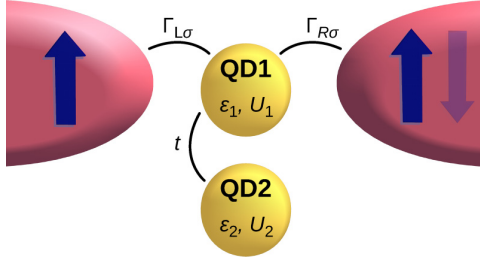


FIG. 1. (Color online) Schematic of a T-shaped double quantum dot coupled to ferromagnetic leads. The first dot is directly coupled to the leads with the coupling strengths  $\Gamma_{L\sigma}$  and  $\Gamma_{R\sigma}$ , while the second dot is coupled to the first one via the hopping matrix element  $t$ . The magnetizations of the leads can form either parallel or antiparallel magnetic configuration.

of the conductance in the parallel configuration on the spin polarization of the leads, which is found to be nonmonotonic. In addition, we analyze the transition from low to high conducting state of the system as a function of the hopping between the two dots at a small but finite temperature,  $T < T^*$ , and show that the exchange field smears out this transition. Finally, we consider the effect of finite magnetic field and level detuning on transport properties, which clearly indicates that transport behavior is conditioned by an intricate interplay between the exchange field and the first and second stage Kondo temperatures,  $T_K$  and  $T^*$ .

The paper is organized as follows. A theoretical description of the system and method used in calculations is presented in Sec. II. The third section is devoted to numerical results and their discussion. We first analyze the case of nonmagnetic leads (Sec. III A), as a starting point for the analysis of the case with ferromagnetic contacts (Sec. III B), where we study the temperature and magnetic field dependence of conductance and TMR for different hoppings between the dots and for different leads' spin polarization. We also analyze how the DQD level detuning affects the transport properties. Finally, the paper is concluded in Sec. IV.

## II. THEORETICAL FORMULATION

The system consists of two single-level quantum dots (QDs) in a T-shaped geometry; see Fig. 1. The dots are coupled to each other and one of the dots (the first dot, denoted QD1) is attached to external ferromagnetic leads. The magnetizations of the leads are assumed to form either parallel or antiparallel magnetic configuration. The Hamiltonian of the system is based on the Anderson model and has the form  $H = H_{\text{DQD}} + H_{\text{cb}} + H_{\text{T}}$ , where

$$H_{\text{DQD}} = \sum_{i\sigma} \varepsilon_i n_{i\sigma} + \sum_i U_i n_{i\uparrow} n_{i\downarrow} + B S_z + \sum_{\sigma} t (d_{1\sigma}^{\dagger} d_{2\sigma} + \text{H.c.}), \quad (1)$$

$$H_{\text{cb}} = \sum_{\vec{k}\sigma r} \varepsilon_{r\vec{k}\sigma} n_{r\vec{k}\sigma}, \quad (r = L, R), \quad (2)$$

$$H_{\text{T}} = \sum_{\vec{k}\sigma r} (V_{r\vec{k}\sigma} d_{1\sigma}^{\dagger} c_{r\vec{k}\sigma} + \text{H.c.}). \quad (3)$$

Here,  $d_{i\sigma}$  annihilates an electron of spin  $\sigma$  in dot  $i$ ,  $n_{i\sigma} = d_{i\sigma}^{\dagger} d_{i\sigma}$ ,  $c_{r\vec{k}\sigma}$  annihilates an electron carrying momentum  $\vec{k}$  and spin  $\sigma$  in the lead  $r$  ( $r = L$  for left and  $r = R$  for right lead), and  $n_{r\vec{k}\sigma} = c_{r\vec{k}\sigma}^{\dagger} c_{r\vec{k}\sigma}$ .  $\varepsilon_i$  ( $\varepsilon_{r\vec{k}\sigma}$ ) denotes the single-electron energy of dot  $i$  (in lead  $r$ , corresponding to momentum  $\vec{k}$  and in spin  $\sigma$ ). The Coulomb energy of two electrons occupying the dot  $i$  is denoted by  $U_i$ , while  $B$  stands for external magnetic field with  $g\mu_B \equiv 1$ . It is assumed that the capacitive coupling between the dots is negligible. We also assume that the Coulomb correlation parameters are the same in both dots,  $U_1 = U_2 \equiv U$ . The term proportional to  $t$  describes hopping between the two dots, while  $V_{r\vec{k}\sigma}$  denotes the respective matrix elements for tunneling between the first dot and external lead  $r$ . We assume  $V_{r\vec{k}\sigma}$  to be independent of  $\vec{k}$  and  $r$ ,  $V_{r\vec{k}\sigma} \equiv V_{\sigma}$ . The coupling to external leads gives rise to broadening of the first dot's level, which is described by  $\Gamma_{r\sigma} = \pi \rho_{r\sigma} |V_{\sigma}|^2$ , where  $\rho_{r\sigma}$  is the normalized density of states at the Fermi level of lead  $r$  for spin  $\sigma$ . For ferromagnetic leads, the coupling can be conveniently expressed in terms of spin polarization  $p_r$  of lead  $r$  as  $\Gamma_{r\sigma} = (1 + \sigma p_r) \Gamma_r$ , where  $\Gamma_r = (\Gamma_{r\uparrow} + \Gamma_{r\downarrow})/2$  and  $p_r = (\rho_{r\uparrow} - \rho_{r\downarrow})/(\rho_{r\uparrow} + \rho_{r\downarrow})$  is the spin polarization of lead  $r$ . In the following we assume that electrodes are made of the same material,  $p_L = p_R \equiv p$ , and the double quantum dot is coupled symmetrically to the leads,  $\Gamma_L = \Gamma_R \equiv \Gamma/2$ .

To analyze the transport properties of T-shaped double quantum dots strongly coupled to ferromagnetic leads, we use the numerical renormalization group (NRG) technique [43]. This method is known as very powerful and versatile in studying various quantum impurity models. It proved to be extremely accurate and useful for explaining experimental data on the Kondo effect in quantum dots and molecules [12,38]. The core of NRG consists in logarithmic discretization of the conduction band and mapping of the discretized Hamiltonian onto a tight-binding chain with exponentially decaying hoppings, which is then solved iteratively. Here, we perform the calculations with the aid of the open-access Budapest NRG code [44]. It allows for calculating static and dynamic properties of the system at arbitrary temperatures by using the full density matrix [45,46] and exploiting an arbitrary number of symmetries that the Hamiltonian possesses. In our calculations we use the Abelian symmetries for the total charge and total spin  $z$ th component. We keep at least 1024 states during iteration and use discretization parameter  $\Lambda = 2$ . Moreover, we calculate the conductance directly from discrete NRG data [47], without the need to invoke broadening procedures which can introduce certain errors [48].

In the linear response regime, for energy-independent couplings to the leads, the conductance can be found from [49,50]

$$G^{\text{P/AP}} = \frac{2e^2}{h} \sum_{\sigma} \frac{2\Gamma_{L\sigma}^{\text{P/AP}} \Gamma_{R\sigma}^{\text{P/AP}}}{\Gamma_{\sigma}^{\text{P/AP}}} \int d\omega \left[ -\frac{\partial f(\omega)}{\partial \omega} \right] \pi A_{\sigma}^{\text{P/AP}}(\omega), \quad (4)$$

where  $\Gamma_{\sigma}^{\text{P/AP}} = \Gamma_{L\sigma}^{\text{P/AP}} + \Gamma_{R\sigma}^{\text{P/AP}}$ ,  $f(\omega)$  is the Fermi function, and  $A_{\sigma}^{\text{P/AP}}(\omega)$  is the spin-resolved spectral function of the first quantum dot, which we calculate by NRG. The superscript denotes either parallel (P) or antiparallel (AP) magnetic configuration. The change of system transport properties when



switching the magnetic configuration of the device can be described by the TMR, which is defined as [51]

$$\text{TMR} = \frac{G^{\text{P}} - G^{\text{AP}}}{G^{\text{AP}}}. \quad (5)$$

To perform the calculations it is convenient to make an orthogonal transformation from the left-right to a new basis, in which the DQD couples only to a single conduction channel with an effective coupling strength  $\Gamma_{\sigma} = \Gamma_{L\sigma} + \Gamma_{R\sigma}$  [32,33,35,37]. This allows us to perform the calculations in the standard single-channel fashion [3]. While generally the spin dependence of the effective coupling  $\Gamma_{\sigma}$  is present in both magnetic configurations [40], for left-right symmetric systems as considered here, it only persists in the parallel configuration. The effective coupling in the given magnetic configuration has then the following form,  $\Gamma_{\sigma}^{\text{AP}} = \Gamma$  and  $\Gamma_{\sigma}^{\text{P}} = (1 + \sigma p)\Gamma$ . This implies that, except for an overall spin-polarization-dependent factor,  $1 - p^2$ , transport properties in the antiparallel configuration are the same as in the case of nonmagnetic leads.

We note that if the left-right symmetry is broken, the effective coupling becomes spin-dependent in the antiparallel configuration. This can result in nontrivial effects, such as the occurrence of the exchange field in both magnetic configurations [40]. Similarly, in the case of left-right symmetry, but when a deviation from collinear alignment of magnetizations in the case of antiparallel configuration occurs, effective exchange field can also arise [52–55]. If the exchange field is smaller than the relevant energy scales in the problem, such as the Kondo temperature, the behavior of the system's transport characteristics will be hardly affected. Consequently, one can expect that relatively small deviations from the left-right symmetry or collinear alignment of magnetizations, which are unavoidable in real experiments, will not change the physics much. Detailed analysis of such effects is however beyond the scope of the present paper.

### III. DISCUSSION OF NUMERICAL RESULTS

In this section we present and discuss the numerical results on the linear conductance and TMR as a function of temperature  $T$ , hopping between the dots  $t$ , external magnetic field  $B$ , and DQD levels' positions. We mainly focus on the case when there is a single electron on each dot, that is, on the transport regime where the (two-stage) Kondo effect occurs. In our analysis we assume the following parameters for the DQD:  $U = 0.5$  and  $\Gamma = 0.1$ , expressed in units of band half-width  $D \equiv 1$ . For  $t = 0$ ,  $\varepsilon_1 = -U/2$ , and  $p = 0$ , the Kondo temperature, defined as the temperature at which  $G(T)/G(0) = 1/2$ , is  $T_{\text{K}} = 3.14 \times 10^{-2}$ .

#### A. The case of nonmagnetic leads

Before analyzing the transport properties for DQD with ferromagnetic leads, let us first discuss the case of nonmagnetic leads as a reference for understanding and elucidating the role of spin-resolved transport on the two-stage Kondo effect. The temperature dependence of the linear conductance for different values of the hopping in the case when the two dots are singly occupied is shown in Fig. 2. For  $t = 0$ , the model corresponds

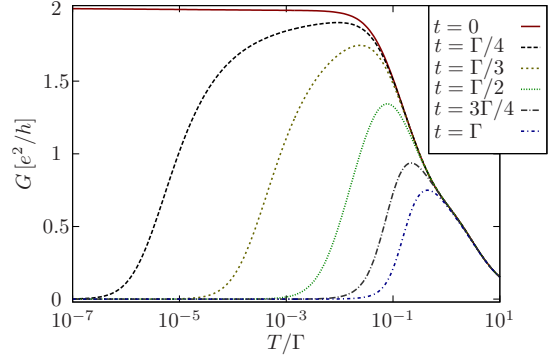


FIG. 2. (Color online) The linear response conductance  $G$  as a function of temperature  $T$  for different values of the hopping  $t$  between the two dots in the case of nonmagnetic leads. The parameters are  $U = 0.5$ ,  $\Gamma = U/5$ ,  $\varepsilon_1 = \varepsilon_2 = -U/2$ , and  $p = 0$ .

to the single-impurity Anderson model and the conductance increases to its maximum value,  $G = 2e^2/h$ , for  $T \ll T_{\text{K}}$ . At low temperatures, the  $T$  dependence of  $G$  is universal with only one relevant energy scale—the Kondo temperature [3].

In the case of finite hopping, however, the temperature dependence of the conductance is not monotonic anymore; see Fig. 2. Finite  $t$  introduces another energy scale in the problem,  $T^*$ , at which the spins of the two dots form a singlet and the conductance through the system becomes totally suppressed for  $T \ll T^*$ . The temperature at which the second stage of the Kondo effect occurs can be expressed as [21–23]

$$T^* = aT_{\text{K}}e^{-bT_{\text{K}}/J_{\text{eff}}}, \quad (6)$$

where  $a$  and  $b$  are constants of the order of unity and  $J_{\text{eff}}$  is the effective antiferromagnetic exchange interaction between the two spins in quantum dots, which is given by [21–23,28]

$$J_{\text{eff}} = 2t^2 \left( \frac{1}{\varepsilon_1 + U_1 - \varepsilon_2} + \frac{1}{\varepsilon_2 + U_2 - \varepsilon_1} \right). \quad (7)$$

In the absence of detuning between the levels,  $\varepsilon_1 = \varepsilon_2$ , and for the same Coulomb correlations in the dots,  $U_1 = U_2 = U$ , the exchange interaction becomes  $J_{\text{eff}} = 4t^2/U$ .

Clearly, decreasing the hopping between the dots suppresses  $T^*$  in an exponential way, and for  $t \rightarrow 0$  the second stage of the Kondo effect does not occur; see Fig. 2. Moreover, if the two energy scales,  $T_{\text{K}}$  and  $T^*$ , are well separated, conductance in the intermediate temperature range,  $T^* \ll T \ll T_{\text{K}}$ , can reach its maximum value; see the case of  $t = \Gamma/4$  in Fig. 2. For larger hopping  $t$ , however, the difference between  $T_{\text{K}}$  and  $T^*$  is decreased and the conductance exhibits smaller increase for temperatures  $T^* < T < T_{\text{K}}$ ; see Fig. 2 in the case of  $t = \Gamma$ . On the other hand, for  $T < T^*$ ,  $G$  decays quadratically with temperature [21].

Numerically, we determine  $T^*$  as the temperature at which the conductance drops to half of its maximum value. In particular, for parameters used in Fig. 2 and for  $t = \Gamma/3$ ,  $T^* = 5.92 \times 10^{-5} = 1.89 \times 10^{-3}T_{\text{K}}$ . From the NRG data we can also estimate the constants  $a$  and  $b$  appearing in Eq. (6), which are equal,  $a \approx 0.48$  and  $b \approx 1.56$ .

### B. The case of ferromagnetic leads

When the leads are ferromagnetic, the behavior discussed in previous section can be drastically changed. Now, another energy scale associated with the exchange field,  $\Delta\varepsilon_{\text{exch}}$ , enters into the problem. The exchange field results from charge fluctuations between the dot and leads, which give rise to the spin-dependent renormalization of the dot levels [31]. As a matter of fact,  $\Delta\varepsilon_{\text{exch}}$ , by splitting the dot levels, acts in a similar way to strong external magnetic field [38]; however, its magnitude and sign can be controlled electrically by tuning the levels with gate voltages. For a single-level quantum dot,  $\Delta\varepsilon_{\text{exch}}$  can be approximated by [31]  $\Delta\varepsilon_{\text{exch}} = \frac{2p\Gamma}{\pi} \log\left|\frac{\varepsilon}{\varepsilon+U}\right|$ . Thus,  $\Delta\varepsilon_{\text{exch}}$  changes sign when crossing the particle-hole symmetry point  $\varepsilon = -U/2$ , while for  $\varepsilon = -U/2$ ,  $\Delta\varepsilon_{\text{exch}} = 0$ . On the other hand, for double dots the formula for the exchange field is more complex [42,56]; nevertheless, the main properties are still very similar to the single-dot case:  $\Delta\varepsilon_{\text{exch}}$  vanishes at the particle-hole symmetry point of the model,  $\varepsilon_1 = \varepsilon_2 = -U/2$ , and its magnitude and sign can be controlled by tuning the DQD levels. Thus, one may expect highly nontrivial behavior of linear conductance and TMR as a function of temperature for various configurations of the DQD levels, which determine the strength of the exchange-field-induced splitting. This is indeed the case, as we show in the following.

As mentioned before, for left-right symmetric systems,  $G$  in the antiparallel configuration is the same as in the case of nonmagnetic leads except for an overall factor of  $1 - p^2$ , which decreases the conductance. However, to make the discussion more comprehensive and enable direct comparison with the case of parallel magnetic configuration, in the following figures we present both  $G^{\text{P}}$  and  $G^{\text{AP}}$ .

#### 1. Temperature dependence for different hoppings $t$

In this section we study the temperature dependence of the linear conductance and TMR for different hoppings between the dots and arrangements of the DQD levels. This corresponds to the situation when for given magnitude of the exchange field we change the effective exchange interaction between the two dots, affecting thus the characteristic energy scale of the second stage of the Kondo effect,  $T^*$  [57].

The temperature dependence of the linear conductance in both magnetic configurations and the resulting TMR for different values of the hopping is presented in Fig. 3. This figure was calculated for  $\varepsilon_1 = \varepsilon_2 = -U/2$ , i.e., for the particle-hole symmetry point of the model where the exchange field is absent. It allows us to determine the effects of spin-dependent couplings, which are not connected with the spin splitting of the DQD levels. As can be seen in Fig. 3, the temperature dependence of the conductance in both magnetic configurations is qualitatively similar. For  $t = 0$ , i.e., when the second dot is decoupled, the Kondo effect occurs in both configurations. For finite  $t$ , both  $G^{\text{P}}$  and  $G^{\text{AP}}$  initially increase when the system is cooled down. For  $T \gtrsim T_K$ , they practically do not depend on  $t$ ; however, at lower temperatures, curves corresponding to different hoppings  $t$  deviate from each other; see Figs. 3(a) and 3(b). At very low temperatures, both conductances eventually approach zero.

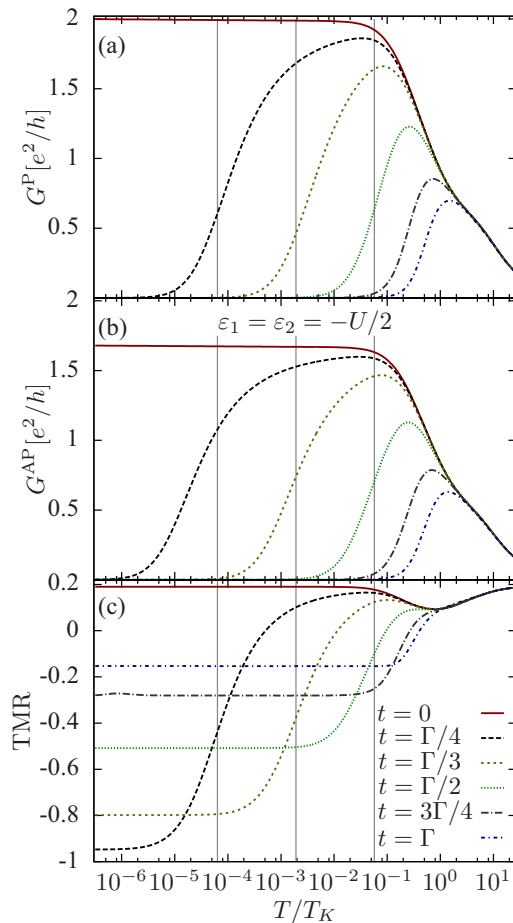


FIG. 3. (Color online) The linear conductance  $G$  in the parallel (a) and antiparallel (b) magnetic configuration and the resulting TMR (c) as a function of temperature. The parameters are  $U = 0.5$ ,  $\Gamma = 0.1$ ,  $\varepsilon_1 = \varepsilon_2 = -U/2$ , and  $p = 0.4$ . The vertical lines correspond to temperatures  $30T^*$ ,  $T^*$ , and  $T^*/30$  in the case of  $t = \Gamma/3$ , indicated for further reference.

Although the behaviors of  $G^{\text{P}}$  and  $G^{\text{AP}}$  with temperature are similar, there are still important quantitative differences: First, the Kondo temperature in the case of parallel configuration is smaller than in the case of antiparallel configuration; i.e.,  $T_K^{\text{P}} < T_K^{\text{AP}}$ . Second, the second stage of the Kondo effect occurs at larger temperature in the parallel magnetic configuration compared to the antiparallel case; i.e.,  $T_p^* > T_{\text{AP}}^*$ . To understand these differences let us invoke the formula for the Kondo temperature in the case of single-level quantum dots for parallel magnetic configuration and for  $\varepsilon = -U/2$  [31],

$$T_K^{\text{P}} = \sqrt{\frac{U\Gamma}{2}} \exp\left[-\frac{\pi U}{8\Gamma} \frac{\text{arctanh}(p)}{p}\right]. \quad (8)$$

Clearly, the spin-polarization-dependent factor in the Kondo temperature leads to decrease of  $T_K^{\text{P}}$  with increasing  $p$ . Note that the Kondo temperature in the antiparallel configuration,  $T_K^{\text{AP}}$ , is the same as in the case of nonmagnetic leads as long as  $p < 1$  (for  $p = 1$  there is no Kondo effect at all). Physically, the decrease of  $T_K$  is associated with asymmetry between

the densities of states for majority and minority electron bands of the ferromagnet, which results in smaller exchange interaction compared to the spin in the dot and the conduction electrons compared to nonmagnetic case. Because  $T_K^P < T_K^{AP}$ , by using Eq. (6), one can immediately see that for the same  $J_{\text{eff}}$ ,  $T_P^* > T_{AP}^*$ ; i.e., the second stage of the Kondo effect occurs at higher temperature in the case of ferromagnetic leads aligned in parallel compared to antiparallel alignment.

The differences between  $G^P$  and  $G^{AP}$  are reflected in the behavior of the TMR, which is depicted in Fig. 3(c). First of all, for  $t = 0$ , the TMR exhibits a behavior which is typical for single quantum dots, where TMR is positive in the absence of exchange field [39]. In the case considered here, however, we observe a strong dependence of the TMR on the hopping parameter  $t$ , which can lead to large negative TMR even in the particle-hole symmetric case. This negative TMR is related to the second stage of screening, at which the conductance decreases as  $\propto T^2$  [21]. Because  $T_P^* > T_{AP}^*$ , the decrease of  $G$  is faster in the parallel configuration compared to antiparallel one, and  $G^P < G^{AP}$  for  $T < T_P^*, T_{AP}^*$ , which results in negative TMR. Moreover, the smaller the hopping  $t$  is, the larger the ratio  $T_P^*/T_{AP}^*$  becomes [cf. Eq. (6)], and, thus, the more negative TMR can be observed. In fact, the TMR approaches the limiting value  $\text{TMR} = -1$  already for  $t = \Gamma/4$ , as can be seen in Fig. 3(c). With increasing the hopping  $t$ ,  $J_{\text{eff}}$  is enhanced and the difference between  $T_P^*$  and  $T_{AP}^*$  becomes reduced, and so does the difference between  $G^P$  and  $G^{AP}$ . This can be seen as a gradual increase of the minimum value of the TMR, which is not close to  $-1$  any more; however, it is still negative. On the other hand, in the high-temperature limit,  $T > T_K^P, T_K^{AP}$ , for all values of the hopping  $t$  considered in the figure, the behavior of the TMR is the same as in the single-dot case [39].

For further reference in Fig. 3 we have marked by vertical lines three different temperatures corresponding to  $30T^*$ ,  $T^*$ , and  $T^*/30$ , with  $T^* \approx 6 \times 10^{-5}$  estimated for the case of  $t = \Gamma/3$ . For these temperatures in Sec. III B 5 we will analyze the dependence of the conductance and the TMR on the positions of quantum dots' energy levels. These temperatures correspond to different transport regimes: the highest one,  $T = 30T^*$ , corresponds to the first stage of the Kondo effect where the Kondo effect develops, the lowest one,  $T = T^*/30$ , to the second stage of the Kondo effect, in which the conductance is suppressed, whereas the intermediate temperature,  $T = T^*$ , corresponds to the crossover region between the two stages; see Fig. 3.

Now, let us turn to the discussion of the case when the exchange field is finite,  $\Delta\varepsilon_{\text{exch}} \neq 0$ . This can be obtained by detuning the position of the DQD levels from the particle-hole symmetry point. We will in particular study what happens when the position of one of the dots' levels is changed to  $\varepsilon_i = -U/3$ . This choice of parameters guarantees that the exchange field effects and, in particular, the interplay between  $T^*$  and  $\Delta\varepsilon_{\text{exch}}$  when changing  $t$ , will be clearly visible in transport characteristics.

The temperature dependence of both  $G^P$  and  $G^{AP}$  together with TMR is shown in Fig. 4. The left column corresponds to the case when  $\varepsilon_1 = -U/2$  and  $\varepsilon_2 = -U/3$ , while the right column is calculated for  $\varepsilon_1 = -U/3$  and  $\varepsilon_2 = -U/2$ . Let us first analyze the former case. In the antiparallel configuration the main difference between  $G^{AP}$  in the case of  $\varepsilon_1 = \varepsilon_2 =$

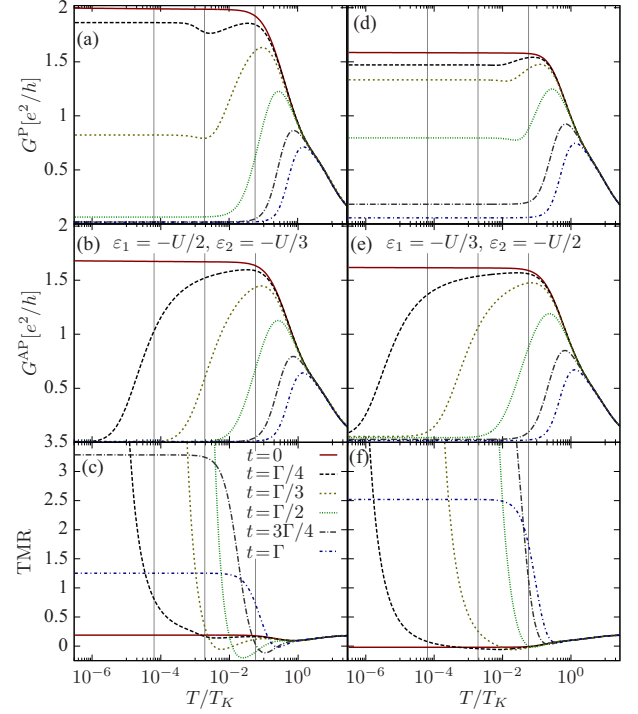


FIG. 4. (Color online) The same as in Fig. 3 calculated in the absence of particle-hole symmetry. The left column corresponds to  $\varepsilon_1 = -U/2$  and  $\varepsilon_2 = -U/3$ , while the right column is calculated for the case of  $\varepsilon_1 = -U/3$  and  $\varepsilon_2 = -U/2$ .

$-U/2$  and that in the asymmetric case is associated with a change of both  $T_K^{AP}$  and  $T_{AP}^*$ ; cf. Eq. (6). More precisely,  $T_K^{AP}$  increases whenever  $\varepsilon_1 \neq -U/2$  [58], while  $J_{\text{eff}}$  increases when either  $\varepsilon_1 \neq -U/2$  or  $\varepsilon_2 \neq -U/2$ . Thus, in Fig. 4(b)  $T_{AP}^*$  is larger compared to that in the case of Fig. 3(b). In the parallel configuration, on the other hand, the situation is more complex due to the presence of exchange field. First of all, we note that for weak hopping between the dots,  $t < \Gamma$ ,  $\Delta\varepsilon_{\text{exch}}$  develops mainly in the second dot where  $\varepsilon_2 = -U/3$ , while the first dot is in its symmetry point  $\varepsilon_1 = -U/2$ . When the hopping increases, however, transport rather occurs through molecular many-body states that can be split by  $\Delta\varepsilon_{\text{exch}}$  [56]. The magnitude of  $\Delta\varepsilon_{\text{exch}}$  can be estimated from the temperature dependence of  $G^P$ , since it corresponds to the energy scale at which the second stage of screening is broken. For example, in the case of  $t = \Gamma/4$ , it corresponds to the small minimum visible around  $T/T_K \approx 3 \times 10^{-3}$ ; see Fig. 4(a). Thus, for assumed parameters one gets an estimate of  $\Delta\varepsilon_{\text{exch}} \approx 3 \times 10^{-3} T_K$ . The most important consequence of the presence of ferromagnetic leads is the suppression of the second stage of the Kondo effect if only  $\Delta\varepsilon_{\text{exch}} > T_P^*$ . Then, the conductance does not decrease but retains a finite, nonuniversal value, which depends on the ratio of  $T_P^*/\Delta\varepsilon_{\text{exch}}$  that can be changed, e.g., by tuning  $t$ . In fact, with increasing the hopping between the dots,  $T_P^*$  raises, cf. Eq. (6), and the second stage of the Kondo effect starts competing with splitting caused by  $\Delta\varepsilon_{\text{exch}}$ , until eventually the  $T$  dependence of  $G^P$  becomes very similar to that of  $G^{AP}$ ; see the case of  $t = \Gamma$  in Figs. 4(a) and 4(b).

The huge difference between conductances in the two magnetic configurations associated with finite  $\Delta\varepsilon_{\text{exch}}$  can be clearly visible in the TMR, which is shown in Fig. 4(c). This difference is most visible for finite but small values of the hopping  $t$ , for which  $G^{\text{P}}$  is large and  $G^{\text{AP}}$  is suppressed due to the second-stage screening. Altogether, it gives rise to greatly enhanced TMR, which is a straightforward signature of the presence of exchange field. We note that  $G^{\text{AP}}$  for  $T \rightarrow 0$  is not precisely zero but takes a small nonuniversal value in the case when the particle-hole symmetry is broken [26]. Nevertheless, this finite value is still a few orders of magnitude smaller than the value of  $G^{\text{P}}$  for  $T \rightarrow 0$ , which leads to giant TMR, of the order of  $10^3$ . With increasing the hopping between the dots, e.g., for  $t = \Gamma$ , the condition  $\Delta\varepsilon_{\text{exch}} > T_{\text{p}}^*$  is not fulfilled any more and the difference between the two magnetic configurations becomes much reduced. The TMR is then still relatively large; however it does not take spectacular values as in the opposite case when the condition  $\Delta\varepsilon_{\text{exch}} > T_{\text{p}}^*$  is satisfied.

In the case when the detuning is induced in the first dot and absent in the second dot, the exchange field effects are more pronounced compared to the opposite case. This is related to the fact that the particle-hole symmetry is broken in the dot that is directly coupled to the leads and thus the spin-dependent charge fluctuations that renormalize the levels are more effective. The respective temperature dependence of  $G^{\text{P}}$ ,  $G^{\text{AP}}$ , and TMR in the case of  $\varepsilon_1 = -U/3$  and  $\varepsilon_2 = -U/2$  is shown in the right column of Fig. 4. Performing an analysis similar to that above, one can estimate the exchange field to be of the order of  $\Delta\varepsilon_{\text{exch}} \approx 3 \times 10^{-2} T_{\text{K}}$ , which is now one order of magnitude larger. In fact, the presence of the exchange field can be observed even in the case of  $t = 0$ , where it leads to a small decrease of the conductance from its maximum value of  $G^{\text{P}} = 2e^2/h$ , which occurs in the case of  $\varepsilon_1 = -U/2$ ; cf. Figs. 4(a) and 4(d). As can be seen in Fig. 4, all the features discussed in the case of  $\varepsilon_1 = -U/2$  and  $\varepsilon_2 = -U/3$  are very similar to those in the case of  $\varepsilon_1 = -U/3$  and  $\varepsilon_2 = -U/2$ . The main difference is associated with the value of hopping for which the condition  $\Delta\varepsilon_{\text{exch}} > T_{\text{p}}^*$  is not satisfied. One can see that now it happens only for large hopping of the order of  $t = \Gamma$ ; see Fig. 4(d). The giant TMR occurs then for most of the hopping values considered in the figure; see Fig. 4(f). Moreover, due to the fact that now  $T_{\text{AP}}^*$  is decreased compared to the previous case, enhanced TMR occurs at slightly lower temperatures; cf. Figs. 4(c) and 4(f).

We also note that in the case when the detunings are present in both dots,  $\varepsilon_1 = \varepsilon_2 = -U/3$  (results not shown), the situation is very similar to the case of  $\varepsilon_1 = -U/3$  and  $\varepsilon_2 = -U/2$ , since finite detuning from the particle-hole symmetry point in the second dot only slightly modifies the strength of the exchange field, which is mainly determined by the detuning of the first dot.

## 2. Temperature dependence for different spin polarizations $p$

To clearly see the effect of  $p \neq 0$ , we now analyze the  $T$  dependence of  $G$  and TMR in the case when the spin polarization of the leads is changed, while hopping between the dots is constant. This corresponds to fixing the exchange interaction between the dots and tuning the magnitude of the exchange

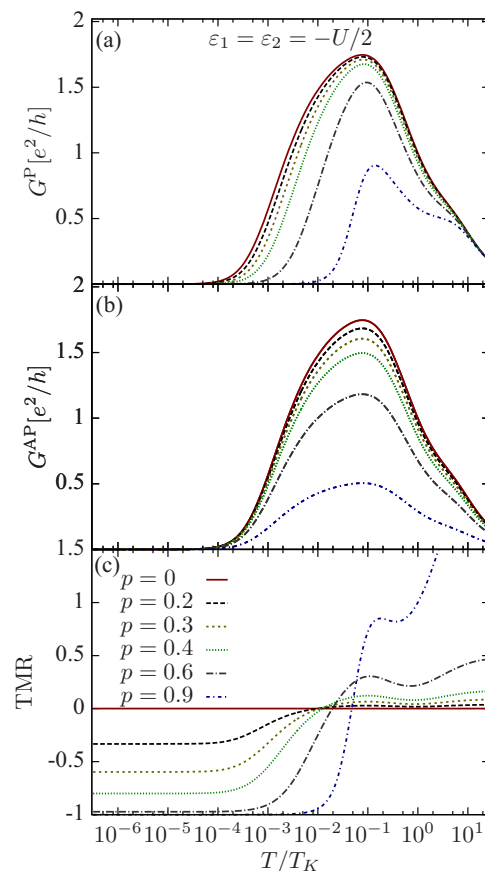


FIG. 5. (Color online) The linear conductance  $G$  in parallel (a) and antiparallel (b) magnetic configuration and the TMR (c) plotted as a function of temperature in the case of  $\varepsilon_1 = \varepsilon_2 = -U/2$  for different spin polarizations of the leads. The parameters are the same as in Fig. 3, except for  $t = \Gamma/3$  and  $p$  indicated in the figure.

field, i.e., the opposite situation to that studied in the previous section.

The temperature dependence of the linear conductance in both magnetic configurations and of the TMR is shown in Fig. 5 in the case of  $\varepsilon_1 = \varepsilon_2 = -U/2$ . In the antiparallel configuration the dependence of  $G^{\text{AP}}$  on the spin polarization  $p$  is trivial and is revealed only through the factor  $1 - p^2$ . In this regard, both  $T_{\text{K}}^{\text{AP}}$  and  $T_{\text{AP}}^*$  do not depend on  $p$ ; see Fig. 5(b). In the parallel configuration, on the other hand, increasing spin polarization leads to a decrease of  $T_{\text{K}}^{\text{P}}$  [cf. Eq. (8)], with immediate increase of  $T_{\text{p}}^*$  [cf. Eq. (6)]. Consequently, the temperature range where  $T_{\text{p}}^* < T < T_{\text{K}}^{\text{P}}$  shrinks with increasing  $t$ , while the maximum value of  $G^{\text{P}}$  decreases; see Fig. 5(a). This behavior is reflected in the temperature dependence of TMR, which is shown in Fig. 5(c). One can see that TMR changes sign approximately at the temperature corresponding to maximum in  $G^{\text{P}}$ . Below this maximum the TMR becomes negative and can reach  $-1$  for  $p \gtrsim 0.6$ , while for temperatures larger than those corresponding to maximum in  $G^{\text{P}}$ , the TMR is positive and can be greatly enhanced for large spin polarization. This behavior results directly from the aforementioned dependence of both  $T_{\text{K}}^{\text{P}}$  and  $T_{\text{p}}^*$  on spin polarization  $p$ .

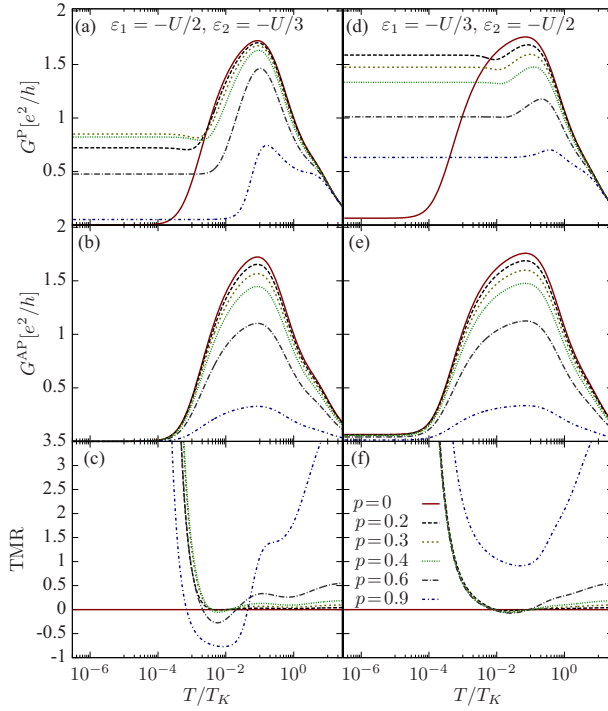


FIG. 6. (Color online) The same as in Fig. 5 calculated for  $\varepsilon_1 = -U/2$  and  $\varepsilon_2 = -U/3$  (left column), and  $\varepsilon_1 = -U/3$  and  $\varepsilon_2 = -U/2$  (right column).

The conductance and TMR as a function of temperature in the case of broken particle-hole symmetry are shown in Fig. 6. Irrespective of whether the detuning from the symmetry point occurs in the first or second dot,  $G^{AP}$  displays qualitatively the same behavior, with  $T_K^{AP}$  ( $T_{AP}^*$ ) larger (smaller) in the case of  $\varepsilon_1 = -U/3$  compared to the case with  $\varepsilon_1 = -U/2$ ; see Figs. 6(b) and 6(e). In the parallel configuration, the effects due to the presence of the exchange field are clearly visible and more pronounced in the case when the detuning occurs in the first dot. The splitting caused by  $\Delta\varepsilon_{\text{exch}}$  suppresses the second stage of the Kondo effect. Similarly to the case discussed in previous section, for  $\Delta\varepsilon_{\text{exch}} \neq 0$ , that is for finite  $p$  and  $\varepsilon_1 \neq -U/2$  or  $\varepsilon_2 \neq -U/2$ , the linear conductance saturates at some finite value; see Figs. 6(a) and 6(d). However, as can be seen in the figure, the low-temperature value of  $G^P$  depends on  $p$  and this dependence is not monotonic. The spin-polarization dependence of  $G^P$  calculated at  $T = 10^{-8}$  (which corresponds to the smallest value used in Fig. 6) is explicitly shown in Fig. 7 for different DQD level positions, indicated in the figure and corresponding to those shown in Fig. 6. Very interestingly, low-temperature  $G^P$  has a maximum for certain spin polarization  $p = p_{\text{max}}$ . Moreover,  $p_{\text{max}}$  clearly depends on the position of DQD levels, i.e., on the strength of the exchange field. The mechanism leading to this behavior is related with the splitting of the triplet states caused by  $\Delta\varepsilon_{\text{exch}}$ . For finite hopping and in the absence of ferromagnetic leads ( $\Delta\varepsilon_{\text{exch}} = 0$ ), the ground state of the system is the spin singlet  $|S\rangle = (|\uparrow\downarrow\rangle - |\downarrow\uparrow\rangle)/\sqrt{2}$ , where  $|\sigma\sigma'\rangle$  denotes a state in which there is a spin- $\sigma$  (spin- $\sigma'$ ) electron in the first (second) dot. Now, if the leads are ferromagnetic, the exchange field does

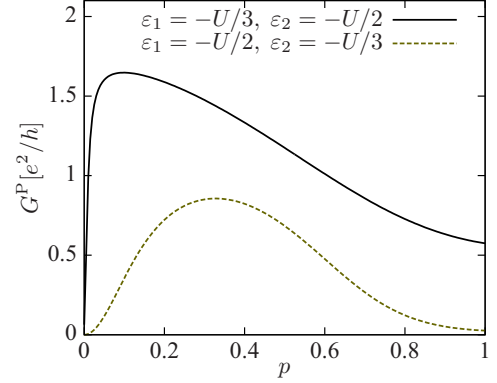


FIG. 7. (Color online) The dependence of the low-temperature value of the linear conductance in the parallel configuration,  $G^P$ , on the spin polarization of the leads  $p$  for different DQD level positions, as indicated, and for  $t = \Gamma/3$  and  $T = 10^{-8}$ . The other parameters are the same as in Fig. 3.

not affect the singlet state; however, it can split the triplet state, which is higher in energy than singlet. Depending on the sign and strength of  $\Delta\varepsilon_{\text{exch}}$ , which can be changed by tuning the DQD levels, for some value of exchange field one of the components of the triplet state, either  $|\uparrow\uparrow\rangle$  or  $|\downarrow\downarrow\rangle$ , can become degenerate with the singlet state. Because such states differ in magnetic quantum number by 1, the usual spin-flip processes responsible for the Kondo effect are possible and the Kondo resonance can be reinstated, though with slightly lower height. This is exactly the physical mechanism responsible for the nonmonotonic dependence of the low-temperature value of  $G^P$  on  $p$ . When increasing the spin polarization,  $\Delta\varepsilon_{\text{exch}}$  becomes enhanced and, for  $p \approx p_{\text{max}}$ , the degeneracy between the singlet state and one component of the triplet state is restored, giving rise to enhancement of  $G^P$ . Another feature visible in Fig. 7 is the difference in  $p_{\text{max}}$  for different arrangements of DQD levels. In agreement with previous observation, the exchange field is stronger in the case when the detuning is present in the first dot, which leads to smaller  $p_{\text{max}}$  compared to the case of  $\varepsilon_1 = -U/2$  and  $\varepsilon_2 = -U/3$ ; see Fig. 7.

Finally, the difference between  $G^P$  and  $G^{AP}$  again leads to giant TMR in the transport regime where the second stage of screening occurs in the antiparallel configuration; see Figs. 6(c) and 6(f). In addition, one can also note very large TMR in the high-temperature regime for spin polarization  $p = 0.9$ . This effect however results directly from the fact that  $G^{AP}$  is smaller by a factor of  $1 - p^2$  than  $G^P$ , which for  $p \rightarrow 1$  translates into infinite TMR.

### 3. Dependence on hopping between the dots $t$

In this section we analyze how the low-temperature conductance in both magnetic configurations depends on the hopping between the dots and the spin polarization of the leads. In calculations we assume very low but finite temperature  $T = 10^{-8}$ , which allows us to study the transition from the low to high conducting state of the system. Note that for  $\varepsilon_1 = \varepsilon_2 = -U/2$ , at zero temperature the conductance should be suppressed in both configurations for any  $t$ , due to the second stage of Kondo screening [21]. Nevertheless, this limit

is experimentally inaccessible and, provided that  $T \ll T_K$ , one should observe the transition in conductance at certain  $t = t_c$  such that  $T^*(t_c) \approx T$ ; cf. Eq. (6). Then, for  $t < t_c$ , one has  $T^* < T$ , and the conductance retains its maximum value due to the first stage of the Kondo effect. We also note that changing the temperature used in calculations (from the value of  $T = 10^{-8}$ ) would only result in a slight shift of the value of hopping  $t_c$  at which the conductance drops, while the results would be qualitatively the same, provided that  $T \ll T_K^P, T_K^{AP}$ .

The dependence of low-temperature conductance in the antiparallel configuration on the hopping  $t$  in the case of particle-hole symmetry is shown in Fig. 8(a). It can be seen that  $G^{AP}$  displays exactly the dependence described in the preceding paragraph:  $G^{AP} = 0$  for  $t > t_c$  and  $G^{AP} = (1 - p^2)2e^2/h$  for  $t < t_c$ . The behavior of  $G^{AP}$  with changing  $t$  is qualitatively the same in the absence of symmetry; the only difference is related to a slight change of  $t_c$ . As expected, for given DQD level arrangement,  $t_c$  does not depend on spin polarization  $p$ , the effect of which is only to suppress the conductance for  $t < t_c$  by a factor of  $1 - p^2$ ; see Fig. 8(a).

In the parallel configuration  $G$  is completely different. In the case of  $\varepsilon_1 = \varepsilon_2 = -U/2$ , increasing  $p$  leads to lowering of  $t_c$ ; see Fig. 8(b). This is due to the fact that the larger the spin polarization is, the smaller the Kondo temperature becomes, cf. Eq. (8), and, thus, the larger  $T_p^*$  is for given  $t$ . Consequently, the condition  $T_p^* \approx T$  becomes satisfied for smaller hopping with increasing the spin polarization. Note also that  $G^P$  for  $t < t_c$  reaches its maximum value of  $2e^2/h$ , irrespective of  $p$ ; see Fig. 8(b). This maximum value also persists in the case when the detuning occurs in the second dot, i.e., in the case of  $\varepsilon_1 = -U/2$  and  $\varepsilon_2 = -U/3$  shown in Fig. 8(c). Now, however,  $t_c$  exhibits a nonmonotonic dependence on the spin polarization. The mechanism leading to such nonmonotonic dependence was already explained in the previous subsection.

Another interesting feature is associated with the change of slope of the transition from  $G = 0$  to  $G = 2e^2/h$  with lowering  $t$ , which is visible for larger spin polarization; see, e.g., the case of  $p = 0.9$  in Fig. 8(c). This is due to the fact that the condition  $|\Delta\varepsilon_{\text{exch}}| < T_K^P$  becomes then only weakly met. On the other hand, in the case of  $\varepsilon_1 = -U/3$  and  $\varepsilon_2 = -U/2$  shown in Fig. 8(d), the violation of this condition can be much stronger. This causes a gradual lowering of  $G^P$  for  $t < t_c$  with increasing spin polarization. In addition, raising  $p$  smears the transition from low to high conducting state and shifts it towards larger values of the hopping  $t$ ; see Fig. 8(d).

#### 4. Magnetic field dependence

Let us now move to the analysis of the influence of external magnetic field on the transport properties. The linear conductance in both magnetic configurations and the TMR as a function of magnetic field for different hoppings between the dots are shown in Fig. 9. This figure was calculated for  $\varepsilon_1 = \varepsilon_2 = -U/2$ , i.e., in the case when the exchange field is absent. For  $t = 0$ , one observes the behavior which is typical for one-stage Kondo effect, when the conductance becomes suppressed once  $B \gtrsim T_K$  [59]; see Figs. 9(a) and 9(b). This situation changes in the case of finite hopping. Now, with

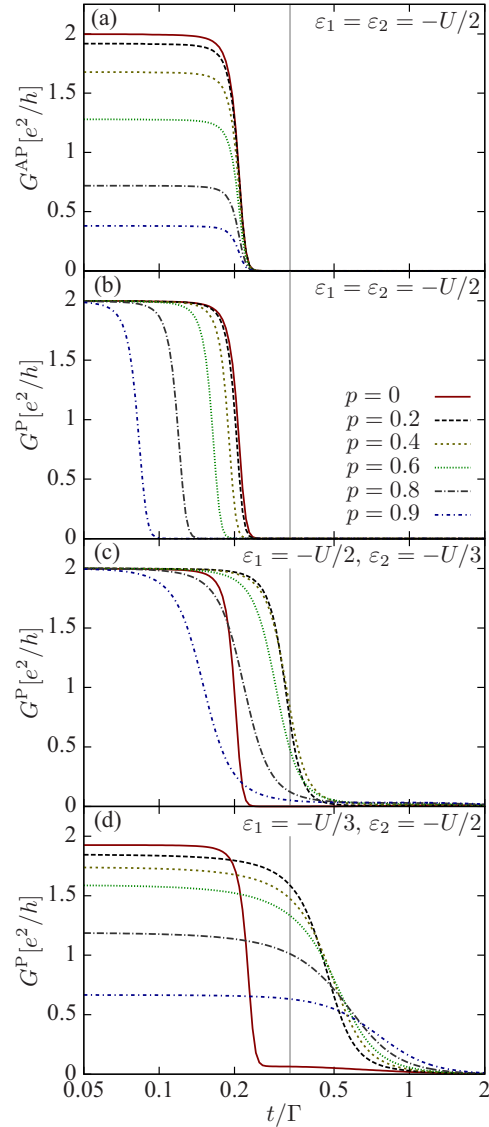


FIG. 8. (Color online) The low-temperature linear conductance in the antiparallel (a) and parallel (b)–(d) configurations as a function of hopping between the dots  $t$  for different spin polarization  $p$ , as indicated. In the case of (a) and (b)  $\varepsilon_1 = \varepsilon_2 = -U/2$ , (c)  $\varepsilon_1 = -U/2$  and  $\varepsilon_2 = -U/3$ , and (d)  $\varepsilon_1 = -U/3$  and  $\varepsilon_2 = -U/2$ . The parameters are the same as in Fig. 3 with  $T = 10^{-8}$ . The vertical line indicates the value of  $t = \Gamma/3$  that was used in Figs. 5 and 6.

lowering magnetic field, the conductance in both magnetic configurations becomes first enhanced for  $B < T_K$  to its maximum value,  $G^P = 2e^2/h$  and  $G^{AP} = 2(1 - p^2)e^2/h$ , respectively. However, with further decrease of  $B$ , both  $G^P$  and  $G^{AP}$  drop to zero once  $B < T^*$ , due to the second stage of the Kondo effect. Though the magnetic field dependence of linear conductance is similar to its temperature dependence, cf. Figs. 3 and 9, there is one important difference. In the presence of external magnetic field, there is always such a field at which the conductance acquires its maximum value for any hopping considered [29], while in the temperature dependence of  $G$

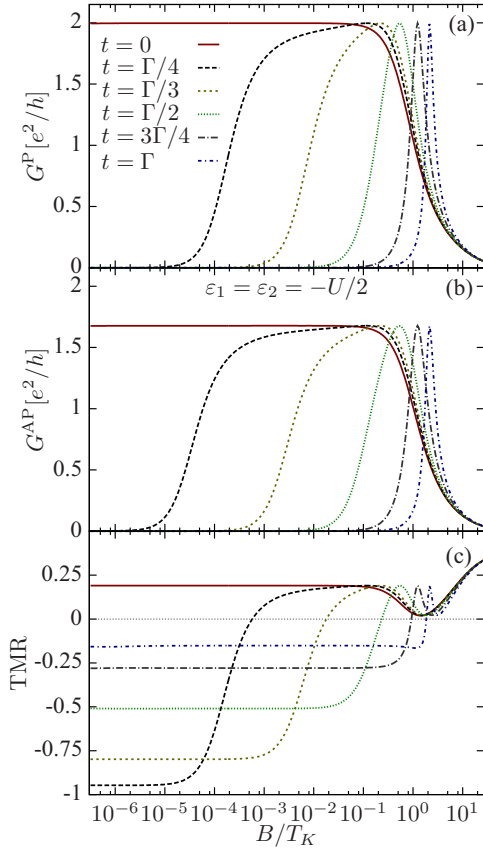


FIG. 9. (Color online) The linear conductance in the parallel (a) and antiparallel (b) magnetic configuration and the TMR (c) as a function of magnetic field for different values of the hopping between the dots, as indicated, and for  $\varepsilon_1 = \varepsilon_2 = -U/2$ . The other parameters are the same as in Fig. 3 with  $T = 10^{-8}$ .

increasing hopping  $t$  lowers the conductance in the intermediate region  $T^* < T < T_K$ . Indeed, as can be seen in Fig. 9, with increasing the hopping between the dots, the region where the conductance is enhanced shrinks; however, its maximum value does not depend on  $t$ . Moreover, one can also note that  $T_P^* > T_{AP}^*$ , in agreement with discussion in previous sections, which implies that  $G^P < G^{AP}$  for magnetic fields  $B < T_P^*, T_{AP}^*$ . This results in a large negative TMR at low magnetic fields; see Fig. 9(c). On the other hand, for magnetic fields where the conductance is enhanced to its maximum value, one generally has  $G^P > G^{AP}$ , yielding positive TMR, which retains its positive value also at higher magnetic fields; see Fig. 9(c).

In the presence of exchange field, the magnetic field dependence of the linear conductance is much more complex. Furthermore, the direction of magnetic field is now important since, if it is opposite to the direction of  $\Delta\varepsilon_{\text{exch}}$  and  $B$  is properly tuned, magnetic field can compensate for the exchange-field-induced splitting of the levels [38]. However, the case of T-shaped double quantum dots is even more subtle, because the splitting caused by the exchange field does not need to be the same in each dot and, moreover, it can have opposite sign [42,56]. One can thus expect that the interplay of  $B$  and  $\Delta\varepsilon_{\text{exch}}$  will be revealed as a nontrivial

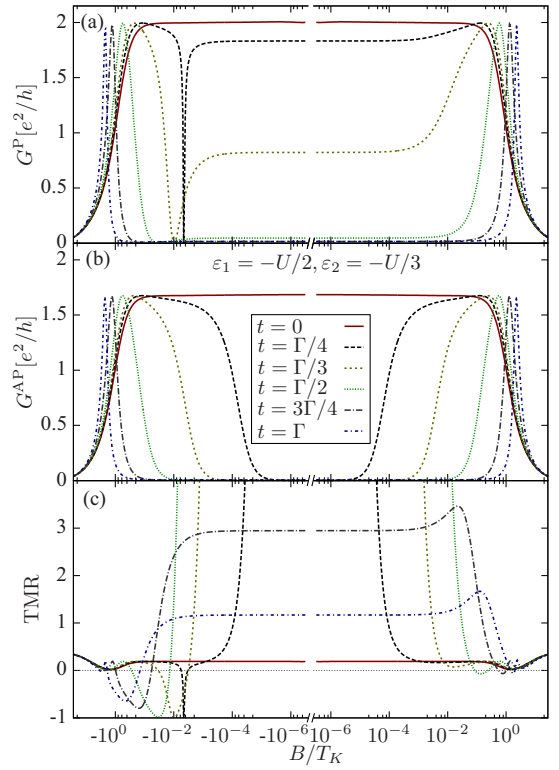


FIG. 10. (Color online) The same as in Fig. 9 calculated for  $\varepsilon_1 = -U/2$  and  $\varepsilon_2 = -U/3$ . Note the logarithmic scale for positive and negative magnetic fields.

behavior of the conductance in the case of finite detuning from the particle-hole symmetry point. This is indeed the case as presented in the following figures.

The linear conductance and TMR in the case of  $\varepsilon_1 = -U/2$  and  $\varepsilon_2 = -U/3$  are shown in Fig. 10. The conductance in the antiparallel configuration is qualitatively similar to the particle-hole symmetric case presented in Fig. 9; therefore we will not discuss it again. Instead, let us focus on the behavior of  $G^P$  and TMR. When  $t = 0$ , the variation of  $G^P$  with  $B$  is similar to that in the antiparallel configuration, since the first dot is in its particle-hole symmetry point. However, when the hopping is finite, the dependence of  $G^P$  becomes asymmetric with respect to the change of magnetic field direction; see Fig. 10(a). First of all, one can see that at very low magnetic fields, the conductance starts decreasing with increasing the hopping  $t$ . This behavior is similar to that discussed in the case of Fig. 4(a) and Fig. 8. When the magnetic field increases ( $B > 0$ ), at certain field the Kondo resonance becomes restored and the conductance reaches its maximum value. The field at which this restoration occurs increases with increasing the value of hopping  $t$ . The occurrence of the Kondo effect is associated with the fact that a properly tuned magnetic field can restore the degeneracy that was lifted by the presence of the exchange field. Very interestingly, the restoration can also occur when the field is reversed, which is contrary to the case of single quantum dots [38]. This can be understood by realizing that, as explained in Sec. III B 2, the restoration of the (single-stage) Kondo effect in DQDs in the magnetic

field results from enforcing the degeneracy between the singlet state and one of the triplet components. The sign change of the magnetic field corresponds to the change of the triplet component. However, it should be noted that due to the existence of the effective exchange field, the restoration occurs at slightly different fields when the direction of the magnetic field is changed. Nevertheless, because the magnitude of the exchange field for  $\varepsilon_1 = -U/2$  and  $\varepsilon_2 = -U/3$  is rather small ( $\Delta\varepsilon_{\text{exch}} \approx 3 \times 10^{-3} T_K$ ) compared to the values of the magnetic field at which the restoration occurs, this effect is hardly visible in Fig. 10(a). Still, detailed analysis of numerical data indeed reveals the shift and confirms that it is of the order of the magnitude of  $\Delta\varepsilon_{\text{exch}}$ .

Besides the Kondo effect restoration, there is another interesting feature visible in Fig. 10(a). For negative magnetic fields and for  $|B|$  slightly below the value where the Kondo effect occurs, the linear conductance reveals a sudden suppression, which is present for small values of the hopping between the dots; see, e.g., the case of  $t = \Gamma/4$  in Fig. 10(a). This suppression is related to the second stage of the Kondo effect, which can be restored by magnetic field. At this field, the spin of the first dot forms a singlet with the spin of the second dot and the conductance becomes suppressed. For larger hopping between the dots, however, the exchange field starts playing a minor role and the magnetic field dependence of  $G$  shows a two-stage character, which is very similar to the case of antiparallel configuration; cf. Figs. 10(a) and 10(b) for  $t \gtrsim \Gamma/2$ .

The related dependence of the TMR on magnetic field is shown in Fig. 10(c). First, we note that for magnetic fields larger than the field where the restoration of the Kondo effect occurs, the TMR is positive and rather independent of  $t$ . Second, for very low magnetic fields, the TMR becomes essentially infinite for small hopping between the dots [see the case of  $t = \Gamma/4$  in Fig. 10(c)], whereas for larger hopping the TMR takes large positive values, which decrease with increasing  $t$ . Third, while for positive magnetic fields of the order of the restoration field one can see a small sign change of the TMR, for negative fields the behavior is much more complex. This is related to the fact that when increasing magnetic field in the opposite direction ( $B < 0$ ), both the first and second stage of screening can be restored. This is revealed in the behavior of the TMR, which changes sign and approaches  $-1$  for fields where the conductance in the parallel configuration is suppressed due to the second stage of the Kondo effect; see Fig. 10(c).

The aforementioned features can be even more pronounced in the case when the exchange field is larger. Such situation is presented in Fig. 11, which corresponds to the case when the detuning occurs in the first dot,  $\varepsilon_1 = -U/3$  and  $\varepsilon_2 = -U/2$ . Now, in the case of  $t = 0$ , one can clearly see that the splitting induced by the exchange field can be compensated for positive direction of the magnetic field, while for negative field no such restoration occurs; see Fig. 11(a). In the case of finite hopping, however, the restoration occurs for both positive and negative fields, however, at different values. Moreover, the restoration and suppression of  $G^P$  for negative fields develop now gradually with increasing the hopping  $t$ . The behavior of the TMR is presented in Fig. 11(c) and is qualitatively similar to the case of  $\varepsilon_1 = -U/2$  and  $\varepsilon_2 = -U/3$ . The main change

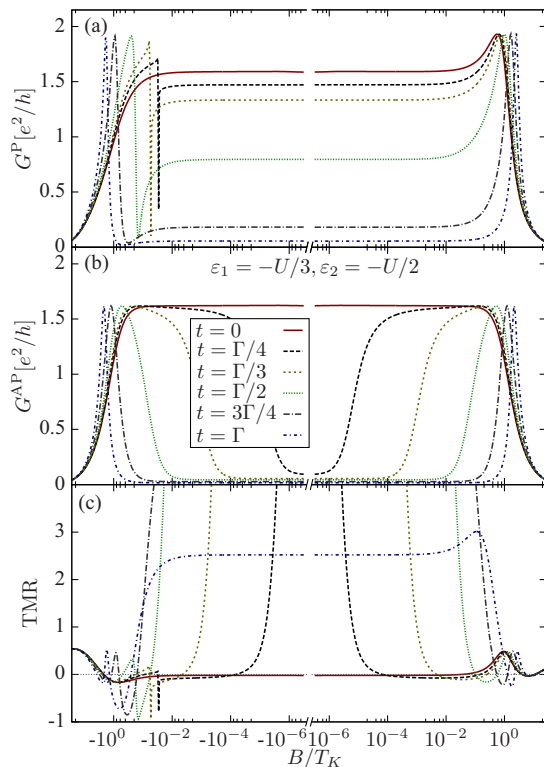


FIG. 11. (Color online) The same as in Fig. 9 calculated for  $\varepsilon_1 = -U/3$  and  $\varepsilon_2 = -U/2$ . Note the logarithmic scale for positive and negative magnetic fields.

is in the values of magnetic field at which the TMR becomes greatly enhanced or suppressed to the value of  $-1$ .

To analyze the behavior of the conductance in the parallel configuration as a function of magnetic field around the point where  $G^P$  becomes suppressed due to the second stage screening, in Fig. 12 we show  $G^P$  from Figs. 10 and 11 in the case of  $t = \Gamma/4$ . We have used  $\tilde{B} \equiv B - B_0$  as a measure of magnetic field detuning from the point where the minimum in  $G^P$  occurs, with  $B_0/T_K = -0.029$  for  $\varepsilon_1 = -U/3$ ,  $\varepsilon_2 = -U/2$ , and  $B_0/T_K = -0.0045$  for  $\varepsilon_1 = -U/2$ ,  $\varepsilon_2 = -U/3$ . In the case where  $\Delta\varepsilon_{\text{exch}}$  is relatively weak, i.e., when detuning from particle-hole symmetry point occurs only in the second dot, the conductance at  $B = B_0$  becomes fully suppressed due to the second stage of the Kondo effect. As can be clearly seen in the inset to Fig. 12, the dependence of  $G^P$  on  $\tilde{B}$  is then quadratic. This is however not the case when the exchange field effects are stronger; see Fig. 12 for  $\varepsilon_1 = -U/3$  and  $\varepsilon_2 = -U/2$ . Then, the minimum in  $G^P$  is much narrower and strongly asymmetric. Moreover, the conductance becomes suppressed only partially, which indicates that in this case the second stage of screening cannot be fully restored by fine-tuning the magnetic field.

### 5. Dependence on the DQD energy levels' positions

To complete our discussion, in this section we relax the condition of fixed dots' levels and study the dependence of the linear conductance and the TMR on  $\varepsilon_1$  and  $\varepsilon_2$ . For that we assume the hopping between the dots  $t = \Gamma/3$ , spin



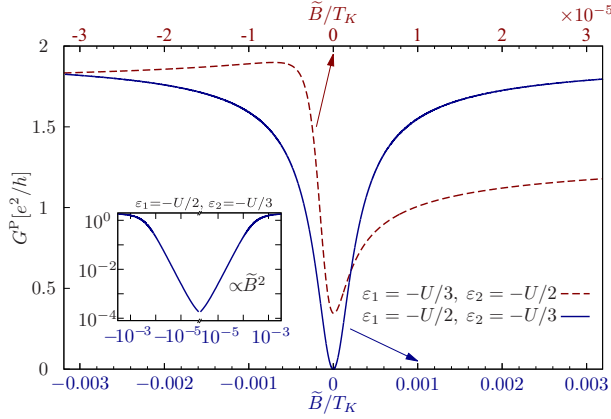


FIG. 12. (Color online) The dependence of the linear conductance in the parallel configuration on magnetic field  $\tilde{B} \equiv B - B_0$  around the point where  $G^P$  becomes suppressed in the case of  $\varepsilon_1 = -U/2$ ,  $\varepsilon_2 = -U/3$  (solid line), and  $\varepsilon_1 = -U/3$ ,  $\varepsilon_2 = -U/2$  (dashed line). Here,  $B_0$  is the magnetic field at which  $G^P$  has local minimum. The inset presents the quadratic scaling of  $G^P$  as a function of  $\tilde{B}$  for  $\varepsilon_1 = -U/2$  and  $\varepsilon_2 = -U/3$ . The other parameters are the same as in Fig. 3 with  $T = 10^{-8}$ .

polarization  $p = 0.4$ , and zero magnetic field. The linear conductance in the parallel and antiparallel magnetic configuration as a function of  $\varepsilon_1$  and  $\varepsilon_2$  is shown in Fig. 13. In this figure each row corresponds to different temperature. The lowest temperature corresponds to the second stage of the Kondo effect, the highest one to the first stage of the Kondo effect, while the intermediate temperature,  $T = T^*$ , corresponds to the crossover regime; see also the vertical lines in Fig. 3.

As can be seen in Fig. 13, the main difference between  $G$  in the parallel and antiparallel magnetic configuration occurs in the case when each dot is occupied by a single electron,  $-U < \varepsilon_1 < 0$  and  $-U < \varepsilon_2 < 0$ . On the other hand, outside this Coulomb blockade valley, the behavior of  $G^P$  and  $G^{AP}$  is qualitatively similar and rather weakly dependent on temperatures considered in Fig. 13. This is due to the fact that the highest temperature  $T = 30T^*$  is still slightly lower than the Kondo temperature and the Kondo resonance in the first dot is present. When the second dot is empty or doubly occupied,  $\varepsilon_2 > 0$  or  $\varepsilon_2 < -U$ , while the first dot hosts a single electron, the linear conductance in the antiparallel configuration reaches its maximum,  $G^{AP} = 2(1 - p^2)e^2/h$ ; see the right column of Fig. 13. At first sight, a similar behavior occurs also in the parallel configuration where the conductance reaches  $G^P = 2e^2/h$  (see the left column of Fig. 13); however, there is a crucial difference, which is related to the width of enhanced conductance region. While in the antiparallel configuration  $G$  is maximum in the whole regime of the first dot being singly occupied,  $-U < \varepsilon_1 < 0$ , in the parallel configuration the width of the maximum is conditioned by the ratio of exchange field and the Kondo temperature. Since for assumed parameters  $T_K$  is relatively large, one needs to induce considerable detuning from particle-hole symmetry point of the first dot to suppress the Kondo resonance. Consequently,

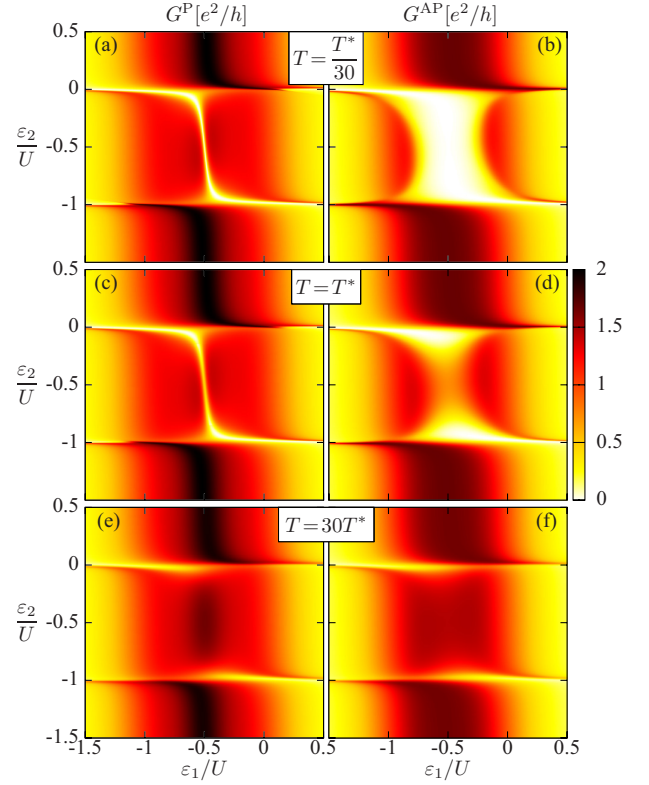


FIG. 13. (Color online) The linear conductance in the parallel (left column) and antiparallel (right column) magnetic configuration as a function of DQD levels calculated at (a)–(b)  $T = T^*/30$ , (c)–(d)  $T = T^*$ , (e)–(f)  $T = 30T^*$ , with  $T^*$  being the second-stage Kondo temperature for  $t = \Gamma/3$ ,  $T^* \approx 6 \times 10^{-5}$ . The parameters are the same as in Fig. 3 with  $t = \Gamma/3$ .

there is relatively small difference between  $G^P$  and  $G^{AP}$  in this transport regime and the dependence of conductance on temperature is rather weak. Nevertheless, with lowering  $T_K$  (decreasing the ratio of  $\Gamma/U$ ), this difference becomes much more pronounced [39].

Similarly, weak dependence on  $T$  can be observed in the case when the first dot is either empty or doubly occupied; see Fig. 13. This is due to the fact that in this case transport is mainly due to cotunneling processes, which do not have such spectacular dependence on temperature as the conductance in the Kondo regime. The difference between the two magnetic configurations results mainly from the coupling asymmetry in cotunneling rates. In the parallel configuration the zero-temperature conductance is proportional to  $G^P \sim 2(1 + p^2)\Gamma^2$ , while in the antiparallel configuration one has  $G^{AP} \sim 2(1 - p^2)\Gamma^2$ . This results in positive TMR, which is given by  $\text{TMR} = 2p^2/(1 - p^2)$  [60].

When each of the dots is singly occupied, the conductance strongly depends on both the magnetic configuration and the temperature. For antiparallel alignment of leads' magnetizations, the conductance is suppressed at low temperatures, see Fig. 13(b), due to the formation of spin singlet between the dots. When temperature increases,  $T = T^*$ , the second stage of the Kondo effect is suppressed by thermal fluctuations and the conductance suppression is absent in the middle of

the Kondo regime. However, the second-stage screening is still present for  $\varepsilon_2$  close to the resonances, yet still in the Coulomb blockade valley; see Fig. 13(d). On the other hand, in the high-temperature regime,  $T = 30T^*$ , the second stage is almost completely smeared out by thermal fluctuations and the conductance shows only a typical enhancement due to the Kondo effect; see Fig. 13(f).

In the parallel configuration the role of exchange field is clearly visible. First of all, the second stage of the Kondo effect becomes destroyed except for a thin line in the  $(\varepsilon_1, \varepsilon_2)$  plane where the exchange-field-induced splitting of the singlet state is absent and the conductance is suppressed. Note that this suppression is present in the case of both  $T = T^*/30$  and  $T = T^*$ , while for antiparallel configuration it was already partially suppressed at  $T = T^*$ ; cf. Figs. 13(c) and 13(d). This is due to the fact that  $T_p^* > T_{AP}^*$ , which implies that the second stage of screening, for such DQD level arrangement when the exchange field effects are absent, is destroyed at higher temperature in the parallel configuration than in the antiparallel one. At  $T = 30T^*$ , instead of the conductance suppression there is an enhancement of  $G$  in the middle of the Coulomb valley with single electron in each dot, which is due to the Kondo effect; see Fig. 13(e). The presence of the exchange field leads to a narrowing of the enhancement regime when sweeping the first dot level position compared to the antiparallel situation; cf. Figs. 13(e) and 13(f).

Large differences between  $G^P$  and  $G^{AP}$  discussed above translate into very nontrivial dependence of the TMR on both the DQD levels' positions and the temperature; see Fig. 14. One can see that for evenly occupied second dot and singly occupied first dot, the TMR can take negative values for such  $\varepsilon_1$  when the conductance is suppressed in the parallel configuration due to the exchange field. On the other hand, when the occupation of the first dot is even, the TMR is generally positive. These two features are rather independent of temperature, see Fig. 14, provided  $T < T_K$ , as considered in the figure. The most striking behavior occurs when the two dots are singly occupied. At low temperatures,  $T = T^*/30$ , when the second stage of the Kondo effect occurs in the antiparallel configuration, giant TMR can be observed; see Fig. 14(a). However, this giant TMR becomes suppressed with increasing temperature and, at  $T = T^*$ , a negative TMR occurs around  $\varepsilon_1 = -U/2$ , which is due to the second-stage screening that is still present in the parallel configuration around this point. Negative TMR also develops around  $\varepsilon_2 = -U/2$  and  $\varepsilon_1 = -U(1/2 \pm 1/4)$ ; see Fig. 14(b). This can be understood by realizing that for  $T = T^*$  the conductance in the antiparallel configuration starts increasing owing to the first-stage Kondo effect, while in the parallel configuration this enhancement is smaller. Moreover, it can be seen that when the second dot level is close to resonance, the TMR can still take giant values. Finally, for higher temperatures, the TMR as a function of the first dot level behaves similarly as in the case when the second dot is evenly occupied; see Fig. 14(c). The behavior of the TMR at  $T = 30T^*$  results only from the interplay of  $\Delta_{\text{exch}}$  and  $T_K$ , since  $T \gg T^*$ . The TMR takes then values that are rather typical for transport through single quantum dots coupled to ferromagnetic leads [39,60].

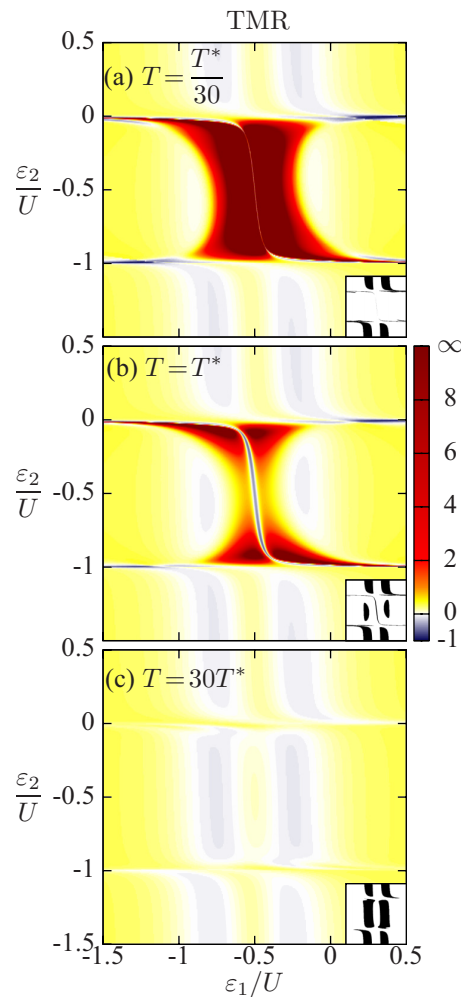


FIG. 14. (Color online) The TMR as a function of DQD levels calculated at (a)  $T = T^*/30$ , (b)  $T = T^*$ , (c)  $T = 30T^*$ , with  $T^* \approx 6 \times 10^{-5}$ . Parameters are the same as in Fig. 3 with  $t = \Gamma/3$ . The black areas in insets mark the regions where TMR is negative.

#### IV. CONCLUSIONS

In this paper we have numerically analyzed the two-stage Kondo effect in T-shaped double quantum dots coupled to ferromagnetic leads. By using the numerical renormalization group method, we determined the behavior of the linear conductance and the TMR on temperature, external magnetic field, DQD levels' positions, hopping between the dots, and spin polarization of the leads. We showed that the two-stage Kondo effect is present in the antiparallel configuration of the system, while in the parallel configuration the second stage of screening is generally suppressed. This suppression is due to the presence of exchange field, which splits the levels of the DQD. Such splitting can be controlled by tuning the DQD levels with gate voltages and results from spin-dependent charge fluctuations between the double dot and the leads. When the electron and hole processes counterbalance each other, which can happen for certain DQD level arrangements,

the exchange field vanishes and the second stage of the Kondo effect can be restored. Such restoration can also occur by fine-tuning the external magnetic field, such that it compensates for the exchange-field-induced splitting. The difference between the conductance in the parallel and antiparallel configuration results in very nontrivial behavior of the TMR, which at low temperatures can take giant values. This giant TMR is reduced when temperature increases above the temperature  $T^*$ , which is the characteristic energy scale of the second stage of the Kondo effect. We also studied the low-temperature transition from the high to low conducting state of the system, which

occurs when changing the hopping between the two dots, and showed that this transition is generally smeared out by the presence of the exchange field.

#### ACKNOWLEDGMENTS

This project was supported by the Polish National Science Centre from funds awarded through the decision No. DEC-2013/10/E/ST3/00213 and Marie Curie FP7 Reintegration Grant No. CIG-303 689 within the 7th European Community Framework Programme.

- [1] W. J. de Haas, J. H. de Boer, and G. J. van den Berg, *Physica* **1**, 1115 (1934).
- [2] J. Kondo, *Prog. Theor. Phys.* **32**, 37 (1964).
- [3] A. C. Hewson, *The Kondo Problem to Heavy Fermions* (Cambridge University Press, Cambridge, 1993).
- [4] L. I. Glazman and M. E. Raikh, *JETP Lett.* **47**, 452 (1988).
- [5] T. K. Ng and P. A. Lee, *Phys. Rev. Lett.* **61**, 1768 (1988).
- [6] D. Goldhaber-Gordon, H. Shtrikman, D. Mahalu, D. Abusch-Magder, U. Meirav, and M. A. Kastner, *Nature (London)* **391**, 156 (1998).
- [7] S. M. Cronenwett, T. H. Oosterkamp, and L. P. Kouwenhoven, *Science* **281**, 540 (1998).
- [8] J. Nygård, D. H. Cobden, and P. E. Lindelof, *Nature (London)* **408**, 342 (2000).
- [9] D. L. Cox and A. Zawadowski, *Exotic Kondo Effects in Metals* (Taylor & Francis, London, 1999).
- [10] L. Borda, G. Zaránd, W. Hofstetter, B. I. Halperin, and J. von Delft, *Phys. Rev. Lett.* **90**, 026602 (2003).
- [11] R. M. Potok, I. G. Rau, H. Shtrikman, Y. Oreg, and D. Goldhaber-Gordon, *Nature (London)* **446**, 167 (2007).
- [12] A. J. Keller, S. Amasha, I. Weymann, P. C. Moca, I. G. Rau, J. A. Katine, H. Shtrikman, G. Zaránd, and D. Goldhaber-Gordon, *Nat. Phys.* **10**, 145 (2014).
- [13] C. Jayaprakash, H. R. Krishna-murthy, and J. W. Wilkins, *Phys. Rev. Lett.* **47**, 737 (1981).
- [14] N. J. Craig, J. M. Taylor, E. A. Lester, C. M. Marcus, M. P. Hanson, and A. C. Gossard, *Science* **304**, 565 (2004).
- [15] G. Granger, M. A. Kastner, I. Radu, M. P. Hanson, and A. C. Gossard, *Phys. Rev. B* **72**, 165309 (2005).
- [16] S. Sasaki, H. Tamura, T. Akazaki, and T. Fujisawa, *Phys. Rev. Lett.* **103**, 266806 (2009).
- [17] P. Petit, C. Feuillet-Palma, M. L. Della Rocca, and P. Lafarge, *Phys. Rev. B* **89**, 115432 (2014).
- [18] M. Pustilnik and L. I. Glazman, *Phys. Rev. Lett.* **87**, 216601 (2001).
- [19] M. Vojta, R. Bulla, and W. Hofstetter, *Phys. Rev. B* **65**, 140405(R) (2002).
- [20] W. G. van der Wiel, S. De Franceschi, J. M. Elzerman, S. Tarucha, L. P. Kouwenhoven, J. Motohisa, F. Nakajima, and T. Fukui, *Phys. Rev. Lett.* **88**, 126803 (2002).
- [21] P. S. Cornaglia and D. R. Grempel, *Phys. Rev. B* **71**, 075305 (2005).
- [22] R. Žitko and J. Bonča, *Phys. Rev. B* **73**, 035332 (2006).
- [23] C.-H. Chung, G. Zarand, and P. Wölfle, *Phys. Rev. B* **77**, 035120 (2008).
- [24] V. M. Apel, M. A. Davidovich, E. V. Anda, G. Chiappe, and C. A. Busser, *Eur. Phys. J. B* **40**, 365 (2004).
- [25] Y. Tanaka, N. Kawakami, and A. Oguri, *Phys. Rev. B* **78**, 035444 (2008).
- [26] R. Žitko, *Phys. Rev. B* **81**, 115316 (2010).
- [27] I. L. Ferreira, P. A. Orellana, G. B. Martins, F. M. Souza, and E. Vernek, *Phys. Rev. B* **84**, 205320 (2011).
- [28] Y. Tanaka, N. Kawakami, and A. Oguri, *Phys. Rev. B* **85**, 155314 (2012).
- [29] L. G. G. V. Dias da Silva, E. Vernek, K. Ingersent, N. Sandler, and S. E. Ulloa, *Phys. Rev. B* **87**, 205313 (2013).
- [30] Ionel Tifrea, Mircea Crisan, George Pal, and Ioan Grosu, *Eur. Phys. J. B* **86**, 102 (2013).
- [31] J. Martinek, Y. Utsumi, H. Imamura, J. Barnaś, S. Maekawa, J. König, and G. Schön, *Phys. Rev. Lett.* **91**, 127203 (2003).
- [32] J. Martinek, M. Sindel, L. Borda, J. Barnaś, J. König, G. Schön, and J. von Delft, *Phys. Rev. Lett.* **91**, 247202 (2003).
- [33] M.-S. Choi, D. Sanchez, and R. Lopez, *Phys. Rev. Lett.* **92**, 056601 (2004).
- [34] A. N. Pasupathy, R. C. Bialczak, J. Martinek, J. E. Grose, L. A. Donev, P. L. McEuen, and D. C. Ralph, *Science* **306**, 86 (2004).
- [35] M. Sindel, L. Borda, J. Martinek, R. Bulla, J. König, G. Schön, S. Maekawa, and J. von Delft, *Phys. Rev. B* **76**, 045321 (2007).
- [36] J. R. Hauptmann, J. Paaske, and P. E. Lindelof, *Nat. Phys.* **4**, 373 (2008).
- [37] I. Weymann and J. Barnaś, *Phys. Rev. B* **81**, 035331 (2010); I. Weymann and L. Borda, *ibid.* **81**, 115445 (2010); M. Misiorny, I. Weymann, and J. Barnaś, *Phys. Rev. Lett.* **106**, 126602 (2011); *Phys. Rev. B* **86**, 245415 (2012); **86**, 035417 (2012).
- [38] M. Gaass, A. K. Hüttl, K. Kang, I. Weymann, J. von Delft, and C. Strunk, *Phys. Rev. Lett.* **107**, 176808 (2011).
- [39] I. Weymann, *Phys. Rev. B* **83**, 113306 (2011).
- [40] K. P. Wójcik, I. Weymann, and J. Barnaś, *J. Phys.: Condens. Matter* **25**, 075301 (2013).
- [41] J. Martinek, M. Sindel, L. Borda, J. Barnaś, R. Bulla, J. König, G. Schön, S. Maekawa, and J. von Delft, *Phys. Rev. B* **72**, 121302 (2005).
- [42] K. P. Wójcik and I. Weymann, *Phys. Rev. B* **90**, 115308 (2014).
- [43] K. G. Wilson, *Rev. Mod. Phys.* **47**, 773 (1975).
- [44] We use the open-access Budapest Flexible DM-NRG code (<http://www.phy.bme.hu/~dmnrg/>); O. Legeza, C. P. Moca, A. I. Tóth, I. Weymann, and G. Zaránd, [arXiv:0809.3143](https://arxiv.org/abs/0809.3143).
- [45] F. B. Anders and A. Schiller, *Phys. Rev. Lett.* **95**, 196801 (2005); *Phys. Rev. B* **74**, 245113 (2006).

- [46] A. Weichselbaum and J. von Delft, *Phys. Rev. Lett.* **99**, 076402 (2007).
- [47] I. Weymann and J. Barnaś, *Phys. Rev. B* **88**, 085313 (2013).
- [48] R. Žitko and T. Pruschke, *Phys. Rev. B* **79**, 085106 (2009).
- [49] S. Hershfield, J. H. Davies, and J. W. Wilkins, *Phys. Rev. Lett.* **67**, 3720 (1991); *Phys. Rev. B* **46**, 7046 (1992).
- [50] Y. Meir and N. S. Wingreen, *Phys. Rev. Lett.* **68**, 2512 (1992).
- [51] M. Julliere, *Phys. Lett. A* **54**, 225 (1975).
- [52] W. Rudziński, J. Barnaś, R. Świrakowicz, and M. Wilczyński, *Phys. Rev. B* **71**, 205307 (2005).
- [53] R. Świrakowicz, M. Wilczyński, M. Wawrzyniak, and J. Barnaś, *Phys. Rev. B* **73**, 193312 (2006).
- [54] D. Matsubayashi and M. Eto, *Phys. Rev. B* **75**, 165319 (2007).
- [55] P. Simon, P. S. Cornaglia, D. Feinberg, and C. A. Balseiro, *Phys. Rev. B* **75**, 045310 (2007).
- [56] K. P. Wójcik, *Eur. Phys. J. B*, doi: 10.1140/epjb/e2015-50821-3.
- [57] Note that the exchange field can also depend on the value of the hopping between the two dots; however, this dependence is much weaker than the dependence of  $T^*$  on  $J_{\text{eff}}$ , which is exponential.
- [58] F. D. M. Haldane, *Phys. Rev. Lett.* **40**, 416 (1978).
- [59] Andrey V. Kretinin, Hadas Shtrikman, David Goldhaber-Gordon, Markus Hanl, Andreas Weichselbaum, Jan von Delft, Theo Costi, and Diana Mahalu, *Phys. Rev. B* **84**, 245316 (2011).
- [60] I. Weymann, J. König, J. Martinek, J. Barnaś, and G. Schön, *Phys. Rev. B* **72**, 115334 (2005); J. Barnaś and I. Weymann, *J. Phys.: Condens. Matter* **20**, 423202 (2008).

**Thermopower of strongly correlated T-shaped double quantum dots**

Krzysztof P. Wójcik\* and Ireneusz Weymann

*Faculty of Physics, Adam Mickiewicz University, Umultowska 85, 61-614 Poznań, Poland*

(Received 13 November 2015; revised manuscript received 29 January 2016; published 18 February 2016)

We theoretically study the thermoelectric transport properties of correlated T-shaped double quantum dots. The calculations are performed with the aid of the numerical renormalization group method. When each of the dots is occupied by a single electron, the system exhibits the two-stage Kondo effect. We identify the signatures of the two-stage screening in transport coefficients such as electrical and heat conductances, Seebeck coefficient, thermoelectric figure of merit, and the power factor. It is shown that the thermopower exhibits maxima for temperatures corresponding to the second stage of screening. Moreover, the normalized heat conductance and the electrical conductance are found to fulfill a modified Wiedemann-Franz law, which however becomes violated when the system is in the weak coupling regime. In addition, we also analyze the effects of external magnetic field, which gives rise to the occurrence of finite spin polarization of the conductance and a significant spin thermopower.

DOI: [10.1103/PhysRevB.93.085428](https://doi.org/10.1103/PhysRevB.93.085428)**I. INTRODUCTION**

As prospective thermoelectric materials one can consider those, which, when embedded between two reservoirs of different temperatures, can produce a sizable voltage bias, and are thus characterized by considerable Seebeck coefficient  $S$  [1]. Such materials draw the attention of researchers due to, in particular, the possibility of using them to capture waste heat of various heat machines [2]. In metals, the Seebeck coefficient  $S$  usually fulfills the Mott formula [3,4], which states that  $S$  is proportional to the temperature  $T$  and the derivative of the conductance  $G$  over the chemical potential  $\mu$ :

$$S = \frac{\pi^2 k_B^2 T}{3e} \frac{\partial G}{\partial \mu}. \quad (1)$$

In low-dimensional systems, when the finite-size effects become important, the dependence of  $G$  on  $\mu$  can contain sharp peaks, leading to strong enhancement of the thermopower [5–7]. For this reason, thermoelectric properties of various nanoscale devices have recently been extensively investigated [8]. In particular, the thermoelectric properties of systems containing a quantum dot (QD) were analyzed theoretically [9–14] and experimentally [15]. It was shown that in such artificial atoms the thermoelectric coefficients can be enhanced compared to conventional bulk materials. Moreover, it turned out that by analyzing the thermoelectric response of the system, one can obtain an extra information about the intrinsic parameters and correlations of the system, as well as important energy scales. This is especially important for quantum dots in the Kondo regime [16–19], where the sign changes of the thermopower when varying temperature were shown to provide further insight into the Kondo correlations and the Kondo temperature  $T_K$  [10].

In more complex quantum dot structures such as, e.g., double quantum dots (DQDs) [20], quantum correlations and interference can lead to even more spectacular behavior of thermotransport characteristics [21–25]. In particular, large

enhancement of the thermoelectric figure of merit  $ZT$  in such systems was found due to the quantum interference [23]. Moreover, transport properties of DQDs reveal a plethora of various interesting phenomena, including the Pauli spin blockade [26], formation of molecular states [27], the Kondo effect [28,29], or Cooper pair splitting [30]. In addition, when the two dots form a T-shaped geometry, the two-stage Kondo effect and Fano interference become important [31–46]. Such a geometry is realized when only one of the two dots, say the first one, is directly coupled to external leads, while the second dot is attached to the first dot [41], as illustrated in Fig. 1.

The goal of this paper is to extend the existing studies on transport through T-shaped double dots by analyzing the thermoelectric transport coefficients, focusing on transport regime where the two-stage Kondo effect and Fano interference are important. In particular, we analyze the fingerprints of these two phenomena on the thermoelectric properties of the system. We also study the effect of external magnetic field on thermotransport characteristics since both effects strongly depend on its magnitude. The calculations are performed by using the numerical renormalization group (NRG) method [47], which allows us to determine the linear response properties of the device in a very accurate manner [48]. We show that the thermopower and figure of merit can be enhanced at temperature corresponding to the second stage of screening, while the normalized heat conductance and the electrical conductance are found to satisfy a modified Wiedemann-Franz law. In addition, we also showed that considerable spin thermopower can occur in the presence of external magnetic field.

The paper is organized as follows. Model and method are described in Sec. II. Then, we present and discuss the numerical results in Sec. III, which is divided into corresponding subsections, each containing description of dependence on different quantities. Finally, Sec. IV concludes the paper.

**II. MODEL AND METHOD**

The considered system is schematically illustrated in Fig. 1. It consists of left ( $r = L$ ) and right ( $r = R$ ) metallic leads,

\*kpwojcik@amu.edu.pl

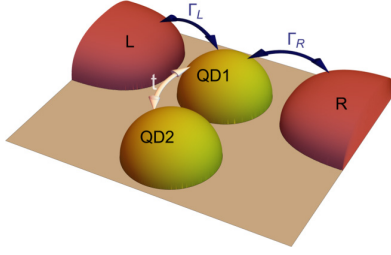


FIG. 1. Schematic illustration of the considered system. The first quantum dot (QD1) is coupled to external left ( $r = L$ ) and right ( $r = R$ ) leads with coupling strength  $\Gamma_r$ , while the second dot (QD2) is connected to the first dot through the hopping matrix element  $t$ .

and the first (QD1) and the second (QD2) quantum dot. The dots form a T-shaped configuration, i.e., QD1 is coupled to both leads and to QD2, while QD2 is not directly coupled to the leads, but only via QD1. We denote the energies of single-electron levels in lead  $r$  by  $\varepsilon_{r\vec{k}}$ , where  $\vec{k}$  stands for quasimomentum. The Hamiltonians of both leads are assumed to have a free-electron form  $H_r = \sum_{\vec{k}\sigma} \varepsilon_{r\vec{k}} n_{r\vec{k}\sigma}$ , where  $n_{r\vec{k}\sigma} = c_{r\vec{k}\sigma}^\dagger c_{r\vec{k}\sigma}$  and  $c_{r\vec{k}\sigma}$  annihilates a corresponding electron with spin  $\sigma$ . To model the double quantum dot, we take into account the on-dot Coulomb interactions  $U$ , which are assumed to be the same for both dots, and allow for hopping between the dots, with  $t$  denoting the respective amplitude. The DQD Hamiltonian has then the following form:

$$H_{\text{DQD}} = \sum_{i\sigma} \varepsilon_{i\sigma} n_{i\sigma} + U \sum_i n_{i\uparrow} n_{i\downarrow} + t \sum_{\sigma} (d_{1\sigma}^\dagger d_{2\sigma} + \text{H.c.}), \quad (2)$$

where  $n_{i\sigma} = d_{i\sigma}^\dagger d_{i\sigma}$ ,  $d_{i\sigma}$  is the annihilation operator of a spin- $\sigma$  electron in the dot  $i$ ,  $\varepsilon_{i\sigma} = \varepsilon_i + \sigma B/2$  denotes its energy ( $\sigma = \pm 1$ ), and  $B$  is the external magnetic field (expressed in such units that  $g\mu_B = 1$ ). Note that we assumed that the capacitive coupling between the dots is negligible. Finally, the Hamiltonian of the whole system can be written in the form  $H = H_L + H_R + H_{\text{DQD}} + H_T$ , where

$$H_T = \sum_{r\vec{k}\sigma} v_{r\vec{k}} (d_{1\sigma}^\dagger c_{r\vec{k}\sigma} + \text{H.c.}) \quad (3)$$

is the tunneling Hamiltonian with the hopping matrix elements  $v_{r\vec{k}}$ . We assume both leads to have flat density of states  $\rho_r$  in the window of width  $2D$  around the Fermi level. The parameter  $D$  is here used as a cutoff for electron energies in the leads and the unit of energy  $D \equiv 1$ . We assume that only  $s$  electrons couple to DQD and consider the wide-band limit, in which the coupling  $\Gamma_r = \pi \rho_r |v_{r\vec{k}}|^2$  is energy independent. We also assume that the system is left-right symmetric  $\Gamma_L = \Gamma_R \equiv \Gamma/2$ .

To reliably analyze the linear-response electric and thermoelectric transport properties of the considered model in the full parameter space, we employ the numerical renormalization group procedure [47,48]. In NRG, the system Hamiltonian is transformed onto the Wilson chain [47], with DQD coupled to the zeroth site of the chain (note that in T-shaped geometry only the first dot is in fact coupled). This Hamiltonian is diagonalized in an iterative fashion by

exploiting the Abelian symmetries for the total charge and total spin. The states discarded during this procedure are then used to build the full density matrix of the system [49,50], which allows us to calculate various correlation functions. Knowing the spectrum of the Hamiltonian and the density matrix, we next calculate the relevant retarded Green's function  $\langle\langle d_{1\sigma}^\dagger |d_{1\sigma} \rangle\rangle^{\text{ret}}(\omega)$  of the first dot level in the Lehmann representation, and hence the spin-dependent spectral function  $A_\sigma(\omega) = -\pi^{-1} \text{Im} \langle\langle d_{1\sigma}^\dagger |d_{1\sigma} \rangle\rangle^{\text{ret}}(\omega)$ , and the transmission coefficient  $\mathcal{T}(\omega) = \pi \Gamma \sum_\sigma A_\sigma(\omega)$ . Then, the relevant transport quantities can be expressed in terms of Onsager integrals [1]

$$L_n = -\frac{1}{h} \int \omega^n \frac{\partial f(\omega)}{\partial \omega} \mathcal{T}(\omega) d\omega, \quad (4)$$

where  $f(\omega)$  denotes the Fermi-Dirac distribution function. The conductance is obviously [51]  $G = e^2 L_0$ . In general, the thermal conductance  $\kappa$  contains an electronic part  $\kappa_{\text{el}}$  and a lattice part due to heat conduction by phonons  $\kappa_{\text{ph}}$ . However, phononic heat transmission through quantum dots in two-dimensional electron gas is usually very poor due to small volume of the system. For this reason, in our model phonons are not taken into account and  $\kappa = \kappa_{\text{el}}$ . Then, the heat conductance can be expressed as

$$\kappa = \left( \frac{\delta J_Q}{\delta T} \right)_{J=0} = \frac{1}{T} \left[ L_2 - \frac{L_1^2}{L_0} \right], \quad (5)$$

where  $\delta J_Q$  denotes the heat current caused by temperature gradient  $\delta T$ , and  $J = 0$  stays for the condition of vanishing of the electric current. Finally, the Seebeck coefficient is given by

$$S = -\left( \frac{\delta V}{\delta T} \right)_{J=0} = -\frac{1}{eT} \frac{L_1}{L_0}, \quad (6)$$

where  $\delta V$  denotes the voltage drop between the leads.

The efficiency of the thermoelectric device  $\eta$  working at its maximal power can be expressed as [52]

$$\eta = \frac{\eta_C}{2} \frac{ZT}{ZT + 2}, \quad (7)$$

where  $\eta_C$  is the Carnot efficiency and the dimensionless parameter  $ZT$  denotes the thermoelectric figure of merit, which is given by

$$ZT = \frac{GTS^2}{\kappa}. \quad (8)$$

Therefore, large values of  $ZT$  are desirable from the application point of view. However, for the efficiency of the device working at fixed heat flow conditions, it is rather the power factor  $P = S^2 G$  which should be maximized [53]. For those reasons, in the following we also study the behavior of both  $P$  and  $ZT$  on various parameters of the system.

In addition, when the system is placed in an external magnetic field  $B$ , and the spin relaxation in the leads is very slow, the spin accumulation may occur, i.e., the voltage may become spin dependent as well,  $\delta V_\sigma = \delta V + \sigma \delta W$ . Then, the spin-dependent transmission coefficient  $\mathcal{T}_\sigma(\omega)$  and the spin-dependent Onsager integrals  $L_{n\sigma}$  are defined in an obvious manner [11,54]. The inequality of conductances in respective

spin channels  $G_\sigma$  gives rise to finite spin polarization of the current [44]

$$\mathcal{P} = \frac{G_\uparrow - G_\downarrow}{G}. \quad (9)$$

On the other hand, the Seebeck coefficient in spin channel  $\sigma$  can be defined as

$$S_\sigma = -\left(\frac{\delta V_\sigma}{\delta T}\right)_{J_\sigma=0} = -\frac{1}{eT} \frac{L_{1\sigma}}{L_{0\sigma}}, \quad (10)$$

where  $J_\sigma$  denotes the current of spin- $\sigma$  carriers. Then, the spin thermopower can be expressed as

$$S_S = \frac{S_\uparrow - S_\downarrow}{2}. \quad (11)$$

### III. RESULTS AND DISCUSSION

The two-stage Kondo effect can occur when each dot is occupied by a single electron. It manifests itself in a nonmonotonic dependence of the linear conductance  $G$  on the temperature  $T$  or the magnetic field  $B$  [36]. This can be explicitly seen in Fig. 2(a), which displays the temperature dependence of  $G$  for different hoppings  $t$ . At high temperatures  $T > U$ , the system is in the free orbital regime and the conductance is rather poor [47,55]. At lower  $T$  the first stage of screening occurs, which corresponds to the usual Kondo effect in the subsystem containing the first quantum dot and conduction band. The conductance  $G$  increases then to become  $G = G_{\max}/2$  at  $T = T_K$ , and  $G = G_{\max}$  for  $T \ll T_K$ . When temperature decreases further, there appears another characteristic temperature  $T^*$  at which the conductance starts decreasing. For relatively weak hopping  $t$ , the conductance suppression is due to the second stage of screening, in which the spin of the second dot becomes screened by the many-body continuum consisting of the first dot strongly interacting with the conduction band [see the curves for  $t \lesssim \Gamma/3$  in Fig. 2(a)]. In the low-temperature limit,  $G$  decreases then as  $G \propto T^2$  [36]. The characteristic temperature  $T^*$  at which the conductance drops to  $G_{\max}/2$  can be estimated from [36,37,39]

$$T^* = a T_K e^{-bT_K/J_{\text{eff}}}, \quad (12)$$

where

$$J_{\text{eff}} = \frac{4Ut^2}{U^2 - (\varepsilon_1 - \varepsilon_2)^2} \quad (13)$$

is an effective exchange interaction between singly occupied dots. When the hopping  $t$  increases, the first-stage Kondo effect still develops when  $T \approx T_K$ , however, further decrease of temperature results in fast suppression of conductance due to the interdot exchange interaction, which leads to the formation of spin singlet state in the double dot [see the curve for  $t = \Gamma/2$  in Fig. 2(a)]. On the other hand, for very large hopping  $t$ , the bonding and antibonding states form in the double dot and the conductance is generally low for all temperatures (no Kondo effect develops) [cf. the case of  $t = \Gamma$  in Fig. 2(a)]. Note that in all cases the low-temperature conductance through the system is blocked, however, the blocking mechanisms are essentially different.

Additional insight into the system behavior can be obtained from the temperature dependence of magnetic susceptibilities

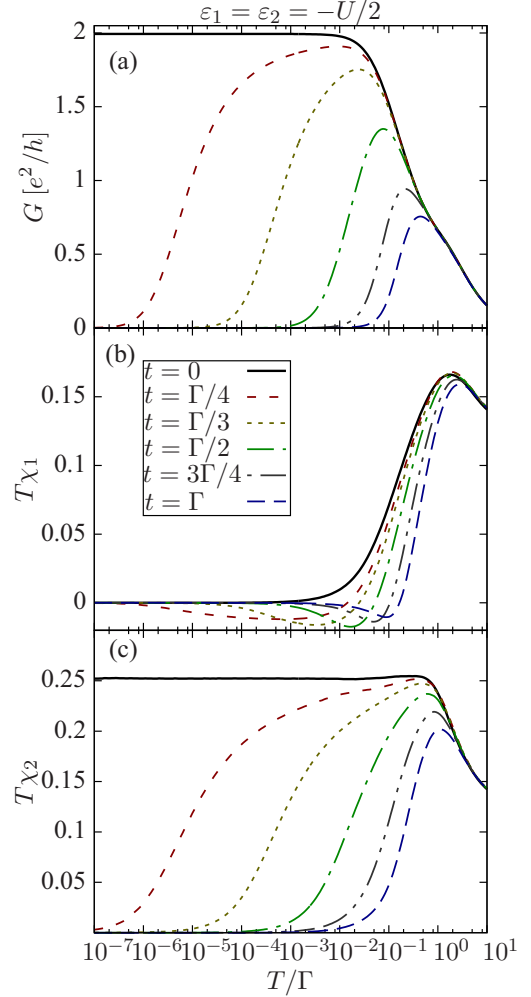


FIG. 2. (a) The linear conductance and magnetic susceptibility of (b) the first ( $\chi_1$ ) and (c) second ( $\chi_2$ ) quantum dots as a function of temperature calculated at the particle-hole symmetry point  $\varepsilon_1 = \varepsilon_2 = -U/2$  and for  $U = 0.5 = 5\Gamma$  and different values of hopping between the dots  $t$ , as indicated. Susceptibilities were for clarity multiplied by  $T$ . Note the logarithmic temperature scale.

of the dots, denoted by  $\chi_1$  ( $\chi_2$ ) for the first (second) dot, which are shown in Figs. 2(b) and 2(c), respectively.  $\chi_i$  is defined as  $\chi_i \equiv \frac{d}{dB} \langle S_{zi} \rangle|_{B=0}$ , where  $S_{zi}$  denotes the  $z$ th component of the spin of dot  $i$  [56]. Let us first discuss the behavior of  $\chi_1$ . When decreasing the temperature,  $T\chi_1$  first grows due to suppression of charge fluctuations and reaches a maximum for  $T \sim \Gamma$  [see Fig. 2(b)]. Relatively large Kondo temperature ( $T_K \approx U/20$ ) corresponding to the parameters of Fig. 2 does not allow for  $T\chi_1$  to reach the free-spin value  $\frac{1}{4}$ . One can see that for  $t \gtrsim \Gamma/2$  the spin of the first dot is screened at  $T$  significantly higher than  $T_K$ . This is associated with the exchange interaction between the dots, which for large  $t$  can suppress even the first-stage Kondo effect. On the other hand, for  $t < \Gamma/2$  the temperature at which  $\chi_1$  is fully screened only slightly depends on  $t$ . Thus, one can deduce that the usual Kondo effect is the leading screening mechanism for

$t \lesssim \Gamma/2$ . Note, however, that  $\chi_1$  becomes negative at  $T^* < T < T_K$ . This is an effect of interdot interaction, which favors antiparallel alignment of the double dot spins. Although this residual magnetic moment is very small  $|T\chi_1| \lesssim 0.02$ , only below  $T^*$  the spin of the first dot becomes fully screened. Clearly, this does not apply to the  $t = 0$  case, where interdot exchange is absent and  $\chi_1 \geq 0$  for all  $T$ .

Figure 2(c) presents the temperature dependence of magnetic susceptibility of the second dot  $\chi_2$ . As can be clearly seen, for  $t = 0$  and  $T \ll \Gamma$ ,  $T\chi_2 = \frac{1}{4}$ , as expected for a single spin- $\frac{1}{2}$ . For  $t \neq 0$ , the local moment of the second dot has a maximum at  $T \approx U/10$ , then it decreases slowly with decreasing  $T$  toward  $T^*$  and vanishes even faster at  $T \approx T^*$ . At zero temperature, the second dot spin is fully screened for any  $t \neq 0$ . Notice, that for  $t < \Gamma/2$  the maximal  $T\chi_2$  almost reaches  $\frac{1}{4}$ , while for stronger interdot couplings the magnetic moment of the second dot is already affected at higher temperatures and  $T\chi_2 < \frac{1}{4}$ .

Let us now analyze how different screening stages of the Kondo effect reveal in thermoelectric properties of the system. Because the Seebeck coefficient vanishes when the electron and hole processes contribute equally to transport, which happens for the particle-hole symmetry point of the model  $\varepsilon_1 = \varepsilon_2 = -U/2$ , we will present results for asymmetric case, when  $\varepsilon_1 \neq -U/2$ . To perform calculations, we assume  $U = 0.5$ ,  $\Gamma = 0.1$ , and  $\varepsilon_2 = -U/2$ , unless explicitly stated otherwise. We note that in the case of  $t = 0$  and for  $\varepsilon_1 = -U/2$ , the Kondo temperature equals [57]  $T_K^0 \simeq 0.022$ .

### A. Temperature dependence

The linear response electric and thermoelectric transport characteristics calculated as a function of temperature for different values of the hopping  $t$  are shown in Fig. 3. The temperature dependence of the conductance is qualitatively similar to that shown in Fig. 2(a) and here is presented to facilitate the estimation of different energy scales. The main difference is a slightly lower value of  $G_{\max}$  due to quite large detuning from the middle of the Kondo valley and a slight change of both  $T_K$  and  $T^*$ .

The temperature dependence of thermal conductance is presented in Fig. 3(b). One can clearly see that  $\kappa$  exhibits a maximum for  $T \sim \Gamma$ , irrespective of the value of the hopping between the dots. A similar maximum in  $\kappa$  as a function of  $T$  was predicted for the single-stage Kondo effect [10]. It results from an enhanced density of states at the Fermi level in the Kondo regime and freezing of thermal transport at low  $T$ . Thus, to analyze the influence of the second stage of Kondo screening on thermal transport, we also plot  $\kappa/T$  versus  $T$  in the inset of Fig. 3(b). According to the Wiedemann-Franz law [58], this quantity should be proportional to the conductance  $\kappa/T = \mathcal{L}_0 G$ , where  $\mathcal{L}_0 = (\pi^2/3) k_B^2/e^2$ . One can clearly see that this is indeed the case by comparison with Fig. 3(a). However, closer inspection of the figure reveals a small shift in  $\kappa/T$  with respect to  $G$  towards lower temperatures. Since the temperature scale is logarithmic, this shift corresponds to rescaling the temperature by a constant factor, which we denote by  $\alpha$ . From the analysis of NRG data we found  $\alpha \approx 2$ . In other words, it is  $\tilde{\mathcal{L}} = \kappa(\alpha T)/[\alpha T G(T)]$  and not the Lorentz number  $\mathcal{L} = \kappa(T)/[T G(T)]$ , which is constant and nearly identical to

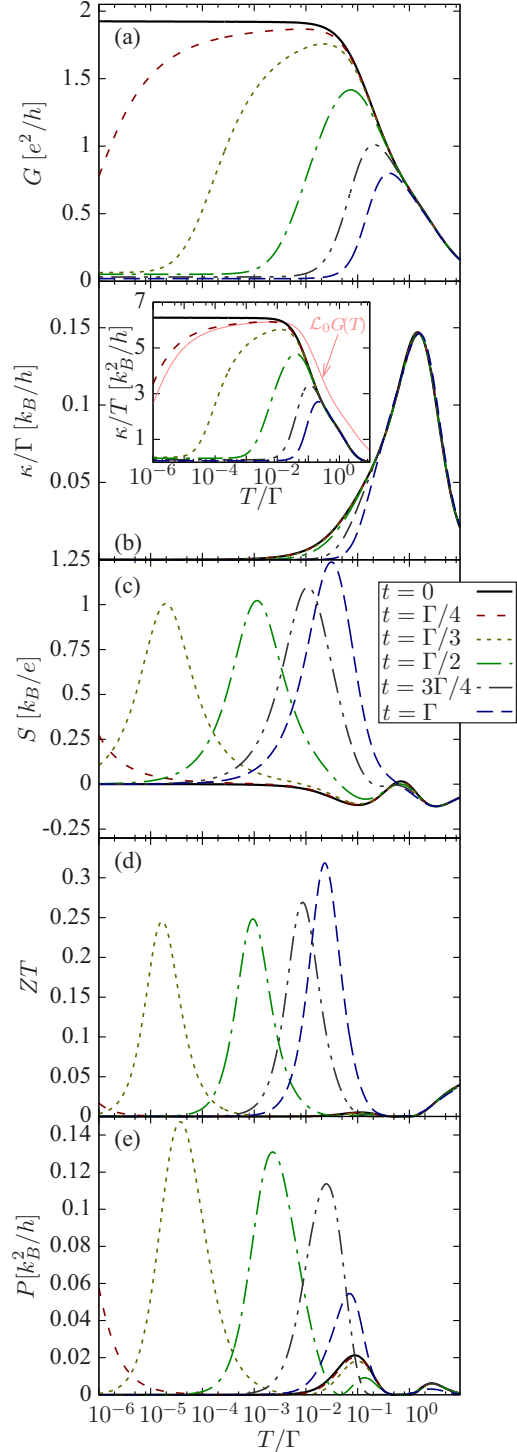


FIG. 3. (a) The electrical conductance and the thermoelectric properties: (b) thermal conductance  $\kappa$ , (c) Seebeck coefficient  $S$ , (d) thermoelectric figure of merit  $ZT$ , and (e) the power factor  $P$  as a function of temperature  $T$  for different values of hopping between the dots  $t$ , as indicated. Inset in (b) shows the thermal conductance normalized by temperature. The parameters are  $U = 0.5$ ,  $\Gamma = 0.1$ ,  $\varepsilon_1 = -U/3$ , and  $\varepsilon_2 = -U/2$ . Note the logarithmic temperature scale.



the universal value  $\mathcal{L}_0$ . To present this feature more explicitly, the curve for  $t = \Gamma/4$  from Fig. 3(a) rescaled by the factor  $\mathcal{L}_0$  (but not shifted) is plotted in the inset of Fig. 3(b) with a bright solid line. When temperature is shifted,  $G(T)$  agrees with  $\kappa(\alpha T)/(\alpha T)$  for  $t = \Gamma/4$  within a few-percent accuracy at  $T < T_K$ . These results can be understood as a generalization of those obtained by Costi and Zlatić for the single-impurity Anderson model, where the shift between  $\kappa(T)/T$  and  $G(T)$  (with  $\alpha \approx 1.9$ ) was found in the Kondo regime [10]. Here, we see that it is also present in more complex systems, and persists in the second stage of screening. Hereafter, let us refer to this property as *the modified Wiedemann-Franz law*. Moreover, when discussing the behavior of  $\kappa$  we will henceforth always plot  $\kappa/T$ .

The Seebeck coefficient  $S$  as a function of  $T$  is presented in Fig. 3(c). In the absence of hopping,  $t = 0$ , the thermopower exhibits typical sign changes as a function of temperature, which signify either electronlike or holelike contributions to conductivity, and vanishes for  $T \ll T_K$  [10]. However, when the hopping is finite,  $S$  exhibits a maximum at certain temperature, which depends on  $t$ : the stronger the hopping, the higher the temperature at which the maximum occurs [see Fig. 3(c)]. The positions of those maxima roughly correspond to  $T^*$  for respective  $t$ . This can be understood by realizing the fact that in the low-temperature limit, when the Sommerfeld expansion is a good approximation, the thermopower  $S$  can be expressed as [10]

$$S \simeq -\frac{\pi^2 k_B^2}{3e} \frac{T}{A(0)} \left. \frac{\partial A(\omega)}{\partial \omega} \right|_{\omega=0}, \quad (14)$$

where  $A(\omega) = \sum_{\sigma} A_{\sigma}(\omega)$  is the (temperature-dependent) spectral function of the first dot, which (at low  $T$ ) behaves qualitatively similar to  $G(T)$ . Thus, for temperatures at which the second stage of screening occurs and conductance drops, there is a large enhancement of the Seebeck coefficient. For the same reason,  $S$  has a minimum for  $t < \Gamma/2$  (with  $S < 0$ ) at  $T = T_K$ . It is much smaller than the peak at  $T^*$  because, due to relatively large  $T_K$  for assumed parameters, the Kondo peak in the spectral function is quite wide, thus, the derivative in Eq. (14) is small. The change of sign corresponds to the fact that  $A(\omega)$  exhibits a (asymmetric) peak of the width  $\sim T_K$  with a (asymmetric) dip of a width  $\sim T^*$ , thus, derivative in Eq. (14) changes sign; see Fig. 4 and Sec. III B for more detailed discussion of the behavior of spectral function. Moreover,  $S$  is also negative at large temperatures  $T \sim U$ , which corresponds to holelike conductivity ( $\varepsilon_1 > -U/2$ ).

Interestingly, the stronger the interdot interaction  $t$  is, the higher is the peak in  $S(T)$  [see Fig. 3(c)]. This reflects itself in relatively high values of the thermoelectric figure of merit  $ZT$ , which exhibits maxima at similar temperatures as thermopower. One can see that these temperatures increase when  $t$  is enhanced [see Fig. 3(d)]. Nevertheless, the values of  $ZT$  are still smaller than unity. Moreover, it can be seen in Fig. 3(a) that with increasing  $t$  the conductance at low temperatures becomes even more suppressed, consequently, the possible applicability of a considered device as a heat pump or a voltage source is rather limited for strong  $t$ . This is also reflected in the temperature dependence of the power factor  $P$ , which is plotted in Fig. 3(e), and the values it takes.

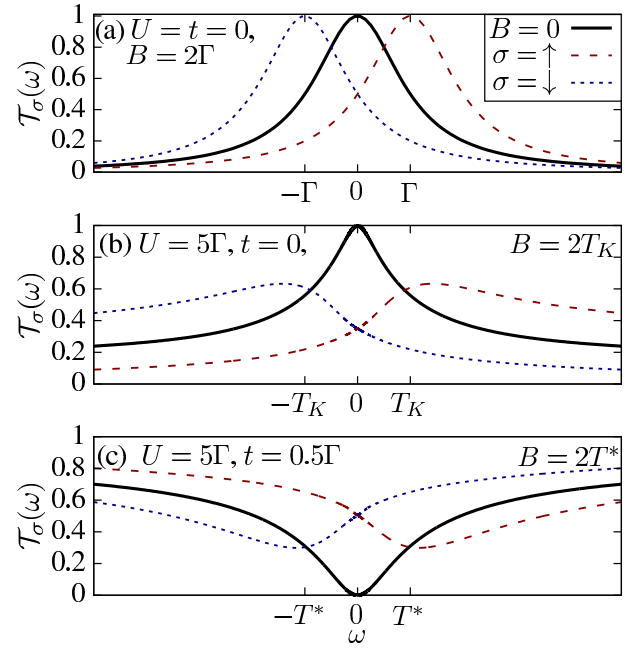


FIG. 4. The zero-temperature spin-resolved transmission coefficient  $\mathcal{T}_{\sigma}(\omega) = \pi \Gamma A_{\sigma}(\omega)$  of the first quantum dot in the particle-hole symmetric case in the presence of external magnetic field  $B$ . The solid lines present for reference the case of  $B = 0$ , while the dashed (dotted) lines show the spin-up (spin-down) contribution. Panel (a) displays the results for  $U = t = \varepsilon_1 = 0$  and  $B = 2\Gamma$ , panel (b) for  $U = 5\Gamma$ ,  $t = 0$ ,  $\varepsilon_1 = -U/2$ , and  $B = 2T_K$ , while panel (c) is calculated for  $U = 5\Gamma$ ,  $t = 0.5\Gamma$ ,  $\varepsilon_1 = \varepsilon_2 = -U/2$ , and  $B = 2T^*$ . The calculations were performed for  $\Gamma = 0.1$ .

As can be seen, the height of maxima in  $P$ , corresponding to peaks of  $ZT$ , significantly decreases with increasing the hopping  $t$ .

### B. Magnetic field dependence

Let us now analyze the effect of external magnetic field on thermoelectric transport properties of the considered device. First, we discuss the behavior of the spin-resolved transmission coefficient of the first dot,  $\mathcal{T}_{\sigma}(\omega) = \pi \Gamma A_{\sigma}(\omega)$ , and then investigate the thermotransport characteristics.

Although the influence of magnetic field on the linear conductance may seem similar to that of finite temperature since both lead to the suppression of conductance once larger than  $T_K$  with a similar dependence on external parameter (either  $T$  or  $B$ ) [59,60] the impact of  $B$  on  $\mathcal{T}_{\sigma}(\omega)$  is more complex. The most important difference is associated with the induced spin polarization of the local density of states and, thus, the linear conductance. The energy dependence of the transmission coefficient calculated for the particle-hole symmetry point and for different transport regimes is shown in Fig. 4. The solid line presents  $\mathcal{T}_{\sigma}(\omega)$  in the case of  $B = 0$  for reference, while the dashed (dotted) line shows the spin-up (spin-down) contribution for finite  $B$ .

First of all, one can see that magnetic field leads to the splitting of the transmission coefficient and to its finite spin

polarization  $\mathcal{T}_\uparrow(\omega) \neq \mathcal{T}_\downarrow(\omega)$ . In the case of noninteracting model and  $t = 0$ , the effect of finite magnetic field  $B$  can be viewed as a shift of  $\mathcal{T}_\sigma(\omega)$  to  $\mathcal{T}_\sigma(\omega - \sigma B/2)$  since  $\mathcal{T}_\sigma(\omega) = \Gamma^2/[(\omega - \varepsilon - \sigma B/2)^2 + \Gamma^2]$ , while the maximum value of  $\mathcal{T}_\sigma(\omega)$  is not affected. This results in the splitting of the transmission coefficient of width given by  $B$  [see Fig. 4(a)]. However, when interactions are relevant both the splitting and magnitude of  $\mathcal{T}_\sigma(\omega)$  may be different.

The effect of magnetic field on transmission coefficient in the case when only the first stage of the Kondo effect is present is shown in Fig. 4(b), while the case of the second stage is depicted in Fig. 4(c). In the former case, the splitting in  $\mathcal{T}(\omega)$  is for  $B \gg T_K$  given by  $2B$  [19]. This is due to the fact that the side peaks of the Kondo resonance occur at energy scale which allows for spin-flip processes between the split spin states of the dot level. Such inelastic scattering becomes effective once  $\omega = \pm B$  and, consequently, a side resonance in  $\mathcal{T}(\omega)$  occurs. Note that in Fig. 4(b) the splitting is slightly smaller than  $2B$ . This is because for parameters used in the figure ( $B = 2T_K$ ), the splitting is not yet fully developed. On the other hand, in the case of second stage of screening, the magnetic field shifts the minimum position of the transmission coefficient to  $\omega = \pm B/2$  [see Fig. 4(c)].

Altogether, while in the noninteracting case the magnetic field has a trivial effect of shifting the maximum in  $\mathcal{T}_\sigma(\omega)$  to  $\omega = \pm B/2$ , in the interacting case its impact is more complex. If  $B$  is larger than the relevant energy scale (either  $T_K$  or  $T^*$  depending on transport regime), the Kondo effect may become suppressed. This results in the suppression of the Kondo peak seen in Fig. 4(b) and conductance minimum due to the second stage of the Kondo effect presented in Fig. 4(c).

For T-shaped DQDs, the dependence of the linear response conductance on magnetic field was analyzed by da Silva *et al.* [44]. It was found that the (first-stage) Kondo effect can be restored (second stage of screening suppressed) by appropriate tuning of  $B$ . This reinstatement is a consequence of restoring the degeneracy between two states differing in magnetic quantum number by unity, which then allows for spin-flip cotunneling processes responsible for enhanced conductance. Alternatively, it can be also understood as a consequence of a shift of the transmission coefficient in each spin channel. In the second stage of screening  $\mathcal{T}(\omega)$  has a dip at the Fermi level with the half-width of the order of  $T^*$  [cf. Fig. 4(c)]. When the magnetic field is applied, this dip is shifted out of the Fermi level and consequently  $G(T=0)$  is increased. For  $T^* < B < T_K$ , the dip in  $\mathcal{T}(\omega)$  characteristic of the second stage of screening is suppressed, but the Kondo peak is still present for  $|\omega - B| < T_K$ . Thus, when changing  $B$ ,  $G(T=0)$  can reach  $2e^2/h$ . Finally, the Kondo resonance can also be affected and eventually destroyed by strong enough  $B$ , leading to the resuppression of  $G$ . This explains the nonmonotonic dependence of  $G$  on  $B$  shown in Fig. 5(a).

The magnetic field dependence of the thermal conductance is shown in Fig. 5(b). One can see that the  $B$  dependence of thermal conductance normalized by temperature is qualitatively the same as that of  $G$ . Moreover, as checked numerically (not shown),  $\kappa$  fulfills the modified Wiedemann-Franz law, i.e., one obtains  $\kappa(\alpha T, B)/(\alpha T) = G(T, B)\mathcal{L}_0$ . Note, however, that  $\alpha > 1$  causes  $\kappa$  to be less suppressed in the second stage of screening compared to  $G$  (for fixed  $T$ ). On the other hand,

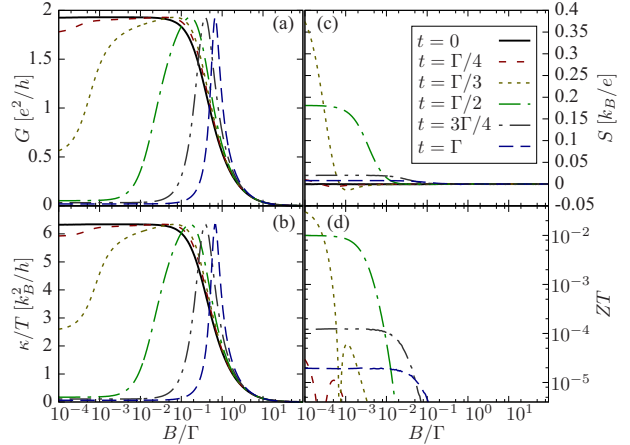


FIG. 5. The magnetic field dependence of (a) the linear conductance, (b) the thermal conductance normalized by temperature, (c) the Seebeck coefficient, and (d) the thermoelectric figure of merit for different values of the hopping  $t$ , as indicated. The parameters are the same as in Fig. 3 with  $T = 10^{-4}\Gamma$ .

the thermopower as a function of  $B$  is shown in Fig. 5(c). Because  $S$  is calculated for relatively low temperatures, its magnitude is rather low. Here, we want to investigate whether finite magnetic field can lead to an increase of  $S$  for such  $B$  that the restoration of the Kondo effect occurs [cf. Fig. 5(a)]. As follows from Fig. 5(c), the general observation is that  $S$  is not enhanced by finite magnetic field, except for intermediate values of  $t$  at low magnetic fields. In fact, an enhancement of  $S$  occurs for such  $t$  that  $T \approx T^*$  (see the case of  $t = \Gamma/3$  in Fig. 5). Then, the maximum in thermopower develops for tiny magnetic fields  $B = T$ . Nevertheless, except for these particular parameters,  $S$  is not especially large. As a consequence, the figure of merit, which is shown in Fig. 5(d), is very low for all values of  $B$  (the same applies to power factor  $P$ , which is therefore not shown here). Low values of  $S$  and  $ZT$  can be understood as follows. Let us recall that  $G \sim L_0$ , while at low temperatures the main contribution to  $\kappa$  comes from  $L_2$  [cf. Eq. (5)], whereas  $S \sim L_1$  [cf. Eq. (6)]. Finite magnetic field splits the transmission coefficient, however, this splitting hardly increases the asymmetry of  $\mathcal{T}(\omega)$  with respect to  $\omega = 0$ , which is necessary for  $L_1$  to increase. Thus,  $S$  can become significant only at temperatures high enough for the asymmetry of  $\mathcal{T}(\omega)$  to be relevant. Consequently, no spectacular enhancement of  $S$  due to finite magnetic field is observed in Fig. 5(c).

### C. Dependence on DQD energy levels

When the hopping between the dots  $t$  becomes relatively large, transport occurs through molecular states of the double dot. When one of such states is narrow and its energy lies within another state that is wide, the Fano effect can occur, reflecting itself as an antiresonance in the linear conductance as a function of DQD's energy levels [36–41]. The antiresonance occurs when the energy of the narrow level coincides with the Fermi level, which effectively corresponds to some condition for  $\varepsilon_1$  or  $\varepsilon_2$ , depending on the interactions and parameters of the

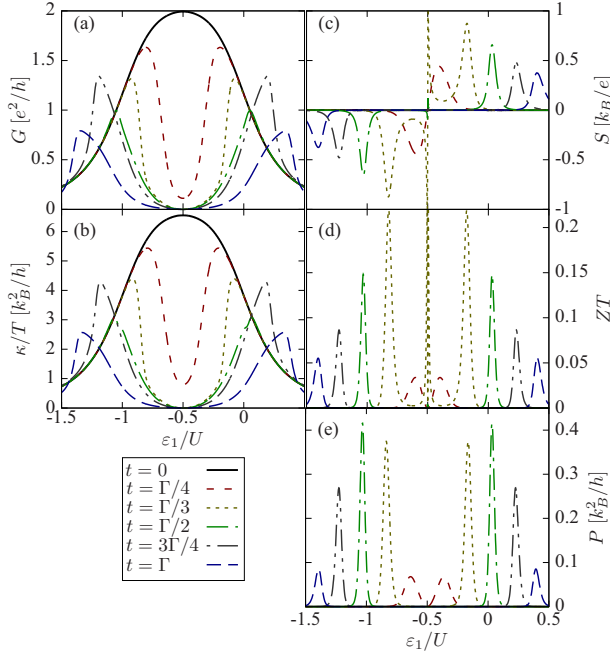


FIG. 6. The first-dot-level dependence of (a) the linear conductance, (b) the thermal conductance normalized by temperature, (c) the Seebeck coefficient, (d) the thermoelectric figure of merit, and (e) the power factor for different values of the hopping  $t$ , as indicated. The parameters are the same as in Fig. 3 with  $T = 10^{-6}\Gamma$ .

system. In fact, Coulomb correlations in the dots can cause a deviation from the exact Fano formula and lead to a broadening of the antiresonance [45]. Interestingly, the suppression of  $G$  due to the Fano effect can be also understood by invoking the two-stage Kondo effect [42]. The presence of the antiresonance is then explained as a consequence of the existence of the second stage of screening, which leads to the suppression of the conductance. A broad minimum in  $G$  occurs then as a function of either  $\varepsilon_1$  or  $\varepsilon_2$  provided that  $T < T^*$ . Moreover, because  $T^*$  is a function of both  $\varepsilon_1$  and  $\varepsilon_2$  [cf. Eqs. (12)–(13)] and generally decreases with increasing the detuning from the particle-hole symmetry point of the model [42,46], the Fano antiresonance in  $G$  strongly depends on temperature. In particular, when  $T > T^*$ , the antiresonance disappears.

In Fig. 6, we analyze the transport properties of the system as a function of  $\varepsilon_1$  while assuming  $\varepsilon_2 = -U/2$ . We chose to tune  $\varepsilon_1$  because for small hopping  $t$  the variation of  $\varepsilon_2$  does not lead to considerable changes in transport, whereas the variation of  $\varepsilon_1$  causes similar consequences as that of  $\varepsilon_2$  for large enough  $t$ . The calculations were performed at  $T = 10^{-6}\Gamma$ , such that the condition  $T < T^*$  was satisfied around the particle-hole symmetry point  $\varepsilon_1 = \varepsilon_2 = -U/2$  for all values of  $t > 0$  considered in the figure. (For  $t = \Gamma/4$ ,  $T$  is in fact of the order of  $T^*$ .) First of all, the Fano antiresonance in the linear conductance for  $t \neq 0$  is clearly visible in Fig. 6(a). One can see that the width of the antiresonance depends on  $t$ . The larger is the hopping between the dots, the wider is the minimum in  $G$ . The existence and width of the antiresonance

are in fact conditioned by the ratio  $T/T^*$ , which can be varied by changing  $t$  and/or levels' positions [42,46].

The Fano effect is also visible in the level dependence of the thermal conductance normalized by temperature, which is shown in Fig. 6(b). As follows from the figure,  $\kappa/T$  behaves qualitatively the same as the linear conductance. Moreover, it satisfies the modified Wiedemann-Franz law (results not shown), which implies that, up to prefactors,  $G(T)$  is equal to  $\kappa(\alpha T)/(\alpha T)$ . This is why the dip in  $\kappa/T$  calculated for  $t = \Gamma/4$  is shallower than that in the linear conductance [cf. Figs. 6(a) and 6(b)].

In the Kondo regime, the low-temperature expression for  $S$  [cf. Eq. (14)] is significantly different from the Mott relation given by Eq. (1), which suggests that  $S$  is proportional to  $\partial G/\partial\mu$ , where the role of the chemical potential  $\mu$  is played by  $\varepsilon_1$ . As can be seen in Fig. 6(c), strong deviations from the Mott relation are also present in the second stage of screening:  $S$  is not proportional to the derivative of the conductance [cf. Fig. 6(a)]. In particular, the thermopower does not change sign for  $\varepsilon_1$  corresponding to the peaks in the linear conductance for  $t \neq 0$ . Nevertheless,  $S$  becomes enhanced for such values of  $\varepsilon_1$ , at the onset of the Fano antiresonance. Despite low temperature, the thermopower reaches then relatively large values of the order of  $\pm k_B/e$  [see Fig. 3(c)]. Note that  $S$  for  $t = 0$  is then negligible due to the fact that  $T \ll T_K$  [10].

Furthermore, all the peaks visible in  $S$  are revealed in both the figure of merit  $ZT$  and the power factor  $P$ , which are shown in Figs. 6(d) and 6(e), respectively. First of all, we note that although  $ZT$  does not exceed unity, it can still take considerable values. One can see that the height of peaks in  $ZT$  as a function of  $\varepsilon_1$  decreases upon increasing  $t$ , until  $t$  reaches  $\Gamma/3$ . Further decrease of  $t$  causes  $ZT$  to decrease rapidly. The height of peaks in  $P$  also depends on  $t$  in a nonmonotonic way. However, the highest peak corresponds to  $t = \Gamma/2$  [see Fig. 3(e)].

In addition, we note that for  $t = \Gamma/3$  there is a sharp peak in both  $S$  and  $ZT$  when approaching the particle-hole symmetry point  $\varepsilon_1 = \varepsilon_2 = -U/2$  from either side [see Figs. 6(c) and 6(d)]. However, these peaks do not correspond to any peak in  $P$  [cf. Fig. 6(e)], which implies that the system does not really conduct heat in this regime and those peaks are therefore unmeasurable. In fact, the peaks in  $S$  (and thus also in  $ZT$ ) result rather from a suppression of the coefficient  $L_0$  than from an enhancement of  $L_1$  [cf. Eq. (6)].

The Fano effect can be strongly affected by an external magnetic field  $B$  [44]. As already explained in Sec. III B, finite magnetic field can restore the Kondo resonance leading to an enhancement of  $G$  [cf. Fig. 5(a)]. Moreover,  $B \neq 0$  splits the Fano antiresonance condition in respective spin channel, which can result in large spin polarization of the linear conductance outside the particle-hole symmetry point [44]. The dependence of the spin polarization on the first dot level position is shown in Fig. 7(a) for  $t = \Gamma/3$  and different values of magnetic field. Since the spin polarization is antisymmetric with respect to the particle-hole symmetry point, let us discuss the dependence for  $\varepsilon_1 > -U/2$ . For small magnetic fields,  $\mathcal{P}$  exhibits one peak around the middle of the Coulomb blockade and another one around the resonance. When  $B > T^*$ , those peaks merge,

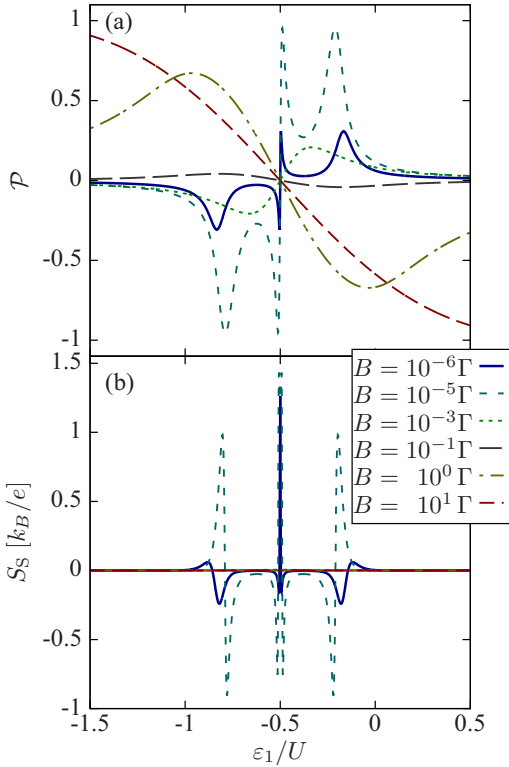


FIG. 7. (a) The spin polarization  $\mathcal{P}$  of the linear conductance and (b) the spin Seebeck coefficient  $S_S$  as a function of  $\varepsilon_1$  calculated for a few values of external magnetic field  $B$  indicated in the figure, and for  $t = \Gamma/3$  and  $T = 10^{-6}\Gamma$ . The other parameters are the same as in Fig. 3.

but the spin polarization is then rather low [see Fig. 7(a)] for  $B = 10^{-3}\Gamma$ . On the other hand, with further increase of  $B$  such that  $B > T_K$ , the spin polarization changes sign and becomes enhanced. As can be seen in the figure, there are a range of parameters where the spin polarization can be enhanced to its maximum value.

When the spin relaxation in the leads is slow, in the presence of magnetic field finite spin thermopower  $S_S$  can emerge in the system. Its dependence on  $\varepsilon_1$  is depicted in Fig. 7(b). As can be seen, the spin Seebeck coefficient is symmetric with respect to the particle-hole symmetry point and significantly differs from zero approximately at positions corresponding to peaks in  $S$  [cf. the curve for  $t = \Gamma/3$  in Fig. 6(c)]. However, the peaks in  $S_S$  are antisymmetric with respect to their center, i.e., spin thermopower changes sign at the point where thermopower has a maximum. As already explained in previous section, only for  $B \lesssim T$ ,  $S$  significantly differs from 0. Similarly, the highest value of  $S_S$  corresponds to  $B = 10^{-5}\Gamma$ , which is only one order of magnitude larger than  $T$ . On the other hand, for weaker fields the peaks in  $S_S$  are much smaller because the magnetic field is not strong enough to break the spin symmetry. Finally, an additional peak around  $\varepsilon_1 = -U/2$  has the same origin as a similar maximum present in  $S$  for  $t = \Gamma/3$  [see Fig. 6(a)].

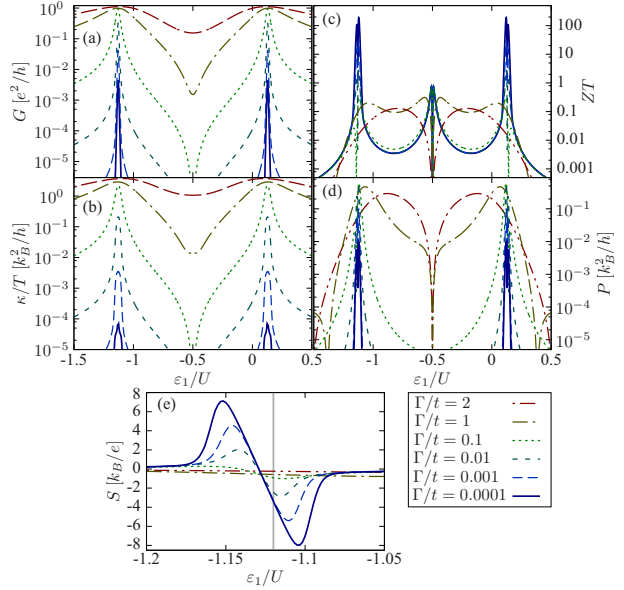


FIG. 8. The dependence of (a) the linear conductance, (b) the thermal conductance normalized by temperature, (c) the figure of merit, (d) the power factor, and (e) the Seebeck coefficient on the position of the first dot level. Each curve corresponds to different coupling  $\Gamma$ , as indicated. The parameters are the same as in Fig. 3 with  $t = 0.1$  and  $T = 0.01t$ . Note the logarithmic scale for the y axes in (a)–(d). The vertical line in (e) indicates the value of  $\varepsilon_1 = -1.12U$ , which is used in further analysis.

#### D. Role of dot-lead coupling strength $\Gamma$

In this section, we analyze how the thermoelectric properties of the considered system change when the coupling to external leads is varied, such that the system crosses over from the strong to the weak coupling regime. To perform this analysis, we fix the hopping between the two dots to be  $t = U/5$  and tune the strength of the coupling  $\Gamma$ . We consider a few different values of  $\Gamma$ , ranging from relatively large  $\Gamma = 2t$  to as small as  $\Gamma = 10^{-4}t$ . Although the latter value may not be relevant from the experimental point of view, we still include it to help understanding the change in the system's transport behavior when the coupling strength is decreased. In the following, we first study the DQD-level dependence of transport properties and then discuss their temperature behavior. Finally, we end this section with the analysis of the role of coupling strength on the spin Seebeck coefficient and conductance spin polarization.

##### 1. Dependence on DQD energy levels

The dependence of thermoelectric transport properties on the position of the first dot level is shown in Fig. 8. The calculations were performed at  $T = 0.01t$ , which roughly corresponds to the temperature at which  $S$  has a peak for  $t = \Gamma$  [see Fig. 3(c)]. To be able to compare the results for significantly different  $\Gamma$ , in Fig. 8 we used the logarithmic scale for vertical axes, except for Fig. 8(e), which presents the thermopower.

Let us start the discussion with the analysis of the linear conductance. For large values of  $\Gamma$  considered in the figure,  $\Gamma \gtrsim t$ , the parameters correspond to the second stage of screening for given  $t$  and  $T$  [cf. Fig. 3(a)]. For this reason, the conductance has only two maxima at resonant energies, while it exhibits an antiresonance for  $\varepsilon_1 = -U/2$  [see Fig. 8(a)]. With decreasing the coupling strength, the conductance becomes generally suppressed. For weak couplings, this suppression is rather due to the Coulomb blockade than the two-stage Kondo effect. On the other hand, when  $\Gamma$  is tuned down, the electron's lifetime in the DQD levels increases, which is reflected in narrowing of resonant peaks.

The level dependence of the thermal conductance normalized by temperature, which is presented in Fig. 8(b), is generally similar to that of  $G$ . For  $\Gamma \gtrsim t$ , the modification of the Wiedemann-Franz law is evident in the vicinity of the particle-hole symmetry point. This results from the shift between  $\kappa(T)/T$  and  $\mathcal{L}_0 G(T)$ , as described by the modified Wiedemann-Franz law introduced in previous sections. However, when the coupling decreases  $\Gamma \lesssim 0.1t$ , the difference between  $G$  and  $\kappa/T$  becomes enhanced and the two quantities cannot be related anymore [cf. Figs. 8(a) and 8(b)]. This is especially visible at resonances, where the thermal conductance becomes strongly suppressed [see Fig. 8(b)], as compared to the electric conductance.

Because the figure of merit is inversely proportional to the thermal conductance [cf. Eq. (8)], suppression of  $\kappa$  translates into an enhancement of  $ZT$ . This effect is clearly visible in Fig. 8(c), which presents  $\varepsilon_1$  dependence of  $ZT$ . With lowering  $\Gamma$ , the figure of merit becomes greatly enhanced at resonances, with values reaching over 100. This originates not only from the suppression of the thermal conductance, but also from an enhancement of the thermopower. Figure 8(e) shows the dependence of the thermopower on the level position around the resonance, where one finds  $|S| \approx 7.5k_B/e$  for  $\Gamma = 10^{-4}t$ . The thermopower in the Coulomb blockade regime does not show any particular enhancement with changing  $\Gamma$ , although its value is finite and can reach  $|S| \approx k_B/e$  (not shown here). Moreover, it can be seen that for weaker couplings  $S$  vanishes for  $\varepsilon_1$  corresponding to the resonance and changes sign at this point, while for stronger couplings  $\Gamma \gtrsim t$ , this effect is not present [see Fig. 8(e)].

To understand the enhancement of the figure of merit and thermopower with decreasing the value of the coupling to external leads, let us for the moment consider the limit of negligible coupling. When  $\Gamma \rightarrow 0$ , the first dot spectral function is given by a sum of the Dirac delta functions, peaked around the energies corresponding to energy differences between the corresponding molecular eigenstates of the DQD. Moreover, at sufficiently low temperatures, only a peak in  $A(\omega)$  which is closest to the Fermi level has a significant thermal weight. We note that the thermoelectric properties of a system whose spectral function possess only one Dirac delta peak have already been analyzed with the aid of simple analytic methods [6,61]. In particular, it was then found that  $ZT \sim 1/\kappa_{\text{ph}}$ . Because in our work we neglected the phonon contribution  $\kappa_{\text{ph}}$ , in the limit of  $\Gamma \rightarrow 0$ , we should obtain  $ZT \rightarrow \infty$  [7]. Using the methodology of Ref. [6], for the considered system we obtained that for  $\Gamma \rightarrow 0$  the Seebeck coefficient reaches a finite limit, which depends linearly on

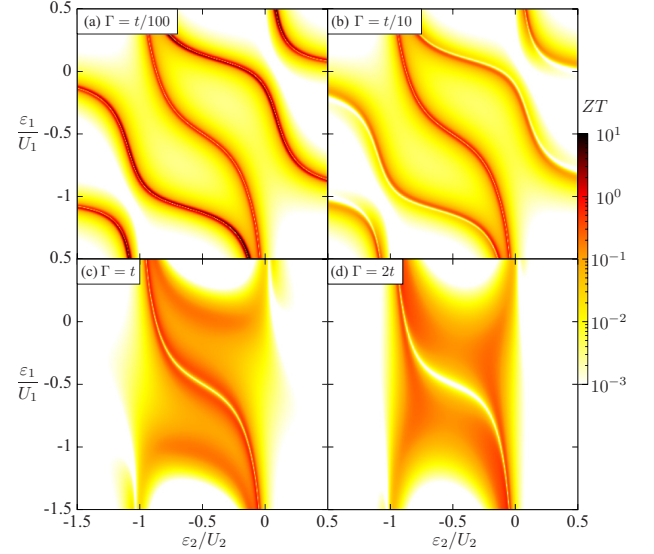


FIG. 9. The thermoelectric figure of merit plotted as a function of  $\varepsilon_1$  and  $\varepsilon_2$  for (a)  $\Gamma = 0.01t$ , (b)  $\Gamma = 0.1t$ , (c)  $\Gamma = t$ , and for (d)  $\Gamma = 2t$ . The other parameters are the same as in Fig. 3 with  $t = 0.1$  and  $T = 0.01t$ .

the distance of the peak in spectral function from the Fermi level, and as a consequence on DQD energy levels  $\varepsilon_1$  and  $\varepsilon_2$ . This is the reason for the linearity of  $S(\varepsilon_1)$  between the peaks visible in Fig. 8(e). Note, however, that the further is the peak in  $A(\omega)$  from the Fermi level, the stronger it is suppressed by the thermal weight. Thus,  $|S|$  reaches maximum and starts to decrease when the distance from the Fermi level exceeds  $T$  [see Fig. 8(e)].

To check whether the observed enhancement of the figure of merit with decreasing  $\Gamma$  has any experimental meaning, we analyze the values of the power factor, which is plotted in Fig. 8(d). First of all, one can see that  $P$  is strongly suppressed in the Coulomb blockade regime, which results from suppressed conductance. On the contrary, the power factor takes considerable values for energies around the resonances. The height of peaks in  $P$  starts decreasing proportionally to  $\Gamma$  when  $\Gamma \lesssim 10^{-2}t$ . At maximum, for  $10^{-1} \lesssim \Gamma/t \lesssim 10^{-2}$ , the height of the peak is  $P \approx 0.6k_B^2/h$ , which is experimentally relevant. For  $\Gamma = 10^{-2}t$ ,  $ZT$  reaches values exceeding unity, however, its magnitude can be increased more when  $\Gamma$  is lowered further.

Finally, in Fig. 9 we plot the dependence of  $ZT$  on both  $\varepsilon_1$  and  $\varepsilon_2$  for different values of the coupling strength  $\Gamma$ , as indicated. This figure in particular demonstrates that the change of  $\varepsilon_2$  has similar consequences as the change of  $\varepsilon_1$ . Moreover, it also shows the crossover between the weak coupling and strong coupling regimes. In the weak coupling regime [see Figs. 9(a) and 9(b) for  $\Gamma = 0.01t$  and  $0.1t$ , respectively], one can clearly see enhanced  $ZT$  at energies corresponding to the resonant energies between the DQD eigenstates. However, in the strong coupling regime, see the panels for  $\Gamma = t$  and  $2t$  in Fig. 9, this landscape drastically changes. In particular, the lines in the  $\varepsilon_1$ - $\varepsilon_2$  plane of enhanced  $ZT$  are not present anymore. This is because the resonant

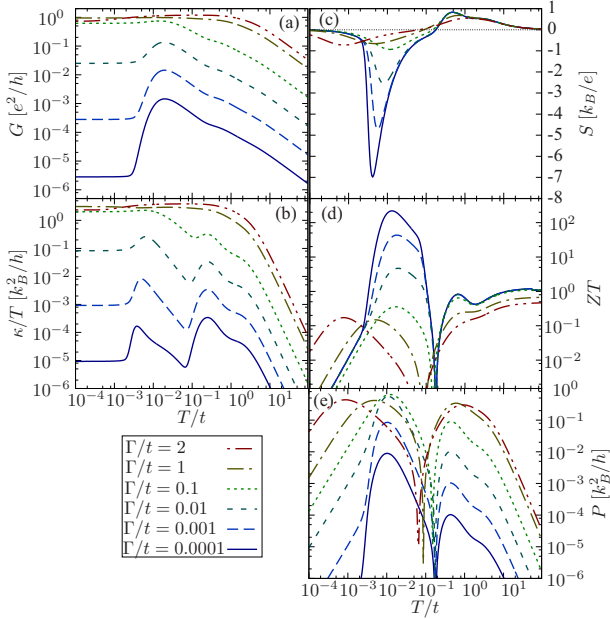


FIG. 10. The temperature dependence of (a) the linear conductance, (b) the thermal conductance normalized by temperature, (c) the Seebeck coefficient, (d) the figure of merit, and (e) the power factor calculated for  $\varepsilon_1 = -1.12U$  and different values of coupling  $\Gamma$  as indicated. The other parameters are the same as in Fig. 8. Note the logarithmic scale in the panels.

energies of DQD eigenstates are not of such a great importance due to large broadening caused by strong interaction with the leads, and nontrivial many-body phenomena taking place in the regime with singly occupied dots. Moreover, for stronger coupling the line of increased  $ZT$  around the middle of the Coulomb blockade regime changes into a valley (see Fig. 9).

## 2. Temperature dependence

To analyze more thoroughly the properties of the system in the vicinity of the enhanced thermoelectric response, which occurs for smaller values of  $\Gamma$  (cf. Fig. 8), in the following we set  $\varepsilon_1 = -1.12U$  and study the temperature dependence. The chosen value of  $\varepsilon_1$  corresponds to some small detuning  $\delta$  from the resonance,  $\delta = 0.045t$ , for which  $S$  has a large finite value, and which is indicated in Fig. 8(e) by a vertical line. We note that although the physical quantities presented in Fig. 10 are the same as in Fig. 3, here we are no longer in the two-stage Kondo screening regime due to the vicinity of the resonance.

The temperature dependence of the linear conductance is shown in Fig. 10(a). One can see that for all considered couplings,  $G$  increases when the system is cooled down. For relatively large couplings  $\Gamma \gtrsim 0.1t$ , at low temperatures the conductance saturates at some rather constant value, which however slightly decreases when reducing the coupling strength. This is due to the fact that the broadening of the resonant peak is still large enough, such that even for  $T < \delta$  there is a considerable weight in the transmission coefficient at the Fermi level, which results in large conductance. The

temperature dependence changes dramatically for smaller couplings  $\Gamma \lesssim 0.01t$  [see Fig. 10(a)]. The reason for such behavior is generally associated with decreased level broadening. Consequently, when  $\Gamma < \delta$ , the resonant peak in  $\mathcal{T}(\omega)$  is not relevant for transport at low temperatures  $T < \delta$ . This results in a nonmonotonic dependence of  $G$  on  $T$ . The conductance first increases and then, for  $T \approx \delta$ , exhibits a maximum. Further decrease of  $T$  leads to a sudden drop of  $G$  to some small nonuniversal value, which depends on the coupling strength as  $G \sim \Gamma^2$  [62,63]. In this transport regime finite conductance is due to cotunneling processes, which explains the  $\Gamma^2$  dependence of  $G$  for  $T < \delta$ .

The thermal conductance (normalized by temperature) as a function of temperature is presented in Fig. 10(b). The most important observation is that the Wiedemann-Franz law becomes now strongly violated, especially for weaker couplings. While cooling the system down,  $\kappa(T)/T$  exhibits two local maxima instead of a single one, as in the case of  $G(T)$ . In addition, for temperatures above the two maxima in normalized thermal conductance,  $\kappa/T$  vanishes much more rapidly with increasing temperature compared to the linear conductance [cf. Figs. 10(a) and 10(b)]. Nevertheless, although the difference between the case of  $\Gamma \geq t$  and  $\Gamma < t$  is pronounced, the approximate proportionality to  $\Gamma$  in high- $T$  regime and to  $\Gamma^2$  in low- $T$  regime, observed for  $G(T)$ , is also valid for  $\kappa(T)/T$ .

The dependence of the thermopower on  $T$  is plotted in Fig. 10(c). One can clearly see that for small values of  $\Gamma$ ,  $S$  exhibits a maximum, the height of which grows with decreasing  $\Gamma$ , while the position only slightly depends on  $\Gamma$ . However, for  $\Gamma \geq t$ , the position of maximum also changes significantly [see in particular the curve for  $\Gamma = 2t$  in Fig. 10(c)]. Interestingly, the curves of  $S(T)$  for different  $\Gamma$  merge at high temperatures. The same happens at very low temperatures, but only for  $\Gamma \lesssim t$ . In fact, in both the low- and high-temperature regimes the thermopower tends to zero [see Fig. 10(c)]. On the other hand, the enhancement of the Seebeck coefficient for intermediate temperatures gives rise to an enhancement of the figure of merit, which is shown in Fig. 10(d). In fact, there is a maximum in  $ZT(T)$  for  $T \approx 0.01t$ , that is, at temperature below which the peak in  $S$  starts forming [see Fig. 10(c)]. It can be seen that the height of the peak in  $ZT$  becomes enhanced when decreasing  $\Gamma$ . This results from both the enhancement of thermopower and the suppression of thermal conductance, which is stronger than predicted by the Wiedemann-Franz law. As already suggested earlier, large value of  $ZT$  is not a sufficient condition for the usability of the device. Therefore, in Fig. 10(e) we analyze the temperature dependence of the second important quantity, namely, the power factor  $P$ . It is evident that while  $P(T)$  exhibits a peak at the same temperature as  $ZT(T)$  does, the height of this peak depends on  $\Gamma$  in a nonmonotonic way [see Fig. 10(e)]. The power factor is the largest for  $0.1 \gtrsim \Gamma/t \gtrsim 0.01$ , and decreases linearly with  $\Gamma$  when the coupling is lowered.

An important observation from Fig. 10 is that there is a quite sharp distinction between the regimes of strong and weak coupling. This is mainly caused by a small detuning  $\delta \neq 0$  from the resonance peak, which was introduced in this section. For weak couplings, the transmission coefficient has then a

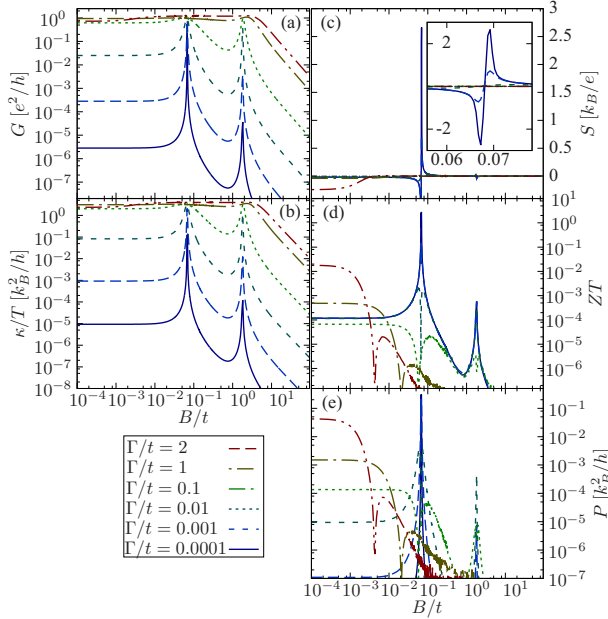


FIG. 11. (a) The linear conductance, (b) the thermal conductance normalized by temperature, (c) the Seebeck coefficient, (d) the figure of merit, and (e) the power factor plotted as a function of magnetic field and calculated for different values of the coupling  $\Gamma$  as indicated. The other parameters are the same as in Fig. 10 with  $T = 10^{-4}t$ . Note the logarithmic scale in the panels. The inset in (c) shows a zoom into the antiresonance visible in  $S$  on the linear scale.

sharp peak near the Fermi level, which becomes broadened with increasing the coupling strength. Thus, the thermoelectric transport properties strongly depend of both the ratio of  $\Gamma/\delta$  as well as  $T/\delta$ , as discussed above.

### 3. Dependence on magnetic field and spin-related effects

To answer the question about the role of magnetic field on transport characteristics in the case when the coupling strength is varied, in Fig. 11 we plot the dependence of thermoelectric coefficients on  $B$ . The  $B$  dependence is calculated assuming the same small value of detuning  $\delta$  from the resonance as in the previous section. The first general observation is that the magnetic field dependence is completely different compared to the temperature dependence presented in Fig. 10. Because the temperature used to calculate this figure is very low,  $T \ll \delta$ , for weak coupling the transport properties out of resonance are mainly determined by second-order tunneling processes. At low enough temperature, as considered in this figure, the rate of such processes is independent of  $T$ . This is why the magnetic field dependence of  $G$  and  $\kappa/T$  is qualitatively the same [see Figs. 11(a) and 11(b)]. In fact, in this transport regime the Wiedemann-Franz law is satisfied. When increasing the magnetic field, both  $G$  and  $\kappa/T$  exhibit peaks at magnetic fields for which the degeneracy between split molecular states of DQD is restored. The width of these peaks increases with increasing the coupling strength. The magnetic field dependence of the thermopower is shown in Fig. 11(c). Interestingly, it exhibits a large antisymmetric resonance for

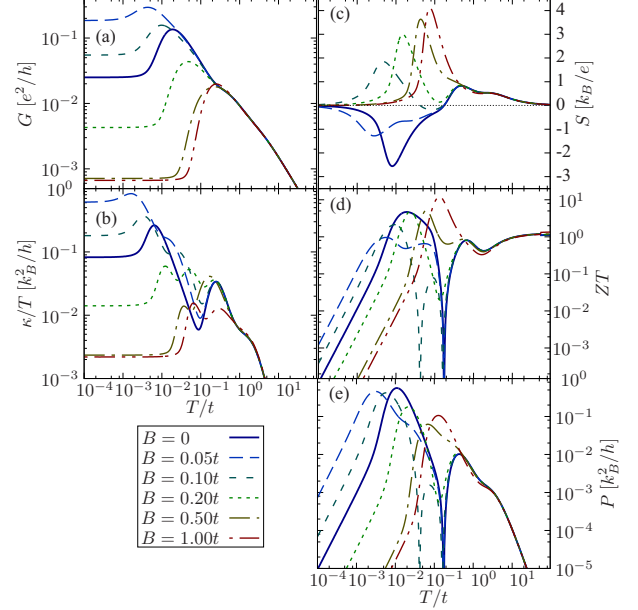


FIG. 12. The same thermoelectric transport coefficients as in Fig. 11 plotted as a function of temperature for  $\Gamma = 0.01t$  and different values of external magnetic field, as indicated. The other parameters are the same as in Fig. 10.

temperatures at which conductance shows first maximum with increasing  $T$ . This resonance strongly depends on  $\Gamma$  and is most pronounced for the smallest value of the coupling considered. The corresponding figure of merit is shown in Fig. 11(d). One can see that, generally, because of assumed low temperature,  $ZT$  is rather low when the magnetic field is varied. The only enhancement can be seen for  $B$  corresponding to the resonance of  $S$ . In addition, Fig. 11(e) presents the magnetic field dependence of the power factor. Similarly to  $ZT$ ,  $P$  is rather low in the whole range of  $B$  and shows only a small maximum for the same magnetic field as  $ZT$  does [cf. Figs. 11(d) and 11(e)].

To check what is the effect of magnetic field on the temperature dependence of thermoelectric coefficients, in Fig. 12 we plot the corresponding  $T$  dependencies for a low value of the coupling strength  $\Gamma = 10^{-2}t$  and a few different values of external magnetic field. Let us first discuss the behavior of the linear conductance, which is shown in Fig. 12(a). Irrespective of the value of  $B$ ,  $G$  first increases with lowering temperature and then suddenly drops at some temperature, different for each value of magnetic field. This suppression occurs approximately at temperature  $T = T_s \sim |\delta - B/2|$ , for which the resonant peak in the transmission coefficient, broadened by  $\Gamma$  and finite  $T$ , goes away from the Fermi level. This is why the low-temperature conductance depends in a nonmonotonic way on  $B$  and takes some nonuniversal values at low temperatures [see Fig. 12(a)].

The normalized heat conductance, clearly not fulfilling the Wiedemann-Franz law at higher temperatures  $T \gtrsim T_s$ , also depends on the magnetic field in a nontrivial way [see Fig. 12(b)]. At low temperatures, similarly to the linear conductance, finite magnetic field can either suppress  $\kappa/T$

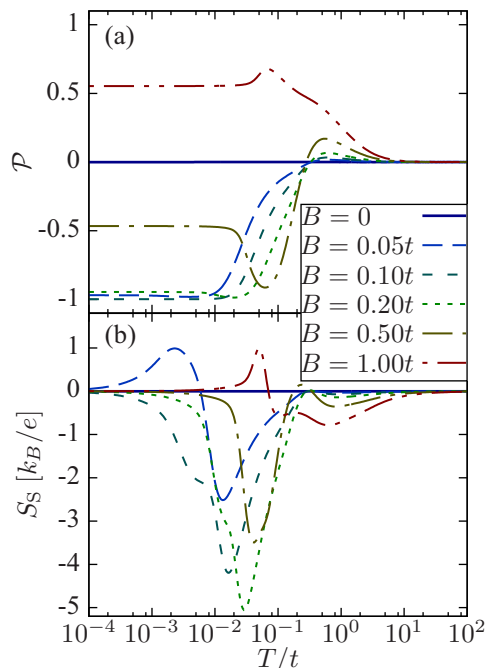


FIG. 13. The temperature dependence of (a) the conductance spin polarization and (b) the spin Seebeck coefficient for different values of external magnetic field, as indicated. The parameters are the same as in Fig. 12.

or increase it. Moreover, magnetic field can suppress the local minimum in the  $B = 0$  case and change it to a third maximum [see, e.g., the curve for  $B = 0.2t$  in Fig. 12(b)].

While at high temperatures the thermopower is rather poor, it is significantly higher when the temperature is lowered [see Fig. 12(c)]. The  $T$  dependence of  $S$  exhibits a large peak, whose position, sign, and height can be tuned by applying different external magnetic field. The peak in  $S$  occurs for  $T \approx T_s$ , i.e., when the suppression of the conductance occurs. Moreover, with increasing the magnetic field, the peak in thermopower changes sign. For  $B \lesssim 0.05t$ ,  $S$  is negative, while for  $B \lesssim 0.1t$ , it becomes positive. This sign change is consistent with magnetic field dependence of  $S$  shown in Fig. 11, where the thermopower changes sign for  $B \approx 0.07t$  [see the inset in Fig. 11(c)].

The magnetic field dependence of the corresponding figure of merit is shown in Fig. 12(d). It can be seen that for all the considered values of magnetic field,  $ZT$  has a peak as a function of  $T$ . Moreover, its maximum value reaches over 10 and for  $B = t$  it is higher than in the case of  $B = 0$ . Again, the peak in  $ZT$  occurs for temperatures at which  $|S|$  exhibits a maximum (cf. Fig. 12). Furthermore, as can be seen in Fig. 12(e), which shows the power factor versus  $B$ , the maximum of  $ZT$  always corresponds to the peak of  $P$ . However, the height of the latter is not necessarily impressive, in particular for strong  $B$ . This is caused by the suppression of transport at large magnetic fields.

There appears a natural question as to whether large thermopower in the presence of external magnetic field corresponds to a large spin thermopower. Figure 13 presents the

temperature dependence of the conductance spin polarization  $\mathcal{P}$  and the spin thermopower  $S_S$  for different magnetic fields calculated for the same parameters as assumed in Fig. 12. One can see that at low magnetic fields, when the linear conductance is higher,  $\mathcal{P}$  is negative and quite large. Already for  $B = 0.05t$ , which corresponds to a maximum value of  $G$  [cf. Fig. 12(a)],  $\mathcal{P} \approx -1$  at  $T \lesssim 0.01t$ . For larger magnetic fields, however, spin polarization changes sign and becomes positive [see the curve for  $B = t$  in Fig. 13(a)]. On the other hand, the spin thermopower  $S_S$  exhibits peaks at positions similar to the positions of peaks in  $S(T)$  [cf. Figs. 12(c) and 13(b)]. The height and position of those peaks depend in a nonmonotonic way on the magnitude of external magnetic field. However, the sign of  $S_S$  is in most cases opposite to the sign of  $S$  and the peaks are much less regular. Unfortunately, the highest values of  $S_S$  correspond to  $B \geq 0.2t$ , when the conductance is strongly suppressed. However, even though  $S_S \rightarrow 0$  for  $B \rightarrow 0$ , for  $B = 0.01t$  the spin thermopower reaches  $k_B/e$  (not shown). On the other hand, at strong magnetic fields the suppression of  $S_S$  occurs [see the curve for  $B = t$  in Fig. 13(b)].

#### IV. CONCLUSIONS

In this paper, we have analyzed the thermoelectric transport properties of correlated T-shaped double quantum dots, exhibiting a two-stage Kondo effect. The calculations were performed with the aid of the numerical renormalization group method, which allowed us to reliably determine transport coefficients in the full parameter space of the model for arbitrary temperatures, magnetic fields, and coupling strength to external leads. The goal of this paper was to analyze the consequences of the two-stage nature of screening on the thermoelectric coefficients of the considered device in the linear response regime.

We showed that the Seebeck coefficient exhibits a maximum for temperatures corresponding to the second stage of the Kondo screening, for which also a relatively large figure of merit and power factor were found. Moreover, we showed that the thermal conductance and electrical conductance can be related by a modified Wiedemann-Franz law, in which, up to prefactors,  $G(T)$  is equal to  $\kappa(\alpha T)/(\alpha T)$ , with  $\alpha \approx 2$ .

We have also analyzed the magnetic field dependence of thermoelectric transport properties. Our analysis has shown that the linear conductance, suppressed by the second stage of screening, can be restored by fine tuning of magnetic field, and the same restoration can also occur in the thermal conductance normalized by temperature. However, despite an enhancement of the heat conductance, the magnetic field was found to have rather inconsiderable impact on the thermopower and figure of merit, which in general could not be increased by magnetic field. On the contrary, the spin Seebeck coefficient, induced by the presence of magnetic field, was found to take considerable values, depending on the position of the DQD levels.

In addition, we found that the thermoelectric coefficients are generally enhanced if the coupling strength between DQD and the leads is diminished. This enhancement is most pronounced when the system is in the vicinity of the resonance.



In fact, a small detuning from the resonance leads then to nontrivial temperature and magnetic field dependence of the thermopower. Moreover, it can also result in considerable spin thermopower and conductance spin polarization.

## ACKNOWLEDGMENT

This research was supported by the National Science Centre in Poland through the Project No. DEC-2012/04/A/ST3/00372.

- 
- [1] R. D. Barnard, *Thermoelectricity in Metals and Alloys* (Taylor&Francis, London, 1972).
- [2] A. I. Hochbaum, R. Chen, R. D. Delgado, W. Liang, E. C. Garnett, M. Najarian, A. Majumdar, and P. Yang, *Nature (London)* **451**, 163 (2008).
- [3] M. Cutler and N. F. Mott, *Phys. Rev.* **181**, 1336 (1969).
- [4] M. Jonson and G. D. Mahan, *Phys. Rev. B* **21**, 4223 (1980).
- [5] L. D. Hicks and M. S. Dresselhaus, *Phys. Rev. B* **47**, 12727 (1993); **47**, 16631 (1993).
- [6] G. D. Mahan and J. O. Sofo, *Proc. Natl. Acad. Sci. USA* **93**, 7436 (1996).
- [7] P. Murphy, S. Mukerjee, and J. Moore, *Phys. Rev. B* **78**, 161406(R) (2008).
- [8] D. Sánchez and H. Linke, *New J. Phys.* **16**, 110201 (2014).
- [9] M. Krawiec and K. I. Wysokiński, *Phys. Rev. B* **73**, 075307 (2006).
- [10] T. A. Costi and V. Zlatić, *Phys. Rev. B* **81**, 235127 (2010).
- [11] T. Rejec, R. Žitko, J. Mravlje, and A. Ramšak, *Phys. Rev. B* **85**, 085117 (2012).
- [12] R. Žitko, J. Mravlje, and A. Ramšak, and T. Rejec, *New J. Phys.* **15**, 105023 (2013).
- [13] S. B. Tooski, A. Ramšak, B. R. Buřka and R. Žitko, *New J. Phys.* **16**, 055001 (2014).
- [14] K. P. Wójcik and I. Weymann, *Phys. Rev. B* **89**, 165303 (2014).
- [15] R. Scheibner, H. Buhmann, D. Reuter, M. N. Kiselev, and L. W. Molenkamp, *Phys. Rev. Lett.* **95**, 176602 (2005).
- [16] J. Kondo, *Prog. Theor. Phys.* **32**, 37 (1964).
- [17] A. C. Hewson, *The Kondo Problem to Heavy Fermions* (Cambridge University Press, Cambridge, 1993).
- [18] D. Goldhaber-Gordon, H. Shtrikman, D. Mahalu, D. Abusch-Magder, U. Meirav, and M. A. Kastner, *Nature (London)* **391**, 156 (1998).
- [19] S. M. Cronenwett, T. H. Oosterkamp, and L. P. Kouwenhoven, *Science* **281**, 540 (1998).
- [20] W. G. van der Wiel, S. De Franceschi, J. M. Elzerman, T. Fujisawa, S. Tarucha, and L. P. Kouwenhoven, *Rev. Mod. Phys.* **75**, 1 (2003).
- [21] K. Brown, M. Crisan, and I. Țifrea, *J. Phys.: Condens. Matter* **21**, 215604 (2009).
- [22] M. Wierzbicki and R. Swirkowicz, *Phys. Rev. B* **84**, 075410 (2011).
- [23] P. Trocha and J. Barnaś, *Phys. Rev. B* **85**, 085408 (2012).
- [24] A. L. Monteros, G. S. Uppal, S. R. McMillan, M. Crisan, and I. Țifrea, *Eur. Phys. J. B* **87**, 302 (2014).
- [25] S. Donsa, S. Andergassen, and K. Held, *Phys. Rev. B* **89**, 125103 (2014).
- [26] K. Ono, D. G. Austing, Y. Tokura, and S. Tarucha, *Science* **297**, 1313 (2002).
- [27] R. H. Blick, R. J. Haug, J. Weis, D. Pfannkuche, K. v. Klitzing, and K. Eberl, *Phys. Rev. B* **53**, 7899 (1996).
- [28] L. Borda, G. Zarand, W. Hofstetter, B. I. Halperin, and J. von Delft, *Phys. Rev. Lett.* **90**, 026602 (2003).
- [29] A. J. Keller, S. Amasha, I. Weymann, C. P. Moca, I. G. Rau, J. A. Katine, H. Shtrikman, G. Zaránd, and D. Goldhaber-Gordon, *Nat. Phys.* **10**, 145 (2014).
- [30] L. Hofstetter, S. Csonka, J. Nygård, and C. Schönenberger, *Nature (London)* **461**, 960 (2009).
- [31] M. Pustilnik and L. I. Glazman, *Phys. Rev. Lett.* **87**, 216601 (2001).
- [32] M. Vojta, R. Bulla, and W. Hofstetter, *Phys. Rev. B* **65**, 140405(R) (2002).
- [33] W. G. van der Wiel, S. De Franceschi, J. M. Elzerman, S. Tarucha, L. P. Kouwenhoven, J. Motohisa, F. Nakajima, and T. Fukui, *Phys. Rev. Lett.* **88**, 126803 (2002).
- [34] N. J. Craig, J. M. Taylor, E. A. Lester, C. M. Marcus, M. P. Hanson, and A. C. Gossard, *Science* **304**, 565 (2004).
- [35] G. Granger, M. A. Kastner, I. Radu, M. P. Hanson, and A. C. Gossard, *Phys. Rev. B* **72**, 165309 (2005).
- [36] P. S. Cornaglia and D. R. Grempel, *Phys. Rev. B* **71**, 075305 (2005).
- [37] R. Žitko and J. Bonča, *Phys. Rev. B* **73**, 035332 (2006).
- [38] P. Trocha and J. Barnaś, *Phys. Rev. B* **76**, 165432 (2007).
- [39] C.-H. Chung, G. Zarand, and P. Wölfle, *Phys. Rev. B* **77**, 035120 (2008).
- [40] Y. Tanaka, N. Kawakami, and A. Oguri, *Phys. Rev. B* **78**, 035444 (2008).
- [41] S. Sasaki, H. Tamura, T. Akazaki, and T. Fujisawa, *Phys. Rev. Lett.* **103**, 266806 (2009).
- [42] R. Žitko, *Phys. Rev. B* **81**, 115316 (2010).
- [43] Y. Tanaka, N. Kawakami, and A. Oguri, *Phys. Rev. B* **85**, 155314 (2012).
- [44] L. G. G. V. Dias da Silva, E. Vernek, K. Ingersent, N. Sandler, and S. E. Ulloa, *Phys. Rev. B* **87**, 205313 (2013).
- [45] K. P. Wójcik and I. Weymann, *Phys. Rev. B* **90**, 115308 (2014).
- [46] K. P. Wójcik and I. Weymann, *Phys. Rev. B* **91**, 134422 (2015).
- [47] K. G. Wilson, *Rev. Mod. Phys.* **47**, 773 (1975).
- [48] We use the open-access Budapest Flexible DM-NRG code (<http://www.phy.bme.hu/dmnrng/>); O. Legeza, C. P. Moca, A. I. Tóth, I. Weymann, and G. Zaránd, arXiv:0809.3143.
- [49] F. B. Anders and A. Schiller, *Phys. Rev. Lett.* **95**, 196801 (2005); *Phys. Rev. B* **74**, 245113 (2006).
- [50] A. Weichselbaum and J. von Delft, *Phys. Rev. Lett.* **99**, 076402 (2007).
- [51] Yigal Meir and Ned S. Wingreen, *Phys. Rev. Lett.* **68**, 2512 (1992).
- [52] C. Van den Broeck, *Phys. Rev. Lett.* **95**, 190602 (2005).
- [53] D. Narducci, *Appl. Phys. Lett.* **99**, 102104 (2011).
- [54] I. Weymann and J. Barnaś, *Phys. Rev. B* **88**, 085313 (2013).
- [55] H. R. Krishna-murthy, J. W. Wilkins, and K. G. Wilson, *Phys. Rev. B* **21**, 1003 (1980); **21**, 1044 (1980).

- [56] M. Hanl and A. Weichselbaum, *Phys. Rev. B* **89**, 075130 (2014).  
[57] F. D. M. Haldane, *Phys. Rev. Lett.* **40**, 416 (1978).  
[58] R. Franz and G. Wiedemann, *Ann. Phys. (Berlin)* **165**, 497 (1853).  
[59] M. Pustilnik and L. Glazman, *J. Phys.: Condens. Matter* **16**, R513 (2004).  
[60] A. V. Kretinin, H. Shtrikman, D. Goldhaber-Gordon, M. Hanl, A. Weichselbaum, J. von Delft, T. Costi, and D. Mahalu, *Phys. Rev. B* **84**, 245316 (2011).  
[61] E. Taylor and D. Segal, *Phys. Rev. B* **92**, 125401 (2015).  
[62] D. V. Averin and Y. V. Nazarov, *Phys. Rev. Lett.* **65**, 2446 (1990).  
[63] K. Kang and B. I. Min, *Phys. Rev. B* **55**, 15412 (1997).

# Strong spin Seebeck effect in Kondo T-shaped double quantum dots

K P Wójcik and I Weymann

Faculty of Physics, Adam Mickiewicz University, Umultowska 85, 61-614 Poznań, Poland

E-mail: [kpwojcik@amu.edu.pl](mailto:kpwojcik@amu.edu.pl)

Received 24 August 2016, revised 14 October 2016

Accepted for publication 1 November 2016

Published 12 December 2016



CrossMark

## Abstract

We investigate, taking a theoretical approach, the thermoelectric and spin thermoelectric properties of a T-shaped double quantum dot strongly coupled to two ferromagnetic leads, focusing on the transport regime in which the system exhibits the two-stage Kondo effect. We study the dependence of the (spin) Seebeck coefficient, the corresponding power factor and the figure of merit on temperature, leads' spin polarization and dot level position. We show that the thermal conductance fulfills a modified Wiedemann–Franz law, also in the regime of suppression of subsequent stages of the Kondo effect by the exchange field resulting from the presence of ferromagnets. Moreover, we demonstrate that the spin thermopower is enhanced at temperatures corresponding to the second stage of Kondo screening. Very interestingly, the spin-thermoelectric response of the system is found to be highly sensitive to the spin polarization of the leads. In some cases spin polarization of the order of 1% is sufficient for a strong spin Seebeck effect to occur. This is explained as a consequence of the interplay between the two-stage Kondo effect and the exchange field induced in the double quantum dot. Due to the possibility of tuning the exchange field by the choice of gate voltage, the spin thermopower may also be tuned to be maximal for desired spin polarization of the leads. All calculations are performed with the aid of the numerical renormalization group technique.

Keywords: Kondo effect, quantum dots, spin caloritronics

(Some figures may appear in colour only in the online journal)

## 1. Introduction

The thermoelectric properties of matter have been drawing the attention of physicists since the first experiments carried out by Seebeck at the beginning of the 19th century. While the properties of bulk materials are already quite well understood [1, 2], the problem of thermoelectricity in confined nanoscale systems still contains issues that need further examination, although these have been intensively researched since the famous publications by Hicks and Dresselhaus [3, 4]. In particular, thermoelectric and spin-thermoelectric properties of strongly correlated quantum dot (QD) systems constitute a field of intensive research [5–17]. It turns out that the understanding of thermoelectric transport properties is not only relevant for possible future applications, but also provides additional information about fundamental interactions and phenomena at the nanoscale. One prominent example is undoubtedly the Kondo effect [18], which in mesoscopic

systems has been of great interest for more than two decades [19, 20]. In fact, the Seebeck coefficient for the Kondo quantum dots was not only reliably calculated [21], but also measured [22]. Moreover, the thermopower was also analyzed for double quantum dot (DQD) systems in the isospin Kondo regime, in which the device was shown to work as a minimal thermoelectric generator [23].

In the presence of magnetic field or when the leads are ferromagnetic, the thermoelectric response of the system becomes spin polarized [6, 8]. Spin caloritronic effects of single quantum dots in the Kondo regime have already been studied theoretically [24–26]. Furthermore, the spin-resolved thermoelectricity has also been analyzed in the case of DQD systems, including the weak coupling regime [27] and the case of nonmagnetic leads [28]. In this paper we extend these studies by investigating the spin caloritronic properties of T-shaped double quantum dots strongly coupled to ferromagnetic leads, as sketched schematically in figure 1. Despite the

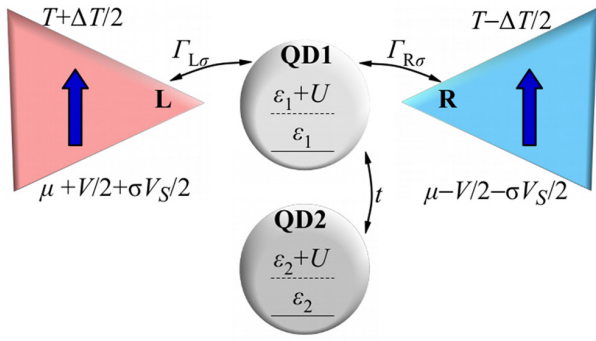


**Figure 1.** Schematic of the system. The left (L) and right (R) leads are coupled to the main quantum dot (QD1) via spin-dependent couplings  $\Gamma_{L\sigma}$  and  $\Gamma_{R\sigma}$ . The second quantum dot (QD2) is directly coupled only to QD1, with a matrix element  $t$ . A small voltage  $V$  (correspondingly spin voltage  $V_S$ ) shifts (spin-splits) otherwise equal chemical potentials  $\mu_L = \mu_R = \mu$  symmetrically. There is also a temperature gradient  $\Delta T$  applied symmetrically to the system.

relative simplicity of the system under consideration, it hosts a variety of interesting many-body phenomena. The screening of subsequent quantum dots gives rise to the two-stage Kondo effect, introducing a cryogenic temperature scale  $T^*$  associated with the second stage of screening [29–32]. On the other hand, the dependence of the Kondo temperature  $T_K$  and  $T^*$  on the DQD level position can lead to Fano-like interference effects [32–38]. These different energy scales, associated with subsequent Kondo screening, can be reflected in the thermoelectric properties of the device [28]. Some aspects of the influence of magnetism on strongly correlated regimes of T-shaped DQDs have also been discussed, mainly in the context of electrical properties, such as linear conductance and current spin polarization. The spin-dependent Fano antiresonance condition in magnetic field [39] and in system with ferromagnetic leads [40] was predicted. Furthermore, the interplay of the two-stage Kondo screening and the ferromagnet-induced exchange field was also studied [41].

The primary goal of the present paper is to analyze the spin caloritronic properties of T-shaped DQD in the case of ferromagnetic contacts. At this point it is worth emphasizing that the presence of ferromagnetic leads is not equivalent to the application of an external magnetic field in the case of DQD with nonmagnetic leads. In fact, we show that the spin caloritronic coefficients are affected, in a very nontrivial manner, by the presence of ferromagnetic correlations. The spin-dependent tunneling results in generation of an effective exchange field, which gives rise to another important energy scale in the problem that conditions the behavior of the spin Seebeck coefficient. We demonstrate that spin polarization of the order of 1% is sufficient to induce a strong spin Seebeck effect in the transport regime where the second stage of screening develops.

Finally, we would like to note that direct observation of the spin Seebeck effect was reported recently in a bulk metallic magnet [42]. In quantum dot systems, experimental evidence remains a challenge. Nevertheless, the closely related spin Peltier effect was observed in a thin metallic layer sandwiched in between two ferromagnets [43]. This setup seems closer to

quantum dot geometry; therefore, we believe that our results will, on one hand, stimulate further experimental efforts and, on the other hand, be of assistance in understanding future experimental data.

The paper is organized as follows. In section 2 the model of the device and method used for its solution are explained. The relevant energy scales are outlined in section 3. Main results, concerning the calculated Seebeck and spin Seebeck coefficients are presented and discussed in section 4. Finally, section 5 concludes the paper.

## 2. Model and methods

The device under consideration consists of two single-level quantum dots in a T-shaped geometry with the first quantum dot (QD1) coupled to external ferromagnetic leads and the second dot (QD2) attached to the first one through the hopping matrix elements  $t$ , see figure 1. The system can thus be described by the following two-impurity Anderson Hamiltonian [44],  $H = H_{\text{DQD}} + \sum_r H_r + H_{\text{tun}}$ . The first term corresponds to an isolated DQD and is given by

$$H_{\text{DQD}} = \sum_{i\sigma} \varepsilon_i n_{i\sigma} + U \sum_i n_{i\uparrow} n_{i\downarrow} + \sum_{\sigma} t (d_{1\sigma}^\dagger d_{2\sigma} + \text{h.c.}), \quad (1)$$

where  $n_{i\sigma} = d_{i\sigma}^\dagger d_{i\sigma}$  and  $d_{i\sigma}^\dagger$  creates a spin- $\sigma$  electron in dot  $i$  with the corresponding energy  $\varepsilon_i$  and  $U$  is the Coulomb correlation parameter in each dot. The ferromagnetic leads are modeled by free-electron Hamiltonian  $H_r = \sum_{\vec{k}\sigma} \varepsilon_{r\vec{k}\sigma} n_{r\vec{k}\sigma}$  ( $r = L$  for left and  $r = R$  for right lead,  $n_{r\vec{k}\sigma}$  denotes the occupation operator for state characterized by momentum  $\vec{k}$ , spin  $\sigma$  and lead  $r$ , while  $\varepsilon_{r\vec{k}\sigma}$  is the energy of the corresponding level). The coupling between the first dot and the leads is described by the tunneling Hamiltonian  $H_{\text{tun}} = \sum_{r\vec{k}\sigma} v_{r\vec{k}\sigma} (d_{1\sigma}^\dagger c_{r\vec{k}\sigma} + \text{h.c.})$ , where  $c_{r\vec{k}\sigma}$  is the corresponding annihilation operator and  $v_{r\vec{k}\sigma}$  denotes the respective tunnel matrix element.

We consider the wide-band limit and assume that only  $s$ -waves couple to the electrodes. This allows us to write the spin-dependent coupling  $\Gamma_{r\sigma} = \pi \rho_{r\sigma} |v_{r\vec{k}\sigma}|^2$  as a constant ( $\rho_{r\sigma}$  denotes the normalized spin-resolved density of states of lead  $r$  at the Fermi level), determined by the leads' spin polarization  $p_r$ . For parallel configuration of the magnetizations of the leads, one then gets  $\Gamma_{r\sigma} = (1 + \sigma p_r) \Gamma_r / 2$ , and  $\Gamma_\sigma \equiv \Gamma_{L\sigma} + \Gamma_{R\sigma} = (1 + \sigma p) \Gamma$ , where  $p = (p_L + p_R) / 2$  is the effective leads' spin polarization and we assumed  $\Gamma_L = \Gamma_R \equiv \Gamma / 2$ . We note that in the antiparallel magnetic configuration, for left-right symmetric systems, the couplings become spin independent and the transport properties are similar to those in the nonmagnetic case with a polarization dependent factor. On the other hand, when the system is not symmetric, the behavior is the same as in the case of a parallel magnetic configuration with some new coupling strength and effective spin polarization [45]. Therefore, in the following we will consider only the case of parallel magnetic configuration.

Let  $I_x$  denote the  $x$ -current ( $x = C$  for charge,  $x = S$  for spin,  $x = Q$  for heat). Using the Boltzmann equation approach and assuming a well-defined Fermi level to be the reference

point for energy scale, one can derive the linear-response coefficients connecting currents with voltage  $V$ , spin voltage  $V_S$  and temperature difference  $\Delta T$  [1]

$$\begin{pmatrix} I_C \\ I_S \\ I_Q \end{pmatrix} = \sum_{\sigma} \begin{pmatrix} e^2 L_{0\sigma} & \sigma e^2 L_{0\sigma} & -e L_{1\sigma}/T \\ -\sigma e \frac{\hbar}{2} L_{0\sigma} & -e \frac{\hbar}{2} L_{0\sigma} & \sigma \frac{\hbar}{2} L_{1\sigma}/T \\ -e L_{1\sigma} & -\sigma e L_{1\sigma} & L_{2\sigma}/T \end{pmatrix} \begin{pmatrix} V \\ V_S \\ \Delta T \end{pmatrix}, \quad (2)$$

where  $e$  is the absolute value of electron charge,

$$L_{n\sigma} = -\frac{1}{\hbar} \int \omega^n \frac{\partial f(\omega)}{\partial \omega} \mathcal{T}_{\sigma}(\omega) d\omega, \quad (3)$$

$f(\omega)$  is the Fermi–Dirac distribution function, and  $\mathcal{T}_{\sigma}(\omega)$  is the spin-resolved transmission coefficient. Henceforth we will also use notation  $L_n = L_{n\uparrow} + L_{n\downarrow}$  and  $M_n = L_{n\uparrow} - L_{n\downarrow}$ .

The transport properties can be calculated from Onsager integrals  $L_{n\sigma}$  using equation (2). In particular, the electrical and spin conductances are

$$G \equiv \partial_V I_C \Big|_{V_S=0, \Delta T=0} = e^2 L_0, \quad (4)$$

$$G_S \equiv \partial_{V_S} I_S \Big|_{V=0, \Delta T=0} = -e \frac{\hbar}{2} \cdot L_0, \quad (5)$$

respectively, where  $\partial_x A|_{y=0}$  denotes partial derivative of  $A(x,y)$  with respect to  $x$ , while the condition  $y = 0$  is fulfilled. Similarly, the heat conductance is given by

$$\kappa \equiv \partial_{\Delta T} I_Q \Big|_{I_C=0, V_S=0} = \frac{1}{T} \left( L_2 - \frac{L_1^2}{L_0} \right), \quad (6)$$

where the conditions  $I_C = 0$  and  $V_S = 0$  in fact determine  $V$  as a function of  $\Delta T$ . In this paper we focus on Seebeck and spin Seebeck coefficients, denoted respectively by  $S$  and  $S_S$ ,

$$S = G^{-1} \partial_{\Delta T} I_C \Big|_{V=0, V_S=0} = -\frac{1}{eT} \frac{L_1}{L_0}, \quad (7)$$

$$S_S = G_S^{-1} \partial_{\Delta T} I_S \Big|_{V=0, V_S=0} = -\frac{2}{\hbar T} \frac{M_1}{L_0}. \quad (8)$$

These are related to the (spin) Peltier coefficient  $\Pi = \partial_{I_C} I_Q \Big|_{V_S=0, \Delta T=0}$

( $\Pi_S = \partial_{I_S} I_Q \Big|_{V=0, \Delta T=0}$ ) by  $\Pi_{(S)} = S_{(S)} T$ . However, we prefer to study  $S_{(S)}$  instead of  $\Pi_{(S)}$ , because Seebeck coefficient better captures caloric properties at low temperatures. Finally, we can define the (spin) figure of merit

$$Z_{(S)} T = S_{(S)}^2 G_{(S)} T / \kappa, \quad (9)$$

which is a measure of thermodynamic efficiency, and the corresponding power factor

$$Q_{(S)} = S_{(S)}^2 G_{(S)}, \quad (10)$$

which is related to maximal power of the device and the performance under the fixed flow conditions [46].

The transmission coefficient is proportional to the imaginary part of QD1's retarded Green function,  $\mathcal{T}_{\sigma}(\omega) = -\Gamma_{\sigma} \text{Im} \langle \langle d_{1\sigma}^{\dagger} | d_{1\sigma} \rangle \rangle^{\text{ret}}(\omega)$ , which we determine with the aid of the numerical renormalization group (NRG) method [47, 48], building the full density matrix from states discarded during the iteration of the NRG procedure [49, 50]. In calculations we use discretization parameter  $\Lambda = 2$  and keep 2048 states at each iteration. To perform the computations, we assume flat densities of leads' states within the cutoff  $D = 2U$  and make a transformation to an even–odd basis [51]. This leads us to an effective single-channel formulation of the problem, where for the parallel magnetic configuration the only parameters corresponding to the conduction bands are those related to an effective one, namely  $\Gamma$ ,  $p$  and  $D \equiv 1$ .

The NRG method allows us to obtain reliable results in the whole parameter space of the model, in particular, at finite temperatures. However, NRG forces us to limit our considerations to the linear response regime, where a single Fermi level can be defined for both leads and, thus, the logarithmic discretization, being a key ingredient of the procedure, is well defined [47].

### 3. Relevant energy scales

The considered device hosts very rich physics at the manifold of energy scales. This can be seen in particular in the temperature dependence of the electrical conductance presented in figure 2. For decoupled second dot (i.e. for  $t = 0$ ), nonmagnetic leads ( $p = 0$ ) and QD1 energy level in the Coulomb valley ( $-U \ll \varepsilon_1 \ll 0$ ), at temperatures below the Kondo temperature  $T_K$ , the conduction band electrons screen the spin of the electron occupying QD1. This screening results in an additional resonance in the local density of states of the first dot at the Fermi level, which gives rise to an enhancement of the conductance  $G$ , see the curves for  $t = 0$  and  $p = 0$  in figures 2(a) and (b). In the Kondo regime  $G$  can achieve the unitary limit  $G = 2e^2/h$ , if the dot is tuned to the point of the particle–hole symmetry (PHS),  $\varepsilon_1 = \varepsilon_2 = -U/2$ , as is done in figure 2(a). The maximal conductance outside the PHS point is slightly smaller, see figure 2(b). For single quantum dots coupled to ferromagnetic leads, the Kondo temperature can be estimated from a scaling approach [52, 53],

$$T_K \approx \sqrt{\frac{\Gamma U}{2}} \exp \left[ \frac{\pi \varepsilon (\varepsilon + U)}{2 \Gamma U} \frac{\text{arctanh}(p)}{p} \right]. \quad (11)$$

Experimentally, the Kondo temperature is typically defined as the temperature at which  $G = G_{\text{max}}/2$ . For parameters assumed in figure 2(a) in the case of  $p = 0$  and  $t = 0$ , from the temperature dependence of  $G$  we find  $T_K \approx 0.32\Gamma$ .

The coupling between quantum dots results in the emergence of another energy scale,  $T^*$ , which for relatively weak  $t \lesssim \Gamma$  is associated with the screening of the second dot's spin by the continuum formed by QD1 and leads. This screening manifests itself through a decrease of  $G$  for temperatures below  $T^*$ , see the curves for  $t = \Gamma/3$ ,  $p = 0$  in figures 2(a) and

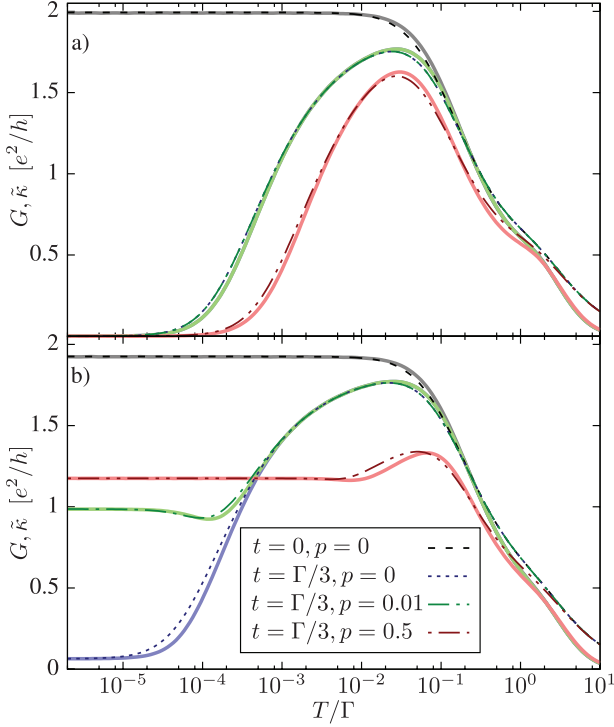


**Figure 2.** Linear conductance  $G$  (dashed lines) as a function of temperature  $T$  calculated for  $\varepsilon_2 = -U/2$ ,  $\Gamma = U/5$  and (a)  $\varepsilon_1 = -U/2$ , (b)  $\varepsilon_1 = -U/3$ . Solid lines indicate the rescaled and shifted thermal conductance,  $\tilde{\kappa} \equiv \mathcal{L}_0^{-1} \kappa(\alpha T)/(\alpha T)$  with  $\alpha = 2$  (see text for details). In (a) the curves for  $p = 0$  and  $p = 0.01$  (both for  $t = \Gamma/3$ ) are on top of each other.

(b). At the PHS point the conductance drops to 0 as  $G \propto T^2$  [30], while outside this point some finite conductance remains even in the  $T = 0$  limit, see figure 2(b). The temperature at which the second stage of screening takes place can be estimated from [30, 37]:

$$T^* = a T_K e^{-bT_K/J_{\text{eff}}}, \quad (12)$$

where  $J_{\text{eff}} = 4Ut^2/[U^2 - (\varepsilon_1 - \varepsilon_2)^2]$  is the effective exchange interaction between the dots and  $a, b$  are numbers of the order of 1. However, similarly to  $T_K$ , we estimate  $T^*$  numerically from the temperature dependence of  $G$ , as the temperature at which the conductance drops to half of its maximum value. For parameters assumed in figure 2(a),  $p = 0$  and  $t = \Gamma/3$ ,  $T^* \approx 5.9 \cdot 10^{-4}\Gamma$ .

Unlike in the case of the magnetic field, the influence of the leads' ferromagnetism on transport properties of the system differs significantly, depending on the presence or lack of particle-hole symmetry in the system. At the PHS point,  $\varepsilon_1 = \varepsilon_2 = -U/2$ , the leads' spin polarization only slightly modifies  $T_K$  and  $T^*$ , see equations (11) and (12), which also causes some minor change in  $G_{\text{max}}$ , see figure 2(a). However, outside the PHS point this influence is much more pronounced, as can be seen in figure 2(b). Even relatively low values of spin polarization (see the curve for  $p = 0.01$ ) block the second stage of Kondo screening, while the value of  $p = 0.5$  is sufficient to suppress the Kondo effect significantly for  $\varepsilon_1$  considered in the figure. This can be inferred from the strongly

reduced maximum value of the conductance and the deviation of the curve corresponding to  $p = 0.5$  from all the other curves at temperatures of the order of  $T_K$ , see figure 2. The suppression of the Kondo effect for large  $p$  is caused by the fact that, in the case of ferromagnetic leads, the renormalization of double quantum dot energy levels due to the hybridization with electrodes becomes spin-dependent, which implies that an effective exchange field  $\Delta\varepsilon_{\text{ex}}$  is induced in DQD. It is worth noticing that  $\Delta\varepsilon_{\text{ex}}$  is in general different in each multiplet of DQD eigenstates [54].

The exchange field  $\Delta\varepsilon_{\text{ex}}$  strongly depends on the DQD level positions, in particular,  $\Delta\varepsilon_{\text{ex}} = 0$  at PHS point (in all multiplets). For  $t \ll \Gamma$ , one can reasonably define  $\Delta\varepsilon_{\text{ex}}$  induced in QD1 and approximate it by the formula for a single quantum dot [53, 54],

$$\Delta\varepsilon_{\text{ex}}^{\text{QD1}} \approx \frac{2p\Gamma}{\pi} \log \left| \frac{\varepsilon_1}{\varepsilon_1 + U} \right|. \quad (13)$$

The determination of the exchange field in the second dot, denoted by  $\Delta\varepsilon_{\text{ex}}^{\text{QD2}}$ , is a more subtle problem [40, 54]. Nevertheless, for  $t \ll \Gamma$ ,  $\Delta\varepsilon_{\text{ex}}^{\text{QD2}}$  can be seen as a consequence of coupling between QD2 and the continuum formed by QD1 and the leads. The effective spin-dependent coupling to the second dot  $\Gamma_{2\sigma}$  is then proportional to  $t^2/\Gamma_\sigma = (1 - \sigma p)\Gamma_2$ , with  $\Gamma_2 = (\Gamma_{2\uparrow} + \Gamma_{2\downarrow})/2$ , instead of simply  $\Gamma_\sigma$  as in the case of QD1. Note that  $\Gamma_2$  is a function of both  $t$  and  $p$ , and the effective spin polarization equals  $-p$ . Consequently, while the coupling to one of the spin species is larger in the first dot, it can be just opposite in the second dot, which implies that  $\Delta\varepsilon_{\text{ex}}^{\text{QD1}}$  and  $\Delta\varepsilon_{\text{ex}}^{\text{QD2}}$  can have different signs [40]. Note that a similar situation cannot be reached by applying external magnetic field, which will have the same sign in both quantum dots. By raising the exchange field, detuning from the PHS point by changing either  $\varepsilon_1$  or  $\varepsilon_2$  will generally suppress the second stage of the Kondo effect once  $|\Delta\varepsilon_{\text{ex}}| \gtrsim T^*$  [41]. Moreover, it can also affect the first-stage Kondo effect if  $|\Delta\varepsilon_{\text{ex}}| \gtrsim T_K$ .

In the strong coupling regime and for  $p = 0$ , the modified Wiedemann-Franz law was predicted [21, 28, 55], which states that at  $T < T_K$ ,  $\mathcal{L} = \kappa(\alpha T)/[\alpha TG(T)]$  is a constant, instead of the Lorentz number  $\kappa(T)/[TG(T)]$ . The value of this constant equals  $\mathcal{L}_0 = (\pi^2/3)k_B^2/e^2$ , while the scale shift  $\alpha$  was estimated to be approximately equal 2. Despite the fact that finite leads' spin polarization significantly changes the fixed point structure of the renormalization group flow, we found the same behavior in this system, although with slightly worse accuracy. This is illustrated in figure 2, where rescaled and shifted heat conductance  $\tilde{\kappa}(T) \equiv \mathcal{L}_0^{-1} \kappa(2T)/(2T)$  is plotted as a function of  $T$  with solid lines. At  $T \lesssim T_K$ , all curves overlap to good accuracy with  $G(T)$ , which implies that the modified Wiedemann-Franz law also holds in the case of T-shaped DQDs with ferromagnetic contacts.

#### 4. Thermopower and spin thermopower

In this section we present and discuss the results on the Seebeck and spin Seebeck coefficients. First, we study their

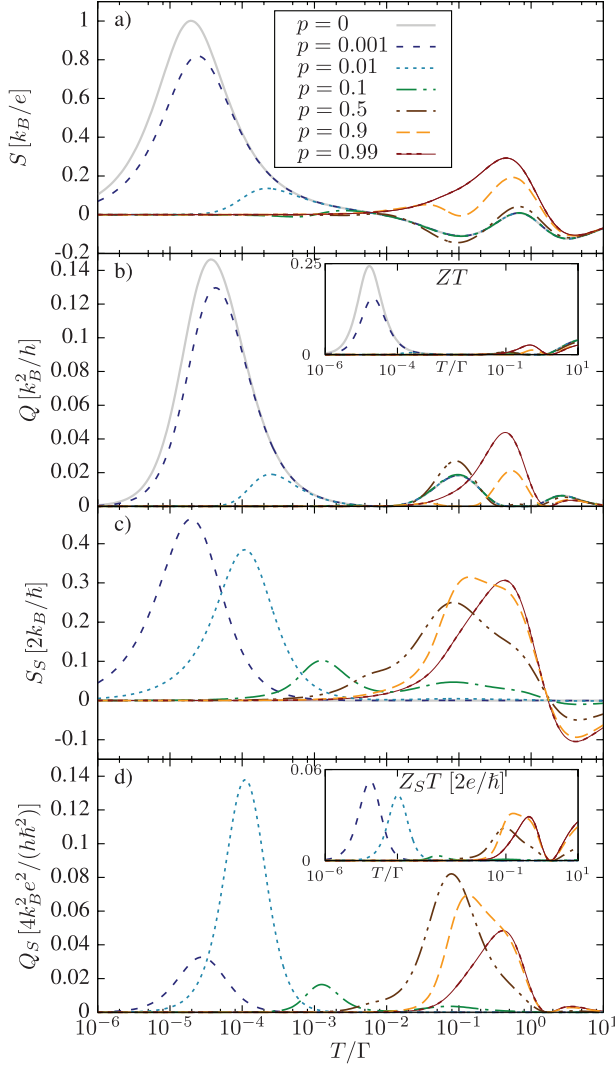


**Figure 3.** Thermopower (a), the corresponding power factor (b) and the related spin counterparts (c), (d) calculated as a function of temperature for  $\varepsilon_1 = -U/3$ ,  $\varepsilon_2 = -U/2$ ,  $t = \Gamma/3$  and  $\Gamma = U/5$ , and for different values of spin polarization  $p$ , as indicated. The insets in (b) and (d) show the temperature dependence of the corresponding figures of merit,  $ZT$  and  $Z_S T$ .

temperature dependence and then analyze what happens when the degree of the leads' spin polarization is varied. Finally, we consider the dependence of thermoelectric coefficients on the position of DQD energy levels.

#### 4.1. Temperature dependence

The full temperature dependence of (spin) thermoelectric coefficients is presented in figure 3 for different values of leads' spin polarization  $p$ . We cover there a wide class of ferromagnetic materials, starting with the nonmagnetic case and ending with half-metals, for which  $p \rightarrow 1$ . This figure was calculated for  $\varepsilon_1 = -U/3$  and  $\varepsilon_2 = -U/2$ , i.e. outside the PHS point, since for  $\varepsilon_1 = \varepsilon_2 = -U/2$ , the thermopower vanishes due to equal contributions from electron and hole processes. For nonmagnetic systems, the second stage of screening leads

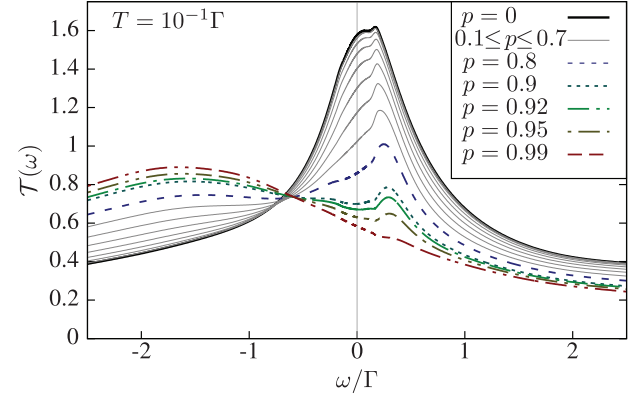


**Figure 4.** Energy dependence of the total transmission coefficient  $\mathcal{T}(\omega) = \sum_{\sigma} \mathcal{T}_{\sigma}(\omega)$  calculated for different values of spin polarization  $p$  and for parameters corresponding to figure 3 with  $T = 10^{-1}\Gamma$ .

to an enhancement of  $S$  at very low temperatures of the order of  $T^*$  [28]. For finite spin polarization, however, a suppression of the second stage of Kondo effect by the exchange field occurs, see figure 2, which suppresses the thermopower peak at  $T < T^*$ , see figure 3(a). Clearly, leads' polarization, even as small as  $p = 0.01$ , is sufficient for the low-temperature peak in  $S(T)$  to be strongly suppressed. This is due to the fact that even very low values of  $p$  give rise to finite exchange field, see equation (13), which for  $p = 0.01$  can already become larger than  $T^*$ . In a similar spirit, larger values of spin polarization resulting in greater exchange field can affect thermopower behavior at higher temperatures. Interestingly, for  $T \approx T_K$  one can then observe a more subtle interplay between the Kondo correlations and the exchange field. For  $p < 0.5$ ,  $S(T)$  exhibits a dip with  $S(T) < 0$  at  $T \approx T_K$ , which is characteristic of the (single-stage) Kondo effect [21]. On the other hand, with increasing spin polarization, thermopower changes sign and a positive peak appears instead, see the curves for  $p \geq 0.9$  in figure 3(a). This can be explained as follows.

For  $T^* < T < T_K$  and  $p = 0$ , there is a Kondo peak visible in the total transmission coefficient,  $\mathcal{T}(\omega) = \sum_{\sigma} \mathcal{T}_{\sigma}(\omega)$ , as can be seen in figure 4, which presents the energy dependence of  $\mathcal{T}(\omega)$  for different spin polarization  $p$ . Because  $\varepsilon_1 > -U/2$ , the Kondo peak displays some asymmetry with respect to the Fermi energy ( $\omega = 0$ ). In fact, finite temperature, which is slightly below  $T_K$ , results in a small shift of the maximum to  $\omega > 0$ . Because of that,  $\mathcal{T}(\omega)$  has a finite slope at  $\omega = 0$ , which is responsible for nonzero thermopower of the device. For  $p \neq 0$  the exchange field appears, which grows with increasing  $p$ . Thus, for sufficiently large spin polarization,  $\Delta\varepsilon_{\text{ex}}$  can become larger than  $T_K$ . If this is the case, the Kondo peak becomes suppressed and split by  $2\Delta\varepsilon_{\text{ex}}$ , see figure 4. Moreover, with increasing spin polarization, the levels of DQD become split and the weight of the transmission coefficient becomes shifted to negative energies. This is visible as a gradual enhancement of the negative- $\omega$  Hubbard peak. For very large spin polarization, due to the factors  $(1 \pm p)$ , the majority spin states are mainly responsible for the enhanced transmission for  $\omega < 0$ . The above-described behavior results in a sign change of the derivative of  $\mathcal{T}(\omega)$  at  $\omega = 0$  with increasing  $p$ , which gives rise

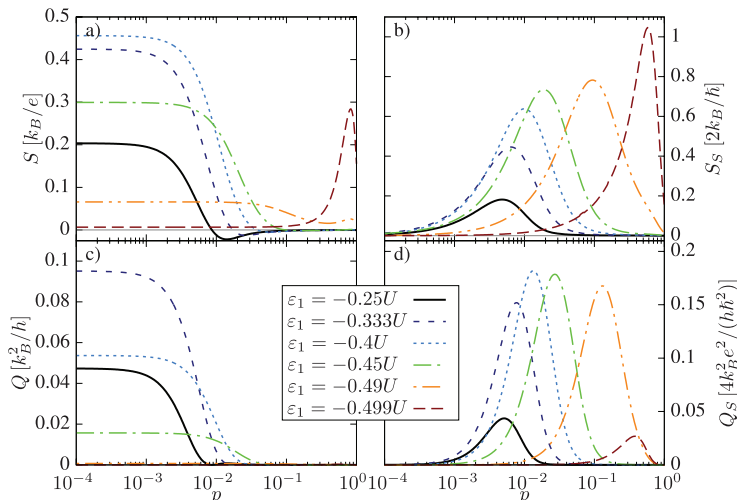


**Figure 5.** Thermopower (a), spin thermopower (b) and the corresponding power factors, (c) and (d), plotted as a function of spin polarization  $p$  for different values of the level position of the first quantum dot, as indicated in the figure. The other parameters are the same as in figure 3 with  $T = 10^{-4}\Gamma$ .

to the associated sign change of the Seebeck coefficient visible in figure 3(a).

One could imagine a similar situation for  $T \approx T^*$ , with a dip in the transmission coefficient corresponding to the second stage of screening being split by  $\Delta\varepsilon_{\text{ex}}$ . However, because  $\Delta\varepsilon_{\text{ex}}$  becomes larger than  $T^*$  at very small values of spin polarization, e.g. at  $p = 0.01$  for parameters assumed in figure 3, the difference between  $(1-p)$  and  $(1+p)$  factors in the spin-resolved transmission coefficient is not significant. For this reason the relative depth of dips remains approximately constant and we do not observe a negative peak at  $T \approx T^*$  for any value of spin polarization considered in figure 3. However, as presented in section 4.2, a sign change of thermopower in the second stage of screening may occur for  $p \approx 0.02$  and is even more pronounced for  $\varepsilon_1 = -U/4$  instead of  $\varepsilon_1 = -U/3$ .

The temperature dependence of the power factor corresponding to the Seebeck coefficient shown in figure 3(a) is presented in figure 3(b). It exhibits local maxima for temperatures corresponding to peaks (or dips) visible in  $S$ , including a small peak at  $T \approx U$ , associated with thermally excited hole-like (due to  $\varepsilon_1 < 0$ ) transport. The inset in figure 3(b) displays the thermoelectric figure of merit  $ZT$  as a function of temperature. It also exhibits all the peaks of  $S(T)$ , however, the contributions at intermediate temperatures,  $T^* < T < T_K$ , are somewhat suppressed by quite large heat conductance; see in particular the curve for  $p = 0.01$  in figure 3(b).

We now move to the discussion of spin thermoelectric properties of the considered device. A large conventional thermopower present at  $T \approx T^*$  gives a hope that breaking the spin-reversal symmetry by finite lead spin polarization will generate a considerable spin thermopower. However, generation of  $S_S$  at such low temperatures is a matter of a delicate compromise. This is because while the spin Seebeck coefficient can be generally enhanced by increasing spin polarization, the second stage of screening and, consequently, the conventional thermopower become strongly suppressed

if  $p$  is too large, as already explained in the discussion of figure 3(a). Nevertheless, as can be inferred from figure 3(c), there are such values of spin polarization for which the symmetry is sufficiently broken and a maximum in  $S_S(T)$  appears, see the curves for  $p = 0.001$  and  $p = 0.01$ . We note that  $\hbar/2 \cdot S_S^{\text{max}} < eS^{\text{max}}$  for  $p = 0.001$  ( $S_S^{\text{max}}$  denotes the maximal value of  $S_S(T)$  for a given value of  $p$ ), while for  $p = 0.01$  the opposite inequality holds. Indeed, in the latter case the spin thermopower exceeds the conventional thermopower.

With increasing the degree of spin polarization of the leads, the maximum in  $S_S$  moves to larger temperatures and for  $p \geq 0.5$  the spin Seebeck coefficient exhibits a peak at  $T \approx T_K$ , see figure 3(c). Contrary to the case of conventional Seebeck coefficient, the peak at  $T \approx T_K$  has the same sign as the low-temperature peak for small spin polarization. This can be surprising, because the peak in  $S(T)$  changes sign when  $T$  increases from  $T \approx T^*$  to  $T \approx T_K$ , see figure 3(a). However, in the case of spin Seebeck coefficient one needs to keep in mind that, for assumed parameters, the exchange field in QD1 is opposite to the exchange field in QD2, which compensates for this effect.

One can be surprised that  $p$  of the order of one percent is sufficient to induce a significant spin Seebeck coefficient. However, it is advisory to recall, that  $S_S$  is in fact a ratio of a small spin bias  $V_S$  and a small temperature gradient  $\Delta T$ . Thus, even the largest value of  $S_S$ , despite its fundamental aspects, does not guarantee a practical importance of the result, if the corresponding power factor  $Q_S$  is too small. For this reason in figure 3(d) we show the temperature dependence of  $Q_S$ . It can be clearly seen that the peak in  $Q_S(T)$  corresponding to  $p = 0.001$  is a few times smaller than the peak corresponding to  $p = 0.01$ . This remains in agreement with intuition, that a lead spin polarization with degree much smaller than 1% cannot induce a significant spin current (although this very small spin current can still be much larger than the corresponding charge current). On the other hand, the peak of  $Q_S(T)$



for  $p = 0.01$  is larger than the peaks corresponding to stronger lead polarization. This implies that the thermoelectric performance of the considered device is best in the regime of the second stage of screening. Nevertheless, the corresponding spin-thermoelectric figure of merit  $Z_S T$ , which is plotted in the inset of figure 3(d), is not too spectacular, with values only slightly exceeding  $0.05 \cdot (2e/\hbar)$ .

#### 4.2. Dependence on the leads' spin polarization

In this section we analyze how the spin thermoelectric properties depend on the magnitude of the exchange field, focusing on the second stage of the Kondo effect. We thus assume the same parameters as in the previous section and set  $T = 10^{-4}\Gamma$ , which is of the order of  $T^*$ , and study the dependence on spin polarization for different values of QD1 level position. According to equation (13), the exchange field is linear in  $p$  and also in  $\varepsilon_1$  near the PHS point, since  $\log|\varepsilon_1/(\varepsilon_1 + U)| \approx 4(\varepsilon_1 + U/2)/U$ . As can be seen in figure 5(a), which displays the dependence of  $S$  on  $p$ , the Seebeck coefficient in the regime of small spin polarization is a nonincreasing function of  $p$  (note the logarithmic scale for  $p$  in the plot). At sufficiently low spin polarization,  $S$  retains its value for a nonmagnetic system. However, for any  $\varepsilon_1$  there is some critical value of  $p$ , which we denote  $p_c$ , above which the Seebeck coefficient becomes suppressed. This critical polarization decreases monotonically with increasing detuning from the PHS point, and is related to some critical value of the exchange field,  $\Delta\varepsilon_{\text{ex}}^c \approx T^*$ , overcoming the second stage of the Kondo effect. As can be seen in figure 5(a), the height of  $S(p)$  maximum depends on  $\varepsilon_1$  in a nonmonotonic manner. This suggests a nontrivial dependence of  $S$  on  $\varepsilon_1$ , which is explained in section 4.3.

Moreover, in figure 5(a) we can also notice a small sign change of  $S(p)$  for  $\varepsilon_1 = -U/4$  and  $\varepsilon_1 = -U/3$ . This is in fact a consequence of the same phenomenon as that responsible for the sign change of  $S(T)$  for  $T \sim T_K$  described in section 4.1. The main difference is that the dip in the transmission coefficient, corresponding to the second stage of the Kondo screening, more easily gets smeared, than split. For this reason, the negative peak of  $S$  is rather small and develops only in a narrow range of parameters, see figure 5(a).

We also note that very close to the PHS point, one can observe a large peak in  $S(p)$ , see the curve for  $\varepsilon_1 = -0.499U$  in figure 5(a). This result, however, may be considered somewhat artificial. According to equation (7),  $S$  is proportional to the ratio of  $L_1$  and  $L_0$ . Exactly at the PHS point,  $L_1$  is always 0 while  $L_0$  decreases with temperature as  $T^2$ . Moreover,  $L_0$  is a symmetric function of the detuning from the PHS point, while  $L_1$  is an anti-symmetric function. Thus, for  $|\varepsilon_1 - U/2| \gtrsim T$ , when  $L_0$  and  $L_1$  are set by detuning,  $S$  may reach really large values. The role of spin polarization is here to split the transmission coefficient dip and cause  $\mathcal{T}(\omega)$  to possess a finite slope at  $\omega = 0$ , which additionally enhances  $L_1$ . However, despite large value of  $S$ , the system does not conduct in this regime (neither heat, nor current, nor spin), so the result is not really physically interesting. This is confirmed by the values of  $Q$ ,

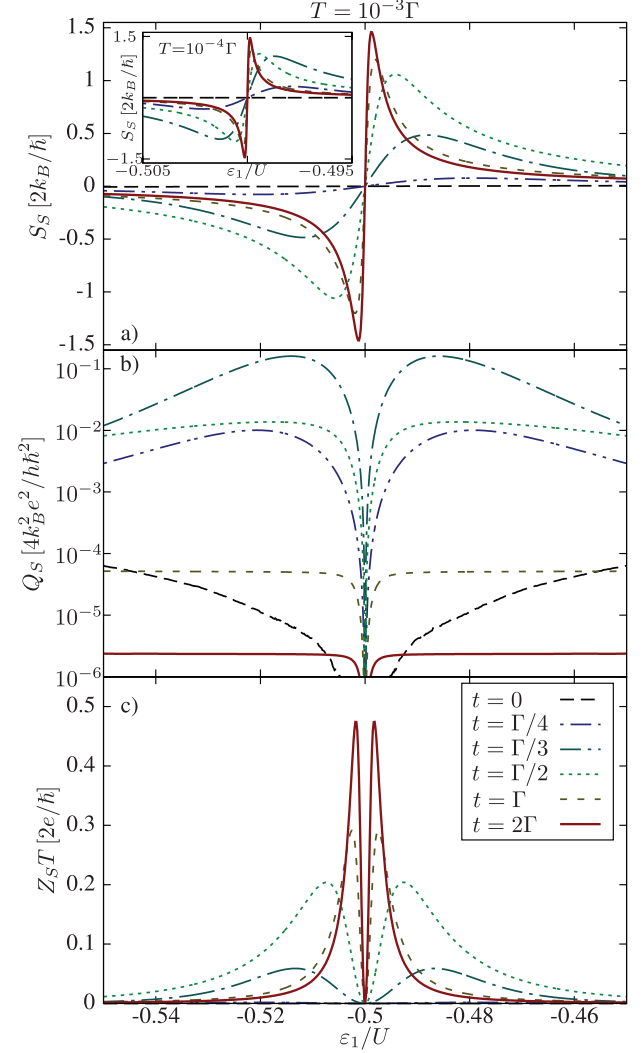


**Figure 6.** Spin thermopower (a), the corresponding power factor (b) and the spin-thermoelectric figure of merit  $Z_S T$  (c) as a function of  $\varepsilon_1$  calculated for different values of hopping between the two dots, as indicated. The parameters are the same as in figure 3 with  $T = 10^{-3}\Gamma$  and  $p = 0.5$ . The inset shows peaks of the spin thermopower at lower  $T = 10^{-4}\Gamma$ .

which are presented in figure 5(c). While for  $\varepsilon_1 > -0.49U$ , the peaks of  $S(p)$  correspond to the peaks of  $Q(p)$ , this is not the case for  $\varepsilon_1 = -0.499U$ ;  $Q$  is not enhanced in the regime of large  $p$ .

The dependence of the spin Seebeck coefficient  $S_S$  on  $p$  is presented in figure 5(b). It significantly differs from the  $p$ -dependence of  $S$ , since  $S_S$  vanishes for  $p = 0$ . In fact,  $S_S(p)$  exhibits a peak, whose position varies with  $\varepsilon_1$  by a few orders of magnitude. The height of the peak increases when  $\varepsilon_1$  approaches the PHS point. The existence of this peak is a consequence of a balance between the exchange field and the second stage of screening. If  $p$  is small enough, spin-reversal symmetry is approximately preserved and  $S_S \approx 0$ . On the other hand, large values of spin polarization result in strong exchange field, which destroys the second stage of the Kondo effect, and thus decrease the spin caloritronic effects.

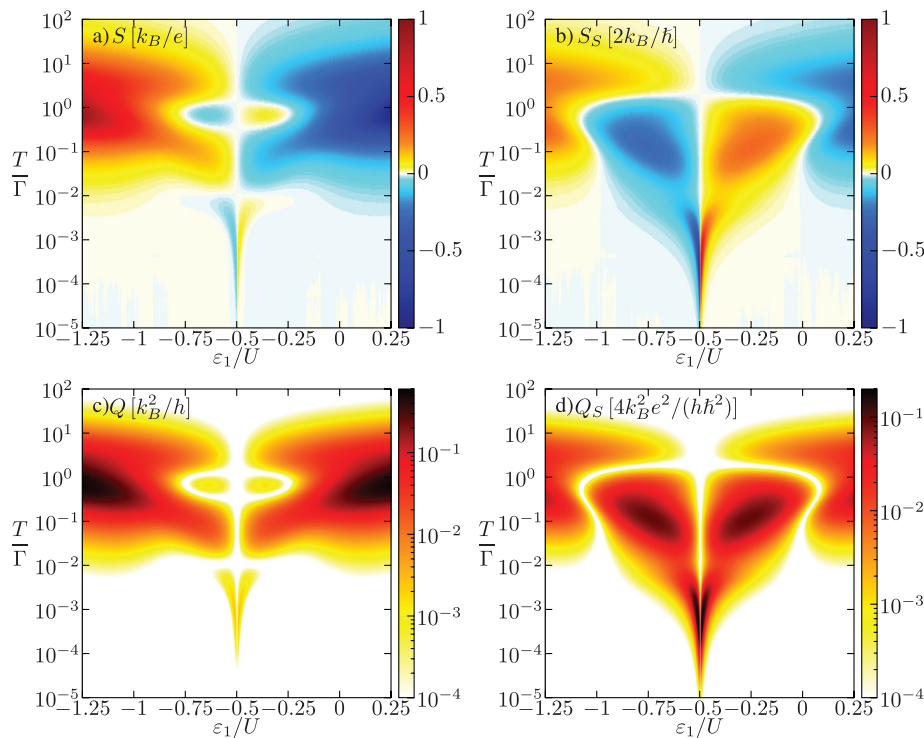


**Figure 7.** Dependence of thermopower (a), spin thermopower (b) and the corresponding power factors, (c) and (d), on the first dot level position  $\varepsilon_1$  and temperature  $T$ . The parameters are the same as in figure 3 with  $p = 0.5$ . Note the logarithmic color scale for the power factors.

The exchange field can also be changed by tuning  $\varepsilon_1$ , which allows for moving the peak in  $S_S(p)$  to the desired range of  $p$ . The flexibility of the device upon this kind of tuning is reduced by the power factor corresponding to spin thermoelectric effects,  $Q_S$ , which is shown in figure 5(d).  $Q_S$  as a function of  $p$  exhibits peaks corresponding to those present in  $S_S(p)$  for all values of  $\varepsilon_1$  considered. The height of these peaks is the largest for  $-0.49U < \varepsilon_1 < -U/3$  and drops significantly for  $|\varepsilon_1 + U/2| < 0.01$ . This is associated with the suppression of the conductance already discussed in the case of conventional Seebeck coefficient. Moreover, as can be seen in figure 5, for a finite value of spin polarization, there exists such a value of  $\varepsilon_1$  for which large peaks in  $S_S(p)$  and  $Q_S(p)$  occur.

#### 4.3. Dependence on the position of QD1 energy level

As follows from figure 5, the dependence of  $S_S$  on  $\varepsilon_1$  for large  $p$  is quite sharp. This is related to Fano-like interference, which occurs between transport paths through a weakly coupled molecular state of DQD that is a resonant one and another, strongly coupled state serving as the background [33, 36–38]. To shed more light on this behavior, in figure 6 we now plot the full  $\varepsilon_1$ -dependence of  $S_S$  for fixed  $p = 0.5$  and the other parameters the same as in figure 5. In this figure we also study the influence of different hopping between the dots  $t$ , which strongly affects the formation of molecular states in DQD and, thus, strongly influences the interference effects.

The dependence of  $S_S$  on  $\varepsilon_1$  calculated at  $T = 10^{-4}\Gamma$ , i.e. for temperature corresponding to that used in figure 5, is shown

as an inset to figure 6(a). However, in this case for the considered range of  $\varepsilon_1$  the spin-thermoelectric power factor  $Q_S$  is quite small, as explained in the previous section (not shown in the plot). Moreover, it becomes even more suppressed with increasing  $t$ . For this reason, the main results shown in figure 6 are calculated at larger temperature,  $T = 10^{-3}\Gamma$ , which is of the order of  $T^*$  for  $t = \Gamma/3$ . At this temperature, outside the PHS point, the conductance is not yet fully suppressed due to the second stage of Kondo effect, and  $Q_S$  values are larger, as can be seen in figure 6(b).

At first sight, one can immediately notice a striking qualitative similarity between the curves shown in figure 6(a) and those in the inset. A closer look, however, reveals some differences. First of all, the two plots have different scales for the horizontal axis. It turns out that the sharp interference peaks get broadened with increasing temperature. Moreover, the width of those peaks scales approximately linearly with  $T$ , while the maximal value of  $S_S$  is rather independent of temperature. We also note that  $S_S$  is anti-symmetric around the PHS point, which is caused by the corresponding sign change of the exchange field  $\Delta\varepsilon_{\text{ex}}$  around this point.

The spin-thermoelectric power factor as a function of  $\varepsilon_1$  is shown in figure 6(b). One can clearly see that  $Q_S$  is optimized for  $t = \Gamma/3$  and only in this case reaches considerable values. For smaller values of hopping  $t$ , the temperature considered in figure 6(b) is above  $T^*$  and  $S_S$  is not enhanced. On the other hand, for larger hoppings,  $T \ll T^*$  and the conductance is generally blocked by the second stage of screening. Since  $Q_S$  must be sufficiently large for any measurement to be possible,

one should not overestimate the meaning of large spin-thermoelectric figure of merit. With this in mind, let us analyze figure 6(c), which presents  $Z_S T$  as a function of  $\varepsilon_1$ .

As can be seen in the figure,  $Z_S T$  exhibits maxima for those values of  $\varepsilon_1$  for which  $|S_S|$  has peaks. Due to the square dependence of  $Z_S T$  on  $S_S$ , see equation (9), the differences in peak heights are now more prominent than in the case of  $S_S$ . The influences of thermal and electrical conductance compensate each other. The maximal  $Z_S T$  equals  $0.5 \cdot 2e/\hbar$ , which is quite large, see figure 6(c). However, it occurs for strong  $t$ , for which  $Q_S$  is rather low and the measurement is hardly possible. On the other hand, for  $t = \Gamma/3$ , corresponding to reasonably large  $Q_S$ , maximal  $Z_S T$  remains of the order of  $0.1 \cdot 2e/\hbar$ .

Finally, to make the analysis of (spin) thermoelectric properties of our magnetic device complete, in figure 7 we present the thermopowers and the corresponding power factors as a function of temperature and QD1 energy level. One can see that both  $S$  and  $S_S$  change sign in the PHS point. However,  $S$  as a function of  $T$  exhibits more sign changes than  $S_S(T)$ . The regimes of large Seebeck and spin Seebeck coefficients can be clearly identified in the figure. While for  $S$  and  $Q$  the largest values are obtained at relatively high  $T$  and large detunings from the PHS point,  $S_S$  and  $Q_S$  are maximized for temperatures of the order of  $T^*$  and close to (but not at) the PHS point.

## 5. Conclusions

We have analyzed the thermoelectric and spin-thermoelectric properties of the DQD in a T-shaped configuration, coupled to two leads magnetized in parallel. The calculations were performed in the linear response regime with the aid of the NRG and we focused on the parameter regime where the system exhibits the two-stage Kondo effect. We determined the full temperature dependence of the (spin) Seebeck coefficient, together with the corresponding power factor and figure of merit. We also studied the dependence of the spin caloritronic properties on the degree of spin polarization of the leads, dot level detuning and the strength of hopping between the dots. It was demonstrated that the thermal conductance fulfills the modified Wiedemann–Franz law found previously for nonmagnetic systems. In addition, we showed that the spin Seebeck coefficient can be strongly enhanced in the regime corresponding to the second stage of the Kondo effect. This enhancement is very sensitive to the value of lead spin polarization. Moreover, it can be tuned by changing the DQD parameters, such as level position and hopping between the dots. We also showed that in order to keep the power factor at an experimentally relevant level, one needs to set the temperature of the order of  $T^*$ . Since  $T^*$  strongly depends on  $t$ , this effect can be tuned by changing the hopping between the dots and the temperature.

We would also like to emphasize that the spin thermoelectric properties of the considered device are very sensitive to the spin polarization of the leads, and even small values of  $p$  (of the order of 1%) can induce large spin Seebeck effect. Such a value of spin polarization may be a consequence of current-induced spin accumulation even for very small driving

currents. It can also occur in the case of the anti-parallel configuration of lead magnetization for two asymmetrically coupled electrodes. Then, even very small coupling asymmetry changes the effective spin polarization from 0 to a finite value of  $p = (\Gamma_L - \Gamma_R)/\Gamma$ . It therefore seems quite realistic to expect  $p \gtrsim 0.01$  in an experiment, which will cause the conventional Seebeck effect to be strongly suppressed (compared to the nonmagnetic case) and the spin Seebeck effect to be present and even possibly strong. All this implies that the effects studied in this paper may also be relevant for a system in which one would not expect them to appear.

## Acknowledgments

This work was supported by the National Science Centre in Poland through Grant No. 2012/04/A/ST3/00372.

## References

- [1] Barnard R D 1972 *Thermoelectricity in Metals and Alloys* (London: Taylor & Francis)
- [2] Zlatić V and Monnier R 2014 *Modern Theory of Thermoelectricity* (Oxford: Oxford University Press)
- [3] Hicks L D and Dresselhaus M S 1993 *Phys. Rev. B* **47** 12727
- [4] Hicks L D and Dresselhaus M S 1993 *Phys. Rev. B* **47** 16631
- [5] Zlatić V, Horvatić B, Milat I and Coqblin B 2003 *Phys. Rev. B* **68** 104432
- [6] Krawiec M and Wysokiński K I 2006 *Phys. Rev. B* **73** 075307
- [7] Grenzebach C, Anders F B, Czucholl G and Pruschke T 2008 *Phys. Rev. B* **77** 115125
- [8] Świrkowicz R, Wierzbicki M and Barnaś J 2009 *Phys. Rev. B* **80** 195409
- [9] Esposito M, Lindenberg K and van den Broeck C 2009 *Europhys. Lett.* **85** 60010
- [10] Kuo D M T and Chang Y-C 2010 *Phys. Rev. B* **81** 205321
- [11] Liu J, Sun Q-F and Xie X C 2010 *Phys. Rev. B* **81** 245323
- [12] Tsaousidou M and Triberis G P 2010 *J. Phys.: Condens. Matter* **22** 355304
- [13] Liu Y-S, Chi F, Yang X-F and Feng J-F 2011 *J. Appl. Phys.* **109** 053712
- [14] Muralidharan B and Grifoni M 2012 *Phys. Rev. B* **85** 155423
- [15] Sanchez R, Sothmann B, Jordan A N and Büttiker M 2013 *New J. Phys.* **15** 125001
- [16] Karwacki Ł, Trocha P and Barnaś J 2013 *J. Phys.: Condens. Matter* **25** 505305
- [17] Hwang S-Y, Lopez R and Sanchez D 2016 *Phys. Rev. B* **94** 054506
- [18] Kondo J 1964 *Prog. Theor. Phys.* **32** 37
- [19] Goldhaber-Gordon D *et al* 1998 *Nature* **391** 156
- [20] Cronenwett S, Oosterkamp T H and Kouwenhoven L P 1998 *Science* **281** 182
- [21] Costi T A and Zlatić V 2010 *Phys. Rev. B* **81** 235127
- [22] Scheibner R, Buhmann H, Reuter D, Kiselev M N and Molenkamp L W 2005 *Phys. Rev. Lett.* **95** 176602
- [23] Donsa S, Andergassen S and Held K 2014 *Phys. Rev. B* **89** 125103
- [24] Rejec T, Žitko R, Mravlje J and Ramsak A 2012 *Phys. Rev. B* **85** 085117
- [25] Weymann I and Barnaś J 2013 *Phys. Rev. B* **88** 085313
- [26] Weymann I 2016 *Sci. Rep.* **6** 19236
- [27] Trocha P and Barnaś J 2012 *Phys. Rev. B* **85** 085408
- [28] Wójcik K P and Weymann I 2016 *Phys. Rev. B* **93** 085428
- [29] Pustilnik M and Glazman L I 2001 *Phys. Rev. Lett.* **87** 216601
- [30] Cornaglia P S and Grepel D R 2005 *Phys. Rev. B* **71** 075305

- [31] Ferreira I L, Orellana P A, Martins G B, Souza F M and Vernek E 2011 *Phys. Rev. B* **84** 205320
- [32] Žitko R 2010 *Phys. Rev. B* **81** 115316
- [33] Fano U 1961 *Phys. Rev.* **124** 1866
- [34] Takazawa Y, Imai Y and Kawakami N 2002 *J. Phys. Soc. Japan* **71** 2234
- [35] Huang R, Wu S-Q and Hou T 2012 *Commun. Theor. Phys.* **57** 161
- [36] Sasaki S, Tamura H, Akazaki T and Fujisawa T 2009 *Phys. Rev. Lett.* **103** 266806
- [37] Žitko R and Bonča J 2006 *Phys. Rev. B* **73** 035332
- [38] Trocha P and Barnaś J 2007 *Phys. Rev. B* **76** 165432
- [39] Dias da Silva L G G V, Vernek E, Ingersent K, Sandler N and Ulloa S E 2013 *Phys. Rev. B* **87** 205313
- [40] Wójcik K P and Weymann I 2014 *Phys. Rev. B* **90** 115308
- [41] Wójcik K P and Weymann I 2015 *Phys. Rev. B* **91** 134422
- [42] Uchida K *et al* 2008 *Nature* **455** 778
- [43] Flipse J, Bakker F L, Slachter A, Dejene F K and van Wees B J 2012 *Nat. Nanotechnol.* **7** 166
- [44] Anderson P W 1961 *Phys. Rev.* **124** 41
- [45] Wójcik K P, Weymann I and Barnaś J 2013 *J. Phys.: Condens. Matter* **25** 075301
- [46] Narducci D 2011 *Appl. Phys. Lett.* **99** 102104
- [47] Wilson K G 1975 *Rev. Mod. Phys.* **47** 773
- [48] We use (modified) open-access Budapest Flexible DM-NRG code, [www.phy.bme.hu/dmnrng/](http://www.phy.bme.hu/dmnrng/), see Legeza O, Moca C P, Tóth A I, Weymann I, Zaránd G 2008 arXiv:0809.3143 unpublished
- [49] Anders F B and Schiller A 2005 *Phys. Rev. Lett.* **95** 196801  
Anders F B and Schiller A 2006 *Phys. Rev. B* **74** 245113
- [50] Weichselbaum A and von Delft J 2007 *Phys. Rev. Lett.* **99** 076402
- [51] Glazman L I and Raikh M E 1988 *J. Exp. Theor. Phys. Lett.* **47** 452  
Glazman L I and Raikh M E 1988 *Pis'maZh. Exp. Teor. Fiz.* **47** 378
- [52] Haldane F D M 1978 *Phys. Rev. Lett.* **40** 416
- [53] Martinek J *et al* 2003 *Phys. Rev. Lett.* **91** 127203
- [54] Wójcik K P 2015 *Eur. Phys. J. B* **88** 110
- [55] Franz R and Wiedemann G 1853 *Ann. Phys.* **165** 497

## **Part III**

### **Appendix**



# Appendix A

## Academic achievements

### A.1. Complete list of publications

1. K. P. Wójcik, *Application of a numerical renormalization group procedure to an elementary anharmonic oscillator*, Acta Phys. Pol. B **44**, 69 (2013).
2. K. P. Wójcik, I. Weymann, J. Barnaś, *Asymmetry-induced effects in Kondo quantum dots coupled to ferromagnetic leads*, J. Phys: Condens. Matter **25**, 075301 (2013).
3. K. P. Wójcik, I. Weymann, *Proximity effect on spin-dependent conductance and thermopower of correlated quantum dots*, Phys. Rev. B **89**, 165303 (2014).
4. K. P. Wójcik, I. Weymann, *Perfect spin polarization in T-shaped double quantum dots due to the spin-dependent Fano effect*, Phys. Rev. B **90**, 115308 (2014).
5. K. P. Wójcik, I. Weymann, *The magnetic field effects on spin polarization of T-shaped double quantum dots coupled to ferromagnetic leads*, Acta Phys. Pol. A **127**, 222 (2015). (Proceedings of the European Conference *Physics of Magnetism*, Poznań 2014).
6. I. Weymann, K. P. Wójcik, *Andreev transport in a correlated ferromagnet-quantum-dot-superconductor device*, Phys. Rev. B **92**, 245307 (2015).
7. K. P. Wójcik, *Ferromagnets-induced splitting of molecular states of T-shaped double quantum dots*, Eur. Phys. J. B **88**, 110 (2015).
8. K. P. Wójcik, I. Weymann, *Two-stage Kondo effect in T-shaped double quantum dots with ferromagnetic leads*, Phys. Rev. B **91**, 134422 (2015).

9. K. P. Wójcik, I. Weymann, *Thermopower of strongly correlated T-shaped double quantum dots*, Phys. Rev. B **93**, 085428 (2016).
10. K. Wójcik, I. Weymann, *Strong spin Seebeck effect in Kondo T-shaped double quantum dots*, J. Phys.: Condens. Matt. **29**, 055303 (2016).
11. S. Głodzik, K. P. Wójcik, I. Weymann, T. Domański, *Interplay between electron pairing and Dicke effect in triple quantum dot structures*, Phys. Rev. B **95**, 125419 (2017).
12. K. Wójcik, I. Weymann, *Andreev conductance through a quantum dot strongly coupled to ferromagnetic and superconducting leads*, accepted in Acta Phys. Pol. A (2017), (Proceedings of XII International School on Theoretical Physics SSPCM, Rzeszów 2016).
13. K. Wójcik, I. Weymann, *Transport properties of a hybrid Majorana wire-quantum dot system with ferromagnetic contacts*, unpublished (2017).

## A.2. List of schools and conferences

1. IV Scientific Camp in Tatra Mountains organized by Physics Students Club SKFiz from University of Warsaw, Bukowina Tatrzańska (Poland), 15-22.09.2009. Delivered **speech** *Statystyki zliczeń fotonów (Photon counting statistics)*.
2. Conference IX Ogólnopolska Sesja Kół Naukowych Fizyków, Toruń (Poland), 11-14.11.2010. Delivered **speech** *Renormalizacja hamiltonianu oscylatora anharmonicznego (Rnormalization of the Hamiltonian of anharmonic oscillator)*.
3. Conference X Ogólnopolska Sesja Kół Naukowych Fizyków "Piknik Naukowy 2011", Brenna (Poland), 5-8.05.2011. Delivered **speech** *Emisja spontaniczna w układzie o skończonej liczbie modów (Spontaneous emission in the system with finite number of modes)*.
4. VI SKFiz Scientific Camp in Tatra Mountains, Bukowina Tatrzańska (Poland), 17-24.07.2011. Delivered **speech** *Dlaczego i jak (pod)układy dążą do najniższej energii (Why and how do the (sub)systems minimize their energy)*.
5. Erasmus Intensive Programme *Soft Mat Control*, Poznań (Poland), 27.02-9.03.2012.
6. Conference II Kopernikańskie Sympozjum Studentów Nauk Przyrodniczych, Toruń (Poland), 9-11.03.2012. Delivered **speech** *Jak wygląda elektron? (How does the*



*electron look?)* and presented **poster** *Jak wygląda elektron w kryształce? (How does the electron in a crystal look?)*.

7. Conference *XI Ogólnopolska Konferencja Kół Naukowych Fizyków Piknik Naukowy 2012*, Wisła (Poland), 17-20.05.2012. Delivered **speech** *Kwantowy opis prądu (Quantum description of current)*.
8. VII *SKFiz* Scientific Camp in Tatra Mountains, Bukowina Tatrzańska (Poland), 15-22.07.2012. Delivered **speech** *Fizyka Mezoskopowa (Mesoscopic physics)*.
9. XXXVI International Conference of Theoretical Physics *Correlations and coherence at different scales*, Ustroń (Poland), 13-18.09.2012. Presented **poster** *Transport through a Kondo quantum dot asymmetrically coupled to magnetic leads*.
10. Conference *XI Ogólnopolska Sesja Kół Naukowych Fizyków*, Warsaw (Poland), 15-18.11.2012. Delivered **speech** *Powszechne efekty relatywistyczne (Common relativistic effects)* and presented **poster** *Nadprzewodniki i druty kwantowe (Superconductors and quantum wires)*.
11. 9th Capri spring school on transport in nanostructures, Anacapri (Italy), 7-14.04.2013. Delivered **speech** *Two-stage Kondo effect in T-shaped quantum dots with ferromagnetic leads*.
12. 15th Czech and Slovak Conference on Magnetism CSMAG'13, Košice (Slovakia), 17-21.06.2013. Presented **poster** *Two-stage Kondo effect in T-shaped double quantum dots with ferromagnetic leads*.
13. VIII *SKFiz* Scientific Camp in Tatra Mountains, Bukowina Tatrzańska (Poland), 30.06-7.07.2013. Delivered **speech** *Efekt Kondo (The Kondo effect)*.
14. 45th IFF Spring School *Computing Solids*, Forschungszentrum Jülich (Germany), 10-21.03.2014.
15. Deutsche Physikalische Gesellschaft Spring meeting 2014, Dresden (Germany), 30.03-4.04.2014. Delivered **speech** *The interplay of the proximity and Kondo effects in spin-resolved transport through quantum dots*.
16. The European Conference Physics of magnetism 2014, Poznań (Poland), 23-27.06.2014. Presented **poster** *Electrically controlled spin polarization in T-shaped double quantum dots coupled to ferromagnetic leads*.

17. IX SKFiz Scientific Camp in Tatra Mountains, Bukowina Tatrzańska (Poland), 13-19.07.2014. Delivered **speech** *Opis przepływu prądu przez kropki kwantowe (Description of the current flow through quantum dots)*.
18. International Summer School of Theoretical Physics *Symmetry and Structural Properties of Condensed Matter*, Rzeszów (Poland), 1-6.09.2014. Presented **poster** *Electric and thermoelectric properties of T-shaped double quantum dots coupled to ferromagnetic leads*.
19. Deutsche Physikalische Gesellschaft Spring meeting 2015, Berlin (Germany), 15-20.03.2015. Delivered **speech** *Spin-dependent Fano effect and two-stage Kondo effect in T-shaped double quantum dots with ferromagnetic leads*.
20. International conference *Frontiers of Quantum and Mesoscopic Thermodynamics*, Prague (Czech Republic), 27.07-1.08.2015. Presented **poster** *Thermoelectric properties of T-shaped double quantum dots exhibiting Fano and Kondo effects*.
21. International conference *SpinTech VIII*, Basel (Switzerland), 10-13.08.2015. Presented **poster** *Spin-dependent thermoelectric effects in Fano-Kondo T-shaped double quantum dots*.
22. Autumn School on Correlated Electrons *Many-Body Physics: From Kondo to Hubbard*, Forschungszentrum Jülich (Germany), 21-25.09.2015. Presented **poster** *Fano and Kondo effects in T-shaped double quantum dot with ferromagnetic leads*.
23. International conference *NEWSPIN4: Transport Beyond Electrons*, Utrecht (Netherlands), 14-16.12.2015. Presented **poster** *Spin-thermoelectric effects in T-shaped double quantum dots with ferromagnetic leads*.
24. Deutsche Physikalische Gesellschaft Spring meeting 2016, Regensburg (Germany), 6-12.03.2015. Presented **poster** *Andreev transport in a correlated ferromagnet-quantum-dot-superconductor device*.
25. International Conference *Spin Caloritronics VII*, Utrecht (Netherlands), 11-15.07.2016. Presented **poster** *Strong spin Seebeck effect associated with two-stage Kondo screening in double quantum dots*.

### A.3. List of awards

2016 – Rector’s award for scientific research at Adam Mickiewicz University in Poznań (further abbreviated AMU) – as a member of awarded team.

- 2015 – Polish Minister of Science and Higher Education Scholarship.
- 2015 – Rector’s award for scientific research at AMU – as a member of awarded team.
- 2015 – Rector’s scholarship for best PhD students at AMU.
- 2014 – Rector’s scholarship for best PhD students at AMU.
- 2012 – Organizers’ award for best talk at the conference *II Kopernikańskie Sympozjum Studentów Nauk Przyrodniczych*, Toruń (Poland), 9-11.03.2012.
- 2012 – Organizers’ award for best poster at the conference *II Kopernikańskie Sympozjum Studentów Nauk Przyrodniczych*, Toruń (Poland), 9-11.03.2012.
- 2011 – Organizers’ award for best talk at the conference *X Ogólnopolska Sesja Kół Naukowych Fizyków Piknik Naukowy 2011*, Brenna (Poland), 5-8.05.2011.

#### **A.4. Experience in scientific projects**

- 2012-2013: Co-investigator in Polish State Committee for Scientific Research grant no. N N202 199739. Project title: *Transport ładunku przez układy kropek kwantowych i molekuł (Charge transport through systems of quantum dot and molecules)*. Project leader: dr hab. Wojciech Rudziński.
- 2012-2014: Co-investigator in the grant of Polish Ministry of Science and Higher Education *Iuventus Plus* no. IP2011 059471. Project title: *Efekty spinowe w transporcie przez hybrydowe układy kropek kwantowych i molekuł (Spin effects in transport through hybrid systems of quantum dots and molecules)*. Project leader: dr hab. Ireneusz Weymann, prof. UAM.
- 2013-2016: Co-investigator in Polish National Science Centre grant *Maestro* no. 2012/04/A/ST3/00372. Project title: *Spinowe efekty termoelektryczne w transporcie przez układy nanoskopowe (Spin thermoelectric effects in transport through nanoscopic systems)*. Project leader: prof. dr. hab. Józef Barnaś.
- 2014-now: (Project in progress.) Main co-investigator in Polish National Science Centre grant *Sonata Bis* no. 2013/10/E/ST3/00213. Project title: *Teoretyczne badania transportu w nanostrukturach magnetycznych (Theoretical studies of transport in magnetic nanostructures)*. Project leader: dr hab. Ireneusz Weymann, prof UAM.

2016-now: (Project in progress.) Principal Investigator in Polish National Science Centre grant *Preludium* no. 2015/19/N/ST3/01030. Project title: *Efekt Kondo w złożonych układach skorelowanych kropek kwantowych* (*The Kondo effect in complex systems of correlated quantum dots*).

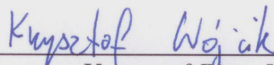
# **Appendix B**

## **Statements concerning authors' contributions**



Hereby, I declare I had the following contribution to the articles constituting the dissertation.

- Article A: I performed all the calculations with the assistance of the Supervisor. I prepared all the figures except for Fig. 1. I contributed extensively to the text of the article. I estimate my contribution as 70%.
- Article B: I performed a part of NRG calculations, implemented the Hilbert transform in a way suitable for calculation of the real part of  $\langle\langle d_{\uparrow}^{\dagger} d_{\downarrow}^{\dagger} \rangle\rangle^{\text{ret}}(\omega)$  and contributed to the text of the article. I estimate my contribution as 40%.
- Article C: I performed all the calculations with the assistance of the Supervisor. I prepared all the figures and contributed extensively to the text of the article. I estimate my contribution as 70%.
- Article D: I performed all the calculations with the assistance of the Supervisor. I prepared all the figures and contributed extensively to the text of the article. I estimate my contribution as 70%.
- Article E: I am the only author, my contribution is 100%.
- Article F: I performed all the calculations with the assistance of the Supervisor. I prepared all the figures and contributed extensively to the text of the article. I estimate my contribution as 70%.
- Article G: I performed all the calculations with the assistance of the Supervisor. I came up with the idea of calculation of power factor. I prepared all the figures and contributed extensively to the text of the article. I estimate my contribution as 70%.
- Article H: I performed all the calculations with the assistance of the Supervisor. I prepared all the figures and contributed extensively to the text of the article. I estimate my contribution as 70%.

  
Krzysztof Piotr Wójcik





Poznań, March 8, 2017

Prof. UAM dr hab. Ireneusz Weymann  
Mesoscopic Physics Division  
Faculty of Physics  
Adam Mickiewicz University in Poznań

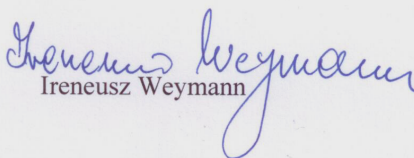
Hereby, I declare that my contribution to the following publications:

- K. P. Wójcik, I. Weymann, *Proximity effect on spin-dependent conductance and thermopower of correlated quantum dots*, Phys. Rev. B **89**, 165303 (2014),  
K. P. Wójcik, I. Weymann, *Perfect spin polarization in T-shaped double quantum dots due to the spin-dependent Fano effect*, Phys. Rev. B **90**, 115308 (2014),  
K. P. Wójcik, I. Weymann, *The magnetic field effects on spin polarization of T-shaped double quantum dots coupled to ferromagnetic leads*, Acta Phys. Pol. A **127**, 222 (2015),  
K. P. Wójcik, I. Weymann, *Two-stage Kondo effect in T-shaped double quantum dots with ferromagnetic leads*, Phys. Rev. B **91**, 134422 (2015),  
K. P. Wójcik, I. Weymann, *Thermopower of strongly correlated T-shaped double quantum dots*, Phys. Rev. B **93**, 085428 (2016),  
K. Wójcik, I. Weymann, *Strong spin Seebeck effect in Kondo T-shaped double quantum dots*, J. Phys.: Condens. Matter **29**, 055303 (2017),

relied on proposing the research topic, assisting in performing calculations, interpreting the results, and preparing the manuscript. For the paper

- I. Weymann, K. P. Wójcik, *Andreev transport in a correlated ferromagnet-quantum-dot-superconductor device*, Phys. Rev. B **92**, 245307 (2015),

I formulated the project, performed part of calculations, contributed to the interpretation of results, and prepared figures together with the initial version of the manuscript.

  
Ireneusz Weymann